Lecture Notes in Civil Engineering

Indrajit Pal · Sreevalsa Kolathayar ·
Sheikh Tawhidul Islam ·
Anirban Mukhopadhyay ·
Iftekhar Ahmed *Editors*

Proceedings of the 2nd International Symposium on Disaster Resilience and Sustainable Development

Volume 2 - Disaster Risk Science and Technology

Springer

Lecture Notes in Civil Engineering

Volume 294

Lecture Notes in Civil Engineering (LNCE) publishes the latest developments in Civil Engineering—quickly, informally and in top quality. Though original research reported in proceedings and post-proceedings represents the core of LNCE, edited volumes of exceptionally high quality and interest may also be considered for publication. Volumes published in LNCE embrace all aspects and subfields of, as well as new challenges in, Civil Engineering. Topics in the series include:

- Construction and Structural Mechanics
- Building Materials
- Concrete, Steel and Timber Structures
- Geotechnical Engineering
- Earthquake Engineering
- Coastal Engineering
- Ocean and Offshore Engineering; Ships and Floating Structures
- Hydraulics, Hydrology and Water Resources Engineering
- Environmental Engineering and Sustainability
- Structural Health and Monitoring
- Surveying and Geographical Information Systems
- Indoor Environments
- Transportation and Traffic
- Risk Analysis
- Safety and Security

To submit a proposal or request further information, please contact the appropriate Springer Editor:

– Pierpaolo Riva at pierpaolo.riva@springer.com (Europe and Americas);
– Swati Meherishi at swati.meherishi@springer.com (Asia—except China, Australia, and New Zealand);
– Wayne Hu at wayne.hu@springer.com (China).

All books in the series now indexed by Scopus and EI Compendex database!

Indrajit Pal · Sreevalsa Kolathayar ·
Sheikh Tawhidul Islam · Anirban Mukhopadhyay ·
Iftekhar Ahmed
Editors

Proceedings of the 2nd International Symposium on Disaster Resilience and Sustainable Development

Volume 2 - Disaster Risk Science and Technology

Springer

Editors
Indrajit Pal
Disaster Preparedness, Mitigation
and Management (DPMM)
Asian Institute of Technology
Khlong Nueng, Pathum Thani, Thailand

Sheikh Tawhidul Islam
Institute of Remote Sensing and GIS
Jahangirnagar University
Dhaka, Bangladesh

Iftekhar Ahmed
School of Architecture and Built
Environment
University of Newcastle
Newcastle, NSW, Australia

Sreevalsa Kolathayar
Department of Civil Engineering
National Institute of Technology
Surathkal, Karnataka, India

Anirban Mukhopadhyay
Disaster Preparedness, Mitigation
and Management (DPMM)
Asian Institute of Technology
Khlong Nueng, Pathum Thani, Thailand

ISSN 2366-2557 ISSN 2366-2565 (electronic)
Lecture Notes in Civil Engineering
ISBN 978-981-19-6296-7 ISBN 978-981-19-6297-4 (eBook)
https://doi.org/10.1007/978-981-19-6297-4

This Springer imprint is published by the registered company Springer Nature Singapore Pte Ltd.
The registered company address is: 152 Beach Road, #21-01/04 Gateway East, Singapore 189721, Singapore

Disaster Risk Science and Technology: Addressing Cross-Cutting Challenges

Technological advancement has always be in the forefront to enhance the capacities of disaster risk management initiatives at various levels. Interdisciplinary approaches to address disaster risk reduction challenges and achieve resilience are the key for sustainable development. The policy ecosystem is deemed crucial for maintaining sustainability and resilient development. Evidence-based approaches to understand the social system are helpful in developing new policies and amending existing policies for sustainability. Understanding the disaster risk through earth observation data is well recognized among the researcher and policy-makers for improving risk understanding and combining science and local voices and knowledge. The comprehensive knowledge covering various aspects of disaster management like earthquakes, flooding, tropical cyclones, and cross-cutting technologies that were developed to mitigate the disasters has been discussed through the various technical papers in this volume.

The proceeding volume is an outcome of the "2nd International Symposium on Disaster Resilience and Sustainable Development" organized by Disaster Preparedness, Mitigation and Management, Asian Institute of Technology, Thailand, brings together research works from some of the critical issues of science and technology in the field of climate change, multiple hazards, and resilience-building measures. The proceeding volume consolidates the research findings and case studies of recent developments in the disaster risk science and technology addressing cross-cutting challenges for sustainability.

Khlong Nueng, Thailand — Indrajit Pal
Surathkal, India — Sreevalsa Kolathayar
Dhaka, Bangladesh — Sheikh Tawhidul Islam
Khlong Nueng, Thailand — Anirban Mukhopadhyay
Newcastle, Australia — Iftekhar Ahmed
Khlong Nueng, Thailand — Ganni Satya Venkata Sai Aditya Bharadwaz

Contents

Disaster Risk Science and Technology: Addressing Cross-Cutting Challenges

Indrajit Pal, Sreevalsa Kolathayar, Sheikh Tawhidul Islam, Anirban Mukhopadhyay, Iftekhar Ahmed, and Ganni Satya Venkata Sai Aditya Bharadwaz

1 Introduction and Background

This book primarily deals with the management of various natural hazards and uses a technological approach for mitigation measures and better preparedness for those disasters. Natural hazards discussed in this book include earthquakes in active faults and fold areas, flooding in the major rivers (such as Brahmaputra and Mekong), pre and post-monsoonal cyclones in the Bay of Bengal, and the South China Sea, etc. South and Southeast Asian countries (such as Thailand, Myanmar, Vietnam, India, Bangladesh, and Nepal) are vulnerable to natural hazards due to their geographic locations and climatic settings. Therefore, comprehensive knowledge covering various aspects of disaster risk management of and cross-cutting technologies developed to mitigate disasters is presented in this book. The solutions proposed are context-specific designed for particular sites, and therefore may not readily be transferable to other locations.

Earthquakes have long been a significant threat to developing countries due to vulnerable structures and post-disaster mismanagement. Analyzing past disasters and simulation of various future scenarios are crucial for better preparedness. Therefore, a devastating earthquake of Mw 6.8 in 1991 in Uttarakhand, India, was analyzed from 13 ground station data. The critical characteristics evaluated were Peak Ground

I. Pal (✉) · A. Mukhopadhyay · G. S. V. S. A. Bharadwaz
Disaster Preparedness, Mitigation and Management, Asian Institute of Technology, Khlong Nueng, Thailand
e-mail: indrajit-pal@ait.ac.th

S. Kolathayar
Department of Civil Engineering, National Institute of Technology Karnataka, Mangalore, India

S. T. Islam
Jahangirnagar University, Dhaka, Bangladesh

I. Ahmed
University of Newcastle, Callaghan, Australia

I. Pal et al. (eds.), *Proceedings of the 2nd International Symposium on Disaster Resilience and Sustainable Development*, Lecture Notes in Civil Engineering 294,
https://doi.org/10.1007/978-981-19-6297-4_1

Acceleration (PGA), Peak Ground Velocity (PGV), Arias Intensity (AI), Predominant Period (Tp), and significant duration. On the other hand, the performance of a -15-storied RC building in Ahmedabad was evaluated using Seismic design codes of USA, Turkey, European Standard and India. The building was fairly resilient in terms of the Life Safety (LS) performance criteria under Maximum Credible Earthquake (MCE) level earthquakes. It is able to withstand damage to non-structural components in case of moderate earthquakes (4–6 MW). A similar study on earthquakes was performed in New Zealand and focused on the 6.8 MW earthquake on 22 February 2011. The study examined critical damages and implemented a sound strategy to enhance and facilitate future research on the performance of buildings and infrastructures in similar seismic regions. In this respect, it is worth mentioning that wavelet analysis provides information on both the time and frequency content of non-stationary signals. Wavelet analysis of M_W 7.8 Gorkha Earthquake (Nepal 2015) depicted response spectra of all recorded ground motions showing a very wide acceleration sensitive region. In addition, some ground motions contain significant velocity pulses. Further investigation using the continuous wavelet transforms (CWT) was carried out to understand the changing time-frequency characteristics of the earthquake ground motions.

Flooding is another significant disaster in South and Southeast Asia. Monsoonal rainfall helps overflow the river basins giving rise to significant floodplains of large rivers like Mekong, Brahmaputra, etc. Hydrologists have been interested in the discharge and runoff caused by precipitation as these parameters are essential for flood modelling. In this book, two conceptual models have been compared, namely TANK and SimHyd, using the Rainfall-Runoff Library (RRL) tool to check their suitability. The TANK model was deemed suitable for the Hemavathi watershed, Cauvery Basin, India, in terms of Nash–Sutcliffe efficiency (NSE) and Correlation coefficient (CC) values. Failure slopes are often made in Southeast Asia to tackle rainfall. This book also describes a failure slope's stability, located at km 34 of the Halong-Vandon highway (Northeast area of Vietnam). Wind-driven hazards are becoming more common as climate change has been directly linked to the intensity and frequency of tropical cyclones. This book provides integrated knowledge and review of research development towards power system vulnerability for cyclone catastrophe models.

2 Addressing Cross-Cutting Challenges

In the modern era, vulnerability assessment and risk management are conducted with the help of GIS-based methods. The Aga Khan Agency for Habitat (AKAH) has developed a standardized hazard, vulnerability, and risk assessment (HVRA) approach for systematic risk screening, developing a DRR plan, and monitoring the impact. The risk index is defined based on two main pillars or indicators: hazard exposure and vulnerability. The HVRA result was generated through GIS tools and

incorporated into village disaster management plans for short- and long-term planning, which is helpful to bridge risk perception gaps between local communities, governments, and experts. Disaster risk reduction in developing countries is hindered mainly due to insufficient information or delay in information. A Hybrid Ladderized Learning Model was developed for the Disaster Risk Management Technical and Vocational Education and Training (DRM-TVET) Program in Higher Education Institutions. Indigenous knowledge can also help mitigate and prevent disasters. The indigenous Chepang community of Nepal has been unknowingly utilizing their indigenous knowledge to tackle disasters in the form of societal functioning and cultural rituals. The authors have successfully established a link between indigenous knowledge and scientific facts to synthesize and propose a new approach that will benefit the government and local communities.

3 DRR and Geo-Environmental Perspective

Raisinghani et al., in their paper "Assessment of the Numerical Methods for the Seismic Resilience of Built Structures in India", evaluated the performance of a 15-storey building for seismic design codes. The authors reviewed regulations and resilience parameters to be followed by the current generation for seismic analysis. The results showed that the building satisfies Life Safety (LS) performance criteria under the highest-level earthquake, and damage to non-structural components is seen in moderate earthquakes (4–6 MW) (IS1893-2016 and IS13920-2016). Also, the various aspects related to the dynamic analysis, linear time history, and modal analysis for seismic design of high-rise buildings have been discussed (Newmark 1959; Chopra and Goel 2002). The study by Sarv Priya and P.K. Goyal in their paper "Wind hazards on the Indian power system and challenges for the future: A review" had integrated the development of research towards power system vulnerability for cyclone catastrophe models. In this study, several essential variables to assess the risk and physical and systemic approaches are used to determine vulnerability. It is found that the distribution subsystem is more vulnerable than the generation and transmission subsystem under extreme wind (Sahoo et al. 2019). The paper "Time-Frequency Analysis of Strong Ground Motions from the Mw 6.8 1991 Uttarkashi Earthquake" by Vinuthna Ambatipudi et al. reviewed the intensity, infrastructure damages, and effects caused by major destructive earthquakes in the state of Uttarakhand. It is found that the amplitude and frequency content of ground motions are the primary variables that affect the behaviour of structures subjected to earthquake forces. The results are consistent with the damage data from the post-earthquake reconnaissance studies conducted using time-frequency analysis after the 1991 Uttarkashi earthquake (Devi and Sharma 2016). Rajnil Rohit Lal et al., in their paper "Earthquake characteristics and ground motions in Christchurch, New Zealand" explained the potentialities and criticalities of identified damages and implemented strategies for future research to enhance the performance of building and infrastructure in high seismic prone regions within the pacific. The results showed that the earthquake-induced shaking is lethal

and dangerous depending on the magnitude and the vulnerabilities of infrastructure and buildings on the ground. The study "Wavelet analysis of Near-Field Ground Motions from the Mw 7.8 2015 Gorkha Earthquake" by Mohammed Ayub Ifan et al. has analyzed the time domain and frequency domain. For conducting the time domain analysis, mainly critical characteristics of the seismic waves are observed, and frequency domain analysis is performed using fast Fourier transforms (FFTs). During the investigation, it is found that during a severe earthquake with high amplitude cyclic forces on a structure, the structure's stiffness degrades with time. The ground motion has seismic waves of lower frequency followed by higher frequency waves, especially if these frequencies are close to the original and changed natural period of the structure.

The "Comparative Analysis of TANK and SimHyd Rainfall-Runoff models in the Hemavathi watershed, Cauvery Basin, India" by Nagireddy Masthan Reddy et al. addressed difficulties faced by hydrologists in selecting the best model for assessing water resources in a specific region. This research was used to determine which of the two conceptual models included in the RRL framework, TANK and SimHyd, was the most appropriate. After the study, the authors suggested that TANK and SimHyd models have shown better performance in terms of CC values during calibration and validation. Overall, TANK is the best model (Jaiswal et al. 2020) based on NSE, showing 0.71 during calibration, which offers good performance and 0.64 during validation which resembles a satisfactory model. Tuan-Nghia Do et al., in their paper "Stability analysis of a failure slope after treatment as regard influence of rainfall", explained the slope failure on the Halong-Vandon highway (Northeast area of Vietnam) as Vietnam is vulnerable to risk of landslides due to its mountainous terrain (Nguyen et al. 2020). However, they are four stages. The loss took place due to the subsidence of the crown at the 1st stage of slope because concrete plates were destroyed throughout the failure surface. To improve the stability of the slope, a 30 m—high MSE wall with four stages has been constructed as a retaining structure. The strength of the slope has been analyzed by estimating the influence of rainfall by the c-phi reduction method coupled with flow analysis, and Plaxis software has been used. The results showed greater stability.

4 DRR, Geo-Physical and Engineering Perspective

The paper "A Study on Seismic Behavior of Hyperbolic Cooling Tower with V and X Columns" by C.L. Mahesh Kumar et al. has determined the seismic response of hyperbolic cooling towers in the form of a natural time period. Also, parameters like Lateral Deformation, base shear (Zhang et al. 2011), and axial forces on columns were compared and analyzed. Two natural draft cooling tower models are developed in this paper, one with Raker Columns and the other with Meridional Columns. Results showed that the time period is greater for the natural draft cooling tower supported on Raker columns than Meridional columns. The paper "Evaluate the durability of RC Bridge under the impact of Climate change in Vietnam" analyzed how climate

change is affecting reinforced concrete structures. In the study, it is found that the structures present in highly aggressive environments have a reduced lifespan. Also, the structures which are near the sea have a faster deterioration rate when compared with structures in inland areas due to a high level of corrosion as stated in studies by Medeiros-Junior (2018) and others. Overall, it is suggested that it is better to develop high strength concrete for the structures present in a strong, aggressive environment. The study "Mechanical Behavior of Geopolymer in Addition with Fibre Reinforced Materials—A Review" by Divya Jat et al.; summarized and discussed the geopolymer's mechanical properties such as compressive strength, flexural strength, tensile strength, and toughness of geopolymer with each fibre. The results showed that glass fibre had shown the maximum mechanical strength compared to other fibres like basalt (Kizilkanat et al. 2015), whereas carbon has been excellent in elevated temperatures. S.M. Anas and Mehtab Alam, in their study "Effect of Additional Transverse Reinforcements on the Performance of Axially Loaded Reinforced Concrete Column under Close-in Blast," had developed a three-dimensional finite element model using a general finite element software package, ABAQUS/Explicit (Kyei and Braimah 2017) equipped with concrete damage plasticity (CDP) model. The study undertaken provides insight into the role of the additional transverse reinforcement used in the RC columns to improve their blast performance and thereby reduce the risk generated by explosive-induced loading. This study also provides insight to mitigate the consequences of blast loading that may trigger progressive collapse risk out of accidental explosions or detonation of the high-yield explosives. The findings of the present research work are useful to structural engineers and the sectional committee for drafting the standard of blast-resistant design of the RC columns. In the study "Ultimate Bearing Capacity of Pipe Buried Near Sand Slopes", Sukanta Das reviewed the effect of slope angles on the bearing capacity of buried pipe and failure wedges. The two-dimensional finite element limit analysis (2D-FEA) is used for the numerical analysis. In general, the bearing capacity increase as the angle of internal friction of soils and the depth of embedment of pipes increase, but a drastic increase in bearing capacity of pipes has been found. It is found that the failure surface beneath the pipe is strongly influenced by the slope angle and the edge distance of the pipe from the crest of the slopes. So, this study will be helpful for the development of pipeline infrastructures in hilly areas, which is still a challenging task for geotechnical engineers. In the paper "Geopolymer concrete—a study of an alternative material for OPC", Ishan Thakar et al. reviewed the different solutions of activators that can improve the strength of geopolymer concrete. As part of the process, various tests have been done. It was concluded that geopolymer delivers greater strength than Ordinary Portland cement and may be used as a cement substitute in the construction industry. Muhammad Hamza Sabir et al., in the paper "Numerical Computation of Code Compliant Beam-Column Joints Made with Low Strength Concrete", studied an exterior RC joint under monotonic loading from published data to check the reliability of numerical prediction using the damaged plasticity constitutive model, available in ABAQUS. It can efficiently help in predicting the failure of reinforced concrete joints as they are the most vulnerable region of frame structures (Behnam et al. 2018). The dilation angle needs to be

calibrated for individual models. It is worth mentioning that the current research is carried out using only the values of concrete compressive strength and steel yield strength. In the study "Seismic Behaviour of Pavements: An Approach Towards Seismic Resistance Design of Pavements" by Sukanta Das et al. reviewed the two-dimensional finite element analysis performed for seismic response of road under surcharge load as traffic loads. Based on extensive numerical analysis and obtained results, a significant amplification has been observed considering seismic soil pavement interaction; less amplification has been found due to less amplitude of the input ground motion. The result shows that road embanks are more vulnerable to seismic excitations, and significant aggravation of ground motion is observed at the top of pavements compared to free field conditions.

5 DRR, Socio-Economic and Cross-Cutting Issues

Apoorva Patel and Ambati Nageswara Rao, in their paper "Policy Ecosystem of Social Entrepreneurship for Sustainable and Resilient Development: A Doctrinal Review", reviewed an inductive approach and exploratory design and explored the dynamic ecosystem of entrepreneurship, specifically the legal framework, and policy concerning social entrepreneurship in India. The practical methods with accurate data integration of the concept of resilience (Avery and Bergsteiner 2011) are one of the important aspects for policymaking, policy implementation, policy analysis, and policy revisions. The results review indicate that the policy ecosystem has a vital role in leveraging or confronting the sustainability and resilience of social entrepreneurship. The study "Indigenous Knowledge of Chepang in Disaster Risk Reduction" by Ganesh Dhungana et al. reviewed the best practices by the community of Chepang from indigenous knowledge interlinked with scientific knowledge and its contribution to DRR. The results revealed that the Chepang community had developed mitigation and preparedness, based on knowledge passed down from previous generations. However, due to negligence and lack of archiving (Khatiwada et al. 2012), lack of social innovation and handover approaches, indigenous knowledge of Chepang has not properly transferred to the newer generation. Rahim Dobariya et al., in their paper "GIS-based HVRA for Risk Anticipation and Disaster Risk Reduction", had reviewed the hazard, vulnerability, and risk assessment (HVRA) approach for systematic risk screening, and developed a DRR plan that of the Aga Khan Agency for Habitat (AKAH). The HVRA is a four-step process that integrates scientific information available with national/international institutions and local community knowledge through participatory risk assessment. HVRA results are considered a baseline to monitor the impact of DRR interventions. World Habitat awarded this work the "World Habitat Gold Award 2020". While the current HVRA is an excellent tool to improve risk understanding and mainstream development planning, the limitation posed by the necessity of being based on onsite and examining current hazards needs to be overcome to factor in remote hazards and the impact of climate change (Fig. 1).

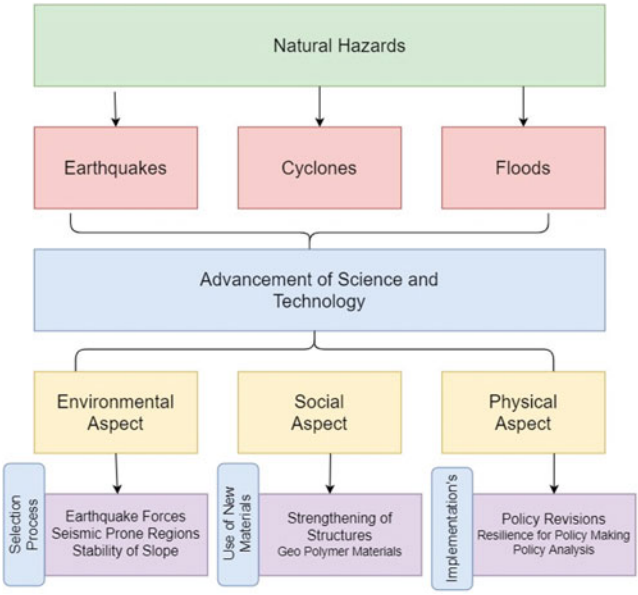

Fig. 1 Framework for addressing cross-cutting issues in the multi-hazard context (*Source* Authors)

Seismic hazards and resilience assessments have been carried out, considering different parameters and variables. The studies based on earthquake disasters in other countries have a variety of susceptibility trigger points and analyses. The studies have adopted various methodologies and parameters based on hazard, vulnerability, and resilience analysis. The study of the impact of wind hazards, specifically cyclones, on the power system in India applies physical and systemic approaches for assessment. It highlights the susceptibility of the power distribution subsystem in the case of extreme wind. Hence, the priority for building the capacity and resilience of the subsystem ought to be prioritized. The comparative analysis of rainfall-runoff models has eased the hydrologists' work to decide on the best model to suit their priorities and goals. Based on one case study, slope failure in a highway has been analyzed by maintaining the stability of the slope considering the estimation of rainfall.

In a case study, the seismic response of a hyperbolic cooling tower in the form of a natural time period and results showed that the time period is more significant for the natural draft cooling tower supported on Raker columns than Meridional columns. Based on another study, it is observed that the structures which are present near the sea are having faster deterioration rate when compared with structures inland areas due to a high level of erosion. Also, in elevated temperatures, it is found that geopolymer fibre has maximum strength when compared with other fibres.

It has been clear that a series of elements are interrelated when we highlight the disasters, their impacts, and priority areas to be examined. These can be individually and holistically based on time and circumstances. The criticality of understanding the social entrepreneurship policies, and writing, analysis, implementation,

and amendment is data-intensive. The policy ecosystem is deemed crucial for maintaining sustainability and resilient development. The study on the knowledge of the indigenous Chepang community for disaster mitigation and preparedness has been reviewed, which showcases the entwining of the scientific ways in the indigenous practices. This, however, has been limited to the older generation due to several issues that ought to be addressed by the future generation for its continuity and recognition. The GIS-based HVRA method has been a promising and recognized concept for improving risk understanding and combining science and local voices and knowledge. There are some drawbacks to the technique which need to be addressed in the future.

Summary

This chapter summarized the contents of the book volume on Disaster Risk Science and Technology: Addressing Cross-Cutting Challenges. All the chapters in this volume are segregated into three sections such as DRR and Geo-environmental perspectives, DRR, Geophysical and Engineering perspective, and DRR, Socio-economic and cross-cutting issues. The book has discussed the management of natural hazards such as earthquakes and floods. The socio-economic aspects of the disaster risk reduction strategies are highlighted in this volume.

References

Avery GC, Bergsteiner H (2011) Sustainable leadership practices for enhancing business resilience and performance. Strategy Leadersh 39(3):5–15. https://doi.org/10.1108/10878571111128766

Behnam H, Kuang JS, Samali B (2018) Parametric finite element analysis of RC wide beam-column connections. Comput Struct 205:28–44. https://doi.org/10.1016/j.compstruc.2018.04.004

Chopra AK, Goel RK (2002) A modal pushover analysis procedure for estimating seismic demands for buildings. Earthq Eng Struct Dyn 31:561–582. https://doi.org/10.1002/eqe.144

Devi V, Sharma ML (2016) Spectral estimation of noisy seismogram using time-frequency analyses. Int J Geotech Earthq Eng 7(1):19–32

IS 13920 (2016) Ductile design and detailing of reinforced concrete structures subjected to seismic forces - code of practice (First Revision). Bureau of Indian Standards (BIS), New Delhi

IS 1893-Part 1 (2016) Criteria for earthquake resistant design of structures: general provisions and buildings. Bureau of Indian Standards (BIS), New Delhi

Jaiswal RK, Ali S, Bharti B (2020) Comparative evaluation of conceptual and physical rainfall–runoff models. Appl Water Sci 10:1–14. https://doi.org/10.1007/s13201-019-1122-6

Khatiwada BP, Ghimire R, Adhikari R, Osti S (2012) Increasing crop water productivity through local crops and technologies: a case from the ethnic Chepang community of Nepal. Hydro Nepal J Water Energy Environ 50–53. https://doi.org/10.3126/hn.v11i1.7204

Kizilkanat AB, Kabay N, Akyüncü V, Chowdhury S, Akça AH (2015) Mechanical properties and fracture behavior of basalt and glass fiber reinforced concrete: an experimental study. Constr Build Mater 100:218–224. https://doi.org/10.1016/j.conbuildmat.2015.10.006

Kyei C, Braimah A (2017) Effects of transverse reinforcement spacing on the response of reinforced concrete columns subjected to blast loading. Eng Struct 142:148–164

Medeiros-Junior RA (2018) Impact of climate change on the service life of concrete structures. Eco-efficient repair and rehabilitation of concrete infrastructures. Elsevier

Newmark NM (1959) A method of computation for structural dynamics. J Eng Mech Div Proc ASCE 67–94

Nguyen LC, Pham VT, Do TN (2020) Deep-seated rainfall-induced landslides on a new expressway: a case study in Vietnam. J Landslides 17:395–407

Sahoo B, Bhaskaran PK, Pradhan AK (2019) Application of weather forecasting model WRF for operational electric power network management—a case study for Phailin cyclone. Theoret Appl Climatol 137(1):871–891

Zhang J-F, Ge Y-J, Zhao L (2011) Effect of latitude wind pressure distribution on the load effects of hyperboloidal cooling tower shell. Tongji University, Shanghai, China

DRR and Geoenvironmental Perspectives

Assessment of the Numerical Methods for the Seismic Resilience of Built Structures in India

B. M. Raisinghani, A. Kumar, A. Jaiswal, T. H. Bhoraniya, and Indrajit Pal

Abstract Earthquakes are a major threat in India owing to the large stock of vulnerable structures combined with high seismicity across the country. The damage survey of Bhuj earthquake (2001) gave impetus for analysing the correct hazard level for design of buildings in Gujarat state. The buildings in Ahmedabad city suffered severe damages to around 70 midrise buildings. The seismic actions on the structure are dynamic in nature and cause low-cyclic fatigue in the structural components leading to the loss of strength and stiffness in each loading cycle. The structural engineers require strong numerical techniques to simulate the behaviour of the structures to ascertain their safety. However, each earthquake does not follow the same pattern and have different characteristics in terms of the PGA, time-period, natural frequency, and the amplification. Hence, the consideration of local seismic hazard is important for the design or evaluation of the buildings for predictable performance and generate resilience in them. The aim is to evaluate the performance of a 15-storey building for the seismic design codes i.e., US, TEC, CEN and IS, to highlight the significance of the current state of knowledge. The building satisfies Life Safety (LS) performance criteria under the highest level earthquake and damage to non-structural components is seen for the moderate earthquakes (4–6 Mw). The inferences from the scenario assumed for the Ahmedabad city can be applied to the other cities in Gujarat where time history records are not available. Resilience benchmarks shall be included in building byelaws to make it a legal obligation. Also, a model is proposed for design that shall be included in code books for multiple earthquake events (4–8 Mw).

B. M. Raisinghani (✉)
Seismic Karyashalal!!, Ahmedabad, Gujarat, India
e-mail: sm.gsdma.eq@gmail.com

A. Kumar · I. Pal
Asian Institute of Technology (AIT), Bangkok, Thailand

A. Jaiswal
National Management Associate, United Nations Volunteer, New Delhi, India

T. H. Bhoraniya
Government Engineering College (GEC), Bhuj, Gujarat, India

I. Pal et al. (eds.), *Proceedings of the 2nd International Symposium on Disaster Resilience and Sustainable Development*, Lecture Notes in Civil Engineering 294,
https://doi.org/10.1007/978-981-19-6297-4_2

Keywords Disaster risk reduction · Time history analysis · Performance-based design · Seismic resilience · Design resilience

1 Introduction

Earthquakes are a major threat in India due to the large stock of vulnerable structures combined with high seismicity across the country. The situation can be understood as the seismic hazards in local context based on visible damages in structures and analysis of its behaviour by time history records. The damage survey of Bhuj earthquake (2001) gave impetus for analysing the correct hazard level for the design of buildings in Gujarat state. The buildings in Ahmedabad city, the business hub of Gujarat, suffered severe damages to around 70 mid-rise buildings (Mishra 2004). The damages in RC buildings in India are due to poor quality of construction, non-code compliance, over-occupancy, and lack of technical expertise in local context to handle complex phenomena like an earthquake (EEFIT 2005). The seismic actions on the structure are dynamic in nature and cause low-cyclic fatigue in the structural components leading to loss of strength and stiffness in each cycle of loading in the buildings. The force-based design caters for the ductility, overstrength and redundancy as a single factor of response reduction (R). Alternately, the parameter for design can be the displacement demand on the structures to resist the impacts of ground shaking (Priestley et al. 2007). Contrary to the above, design of high-rise buildings depends more on the higher modes for the estimation of seismic response for which the methods need to be evaluated.

The numerical techniques that are needed to draw useful deductions for quantitative assessment of the earthquake safety in structures are based on the principles of dynamics. The structural dynamics developed with the contributions from Newton (1642–1727) and Leibniz (1646–1716). The modal analysis of building was shaped through a series of developments laid forward initially by Johann Bernoulli (1742) to finally by Routh (1920). The integral equations were used to represent the high-rise building structures. The response spectrum was proposed by M.A. Biot (1932), he inferred the vibration of a system as a superposition of harmonics. Newmark (1959) proposed a computational method for structural dynamics, a time-domain procedure. The time integration method, Wilson-θ, is done for a time interval of ($\theta . \Delta t$) following the linear acceleration routine. The developments in the linear and non-linear dynamics through mathematical formulations are computerized into the software for structural inferences. The documented procedures for response spectrum are important to trace back its developments (Ebeling 1992). The tall buildings shall respond properly to the strong earthquake shaking, damage shall be distributed over the structure and is of moderate intensity to bring them back into service (Jennings 1997).

Seismic resilience aims to broaden the traditional design approach for damage controlled to the higher criteria including the time and cost optimization with assumptions of scenario conditions for a faster system recovery. Considering the importance of recovery to be included in the design stage itself, it is essential to validate the procedures that can suit the purpose with efficiency and can be used for predicting the performance of structures. The research carried out for disaster mitigation with high end procedures need to be checked for the larger target of seismic resilience. This paper studies the displacement-based design methods, time integration methods and code procedures for design of mid-high-rise building in Ahmedabad city. The scenario condition assumed for the study is the Bhuj (2001) earthquake considering that the many buildings got damaged. Also, with the local seismic hazard estimation done by ISR, Gujarat for the city it is now apt to capture the gap between the resistance and the resilience framework for design of structures in India through a pilot study.

2 Problem Design

The design of a regular 15-storey RC framed building (see Fig. 1) is to be dealt in a step-by-step format to check the adequacy of the numerical methods for understanding the structural behaviour and the improvements for inducting resilience in the design procedure. The building shall satisfy the performance in the range of LS-CP for the magnitude of 7.0 Mw considering the life and the asset values to be protected. The review of the design of RC building using IS1893-2016 and IS13920-2016 is carried out to ascertain the level of performance that can be expected from the current prescription-based design procedure for the residential buildings. The system performance for the early occupancy criteria of the residents is to be obtained from the current methods for earthquake resistance. The idea is to evaluate the performance of the building located in Ahmedabad city, designed with the minimalistic needs of the code to comment on the design resilience. The flow of evaluation is mentioned below for the study (see Fig. 2).

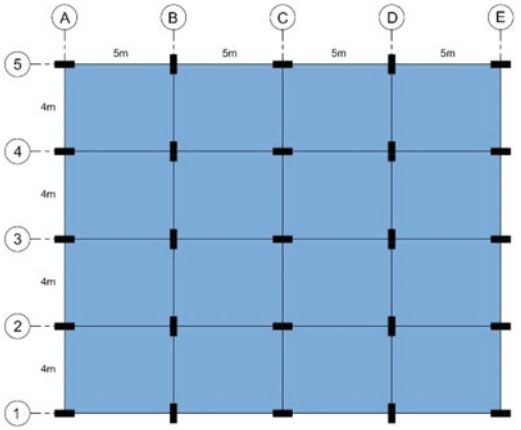

Columns (300 x D mm):
- IS Code

1-3:800 ; 4-10:750 ; 11+: 700
- ACI Code

1-3:900 ; 4-10:850 ; 11+:800
- EC-8 & TSS-500

1-3:900 ; 4-9:850 ; 10+:800
- TSS-500

1-3:1000 ; 4-9:900 ; 10+:800

Beams (all cases):
1-15: 300 x 500mm
Slabs (all cases): 1-15: 120mm
Time Period (T):
X-dir: 0.90s
Y-dir: 1.01s
Storey height (h): 3m
Soil type: Medium

Fig. 1 Details of the 15-storey RC building for performance evaluation

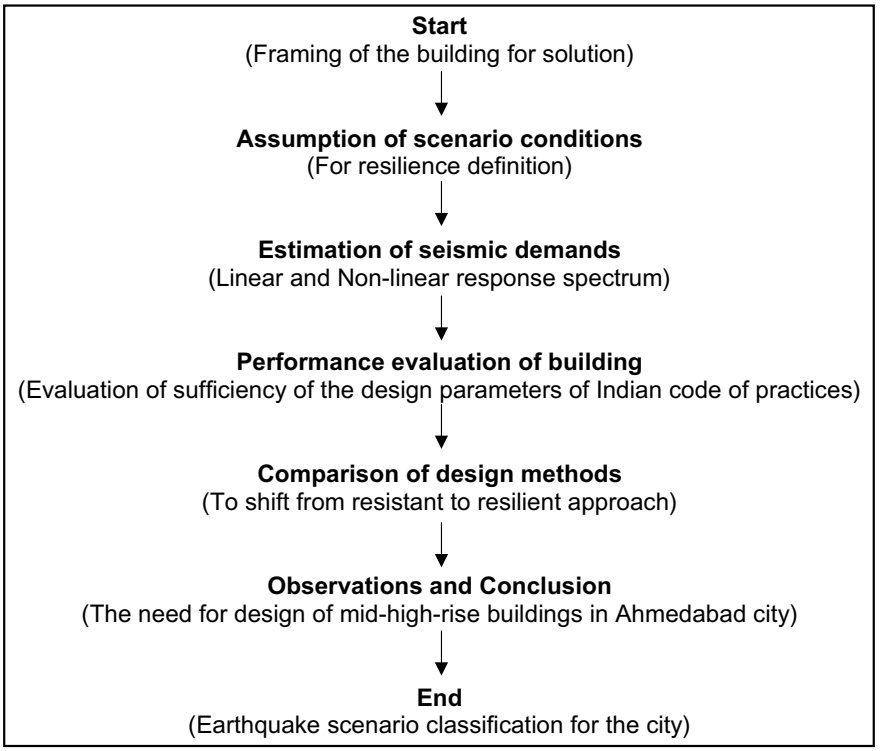

Fig. 2 Proposed procedure for evaluation of building design

3 Review of Parameters for Performance Evaluation

The inference for performance definition of RC buildings in the Ahmedabad city (typical representation for India) can be taken from the damages that occurred during the Bhuj (2001) earthquake. The damage survey of buildings in the city showed many vulnerabilities in the structures that gave earthquake the opportunity to cause partial to complete collapse. Moreover, the buildings are skying new heights, lengths and depths in the city owing to rapid urbanization and being the business capital of Gujarat. It is necessary to review the changes done in the code of practice for earthquake resistant design of RC buildings i.e., IS1893 and IS13920, for better performance of the structures. The assessment of the senior analyst at FEMA mentioned that the unregulated construction industry and non-compliance to the building byelaws were the prominent reasons for large scale disaster in the state of Gujarat (Langenbach et al. 2002). The old buildings that survived the earthquake with presence of masonry infills and planning cannot be overlooked as they represent the local economy and culture rather than technologically rich buildings in the west. The mitigation actions taken till date after the Bhuj (2001) earthquake will provide a necessary outline for the future needs (Fig. 3).

The following inferences can be made from the past-experience of earthquake damages and analytical procedures that have made way in the formation of new earthquake design code of practice in India (see Table 1):

(a) lack of confining reinforcement

(b) shear failure of column in Mansi complex

(c) hinges formed in columns of OGS buildings

(d) soft storey damages in newly constructed Shikhar building

Fig. 3 Identification of damages occurring in RC buildings in Ahmedabad city (Humar et al. 2001)

Table 1 Design changes in the code of practice for RC buildings

Parameters	IS1893-2002/IS13920-2002	IS1893-2016/IS13920-2016
Zone factor (Z)	0.16	0.16
Ductility class (R)	5	5
Analysis methods	Linear	Linear & non-linear
Torsion modes	Irregularities defined for various modes of torsion	Extended, first two modes cannot be torsion
Infill modeling	Not prescribed	Prescribed
Stiffness modifiers	Not prescribed	Prescribed
Response spectrum	Defined up to 4 s time-period	Defined up to 6 s time-period
OGS design	Possible with multiplication factor of 2.5 for brick infill	Need to prove the adequacy of design of OGS columns with suitable method
Minimum strength	Not specified	Specified
Importance factor	Two classes defined	Three classes defined for residential buildings with higher occupancy
Dynamic analysis	For buildings with height more than 90 m for regular and 40 m for irregular configuration in Zone III	For all buildings except the regular buildings lower than 15 m in Zone II
RC Structural Wall plan density	Not specified	Minimum 2% in each principal plan direction for Zone III and above
Liquefaction potential estimation	Not specified	Specified as appendix
Ductile detailing	Prescribed	Improved

- *Inference 1*: Dynamic analysis i.e., high-end numerical procedure is more depended upon for the earthquake design. The modal analysis and linear time history analysis are necessary for high rise structures in Ahmedabad.
- *Inference 2*: The modelling of buildings with higher accuracy considering the cracked section properties, staircase and infills will lead to higher accuracy in understanding the behaviour of buildings. This helps to locate the vulnerabilities at design stage itself.
- *Inference 3*: The seismic micro-zonation of Ahmedabad city gave information on the areas in which soil amplification is expected to the range of 1.5–2.0. Also, the estimate EPGA by ISR, Gujarat is 0.18 g which needs to be updated in design code.
- *Inference 4*: The ductile detailing of the buildings is improved by increase in the minimum section size of column and minimum area of steel for stirrups. This will generate ductility in the system and give better resistance to lateral forces. The capacity-based design factor of 1.4 is an attempt to create beam mechanism at failure for buildings subjected to earthquakes.

Hence, the earthquake resistant design code has targeted the mood points that caused damage in buildings during Bhuj (2001) earthquake in India i.e., ductile detailing, torsion prevention, capacity-based design for beam mechanism, OGS frame design, short column effects in design and member modelling for dynamic analysis. With these factors the building of 45 m height is designed in Ahmedabad city considering the seismic hazard of 0.16 and 0.18 g owing to the available seismic micro-zonation results (Rastogi et al. 2018; 2019).

4 Performance Evaluation of Building

4.1 Review of Performance as Per Seismic Design Codes

The building is designed in software package ETABS v2015 for the Indian standard code of practice and compared with the performance of the same building designed for ACI-318, EC8 and TEC07 i.e., USA, Europe, and Turkey. The changes in the column size (see Fig. 1) with requirement of reinforcement for three design codes is considerable (see Table 2). The reinforcement in the building is highest for IS1893 code designed building as per the routine of response spectrum method (RSM). However, the percentage of reinforcement in upper stories is more for ACI318 and EC8/TEC07 earthquake design codes. This gives the information on the pattern of loading by different codes to distribute the storey shears and mode of failure considered for building. The parabolic loading pattern followed by IS1893 is suitable for flexure governed buildings while the triangular loading and 1st mode loading pattern followed by ACI-318 and EC8 is suitable for shear governed failure mode of a building.

The nonlinear relationship of base shear (V_b) and deformation (Δ) was done using the pushover analysis. This numerical procedure converts the MDOF system to SDOF system and lateral loads are monotonically increased till the collapse state of the structure has reached. The software follows the predefined backbone curve of ASCE41 while the performance limits are also prescribed by EC8 and TEC07. The displacement coefficient method (DCM) was adopted for the building considering it as the better replacement of capacity spectrum method (CSM). The performance point for the building on the capacity curve for seismic demand of 0.16 and 0.18 g was obtained (see Fig. 4). The capacity of base level corner column for the design and detailing was compared (see Fig. 5). However, the failure mode at the end of pushover analysis displayed the efficiency of ACI-318, EC8 and TEC07. The building had better response due to correct distribution of steel with the height of building and the failure was located only in the base level columns in comparison to the IS1893-2016 (see Fig. 6).

Table 2 Comparison of reinforcement in corner column

Storey	IS1893	ACI-318	EC8/TEC07
15	12-12ϕ (0.8%)	12-16ϕ (1.0%)	12-16ϕ (1.0%)
14	12-12ϕ (0.8%)	12-16ϕ (1.0%)	12-16ϕ (1.0%)
13	12-12ϕ (0.8%)	12-16ϕ (1.0%)	12-16ϕ (1.0%)
12	12-12ϕ (0.8%)	12-16ϕ (1.0%)	12-16ϕ (1.0%)
11	12-12ϕ (0.8%)	12-16ϕ (1.0%)	12-16ϕ (1.0%)
10	12-12ϕ (0.8%)	12-16ϕ (1.0%)	12-16ϕ (1.0%)
9	10-16ϕ (1.03%)	12-16ϕ (1.0%)	12-16ϕ (1.0%)
8	10-16ϕ (1.03%)	8-20ϕ + 2-16ϕ (1.14%)	8-20ϕ + 2-16ϕ (1.14%)
7	12-16ϕ (1.24%)	8-20ϕ + 2-16ϕ (1.14%)	8-20ϕ + 2-16ϕ (1.14%)
6	10-20ϕ (1.61%)	8-20ϕ + 2-16ϕ (1.14%)	8-20ϕ + 2-16ϕ (1.14%)
5	12-20ϕ (1.93%)	8-20ϕ + 2-16ϕ (1.14%)	8-20ϕ + 2-16ϕ (1.14%)
4	10-25ϕ (2.52%)	8-20ϕ + 2-16ϕ (1.14%)	8-20ϕ + 2-16ϕ (1.14%)
3	10-25ϕ + 2-20ϕ (2.6%)	8-20ϕ + 2-16ϕ (1.14%)	10-20ϕ (1.16%)
2	8-32ϕ (3.06%)	8-20ϕ + 2-16ϕ (1.14%)	10-20ϕ (1.16%)
1	12-32ϕ (4.6%)	10-25ϕ (1.82%)	10-20ϕ (1.16%)
%change	–	−12%	−15%

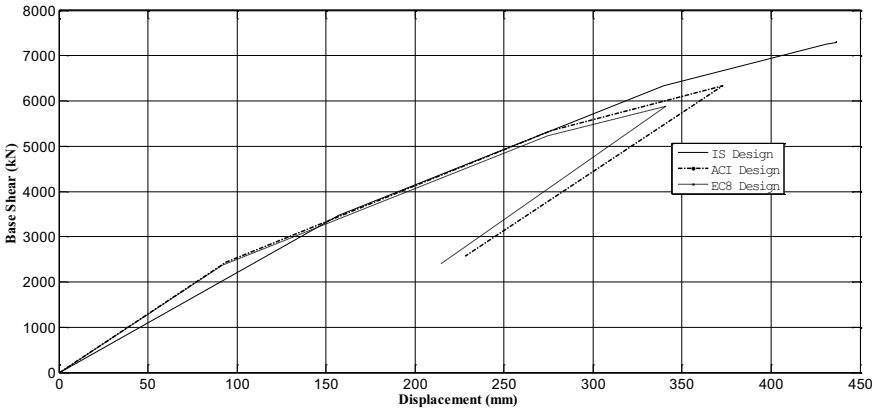

Fig. 4 Capacity curve of building as per DCM routine in ETABS

4.2 Review Based on the Displacement Methodology

The development of direct displacement-based design procedure (DDBD) was the pioneering change as the displacement is an action effect of earthquake on buildings due to which stresses get generated. Hence, rather than calculating the forces based on the acceleration-based response spectrum prescribed by the design codes, the

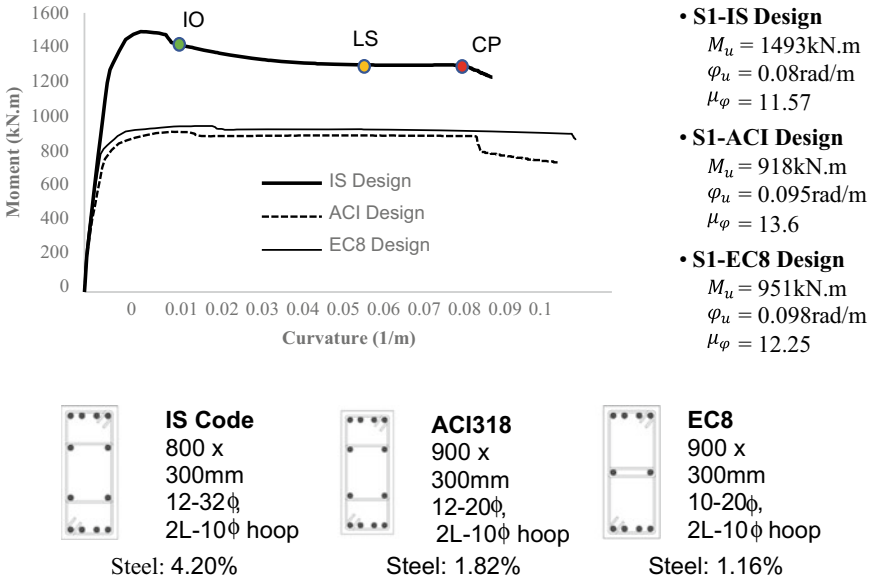

Fig. 5 Capacity of base level corner column—SEMAp (Mander et al. 1988; Ozmen et al. 2007)

displacement shall be estimated for different levels of nonlinear seismic demands (Priestley et al. 2007). The response reduction factor (R) and the damping considered by the code does not relate directly to the nonlinear behaviour of the buildings. DDBD procedure gives the rough estimate of the capacity of the building for the drift assumed for the performance level (PL) to be achieved. In this study, the drift of 2% is considered for design of building for MCE level earthquake. The nonlinear drift when divided by the displacement ductility will give the elastic level drift for the building. IS1893-2016 prescribes inter-storey drift limit of 0.4% as a check at the end of the analysis which is for the elastic condition of the building. Program calculations for DDBD suggested for increase in the depth of beams to achieve the higher displacement ductility in the system as current beam depth gave only a value of 2.0. The maximum base shear the building can survive before collapsing was 50,000 kN and displacement of 500 mm. The base shear of the building as per the pushover curve in ETABS software is quite high i.e., 55,000–70,000 kN. The time-period of the building was estimated as 1.6 s as against the 1.35 s obtained in the software. The displacement response spectrum, linear and nonlinear, was developed to check the system for DDBD procedure and POA procedure to churn a comparison of displacement demands i.e., 100–600 mm range (see Fig. 7).

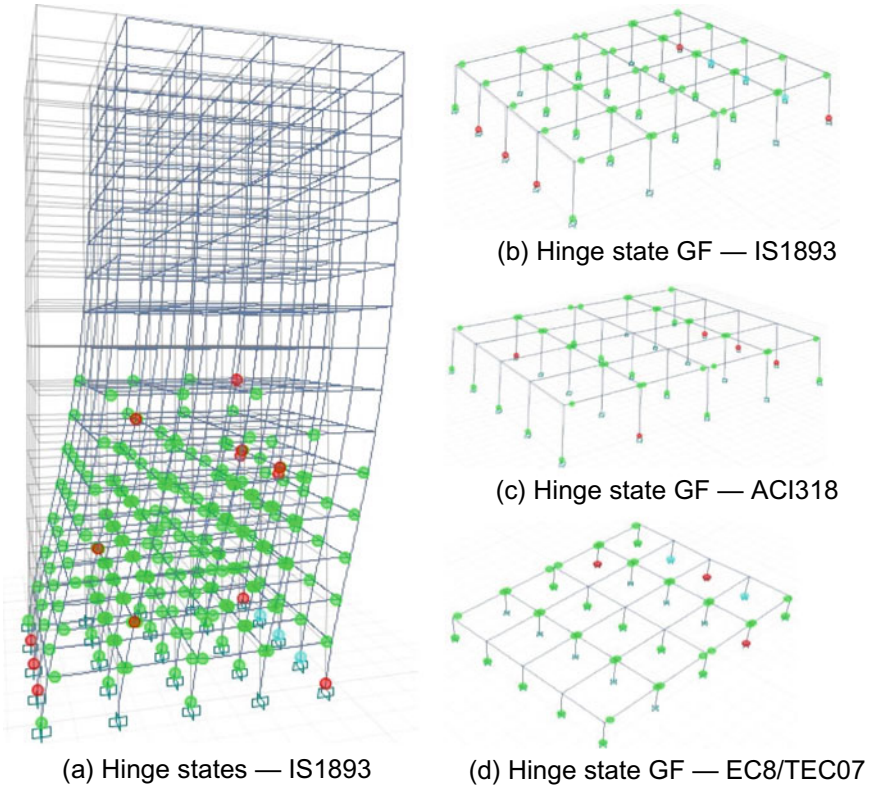

Fig. 6 Review of hinge states at the end of pushover analysis

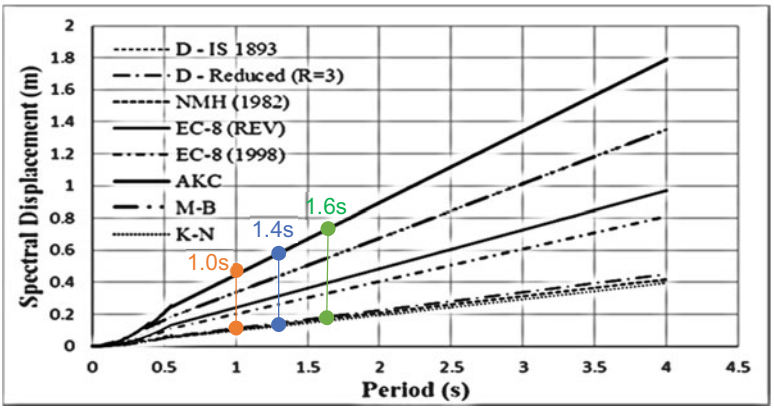

Fig. 7 Displacement response spectrum based on IS1893-Z3 (Bathe and Wilson 1972)

4.3 Review of the Analysis Methods for MDOF Systems

The direct integration methods are useful for the estimation of the demands for the design of buildings. The linear and non-linear method for dynamic analysis was developed using time stepping integration method (Newmark et al. 1959). The calculation of response at interval step of 'Δt' for the time history record need high computational processing unit. The suitability of this method is based on the 'α' and 'β' parameters. This method was transformed into the form of matrix considering linear acceleration between the time steps and a modified time step of θ. Δt, where the factor keeps the equation unconditionally stable for any value greater than 1.37 and taken as 1.4 for nonlinear systems. However, this method is not good for capturing higher modes as it has high damping for higher modes and low damping for lower modes (Wilson et al. 1962). The comparison of mode superposition method for linear analysis with linear time history analysis can give faster results. The modal analysis determines the dynamic properties of systems in the frequency domain considering the stiffness and strength as constant parameters. The modal pushover analysis (Chopra and Goel 2002) is an attempt to replace the nonlinear dynamic analysis based on the time-step integration methods. The time integration methods used for the linear and nonlinear analysis are based on the explicit and implicit methods of consideration (see Fig. 8).

The inter-storey drift for the building is estimated using the Newmark-Beta method for dynamic analysis in MATLAB program (see Table 3). This procedure is suitable for MDOF system under time history using time-step integration to achieve a successful solution to give the parameters for design. The Chamoli earthquake time history (VDC, COSMOS) is near to the MCE level response spectrum for the Ahmedabad city (Raisinghani et al. 2021) and gives around 2.5% drift at mid-level of the building which is like the seismic demand seen in the pushover analysis (refer Fig. 6). The Izmit (1999) earthquake result gives the DBE level demands of 0.4–0.5% drift limit for linear analysis as per IS1893 and the Duzce (1999) earthquake estimate represents the foreshock and aftershock drift needs of the building

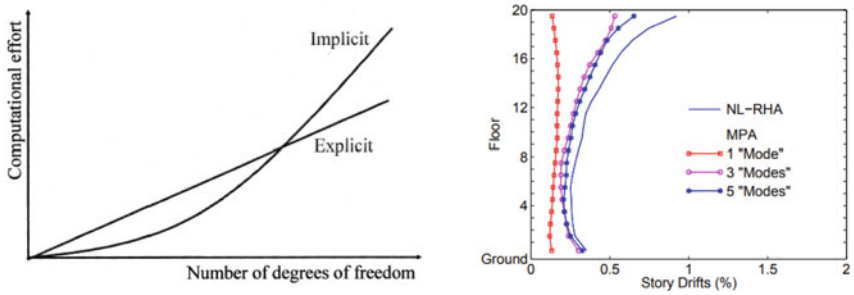

a. time integration methods for MDOF [16] b. modal pushover analysis [23]

Fig. 8 Methods for estimation of demands for MDOF systems

Table 3 Inter-storey drift (ISD) of building using Newmark-Beta method

Storey	India			Turkey	
	Uttarkashi (%)	Chamoli (%)	Bhuj (%)	Izmit (%)	Duzce (%)
15	3.93	2.33	0.89	0.46	0.22
14	3.97	2.34	0.87	0.45	0.20
13	3.97	2.32	0.85	0.44	0.17
12	4.81	2.78	1.00	0.52	0.19
11	4.66	2.68	0.94	0.49	0.21
10	4.41	2.55	0.91	0.45	0.22
9	4.15	2.38	0.87	0.43	0.22
8	3.86	2.20	0.82	0.40	0.22
7	3.51	2.00	0.76	0.36	0.21
6	3.11	1.78	0.69	0.32	0.19
5	3.33	1.94	0.75	0.35	0.20
4	2.74	1.63	0.62	0.29	0.18
3	2.11	1.28	0.48	0.22	0.16
2	1.43	0.89	0.33	0.15	0.12
1	0.73	0.45	0.17	0.08	0.06

(4–5 Mw). This information can be useful for planning the building needs by integration with the other factors of resilience i.e., community, local resources, medical facility, economics, fatality rate, etc.

5 Observations and Discussion

The following observations can be inferred from this study and discussed below for summarizing the difference between the resistant and resilient framework for design using the modern methods for seismic engineering of buildings in Ahmedabad city (pilot study):

- No time history record for Ahmedabad city is available as it located about 250 km from the epicentre location in Kutch. The ETABS provides a feature to match the available time histories with the response spectrum given by IS1893 for Zone-III (see Fig. 9).
- Considering the amplification levels in different zones of the city, the response spectrum for each zone shall be made available for use in the bye-law book and increase the accuracy of hazard as input for building design.
- The pushover analysis procedure showed good results for the building designed as per IS1893-2016 and detailed as per IS13920-2016. The width of the column

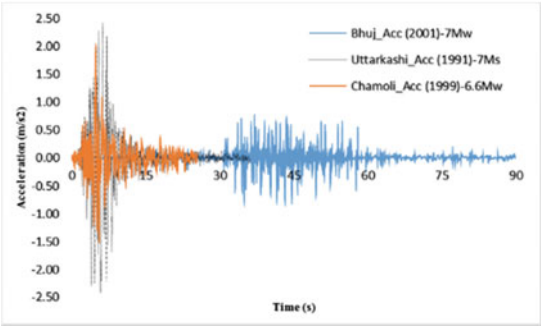

a. Strong motion with 7Mw earthquakes

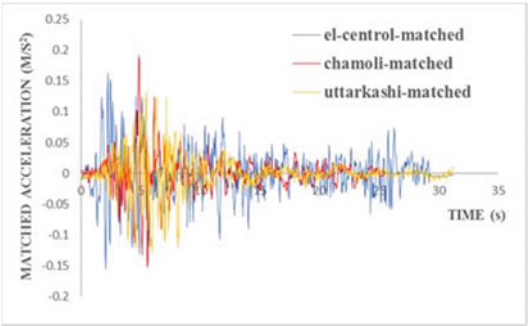

b. Matching of time history records for Zone-3

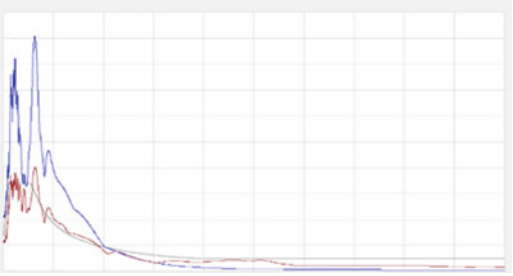

c. Matched response spectrum — Uttarkashi

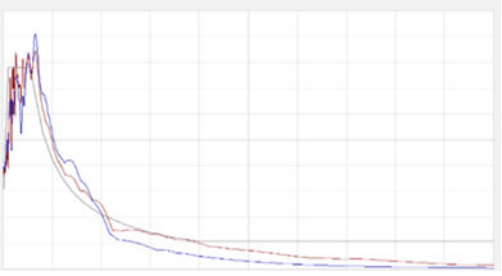

d. Matched response spectrum — Chamoli

Fig. 9 Time history and response spectrum matching for Ahmedabad

is controlled by the minimum provision of Max(300, $20d_b$)mm which gives increased shear capacity to the columns oriented in two direction (X, Y).

- The direct integration methods give good estimate of the problem until the mathematical models are assumed correctly. The energy dissipation model used for nonlinear time history analysis (NLTHA) is essential to give the correct estimate of demand and weakness in the structures.
- The DDBD procedure gave a negative impression of the capacity of the building as the ductility achieved was only 3 while the assumed value was 5.
- The displacement response spectrum developed from the IS1893-2016 code-based spectrum includes the nonlinearity of the system directly through a graph. However, this procedure is applicable when the MDOF is converted to equivalent SDOF system (see Fig. 8). The results of this procedure can be compared with the pushover analysis as both are following the equivalent SDOF system policy.
- The inter-storey drift (ISD) values obtained for the MDOF system from the numerical procedure programmed in MATLAB software following the Newmark-Beta regime is beneficial to identify the time histories that can be used for defining the resilience-based performance parameters i.e., fatality scenario, re-occupancy time and cost.

6 Conclusion

The performance evaluation of the regular RC building located in Ahmedabad which is 300 km from the epicentre in Kutch gave confidence on the design of buildings for seismic design i.e., IS1893-2016 and IS13920-2016. The various aspects related to the dynamic analysis using linear time history and modal analysis of the building, which is pre-requisite for seismic design of high-rise buildings as per the code, were evaluated in detail to show the difference in approach towards defining the seismic demands and performance criteria to be followed for a city situated farther from the fault but had suffered serious damage in the past earthquake (see Fig. 10). The current generation for seismic analysis and design must include the resilience parameters based on the locality index in which the building is to be made. The design parameters shall change as per the change in the locality index i.e., design resilience to be high, medium, or low. The stringent requirement shall be based on the quality of construction, business centres, expected loss and medical infrastructure available. Considering the overall need of the resilience-based performance evaluation of buildings, the building byelaws shall govern the resilience parameters and the code shall regulate the general procedure to be adopted for the design of buildings as the large area of the country is susceptible to earthquakes (4–8 Mw).

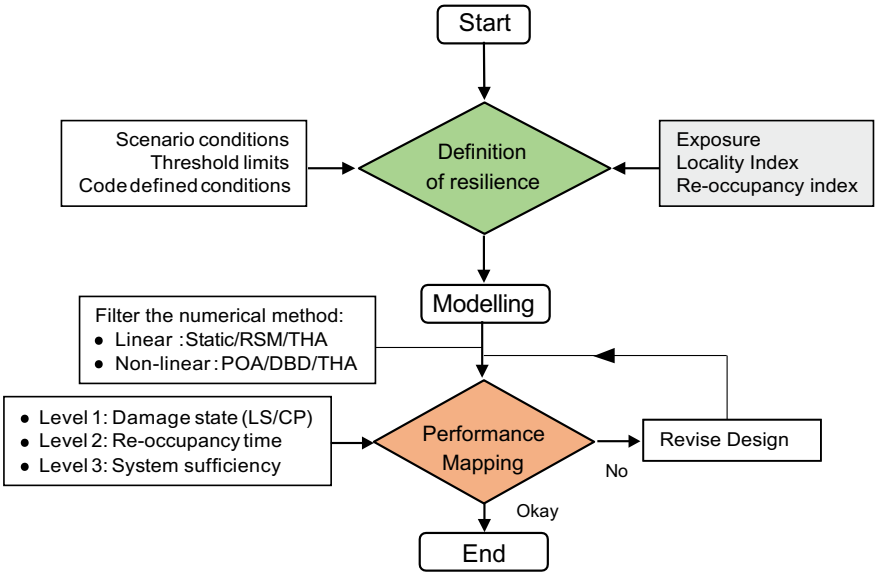

Fig. 10 Proposed design and research model for seismic resilience in code books

References

ASCE 41 (2017) Seismic rehabilitation of existing buildings. American Society of Civil Engineers, ASCE/SEI Standard 41, Reston, VA

Bathe KJ, Wilson EL (1972) Stability and accuracy analysis of direct integration methods. Earthq Eng Struct Dyn 1:283

CEN (2004) Design of structures for earthquake resistance – part 1: general rules, seismic actions and rules for buildings. EN 1998-1:2004, EC-8, Cmite Europeen de Normalisation, Brussels

Chopra AK, Goel RK (2002) A modal pushover analysis procedure for estimating seismic demands for buildings. Earthq Eng Struct Dyn 31:561–582. https://doi.org/10.1002/eqe.144

Chopra AK, Goel RK (2004) Modal pushover analysis of SAC buildings. In: SEAOC convention, Sandiego, California

Dorheim H (2012) Methods for earthquake analysis. NTNU, Trondheim (Thesis)

Dwivedi V, Dubey RK, Pancholi V, Rout MM, Singh P, Sairam B, Chopra S, Rastogi BK (2019) Multi-criteria study for seismic hazard assessment of UNESCO world heritage Ahmedabad city. Bull Eng Geol Environ 79:1721–1733

Ebeling RM (1992) Introduction to the computation of response spectrum for earthquake loading. Department of the Army, US Army Corps of Engineers, Technical report ITL-92-4. NSN 7540-01-280-5500

Humar JM, Lau D, Pierre J (2001) Performance of buildings during the 2001 Bhuj earthquake. Can J Civ Eng 28:979–991

IS 13920 (2016) Ductile design and detailing of reinforced concrete structures subjected to seismic forces - code of practice (First Revision). Bureau of Indian Standards (BIS), New Delhi

IS 1893-Part 1 (2016) Criteria for earthquake resistant design of structures: general provisions and buildings. Bureau of Indian Standards (BIS), New Delhi

Jennings PC (1997) Earthquake response of tall regular buildings. Technical report no EERL 97-01, California Institute of Technology, Pasadena, California, January

Madabhushi SPG, Haigh SK (2005) The Bhuj, India earthquake of 26th January 2001 – a field report by EEFIT. The Institution of Structural Engineers, United Kingdom. ISBN0901297372

Mander JB, Priestley MJN, Park R (1988) Theoretical stress-strain model for confined concrete. J Struct Eng ASCE 114(8):1804–1825

Mishra PK (2004) The Kutch earthquake 2001: recollections, lessons and insights. National Institute of Disaster Management (NIDM), report, New Delhi, India

Newmark NM (1959) A method of computation for structural dynamics. J Eng Mech Div Proc ASCE 67–94

Ozmen HB, Inel M, Bilgin H (2007) Modelling nonlinear behaviour of reinforced concrete members. In: 6th national conference on earthquake engineering, Istanbul, Turkey, 16–20 October, pp 207–2015

Priestley MJN, Calvi GM, Kowalsky JM (2007) Displacement based seismic design of structures. IUSS Press, Pavia. ISBN 978-88-6198-000-6

Raisinghani BM, Morbia HH (2018) Evaluation of displacement limits for RC buildings. In: 16th symposium on earthquake engineering (16SEE), 20–22 December, IIT Roorkee, paper no 334

Raisinghani BM, Bhoraniya TH, Noroozinejad E (2021) Scientific perspectives to earthquake resistant design of RC buildings – a global approach. In: Virtual conference on earthquake engineering (VCDRR), NITK, India, 15–20th March, paper no 033

Sairam B, Rastogi BK, Patel V, Pancholi V (2018) Site effects: case study of the 2001 Bhuj earthquake damages in the Ahmedabad city. Bull Seismol Soc Am 4:2170–2182. https://doi.org/10.1785/0120170266

Soroushian A, Farjoodi J, Bargi K, Rajabi M, Saaed A, Arghavani M, Sharifpour MM (2011) Two versions of the Wilson-θ time integration method. In: International conference on vibration problems (ICoVP), Lisbon, 9–12 September, pp 1–6

Turkish Earthquake Code (TEC-2007) Specifications for buildings to be built in seismic areas. Ministry of Public Works and Settlement, Ankara, Turkey

Virtual data center (VDC) (2012) Consortium of organizations for strong motion observation systems (COSMOS). University of California Santa Barbara. https://strongmotioncenter.org/vdc

Wilson EL, Farhoomand I, Bathe KJ (1972) Nonlinear dynamic analysis of complex structures. Earthq Eng Struct Dyn 1:241

Wind Hazards on the Indian Power System and Challenges for the Future: A Review

Sarv Priya and Pradeep K. Goyal

Abstract The Indian subcontinent is one of the most sensitive cyclone prone regions in the world. Approximately, India consists of almost 7500 km of coastline and around 10% of the world's tropical cyclones influence this coastline. Cyclones have serious impacts on the power system along the coastline in India. Various researchers have developed vulnerability models to analyze the hazards on power systems due to cyclones. This paper aims to integrate and review the development of research towards power system vulnerability for cyclone catastrophe models. In addition, challenges and future investigation are also discussed in this paper.

Keywords Tropical cyclone · Power transmission system · Vulnerability curve

1 Introduction

Natural hazards such as cyclones, earthquakes, floods, and landslides have been occurring in different parts of the world every year and they are persuading considerable damage to buildings and structures, and crops, apart from the loss of human and animal lives. When examined the natural hazards based on severity, duration, and areas of devastation, cyclones are described as the most disastrous among all the natural hazards (Shanmugasundaram et al. 2000). The power system has specific importance for social and economic development. Under extreme weather conditions like typhoon/cyclone causes considerable damages on power system (Yang et al. 2017).

Overhead lines, underground cables, transformers, and switching stations cover the key elements in transmission and distribution systems more vulnerable in intense weather conditions (Sahoo et al. 2019). Climate change, higher climatic loads are

S. Priya (✉)
Research Scholar, Department of Civil Engineering, Delhi Technological University, Delhi, India
e-mail: ersharma1980@gmail.com

P. K. Goyal
Department of Civil Engineering, Delhi Technological University, Delhi, India

I. Pal et al. (eds.), *Proceedings of the 2nd International Symposium on Disaster Resilience and Sustainable Development*, Lecture Notes in Civil Engineering 294,
https://doi.org/10.1007/978-981-19-6297-4_3

subjected in certain regions around the world and can consequently affect the performance of overhead transmission and distribution lines (Cheng et al. 2007, 2011, 2012; Cheng et al. 2014). As the standard deviation of mean wind speed increases, the probability of damage to the tower increases (Deoliya and Datta 2000). Field measurement, wind tunnel test, theoretical analysis, and numerical simulation are the four current alternatives for investigating the field of wind engineering. Previous research of cyclonic effect on power system was mainly carried out by considering the statistical approach to investigate the crucial points, including the environment or structural variables. Environmental variables consist of cyclone wind speed, cyclone rainfall, type of land cover, tree type, etc. (Liu et al. 2005) and these variables are applied to a negative binomial regression model to forecast the power outage. This regression model was also used by Han et al. (2009) considering local climatology and geographical sensibility. Liu et al. (2017) employed a statistical model in addition to a spatial generalized linear mixed modeling approach to describe the power outage and other infrastructures network in natural disasters. Vulnerability analysis is essential in a power system to decide the degree of hazards a power system and is used to determine and classify the significantly critical components of a power system under any unforeseen events (Kröger and Zio 2011). The vulnerabilities are classified as physical, social, economic, territorial, organizational, environmental, and systematic (Kundak 2013). Physical and systemic vulnerabilities are more popular among all the vulnerabilities to analyze the risk. Physical vulnerability expresses the degree of damage of a component due to the external load (Pascale et al. 2010) even though systemic vulnerability expresses the redundancy, performance and, reliance of a component in a network or collapse of interconnected networks (Veen and Logtmeijer 2005).

Indian Transmission line structure is remarkably vulnerable to the effect of natural hazards like storms, earthquakes, tropical cyclones, floods, and localized wind. Every disaster has some usual characteristics. Therefore, the objective of this paper provides a review of advancement in research towards vulnerability for cyclone catastrophe models. In addition, the effect of a tropical cyclone on the Indian power system, challenges, and future investigation are also discussed in this paper.

2 Structure of Electrical Power System

An electrical power system is an interconnected network that brings the produced power to the end users in an economic, reliable, and safe manner. It is the combination of power generation, transmission, and distribution subsystems (Fig. 1). The function of an electrical power system is to change the form of energy (for example, coal, oil, gas) into electrical energy. An electrical power system consists of various appliances like motor, synchronous generator, transformer, circuit breaker, conductor, etc. that associated with the system.

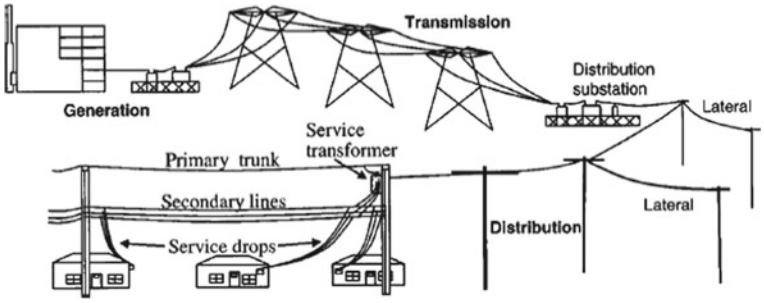

Fig. 1 Structure of electric power system (Davidson et al. 2003)

2.1 Power Generation Subsystem

Power plants generate electric power that is mainly classified as thermal power plants, hydropower plants, and nuclear power plants. Power plants generate electricity at voltage varying from 11 to 25 kV and this voltage cannot be much greater as a result of technical limitations.

2.2 Power Transmission Subsystem

Generating stations have produced the electricity in bulk and then transferred over long distances to the load centers. All the generating stations interconnect to the transmission subsystem. High voltage requires to operate the transmission lines so the generated voltage is stepped up transmission level in the range of 66 to 765 kV or higher (Kothari and Nagrath 2003). A commonly meshed structure is adopted in transmission networks to provide different optional ways for electricity to flow from generators to load centers. The Transmission network is formed with cables strung between 150 ft high, lattice type steel towers spaced around 800 ft away (Willis and Philipson 2018).

2.3 Power Distribution Subsystem

The distribution serves as the ultimate stage of electricity transfer to the end users. The distribution network is typically linked to the radial formation. Typically, the distribution subsystem operates at voltage between 11 and 33 kV. At this voltage level, power is supplied by the primary feeder to the small industry.

The power system is seriously damaged under cyclonic hazards (Feng et al. 2005). Therefore, it is essential to investigate the risk assessment of power systems under cyclonic hazards to minimize the damage and power outage.

3 Effect of Tropical Cyclones on Indian Power System

The Indian subcontinent is geographically extended from 8° N to 37° N and 68° E to 97° E respectively and due to this topographical variation across the country resulting in the wide variation in weather conditions (Kale 2014). India is susceptible to different types of natural hazards such as landslides, cyclones, heavy rainfall, thunderstorm, heat waves/cold waves, floods, earthquakes, forest fires, and drought (Fig. 3). In India, main coal based power plants are densely located in the eastern part of India due to the availability of coal even though gas based plants are located in the western part of India due to the availability of local gas and imported gas/liquid fuels (Kumar et al. 2019). India consists of almost 7500 km of coastline and around 10% of the world's tropical cyclones influence this coastline with different frequency and intensity (NDMP 2016). According to the electronic atlas, cyclones are arranged into two categories as cyclone storms varying the maximum sustained wind speed 34–47 knots (18–24 mps) and severe cyclone storms varying maximum sustained 48 knots (25 mps) or higher. Very severe cyclonic storms and super cyclonic storms come under the category of severe cyclonic storms. The metrological department of India (IMD) is a government organization that supplies information about climatic conditions in India related to cyclones. The Metrological department of India (IMD) adopted the criteria to classify the tropical cyclone as shown in Table 1 on the basis of wind speed. The eastern coast of India from Kolkata to Tamil Naidu is most vulnerable for storms as well as depressions (Figs. 2 and 3) and observed during 1974-99 in Kolkata-Vishakhapatnam coast, 36.78% of the total storms and depressions passed over this coastal line and 29.89% of total storms and depressions passed over Vishakhapatnam–Tamilnadu coast of India (Alam et al. 2003).

Tropical cyclones formation in the area between tropics of Capricorn and cancer where the extremely low pressure occurs over the tropical or subtropical waters, and described by their detrimental potential to damage the buildings, power system, roads, bridges, culverts, and crops, etc. Cyclones probably have impacted on generation, transmission, and distribution subsystem as a result of transmission line tripping /breakdown, tower collapse and damage to several distribution lines, etc. The impact of major cyclones on the Indian power system has been summarized in Table 2.

Table 1 Category of the tropical cyclone in the Indian Ocean (Metrological department of India)

Type of cyclonic disturbance	Wind speed in Km/hr	Wind speed in knot (mps)
Low pressure area (L)	Less than 31	Less than 17 (09)
Depression (D)	31–49	17–27 (9–14)
Deep depression (DD)	50–61	28–33 (15–17)
Cyclonic storm (CS)	62–88	34–47 (18–24)
Severe cyclonic storm (SCS)	89–118	48–63 (25–32)
Very severe cyclonic storm (VSCS)	119–221	64–119 (33–61)
Super cyclonic storm (Sup. CS)	222 or more	120 (62) or more

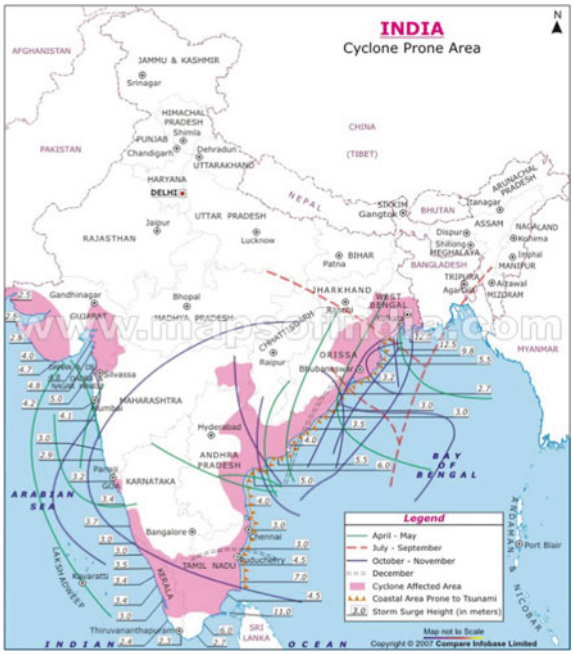

Fig. 2 Cyclone prone areas in India (mapsofindia.com)

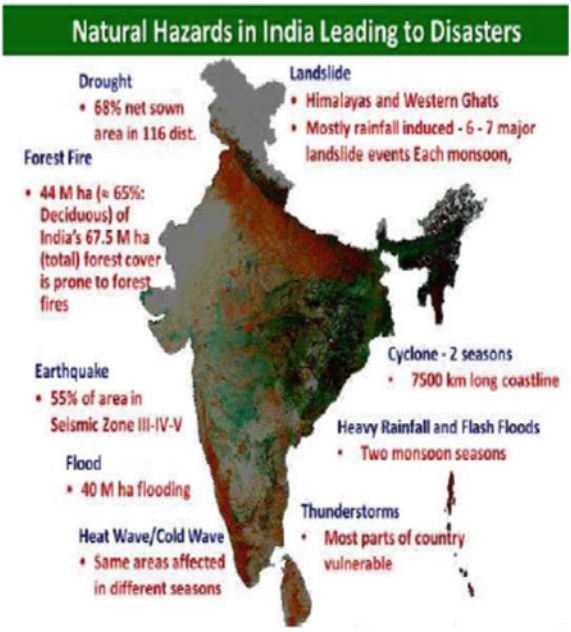

Fig. 3 Natural disaster risk on the power system in India (Kumar et al. 2019)

Table 2 Major impact of cyclones on the Indian power system

S. No.	Name of the cyclone	3-min sustained wind speed (Km/hr)	Category	Impact of the cyclone on power system
1	Hudhud (2014)	185	Very severe cyclonic storm	Transmission Line tripping: 28 no of 400 kV, 37 no of 220 kV and 85 no of 132 kV; Traction station effected: 12 (Soonee et al. 2015)
2	Vardah (2016)	130	Very severe cyclonic storm	Generating Unit tripping: 9 (2430 MW Gen loss), Tower collapse: 33 (230 kV), Transmission Line tripping: 14 no of 400 kV and 19 no of 230 kV; Traction station damaged: 4 (Soonee et al. 2015)
3	Ockhi (2017)	155	Very severe cyclonic storm	Transmission Line tripping: 3 no of 220 kV especially 110 kV system and distribution system was damaged (Kumar et al. 2019)
4	Titli (2018)	150	Very severe cyclonic storm	Transmission Line tripping: 2 no of 765 kV, 4 no of 400 kV, 6 no of 220 KV, 8 no of 132 kV; Substation Dead: One 220 kV and One 765 kV substation became dead (Bala and Pattanayak 2019)
5	Fani (2019)	215	Very severe cyclonic storm	Minor damage to the Transmission system while distribution system was affected including 202 substations, 13,400 transformers, and nearly 80,600 km of distribution lines (Mohanty et al. 2020)

(continued)

Table 2 (continued)

S. No.	Name of the cyclone	3-min sustained wind speed (Km/hr)	Category	Impact of the cyclone on power system
6	Amphan (2020)	240	Super cyclonic storm	448 No. of 33/11 kV substations and 1,26,540 distribution transformers were fully and partially were damaged (www.newindianexpress.com)

The Super Cyclone Ampham was the most recent catastrophic tropical cyclone that formed over the Bay of Bengal and caused huge damage in the east part of India especially West Bengal and Odisha in May 2020. The east part of Kolkata city was destroyed by the tremendous storms and in the continuation of a few hours, the cyclone damaged electricity and telecommunication towers (Syam 2020). Some examples of partially and completely damaged transmission towers in Kolkata city by Amphan cyclone are shown in Figs. 4, 5, 6, 7 and 8. Figures 4, 5 and Figs. 6, 7, 8 are shown partially and completely damaged transmission towers respectively.

Fig. 4 Partially damaged Cross Arm of Transmission Tower

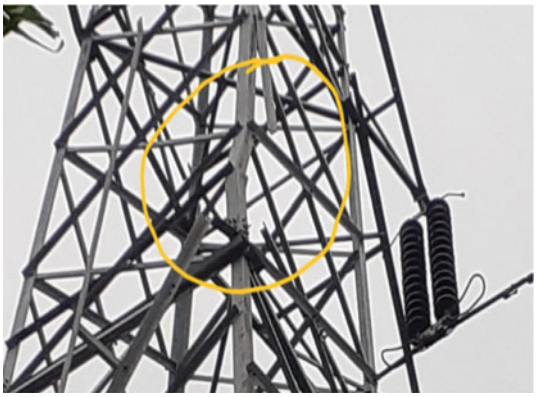

Fig. 5 Partially damaged leg of Transmission Tower

Fig. 6 Completely damaged Transmission Tower due to failure connection with Foundation

Fig. 7 Completely Damaged Transmission Tower due the Torsional Effect

Fig. 8 Completely damaged Transmission Tower due to the shear failure of connection

4 Methods of Evaluation of Hazards

Catastrophe risk is associated with the three elements hazards, exposure, and vulnerability (Crichton 1999). Cyclone is the main threat to the Indian transmission system. The transmission line along with the Indian coastal line is vulnerable to cyclonic hazards. Deterministic and probabilistic approaches are used to identify the hazards, exposure, and vulnerability. In the deterministic approach, the output of the system is well known without the involvement of any uncertainty so the level of reliability of the system can be effectively studied under the expected accident. A probabilistic

approach is used to gain the prediction of different events through the degree of possible risk and different statistical values. Therefore, the probabilistic approach is more inclusive than the deterministic approach. The probabilistic method can be classified into analytical method and simulation method. The analytical method includes the Markov process, Bayesian network, frequency and duration method, series and parallel network method, faulty tree, probability convolution method, and so on. The simulation method can be categorized into State enumeration method and Monte Carlo method. Advantages and disadvantages of Analytical methods and simulation methods are described in Table 3.

The estimation of vulnerability is an essential part of the catastrophe model. There are many vulnerability estimation methodologies available in published technical literature. Power networks can be investigated on various levels as at the component level, the network level, and the interdependency between various infrastructures networks. Holmes (2001) provides an overview of the effect of wind load on transmission lines and towers along with related vulnerability models. The vulnerability of electric power systems is built in its configuration so a new approach is adopted to estimate the level of redundancy inside the power network (Albert et al. 2004). An original method is adopted by Ahmed et al. (2010) to analyze the vulnerability of lattice type high voltage transmission towers using the data available in the literature. The study was carried out by applying severe wind on towers to find out the probable failure of collapse and plotted against the ratio of impacted wind speed to the modified strength of a tower (Fig. 9). Other parameters like partial damage, cable breakage, and equipment damage of transmission towers have not been considered in the investigation.

A vulnerability model (Fig. 10) is proposed by Bjarnadottir et al. (2014) to evaluate the impact of cyclones on distribution poles based on particular wind speed. They also added a part in the model to estimate the effect on pole age by the possible deterioration of strength.

Winkler et al. 2010 used a vulnerability model to predict the damage separately for transmission and distribution network elements without considering the coupling effect between the transmission tower line system while (Xue et al. 2020) considered coupling effect in investigation and developed the fragility curves for singly stand transmission tower considering without tower-cable interaction and transmission line system shown in Figs. 11(a) and (b) respectively and found that performance level of singly stand tower is much higher than the transmission line tower.

Yang et al. (2017) developed a vulnerability model having a random probability distribution and platted a fragility curve against probability failure and weather intensity. Further, the failure probability is correlated with random data t from the uniform distribution U (0, 1). This study reveals that the transmission line breaks down if the failure probability is more than t.

Table 3 Advantages and disadvantages of Analytical methods and simulation methods

Analytical methods		
Advantages	Disadvantages	References
Probability convolution method		
• It can be used to evaluate the hazards by differencing the two random variables • It has fewer variables and easy to determine the hazards	• This method can not be applied to assess the hazards for multivariable and complex power systems	(Yuan et al. 2013), (Li 2014)
Series and parallel network method		
• It has fewer variables and easy to determine the hazards • This method is suitable for computer programming	• It cannot be used to complex power system	(Čepin 2011), (Li 2014)
Bayesian network method		
• This method provides a mathematically logical and robust structure for the investigation • This method is useful to model uncertain and complex situations	• This is a visual probabilistic model that depends on different variables conditionally so the probabilities of all the random variables need to be simplified to get an effective outcome	(Uusitalo 2007), (Mensah and Dueñas-Osorio 2016)
Markov method		
• Markov method can be used to model the environments and problems based on statistical decisions overtime • This is a powerful tool for making predictions	• It is not able to provide explanations of events	(Čepin 2011), (Zhao et al. 2017)
Faulty tree method		
• It is good to analyze the probabilistic damage • It is useful to set up the priorities of a system • It is useful to identify the interrelationship between failures and subsystems	• The faulty tree is a binary method so it does not provide the information about each hypothesis whether it is validated or not • It is a unidirectional method and it does not take into consideration the time	Wang et al. (2010), Liu et al (2017)
Frequency and duration method		
• It is the precise and speedy method • It can examine the extensive power system without taking more computing time	• It usually provides the under or over estimated response	Renuga et al. (2006), Čepin (2011)

(continued)

Table 3 (continued)

Analytical methods		
Advantages	Disadvantages	References
Simulation method		
State enumeration method		
• It is an accurate and efficient method. It is also useful to identification of the weak points of the system	• It does not consider high order failure	Li (2014), Liu et al. (2017)
Monte Carlo method		
• It enhances the computing power • It is useful in the nonlinear and dynamic models	• Building of simulation is more expensive and time taking	Li et al. (2013), Quiring et al. (2014)

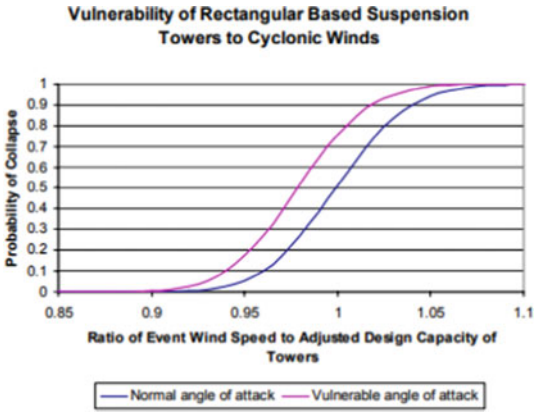

Fig. 9 Vulnerability of rectangular based suspension towers to cyclonic wind (Ahmed et al. 2010)

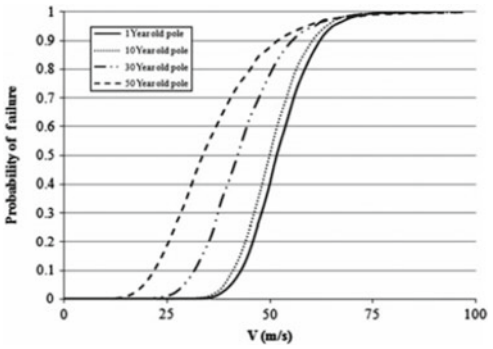

Fig. 10 Vulnerability of distribution poles to a cyclone on particular wind speed (Bjarnadottir et al. 2014)

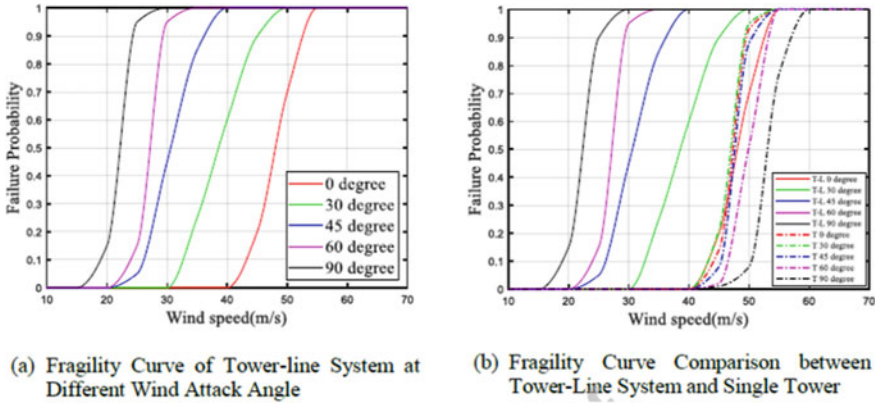

Fig. 11 **a** and **b**: Fragility curve of transmission tower line network and single tower (Xue et al. 2020)

5 Challenges and Future Research Directions

Based on the literature survey and observations, we can identify the following emerging points that necessitate further research work.

1. Several failure models have been developed to evaluate the wind hazards on power systems but still, more research is needed to develop comprehensive failure models. Most of the researchers have applied vulnerability curves for failure modeling without capturing the effect of space and time of extreme wind. Vulnerability curves cannot give the real understanding and direction of the extreme wind as well as its hazards on devices of the power systems. The development of comprehensive and exact failure models can be achieved by synthesizing the pattern based simulation approaches with more exact vulnerability curves.
2. The interrelationship between interdependent power subsystems needs to be broadly analyzed to assess the effect of the failure of each subsystem component on the other linked subsystem component.
3. More researches are required to describe the effect of climate change on the physical infrastructure and operational conditions of the power system.
4. Mostly, vulnerability models have been established internationally considering their geographical conditions, therefore, a model needs to be developed considering Indian subcontinent conditions.

6 Conclusion

The damage to the power system due to the cyclone is a serious concern. This paper presents the impact of tropical cyclones on the Indian power system, development,

challenges, and future trends to evaluate the power system vulnerability in catastrophic models. The new catastrophic models have used several essential variables to assess the risk. In the survey, it is found that the distribution subsystem is more vulnerable than the generation and transmission subsystem under extreme wind. Two approaches are widely used to assess vulnerability, namely physical and systemic vulnerability. Physical and systemic vulnerability approaches employ to predict the damage of components within the subsystem and interconnected subsystems respectively which are an essential step in direction of resilience modeling.

References

Ahmed A, Arthur C, Edwards M (2010) Collapse and pull–down analysis of high voltage electricity transmission towers subjected to cyclonic wind. In: IOP conference series: materials science and engineering, vol. 10, no 1. IOP Publishing, p 012004

Alam MM, Hossain MA, Shafee S (2003) Frequency of Bay of Bengal cyclonic storms and depressions crossing different coastal zones. Int J Climatol J Royal Meteorol Soc 23(9):1119–1125

Albert R, Albert I, Nakarado GL (2004) Structural vulnerability of the North American power grid. Phys Rev E 69(2):025103

Bala SK, Pattanayak SK (2019) Very severe cyclonic storm 'Titli': impact on Indian power system. In: 2019 IEEE 1st international conference on energy, systems and information processing (ICESIP). IEEE, pp 1–6

Bjarnadottir S, Li Y, Stewart MG (2014) Risk-based economic assessment of mitigation strategies for power distribution poles subjected to hurricanes. Struct Infrastruct Eng 10(6):740–752

Čepin M (2011) Assessment of power system reliability: methods and applications. Springer

Cheng CS, Auld H, Li G, Klaassen J, Li Q (2007) Possible impacts of climate change on freezing rain in south-central Canada using downscaled future climate scenarios. Nat Hazard 7(1):71–87

Cheng CS, Auld H, Li Q, Li G (2012) Possible impacts of climate change on extreme weather events at local scale in south–central Canada. Clim Change 112(3):963–979

Cheng CS, Li G, Auld H (2011) Possible impacts of climate change on freezing rain using downscaled future climate scenarios: updated for eastern Canada. Atmos Ocean 49(1):8–21

Cheng CS, Lopes E, Fu C, Huang Z (2014) Possible impacts of climate change on wind gusts under downscaled future climate conditions: updated for Canada. J Clim 27(3):1255–1270

Crichton D (1999) 'the Risk Triangle.' In: Ingleton J (ed) Natural disaster management. Tudor Rose, London, pp 102–103

Davidson RA, Liu H, Sarpong IK, Sparks P, Rosowsky DV (2003) Electric power distribution system performance in Carolina hurricanes. Nat Hazard Rev 4(1):36–45

Deoliya R, Datta TK (2000) Reliability analysis of a microwave tower for fluctuating mean wind with directional effect. Reliab Eng Syst Saf 67(3):257–267

Feng Z, Qiuhan W, Jihong L (2005) Hazard of Typhoon 'Yunna'to Zhejiang power grid and precautionary measures. Electric Power 38(5):39–42

Han SR, Guikema SD, Quiring SM, Lee KH, Rosowsky D, Davidson RA (2009) Estimating the spatial distribution of power outages during hurricanes in the Gulf coast region. Reliab Eng Syst Saf 94(2):199–210

Kale VS (ed.) (2014) Landscapes and landforms of India. Springer, Dordrecht

Kothari DP, Nagrath IJ (2003) Modern power system analysis. Tata McGraw-Hill Education, New Delhi

Kröger W, Zio E (2011) Challenges to methods for the vulnerability analysis of critical infrastructures. In: Vulnerable systems. Springer, London, pp 33–39

Kumar C, Basak AK, Sahay SK, Banerjee S (2019) Impact of high impact low frequency (HILF) events on Indian power system

Kundak S (2013) Cascading and unprecedented effects of disasters in urban system. In: Intelligent systems and decision making for risk analysis and crisis response, pp 743–748

Li G, Zhang P, Luh PB, Li W, Bie Z, Serna C, Zhao Z (2013) Risk analysis for distribution systems in the northeast US under wind storms. IEEE Trans Power Syst 29(2):889–898

Li W (2014) Risk assessment of power systems: models, methods, and applications. Wiley, New York

Liu B, Li Z, Chen X, Huang Y, Liu X (2017) Recognition and vulnerability analysis of key nodes in power grid based on complex network centrality. IEEE Trans Circuits Syst II Express Briefs 65(3):346–350

Liu H, Davidson RA, Apanasovich TV (2008) Spatial generalized linear mixed models of electric power outages due to hurricanes and ice storms. Reliab Eng Syst Saf 93(6):897–912

Liu H, Davidson RA, Rosowsky DV, Stedinger JR (2005) Negative binomial regression of electric power outages in hurricanes. J Infrastruct Syst 11(4):258–267

Liu X, Shahidehpour M, Cao Y, Li Z, Tian W (2015) Risk assessment in extreme events considering the reliability of protection systems. IEEE Trans Smart Grid 6(2):1073–1081

Mensah AF, Dueñas-Osorio L (2016). Efficient resilience assessment framework for electric power systems affected by hurricane events. J Struct Eng 142(8):C4015013

Mohanty SK, Chatterjee R, Shaw R (2020) Building resilience of critical infrastructure: a case of impacts of cyclones on the power sector in Odisha. Climate 8(6):73

National disaster management plan (NDMP) (2016) A publication of the national disaster management authority Govt. of India, May 2016

Pascale S, Sdao F, Sole A (2010) A model for assessing the systemic vulnerability in landslide prone areas.Nat Hazards Earth. Syst Sci 10(7):1575–1590

Quiring SM, Schumacher AB, Guikema SD (2014) Incorporating hurricane forecast uncertainty into a decision-support application for power outage modeling. Bull Am Meteor Soc 95(1):47–58

Reed DA (2008) Electric utility distribution analysis for extreme winds. J Wind Eng Ind Aerodyn 96(1):123–140

Renuga P, Ramaraj N, Primrose A (2006) Frequency and duration method for reliability evaluation of large scale power generation system by fast fourier transform technique. J Energy Environ 5:94–100

Sahoo B, Bhaskaran PK, Pradhan AK (2019) Application of weather forecasting model WRF for operational electric power network management—a case study for Phailin cyclone. Theoret Appl Climatol 137(1):871–891

Shanmugasundaram J, Arunachalam S, Gomathinayagam S, Lakshmanan N, Harikrishna P (2000) Cyclone damage to buildings and structures—a case study. J Wind Eng Ind Aerodyn 84(3):369–380

Soonee SK, Narasimhan SR, Nallarasan N, Rathour HK, Yadav G, Bhan SC, Mali RR (2015) Impact of very severe cyclone 'HudHud'on power system operation. In 2015 annual IEEE India conference (INDICON). IEEE, pp 1–5

Syam S (2020) Importance of urban forestry in cyclonic risk mitigation through GIS and remote sensing: a case study of the severe cyclonic storm Amphan in West Bengal. Editorial Board 9(8)

Uusitalo L (2007) Advantages and challenges of Bayesian networks in environmental modelling. Ecol Model 203(3–4):312–318

Van Der Veen A, Logtmeijer C (2005). Economic hotspots: visualizing vulnerability to flooding. Nat Hazards 36(1-2):65–80

Wang A, Luo Y, Tu G, Liu P (2010) Vulnerability assessment scheme for power system transmission networks based on the fault chain theory. IEEE Trans Power Syst 26(1):442–450

Willis HL, Philipson L (2018) Understanding electric utilities and de-regulation, vol 27. CRC Press

Winkler J, Duenas-Osorio L, Stein R, Subramanian D (2010) Performance assessment of topologically diverse power systems subjected to hurricane events. Reliab Eng Syst Saf 95(4):323–336

Xiaowei Y, Wenxue Q, Liyang X (2008) A method for system reliability assessment based on Bayesian networks. Acta Aeronautica et Astronautica Sinica 6

Xue J, Mohammadi F, Li X, Sahraei-Ardakani M, Ou G, Pu Z (2020) Impact of transmission tower-lineinteraction to the bulk power system during hurricane. Reliab Eng Syst Saf 203:107079

Yang YH, Xin YL, Zhou JJ, Tang WH, Li B (2017) Failure probability estimation of transmission lines during typhoon based on tropical cyclone wind model and component vulnerability model. In: 2017 IEEE PES Asia-Pacific power and energy engineering conference (APPEEC). IEEE, pp 1–6

Yuan Z, Jin Z, Jingjing L, Kaigui X (2013) A convolution model for bulk power grid reliability evaluation. Power Syst Technol 37(9):2466–2473

Zhao L, Mao T, Xu W, Luan J, Wu J, Qi G (2017) A review of risk assessment methods for power system. In: MATEC web of conferences, vol 139. EDP Sciences, p 00175

Time-Frequency Analysis of Strong Ground Motions from the Mw 6.8 1991 Uttarkashi Earthquake

Vinuthna Ambatipudi, Kanuka Mareddy, Jayaprakash Vemuri, and K. V. L. Subramaniam

Abstract The stress build-up along the plate boundary of the Indian and Asian plates is a source of major destructive earthquakes in the state of Uttarakhand. The high seismic hazard in the region has led the Indian Standard Code 1893:2016 to place the entire state of Uttarakhand in seismic zone IV and V, corresponding to seismic intensity levels of severe and very severe, respectively. On 20th October 1991, a strong earthquake having a moment magnitude Mw 6.8, occurred along the Main Central Thrust in the Uttarkashi and Garhwal regions. Field observations indicated that the maximum damage intensity corresponded to a level of IX as per the modified Mercalli Intensity scale. Reconnaissance studies performed in the aftermath of the earthquake indicate that the high lateral forces generated by the horizontal shaking associated with the strong ground motions caused severe destruction of stone masonry and concrete block structures prevalent in the region. Strong ground motions from the 1991 Uttarkashi earthquake are obtained from 13 stations with hypo-central distances varying from 22 to 155 km. The 26 horizontal waveforms are analyzed and their key characteristics, such as Peak Ground Acceleration (PGA), Peak Ground Velocity (PGV), Arias Intensity (AI), and Predominant Period (Tp) and significant duration are tabulated. The frequency content is analyzed using fast Fourier transforms and the time-frequency analyses are performed using continuous wavelet transforms. The results indicate that the arrival of high-amplitude waves with high frequencies corresponding to the resonant frequency range of low-rise structures at several sites corresponds to observed enormous damage to the structures.

Keywords Frequency content · Fast Fourier transforms · Continuous wavelet transform · Time-frequency analysis · Uttarkashi

V. Ambatipudi · K. Mareddy (✉) · J. Vemuri
Mahindra University, Bahadurpally, Hyderabad 500043, India
e-mail: kanukareddy170110@mechyd.ac.in

K. V. L. Subramaniam
Indian Institute of Technology Hyderabad, Sangareddy 502285, India

I. Pal et al. (eds.), *Proceedings of the 2nd International Symposium on Disaster Resilience and Sustainable Development*, Lecture Notes in Civil Engineering 294,
https://doi.org/10.1007/978-981-19-6297-4_4

1 Introduction

The Mw 6.8 1991 Uttarkashi earthquake occurred along the main central thrust of the Himalayas and caused unprecedented damage in the Garhwal Himalayas (Cotton et al. 1996). Several villages, e.g. Bhatwari-Maneri, Ghansyali, Guptkashi-Ukhimath, were destroyed. Over 50% of structures in the town of Uttarkashi town sustained serious damage. Over a thousand fatalities and damage to over 50,000 structures were reported with severe damage reported from villages located on loose terrace deposits (Gupta et al. 1994). It has been reported that the maximum observed damage intensity was IX on the Modified Mercalli Intensity (MMI) scale felt over a region of 20 sq. km. (Jain and Das 1993). All three components of ground motions are available from 13 stations (Kumar et al. 2011). Figure 1 shows the epicentre and the location of the 13 stations, with distances ranging from 22 to 154 km, where ground motions were recorded. Reconnaissance studies conducted in the aftermath of the earthquake reported that two towns, Bhatwari and Uttarkashi experienced damage corresponding to MMI level VIII; one town, Ghansiali experienced damage intensity corresponding to MMI level VII; eight towns, Rudraprayag, Tehri, Srinagar, Barkot, Koteshwar, Karnprayag, Purola, and Koti, had MMI intensity of level VI; and two towns, Kosani and Almora had associated MMI levels of V (Jain and Das 1993).

The Uttarkashi region lies in the seismic gap zone between the 1905 Kangra earthquake and the 1934 Bihar earthquake (Kayal 1996). Earthquakes in this region take place along the Indian-Asian plate boundary along three faults zones—Main Boundary Thrust (MBT), Main Central Thrust (MCT), Central Counter Thrust (CCT) which extend longitudinally throughout the Himalayan region. There have been

Fig. 1 Epicentre and the 13 recording stations. 1) Bhatwari 2) Uttarkashi 3) Ghansiali 4) Tehri 5) Barkot 6) Rudraprayag 7) Srinagar 8) Koteshwar 9) Karnprayag 10) Purola 11) Koti 12) Kosani 13) Almora (*) Earthquake Epicentre

several recurrent earthquakes along these thrusts due to the enormous build-up of Coulomb stress due to past earthquakes (Gupta et al. 2015). The 1991 earthquake struck in a complex geological setting at the MCT (Kayal 1996) and the Munsiari fault has been identified as the causative fault for the earthquake (Joshi 1997). The focal depth of the earthquake was estimated by USGS as 10.3 km and by IMD as 12 km (Thakur and Kumar 1994). The focal parameters, such as dip, strike directions, and slip angle have been estimated by researchers (Paul et al. 1998). The 1991 Mw 6.8 Uttarkashi earthquake is reported to have triggered the swarms of minor earthquakes in the Garhwal Himalayas (Shanker et al. 2003). Time-frequency analysis on ground motions has been performed by several researchers in recent years (Cui and Hong 2021; Devi and Sharma 2016; Ramkrishnan et al. 2022). This paper presents results from a time-frequency analysis of ground motions recorded in the 1991 Uttarakashi earthquake using CWTs.

2 Characteristics of Ground Motions

Table 1 shows the important characteristics of ground motions, namely PGA (in m/sec^2), PGV (in m/sec), Ratio of PGV and PGA (in sec), Predominant Period (in sec), and Mean Period (in sec). The maximum PGA of 0.3 g was recorded in the town of Uttarkashi situated at a distance of 34 km, while Bhatwari town located at a distance of 21.7 km also experienced a high PGA of 0.25 g. The maximum PGV of 0.295 m/s was recorded in the town of Bhatwari, while Uttarkashi town also experienced a PGV of 0.189 m/s. The single parameter estimates of the frequency content, i.e. T_p, $T_{m,}$ and V/A are often used to estimate the frequency content. The predominant period, T_p, varies from 0.08–0.62 s, while the mean period, T_m, of ground motions varies from 0.15–0.71 s. The range of V/A was 0.038–0.122 s.

Table 1 Characteristics of ground motions

S. No.	Station	Distance (km)	Direction	PGA (m/sec^2)	PGV (m/sec)	V/A (sec)	T_p (sec)	T_m (sec)
1	Bhatwari	21.7	Radial Transverse	2.48 2.42	0.169 0.295	0.068 0.122	0.28 0.62	0.42 0.54
2	Uttarkashi	34.0	Radial Transverse	2.37 3.04	0.189 0.183	0.080 0.060	0.24 0.3	0.29 0.34
3	Ghansiali	39.3	Radial Transverse	1.16 1.15	0.094 0.071	0.081 0.062	0.2 0.18	0.30 0.26
4	Tehri	50.6	Radial Transverse	0.714 0.611	0.046 0.090	0.065 0.147	0.32 0.26	0.42 0.71

(continued)

Table 1 (continued)

S. No.	Station	Distance (km)	Direction	PGA (m/sec^2)	PGV (m/sec)	V/A (sec)	T_p (sec)	T_m (sec)
5	Barkot	55.8	Radial Transverse	0.932 0.805	0.074 0.051	0.079 0.063	0.12 0.26	0.23 0.25
6	Rudraprayag	56.2	Radial Transverse	0.523 0.508	0.020 0.024	0.038 0.047	0.12 0.12	0.15 0.17
7	Srinagar	58.8	Radial Transverse	0.654 0.494	0.035 0.029	0.053 0.059	0.08 0.08	0.16 0.19
8	Koteshwar	61.3	Radial Transverse	0.988 0.652	0.061 0.040	0.062 0.061	0.24 0.28	0.30 0.33
9	Karnprayag	69.6	Radial Transverse	0.61 0.773	0.038 0.042	0.062 0.054	0.34 0.34	0.34 0.33
10	Purola	70.0	Radial Transverse	0.739 0.917	0.042 0.055	0.056 0.060	0.2 0.18	0.29 0.28
11	Koti	98.7	Radial Transverse	0.206 0.409	0.024 0.033	0.115 0.082	0.34 0.36	0.54 0.45
12	Kosani	148.2	Radial Transverse	0.283 0.315	0.022 0.018	0.076 0.056	0.2 0.18	0.25 0.24
13	Almora	153.5	Radial Transverse	0.174 0.21	0.014 0.013	0.082 0.062	0.26 0.22	0.39 0.40

3 Fast Fourier Transforms

Figures 2, 3, 4, 5, 6, 7, 8, 9, 10, 11, 12, 13 and 14 show the FFTs derived for the horizontal components of the ground motions from the thirteen stations. The X-axis shows the Frequency and Y-axis shows the Fourier Amplitude of the ground motion. Low-frequency content is observed in almost all the records (0–10 Hz). The ground motions from Srinagar exhibit a higher frequency content (0–20 Hz) while Karnprayag and Koti exhibit lower frequency content than all the other stations (0–5 Hz).

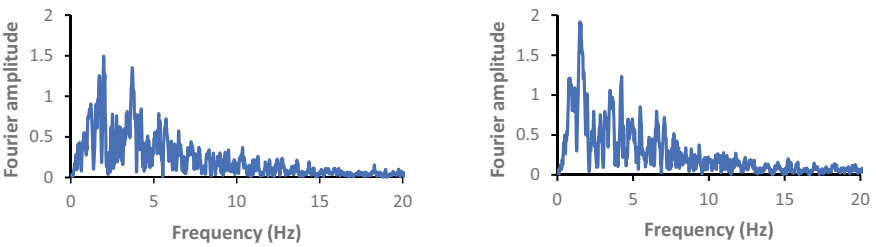

Fig. 2 FFTs of Bhatwari, radial (left) and transverse (right)

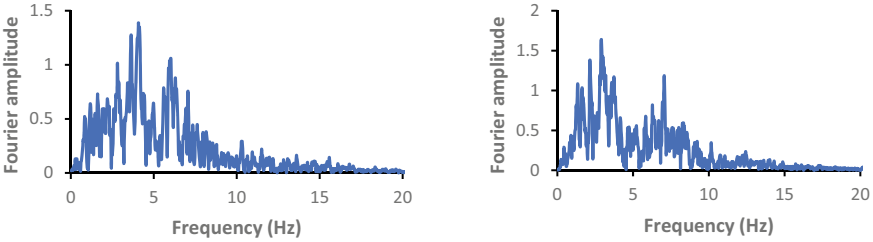

Fig. 3 FFTs of Uttarkashi, radial (left) and transverse (right)

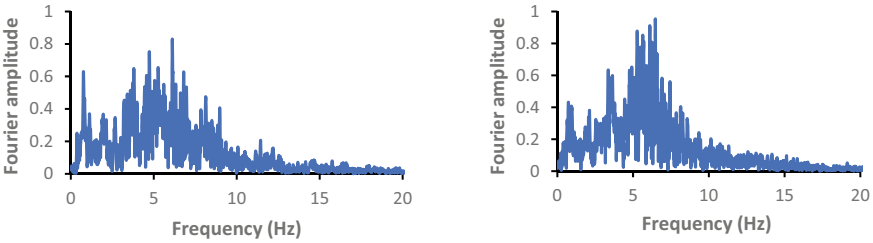

Fig. 4 FFTs of Ghansiali, radial (left) and transverse (right)

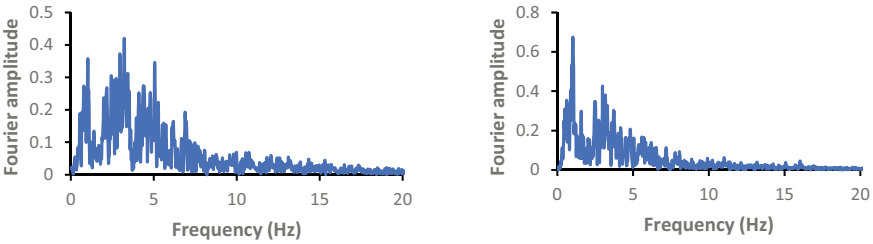

Fig. 5 FFTs of Tehri, radial (left) and transverse (right)

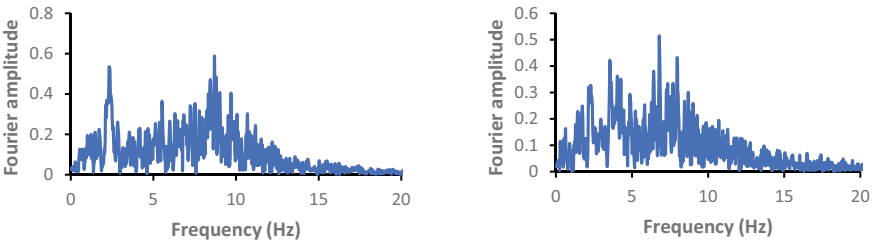

Fig. 6 FFTs of Barkot, radial (left) and transverse (right)

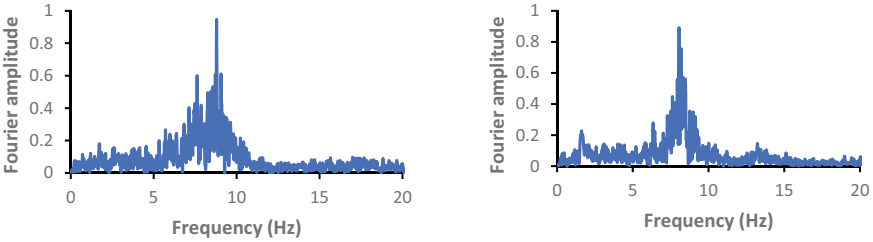

Fig. 7 FFTs of Rudraprayag, radial (left) and transverse (right)

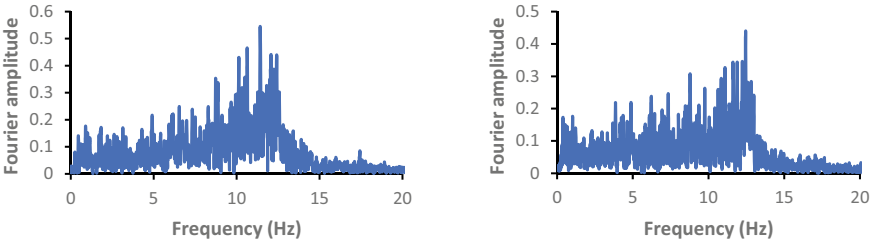

Fig. 8 FFTs of Srinagar, radial (left) and transverse (right)

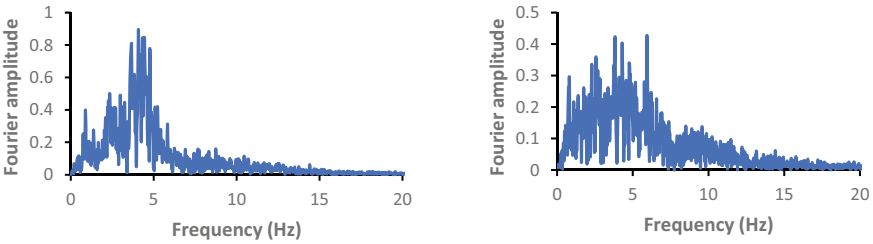

Fig. 9 FFTs of Koteshwar, radial (left) and transverse (right)

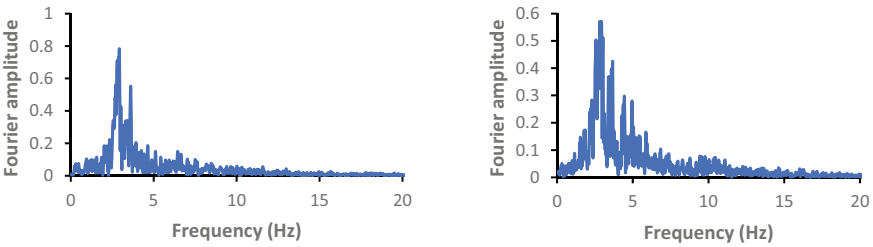

Fig. 10 FFTs of Karnprayag, radial (left) and transverse (right)

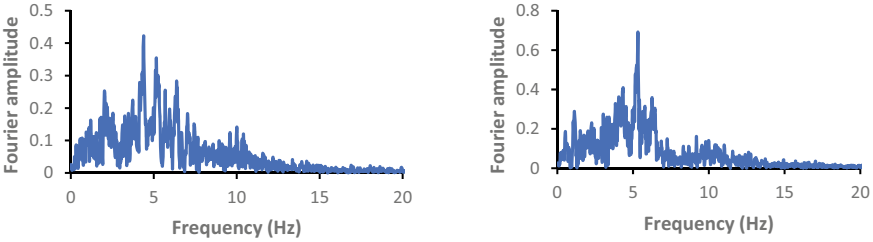

Fig. 11 FFTs of Purola, radial (left) and transverse (right)

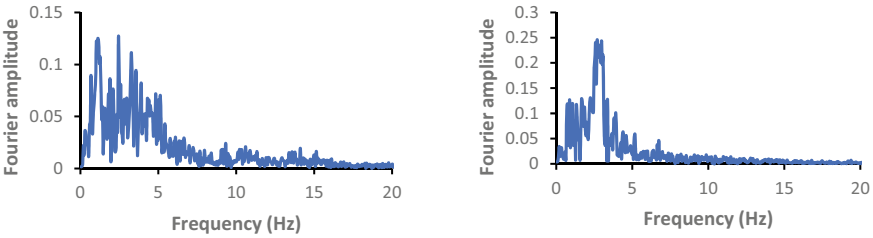

Fig. 12 FFTs of Koti, radial (left) and transverse (right)

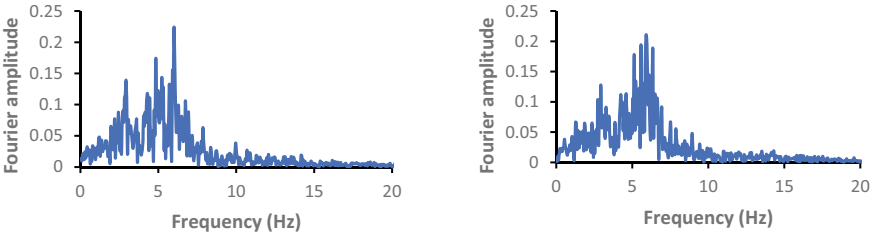

Fig. 13 FFTs of Kosani, radial (left) and transverse (right)

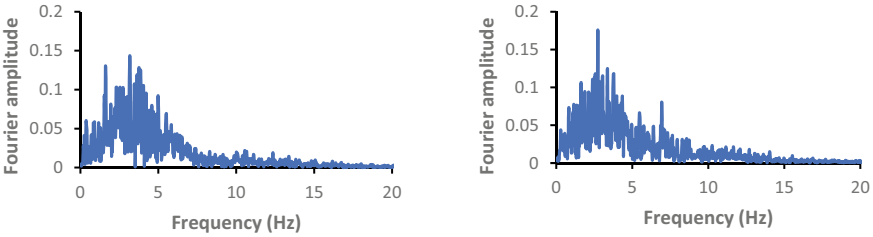

Fig. 14 FFTs of Almora, radial (left) and transverse (right)

4 Continuous Wavelet Transforms

Figures 15, 16, 17, 18, 19, 20, 21, 22, 23, 24, 25, 26 and 27 (left and right) represent the continuous wavelet transforms (CWTs) for the thirteen stations of Uttarkashi in 3D Scalograms. CWTs decompose signals into wavelets and are preferred over other transforms due to their better resolution. The X-axis shows the time (in seconds), the Y-axis shows the frequency (in Hz) and Z-axis represents the magnitude of the seismic wave. The sampling frequency was 50 Hz, i.e. time step was 0.2 s. From Fig. 15 which shows the CWTs for Bhatwari town, it is observed that high amplitude seismic waves carrying multiple frequencies corresponding to a period ranging from 0.1 to 0.5 s, were observed from the 3rd–7th second in the earthquake ground motion record. These observations correlate well with the damage recorded in the reconnaissance surveys which assigned a damage intensity of the level of VIII+ to the town (Thakur and Kumar 1994). Such high energy content in a short duration of time was particularly damaging to low-rise structures (1–5 storeys high), which have a natural period in the range of 0.1–0.5 s. Similarly, the town of Uttarkashi was also assigned an intensity level of VIII+ (Thakur and Kumar 1994) and Fig. 16 shows that the town experienced high amplitude seismic waves having frequencies corresponding to a period of 0.1–0.3 s during a short duration of time (3rd to 7th second in the earthquake ground motion record). Figure 17 shows the CWTs for the town of Ghansiali which experienced high amplitudes at periods of 0.2–0.3 s, causing structural damage to low-rise buildings 2–3 storey high. Figure 18 shows the CWTs for the town of Tehri which experienced seismic waves of high amplitude at various frequencies in the period range of 0.2–0.4 s impacting low-rise, 2 to 4 storey structures. The town was assigned an intensity level of VII (Thakur and Kumar 1994). The transverse component of the Tehri record also exhibits a high amplitude seismic wave, of short duration during the 6th–7th second, having a frequency corresponding to 1 s. The town of Barkot was also assigned an intensity level of VIII+ (Thakur and Kumar 1994) and Fig. 19 shows that the town experienced high amplitude seismic waves having frequencies corresponding to a period of 0.1–0.5 s during a short duration of time (5th to 10th second in the earthquake ground motion record). Figure 20 shows the CWTs for the town of Rudraprayag which observed high amplitude seismic waves at periods of 0.1–0.2 s, for a long duration of time. The town experienced damage corresponding to an intensity level of VI (Thakur and Kumar 1994). Similarly, Figs. 21, 22, 23, 24, 25, 26 and 27 show the CWTs for the towns of Srinagar, Koteshwar, Karnprayag, Purola, Kosani, Koti, and Almora. In the CWT plots, for towns situated at larger distances from the epicentre, the magnitude of the observed scalogram peaks is lower as compared to the peaks observed in CWT plots for towns situated closer to the epicenter.

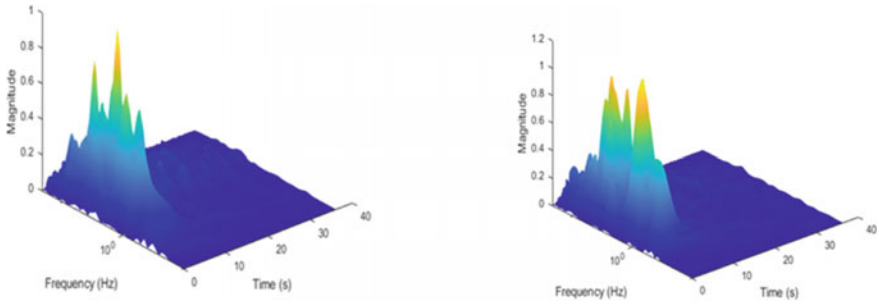

Fig. 15 Scalogram 3D of Bhatwari, radial (left) and transverse (right)

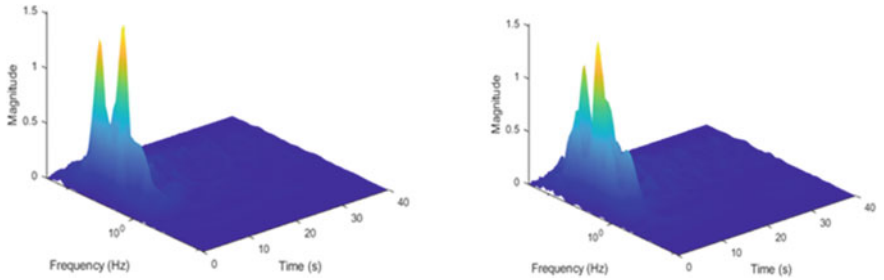

Fig. 16 Scalogram 3D of Uttarkashi, radial (left) and transverse (right)

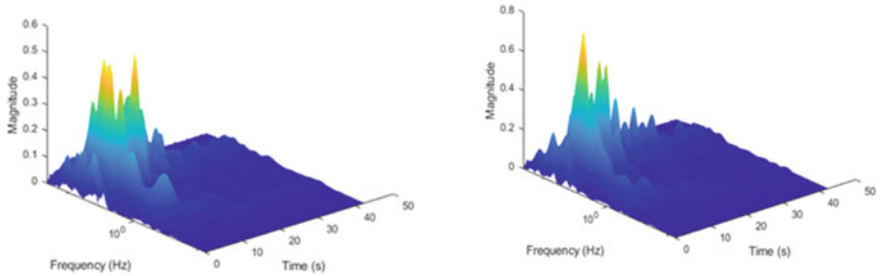

Fig. 17 Scalogram 3D of Ghansiali, radial (left) and transverse (right)

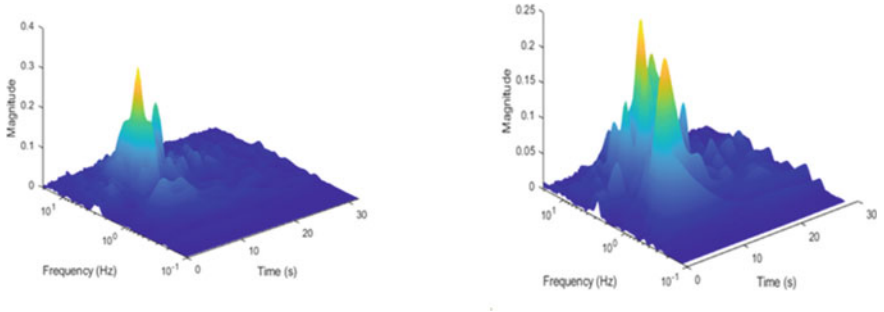

Fig. 18 Scalogram 3D of Tehri, radial (left) and transverse (right)

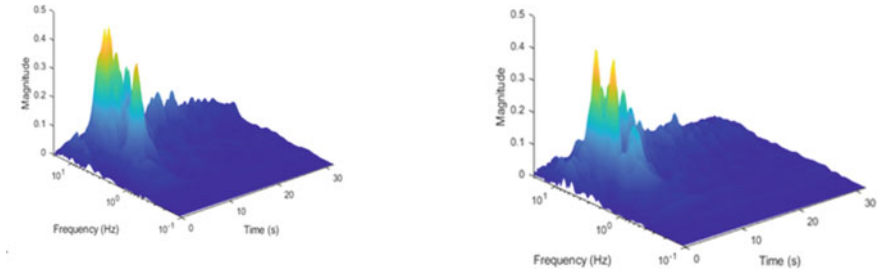

Fig. 19 Scalogram 3D of Barkot, radial (left) and transverse (right)

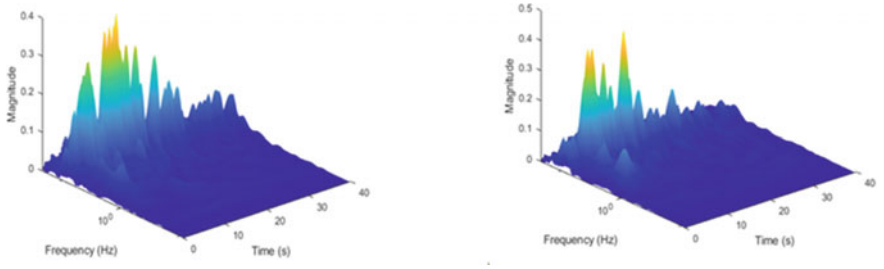

Fig. 20 Scalogram 3D of Rudraprayag, radial (left) and transverse (right)

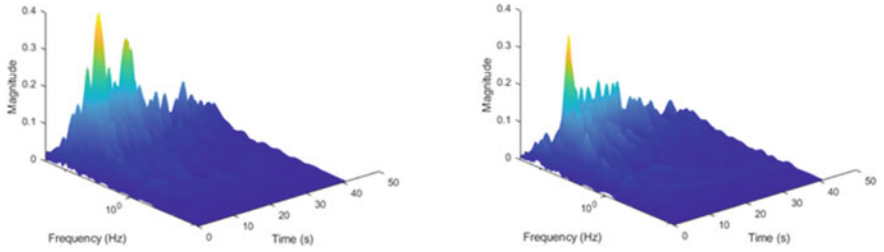

Fig. 21 Scalogram 3D of Srinagar, radial (left) and transverse (right)

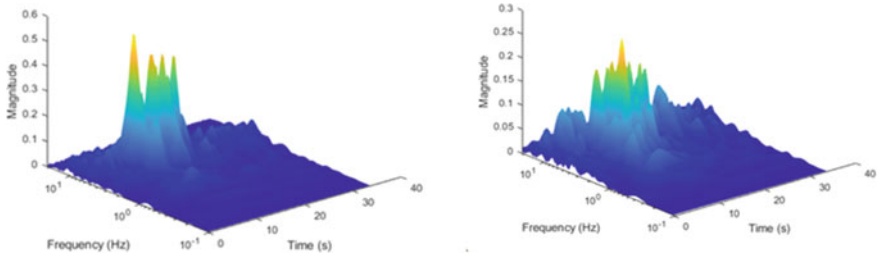

Fig. 22 Scalogram 3D of Koteshwar, radial (left) and transverse (right)

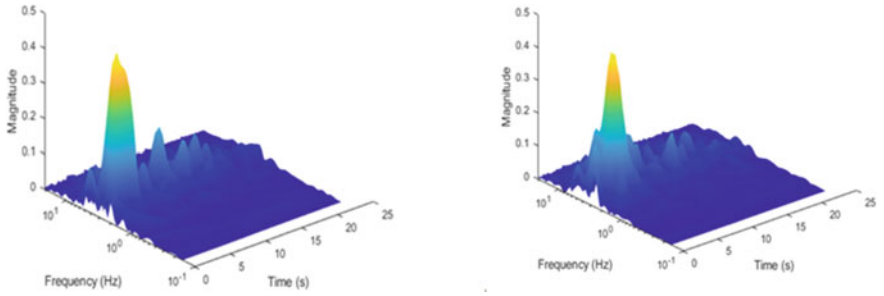

Fig. 23 Scalogram 3D of Karnprayag, radial (left) and transverse (right)

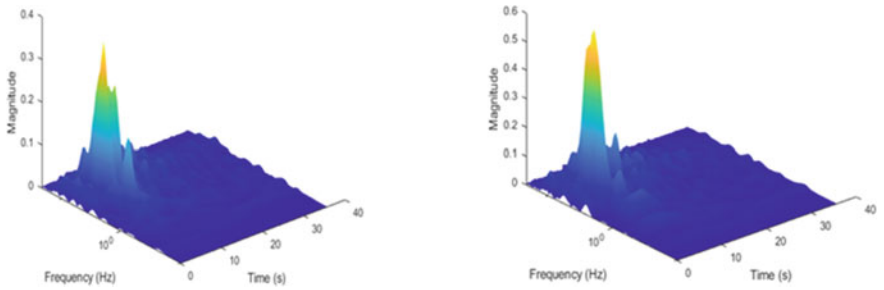

Fig. 24 Scalogram 3D of Purola, radial (left) and transverse (right)

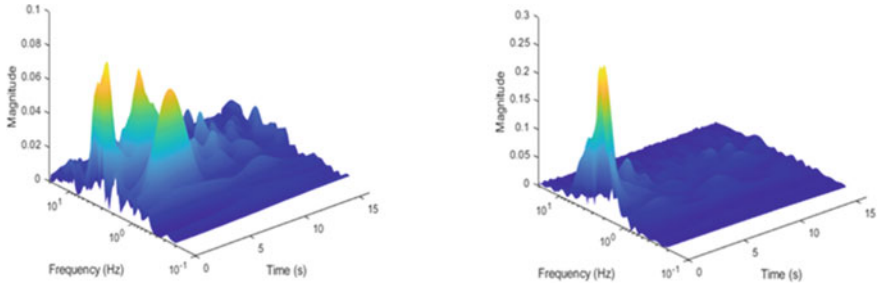

Fig. 25 Scalogram 3D of Koti, radial (left) and transverse (right)

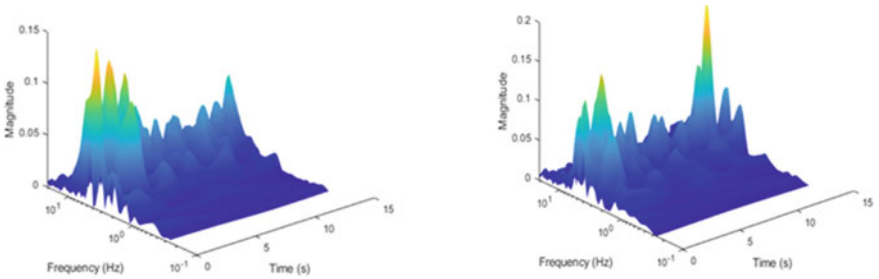

Fig. 26 Scalogram 3D of Kosani, radial (left) and transverse (right)

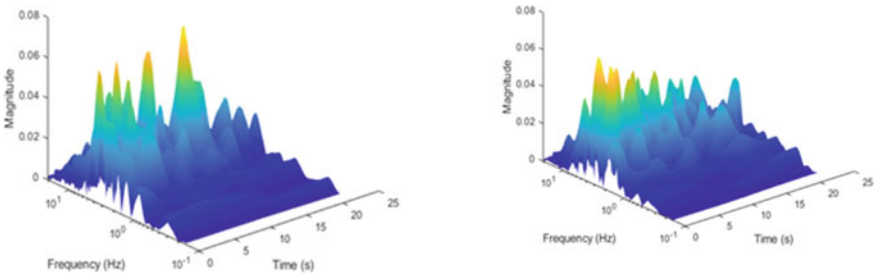

Fig. 27 Scalogram 3D of Almora, radial (left) and transverse (right)

5 Conclusions

The amplitude and frequency content of ground motions are the primary variables that affect the behaviour of structures subjected to earthquake forces. These two variables are obtained separately using the time-acceleration and Frequency-Fourier representations, respectively. However, both descriptions carry incomplete information and do not enable the proper correlation of ground motion characteristics to structural damage. In this paper, first, the FFTs are used to estimate the frequency content of the earthquake. Single parameter estimates of the frequency content, i.e. T_p, $T_{m,}$ and V/A are also tabulated. Next, the continuous wavelet transform technique is used to perform time-frequency analyses of 26 horizontal strong ground motions recorded in the 1991 Uttarkashi earthquake. Further, the earthquake-induced physical damage to infrastructure, at various locations in Uttarakhand, was obtained from multiple reconnaissance-based damage surveys. The observations from the continuous wavelet transforms are correlated with the observations from reconnaissance surveys. In certain ground motions, high amplitude seismic waves with high frequencies were also sustained in time, thus severely affecting low-rise structures. The results are consistent with the damage data from the post-earthquake reconnaissance studies conducted in the aftermath of the 1991 Uttarkashi earthquake.

References

Cotton F, Campillo M, Deschamps A, Rastogi BK (1996) Rupture history and seismotectonics of the 1991 Uttarkashi, Himalaya Earthquake. Tectonophysics 258(1–4):35–51

Cui XZ, Hong HP (2021) A Time–frequency representation model for seismic ground motions. Bull Seismol Soc Am 111(2):839–856

Devi V, Sharma ML (2016) Spectral estimation of noisy seismogram using time-frequency analyses. Int J Geotech Earthq Eng 7(1):19–32

Gupta RP, Saraf AK, Saxena P, Chander R (1994) IRS detection of surface effects of the Uttarkashi earthquake of 20 October 1991, Himalaya. Int J Rem Sens 15(11):2153–2156

Gupta DK, Bhowmick D, Roy PNS (2015) Himalayan hazard study on the basis of stress and strain state of 1991 Uttarkashi earthquake using coulomb stress transfer model. Geomat Nat Haz Risk 6(2):131–148

Jain SK, Das S (1993) Analysis of strong motion records from Uttarkashi earthquake for assessment of code provisions for different seismic zones. Earthq Spectra 9:739–739

Joshi A (1997) Modelling of peak ground accelerations for Uttarkashi Earthquake of 20th October 1991. Bull Indian Soc Earthq Technol 34(2):75–96

Kayal JR (1996) Precursor seismicity, foreshocks and aftershocks of the Uttarkashi earthquake of October 20, 1991 at Garhwal Himalaya. Tectonophysics 263(1–4):339–345

Kumar D, Teotia SS, Sriram V (2011) Modelling of strong ground motions from 1991 Uttarkashi, India, Earthquake using a hybrid technique. Pure Appl Geophys 168(10):1621–1643

Paul A, Sharma ML, Sing V (1998) Estimation of focal parameters for Uttarkashi earthquake using peak ground horizontal accelerations. ISET J Earthq Technol 35(1–3):1–8

Ramkrishnan R, Devaraj D, Kolathayar S, Sitharam TG (2022) Joint time frequency analysis based synthesis of acceleration-time history and response spectra for Japanese earthquakes. In: Earthquakes and structures. Springer, Singapore, pp 21–31

Shanker D, Kapur N, Singh VP (2003) Evidence on triggered seismicity associated with the October 20, 1991 Uttarkashi earthquake (Garhwal Himalaya). Acta Geodaetica Et Geophysica Hungarica 38(3):363–374

Thakur VC, Kumar S (1994) Seismotectonics of the 20 October 1991 Uttarkashi earthquake in Garhwal, Himalaya, North India. Terra Nova 6(1):90–94

Earthquake Characteristics and Ground Motions in Christchurch, New Zealand

Rajnil Rohit Lal, Joeli Varo, and Sujoy Kumar Jana

1 Introduction

The devastating earthquake which struck in new Zealand's South Island resulted in significant structural and non-structural damages. One of the key aspects relating to the associated damages was the variation in the ground acceleration from region to region. Summarised below are the seismological details of the 2010 Darfield and 2011 Christchurch earthquake.

2010-Darfield Earthquake
The ruptured fault with an epicentre of 30–40 km from New Zealand's Christchurch city resulted in an $M_w = 7.1$ earthquake that caused severe damages in the districts located near to the strong shake location; epicentre on at 4:45 am NZT on the 4th of September, 2010. The duration of this earthquake was relatively short at 15 s in comparison to the 2003 Hokkaido earthquake, which lasted for 45 s. This earthquake exceeded New Zealand's strong ground motion data since the beginning of the recording, which established in the 1960's. The peak recorded horizontal acceleration was 0.82 g, and peak velocity was found to be above 1 m/s. Surprisingly, one site located near to the fault recorded the vertical acceleration of 1.26 g. For Christchurch CBD, the return period of 400–500 years was generated for a period below 2 s. And or periods above 2 s, the return period was found to be between 1000–3000 years (Brando et al. 2012; Palermo 2010).

R. R. Lal · J. Varo (✉)
School of Building and Civil Engineering, Fiji National University, Derrick Campus, Samabula, Fiji Islands
e-mail: joelivaro@gmail.com

S. K. Jana
Department of Surveying and Land Studies, Papua New Guinea University of Technology, Lae, Morobe Province, Papua New Guinea

I. Pal et al. (eds.), *Proceedings of the 2nd International Symposium on Disaster Resilience and Sustainable Development*, Lecture Notes in Civil Engineering 294,
https://doi.org/10.1007/978-981-19-6297-4_5

Christchurch Earthquake

The magnitude (M_w) 6.3 earthquake resulted in a strong shaking within the Central and Eastern region of Christchurch. Massive bridge damages were noticed within this region. This damage was mainly due to liquefaction and lateral spreading of riverbanks on the 22nd February, 2011 (Brando et al. 2012; Palermo 2010).

The epicentre of the earthquake was located near the town of Lyttelton, 10 km south of Christchurch CBD. Although the magnitude of this earthquake was lower than the 2010 Darfield earthquake having similar localised effects. The Peak Ground Acceleration (PGA) for this earthquake ranged from 0.5 to 2.2 g, exceeding the values that are used in the design of NZ road highway bridges. The horizontal Peak Ground Acceleration ranged from 0.37–0.51 g for bridges situated in the Christchurch CBD; Colombo Street Bridge, bridge of Remembrance, Antigua Street Footbridge, and Moorhouse Avenue Overpass. Bridges within 10 km of the Christchurch earthquakes epicentre recorded the horizontal PGA ranging from 0.25 to 1.4 g (Palermo and Brando 2013; Wotherspoon et al. 2011).

Shallow epicentral depth less than 10 km resulted in higher intensity shaking in Christchurch in comparison to the 2010 Darfield event. The duration of the ground shaking was observed to be in between 15–20 s. Although having a short duration, this event recorded one of the highest peak ground acceleration (PGA) = 2.1 g, close to the epicentre in the world. In Christchurch CBD, high vertical acceleration also characterised the ground motion, resulting from reversing thrust mechanism. Following the occurrence of this severe earthquake, aftershocks were experienced in the following months with the strongest one recorded on 13th June 2011 with a magnitude ($M_w = 6$) with the epicentre located on the same south-east edge where the earthquake occurred on 22nd February 2011 (Brando et al. 2012; Wotherspoon et al. 2011) (Table 1).

A response spectrum was then formed based on the ground motion of both Darfield and Christchurch earthquake recorded at the nearest record stations. The response spectra for an Importance Level 2 for a return period of 500 years was plotted, and a comparison was made based on the spectral acceleration for different periods of the bridges. This analysis was done to monitor what percentage of the design code acceleration was activated.

Table 1 Comparison the peak ground acceleration for Darfield, Christchurch, and Sumner events. *Source* (Palermo et al. 2012)

Event	M_w	Peak Ground Acceleration (PGA)	
		Maximum horizontal (g)	Maximum vertical (g)
Darfield, September 4, 2010	7.1	0.8	1.3
Christchurch, February 22, 2011	6.2	1.7	2.2
Sumner, June 13, 2011	6.0	2.0	1.1

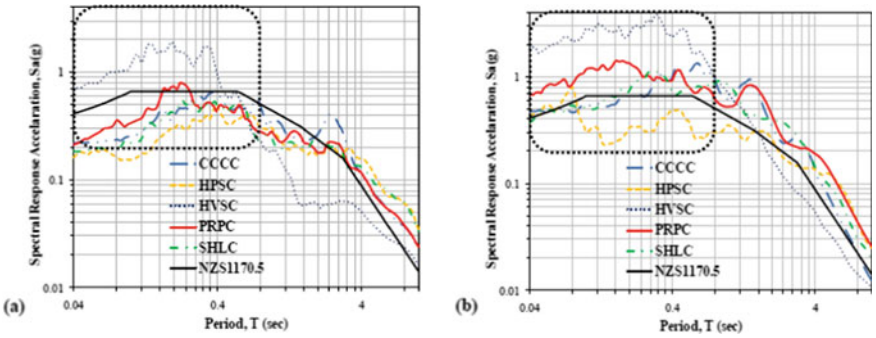

Fig. 1 Response spectra of the geometric mean of the horizontal acceleration and strong motion station recording in central and eastern Christchurch compared to NZS1170.5 design response spectrum for Christchurch, site soil class D for 500-year return period: **a** 2010 Darfield earthquake; **b** Christchurch earthquake. The four (4) letter symbols represents the different strong motion stations. *Source* (Palermo et al. 2012)

2 Background and Methodology

Considering the records from Catholic Cathedral College (CCCC), the 2010 earthquake demand in the natural period range of the bridge structure is below the NZS 1170.5 Design spectral acceleration whereas, the 2011 earthquake demand matches the Code spectral acceleration at period range of 0.17 to 0.27 (Fig. 2 and Table 2).

The recorded Peak Ground Acceleration from the Health Cote Valley school station (HVSC) was above the NZS1170.5 Design Spectral acceleration for both 2010 (0.16–0.25 g) and 2011 (0.37–0.52 g) earthquakes. It was also noted that the 2011 Christchurch earthquake's epicentre was closest to HVSC record station. Due to the topographic effects, seismic waves were amplified due to the station being located on a raised mass of land. Port Hills Overbridge was located very close to the Health Cote Valley school station (Code: HVSC). Therefore, it sustained substantial damages during the 2011 Christchurch earthquake. The ground motions recorded near the source had different characteristics in comparison to the locations situated far from the epicentre (Brando et al. 2012; Palermo et al. 2012; Wotherspoon et al. 2011).

1) **Regional geotechnical conditions**
   Christchurch city sits on the central coast of the Canterbury plains; 50 km wide and 160 km long region created by converging alluvial fans of rivers that flows eastward from the Southern Alps. New Zealand South Island is situated on a plate boundary where the Australian (A) and Pacific (P) plates meet. Subduction zone formed due to the Hikurangi Plateau, there exists a collision of the continents linked with the Chatham Rise and the Continental crust of the Australian (A) plate. This results in oblique convergence of the Australian (A) AND Pacific (P)

Table 2 The variation between the ground motion across the Christchurch region is shown below for both the 2010 Darfield and 2011 Christchurch earthquake. *Source* (Cubrinovski et al. 2011)

Station Name	Code	Site Class[a]	4th September 2010			22nd February 2011		
			R_{rup}[b] (km)	PGA[c] (g)	PGV[d] (cm/s)	R_{rup}[b] (km)	PGA[c] (g)	PGV[d] (cm/s)
Canterbury Aeroclub	CACS	D	11.70	0.20	39.20	12.80	0.21	20.00
Christchurch Botanic Garden	CBGS	D	14.40	0.16	36.20	4.70	0.50	46.30
Christchurch Cathedral College	CCCC	D	16.20	0.22	53.80	2.80	0.43	56.30
Christchurch Hospital	CHHC	D	14.70	0.17	38.30	3.80	0.37	50.90
Cashmere High School	CMHS	D	14.00	0.24	31.30	1.40	0.37	44.40
Hulverstone Dr Pumping Station	HPSC	E	21.70	0.15	39.30	3.90	0.22	36.70
Healthcode Valley School	HVSC	C	20.80	0.61	28.80	4.00	1.41	81.40
Kaipoi North School	KPOC	E	27.60	0.34	35.70	17.40	0.20	18.90
Lincoln School	LINC	D	5.90	0.44	34.40	13.60	0.12	12.70
Lyttelton Port	LPCC	B	22.10	0.29	19.10	7.10	0.92	45.60
Lyttelton Poet Naval Point	LPOC	C	-	-	-	6.60	0.34	69.10
North New Brighton School	NNBS	E	23.10	0.21	35.60	3.80	0.67	35.10
Papnui High School	PPHS	D	15.30	0.22	54.80	8.60	0.21	36.70
Pages Rd Pumping Station	PRPC	E	19.30	0.21	44.90	2.50	0.63	72.80
Christchurch Resthaven	REHS	D	15.80	0.25	42.60	4.70	0.52	65.40
Riccarton High School	RHSC	D	10.00	0.21	39.30	6.50	0.28	29.80
Rolleston School	ROLC	D	2.20	0.34	73.70	19.60	0.18	84.00
Shirley Library	SHLC	D	18.60	0.18	43.00	5.10	0.33	67.80
Styx Mill Transfer Station	SMTC	D	17.50	0.18	36.10	10.80	0.16	27.60
Templeton School	TPLC	D	3.00	0.27	55.60	12.50	0.11	11.30

plates by approximately 48–39 mm per year. The resultant of the collision generates high energy results in earthquakes throughout New Zealand (Cubrinovski et al. 2011).

The right lateral displacements due to the fault at Marlborough fault zone results in a mountainous uplift. These faults are linked with the Alpine faults which consider the boundary motions between the Australian (A) and Pacific (P) plates resulting in 27 ± 5 mm/year strike-slip and 5–10 mm/year of displacement slip. The Greendale fault was the source for the 2010 Darfield earthquake. When the plates converge, most of the motion is accounted for by the more significant faults such as Porter Pass Fault, as it has a slip rate of 3–7 mm/year. GNS seismologists have analysed and predicted that the 2010 Darfield earthquake initiated a rupture that had a component of reverse faulting behaviour; oblique east-side down slip on the N-W striking western portion of the fault resulted in the diversion of Hororata River (Cubrinovski et al. 2010) (Fig. 3).

The 2011 Christchurch earthquake occurred on a previously unmapped fault. That is the largest fault known as Port Hills Fault that is situated in Port Hills south of Christchurch. The epicentre was located on 43.598°S, 172.714°E. at a focal depth of 4 km. This fault had a reversal behaviour. The distance from

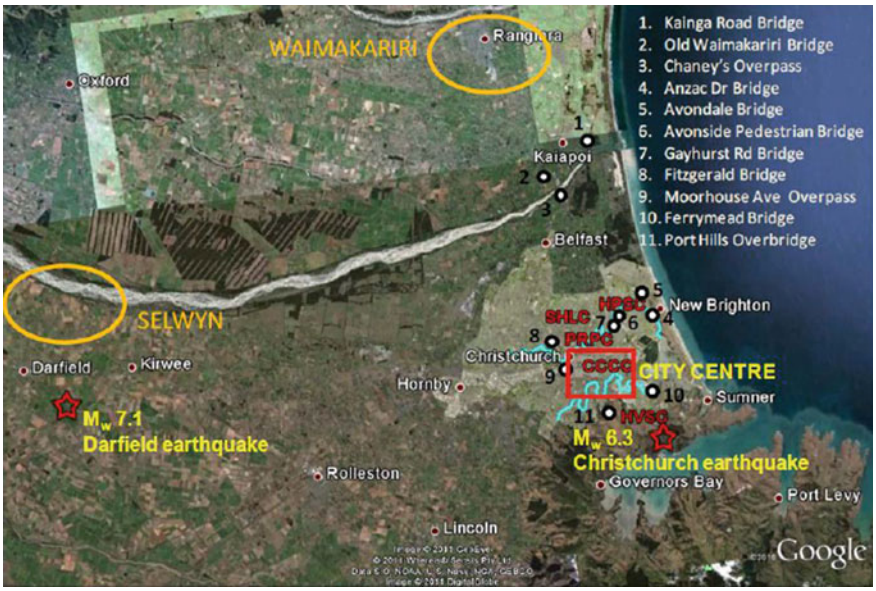

Fig. 2 Overview of Christchurch and the surrounding region, indicating locations of damaged bridges, strong motion stations and the epicentres of the 2011 Christchurch earthquake *Source* (Palermo et al. 2012)

Christchurch to the epicentre of this 2011 earthquake was approximately 8 km, but the ruptured fault was underneath the Health Cote Valley located right beside Christchurch.

The layers of soil strata are characterised as Holocene aged silt, sand and gravel. The groundwater table for the eastern part of Christchurch is only 1–2 m below the surface with the depth of the water table increasing towards the west. The 2011 Christchurch earthquake had shown a significance of liquefaction in Christchurch CBD that was widespread in developed areas that were not prevalent in the 2010 Darfield earthquake. In fact, there was no sign of liquefaction in the CBD during the 2010 Darfield earthquake (Cubrinovski et al. 2012a).

3 Discussion and Analysis

Following the Darfield earthquake in 2010, several geotechnical investigations were carried out on the eastern suburbs of Christchurch. Results confirmed that the soil practically consisted of silty sand and clean fine to medium sand with the groundwater table of the approximate depth of 0.3–2.5 m. The Cone Penetration test and The SPT test indicated that the soil up to 10 m depth had very low cyclic shear resistance. This confirmed that the upper layers were mostly liquefied wherein, the sandy soil deposits settle on top (Smyrou et al. 2011).

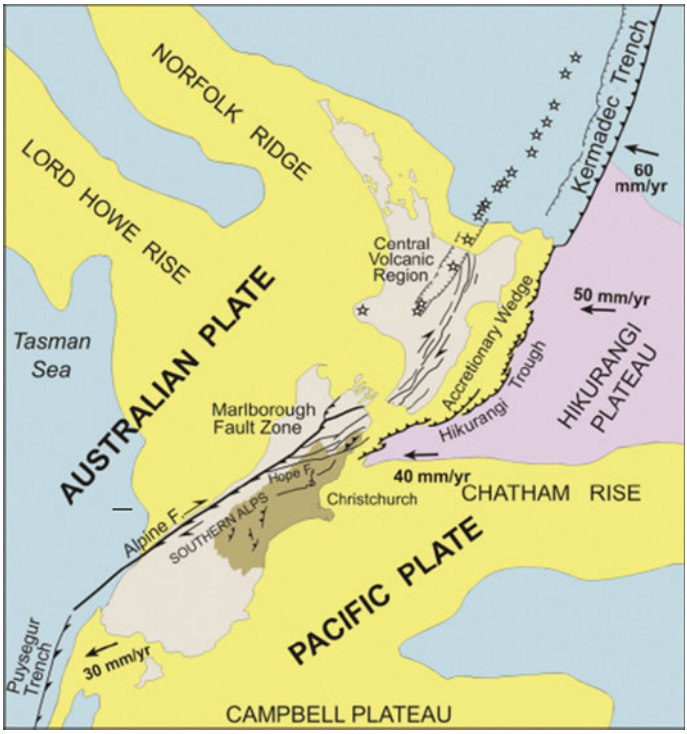

Fig. 3 Australian-Pacific plate through the New Zealand and convergence rates of Pacific relative to Australian Plate *Source* (Cubrinovski et al. 2010)

2) **Wider damage and impacts on Built Environment**
See Fig. 4.

The suburbs that were affected by liquefaction along the Avon River to the east of Christchurch CBD (Avonside, Dallington, Avondale, Burwood, Bexley) consisted of loose fluvial deposits of sand and plastic silts with the top layer (5–6 m) deep being in a very loose state. Liquefaction caused differential settlement and instability within the soil strata that resulted in lateral movement of foundations and rotation of bridge piers. Lateral spreading was a major contributor for the unexpected damages during this event. The magnitude of peak lateral displacement due to lateral spreading was between 0.5 to 3.0 m at the Avon river banks. This drove the spreading inland of about 100–250 m from the riverbank, as shown in Fig. 5 (Cubrinovski et al. 2012b).

Lateral displacements from the spreading behind the abutment resulted in extensive cracks in the abutments due to abutment rotation. In most cases, the abutment wall was restrained on top by the bridge superstructure, and it pushed and rotated the abutment wall outwards at the bottom due to the lateral displacement towards the river. Slope failure was also widespread through the

Port Hills region with almost every cliff experiencing rockfall and landslide as shown in the Fig. 6 (Cubrinovski et al. 2011; Palermo et al. 2012).

Bridge Damages and Its Impacts

A back rotation of approximately 7–8° was observed on abutments. Structural cracks were also seen together with spalling and crushing of concrete. These failures were influenced by the lateral spreading due to liquefaction. Deep abutments showcased more of this failure where plastic hinges developed on abutment piles due to high rotation demands imposed on the bridge structure (Palermo et al. 2012).

Piers performed well without forming plastic hinges due to the vibration of the ground. However, large moments developed at the pier-deck interface due to lateral spreading that resulted in structural cracks from the high flexure demands. Only the Moorhouse Overpass bridge in the Christchurch CBD encountered pier failure which disrupted the traffic flow with the Christchurch CBD. Due to this failure, the bridge was closed for five (5) weeks and repair works commenced easing the flow of traffic within CBD. A temporary prop was provided beside the failed piers to resist the vertical traffic load. This was done by providing a Steel cross braces fixed the UB steel columns that were placed beside the piers. Extensive brittle failures were observed as the bars buckled and the vertical load-carrying capacity of the bridge

Fig. 4 Typical spreading induced damage to bridges (South Brighton Bridge): **A** Lateral ground displacement is resisted by the upper bridge structure. **B** Abutment back-rotation due to the pinning effect and lateral displacement of foundation soils. **C** Spreading-induced damage (bending cracks) at the top of abutment piles *Source* (Cubrinovski et al. 2012b)

diminished. Shear failure was observed on the columns and piers due to lack of confinement provided by transverse stirrups. Anzac Bridge and the South Brighton Bridge also experienced severe damages like Moorhouse Overpass Bridge (Palermo et al. 2012) (Figs. 7 and 8).

Approaches experienced large offsets between bridge deck and approach. At some points where the bridge was extremely rigid, approaches were significantly damaged, and access to the bridge was impossible. Pavement cracks parallel to the axis was seen on the approaches.

Most of the Highway bridges went through the seismic assessment phase where retrofitting was done by providing a steel shear key at the ends of the abutments

Fig. 5 Induced Lateral spreading effect from Avon River into the CBD *Source* (Cubrinovski et al. 2012b)

Fig. 6 Rock falls and sliding on the Port Hills *Source* (Cubrinovski et al. 2011)

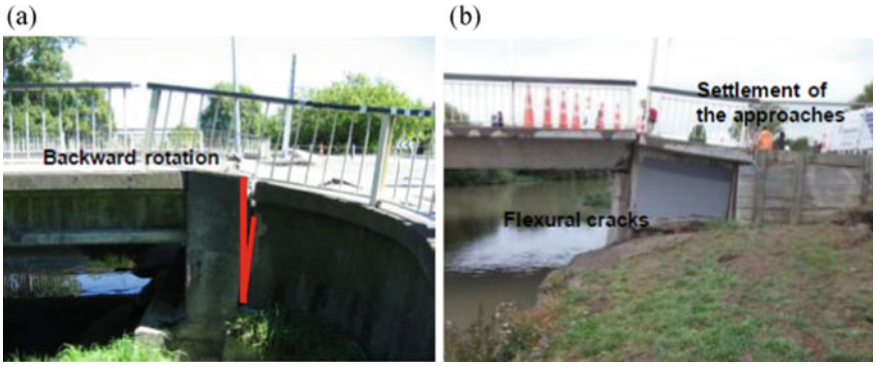

Fig. 7 **A** Back rotation of abutment, and **B** settlement of approaches *Source* (Palermo et al. 2012)

linking the deck to the abutment. This proved quite useful to counteract the rotation demands and the transverse demands imposed on the structure during the time of the event. The Port Hills Overpass Bridge sustained severe damage although retrofitting was done prior to the 2010 Darfield and 2011 Christchurch earthquake. It was predicted based on the damages observed that if retrofitting would not have been done on this bridge. There was a high probability of this bridge to collapse (Palermo 2010; Palermo et al. 2012).

Residential Buildings

The residential buildings consisting of slab on grade foundation consisting of low-grade wire mesh that was built in the 1960's. These foundations sustained massive damages due to lateral spreading as the foundation lost its load-bearing capacity due to the influence of large displacement, as shown in Fig. 9. This resulted in rupture of the floor slab and propagation of cracks through the structural wall to the roof elements. Large sand deposits were ejected from the ground that piled around houses. Differential settlements lead to severe sand boils that tilted many houses due to the loss of foundation due to a huge reduction of the bearing capacity of the soil. (Cubrinovski et al. 2012b; Yamada et al. 2011).

Multi-Storey CBD Structures

Lateral spreading from narrow zones of Avon river had a high influence on the foundation of tall multi-storey buildings. As the foundation of tall buildings stretched, the expansion joints up the height of the building opened. A failure such as shear cracks and column rotations were prevalent in the CBD region. Due to massive structural failures, the heritage buildings were demolished as the damages were beyond the economical repairing mode. Moreover, bridges sustained minimal damages in comparison to the vertical structures. Overall, the monolithic bridges performed better. The performance of the precast concrete bridges in the Christchurch CBD

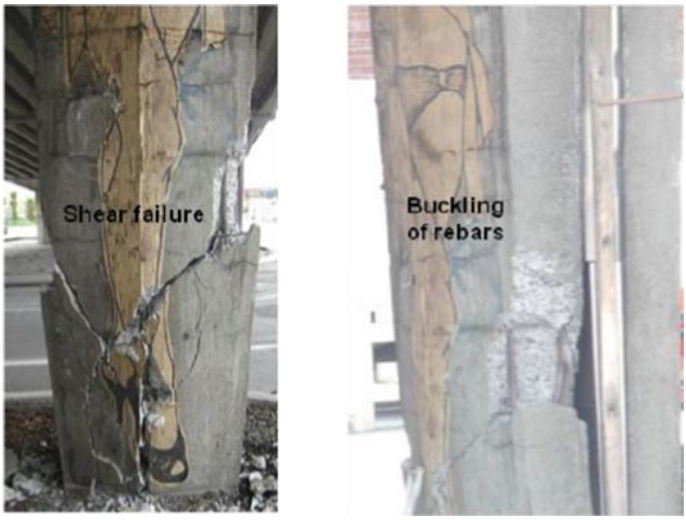

Fig. 8 The shear failure mechanism of the pier *Source* (Palermo et al. 2012)

was satisfactory. However, due to the lack of efficiency between deck to the abutments resulted in high rotation and displacement demands imposed on abutments (Cubrinovski et al. 2012a) (Fig. 10).

Leeves on the edge of the riverbanks sat on a sandy soil which was very close to the groundwater table. During the construction of the leaves, the base coarse was compacted with rollers. However, liquefaction causes huge dames to this leeves which was non-functional after the 2011 Christchurch earthquake. The leeves were mostly damages at the East of State Highway 1 (SH1) as shown in Fig. 11 (Cubrinovski et al. 2012a).

3) **Overall bridge stock damage characteristics**
This section addresses the overall damages within the Canterbury region bridge stock during the 2011 Christchurch earthquake. The bridge stock was inspected by road consultants and researchers from the University of Canterbury. This was done to ensure safety, mark the observed damages and establish a criterion to enforce smooth traffic flow if the bridges remained in an operational state.

To assess the damages, both qualitative and quantitative approach was utilised. To ease the assessment criteria and to obtain the precise results, the damages associated with the bridge stock was divided into nine different categories. The categorisation was based on the location of damages on various components of the bridge structure. These include deck and superstructure, bearing between

deck and abutment or piers, piers, abutments, bridge surface pavement, approach pavement, approach settlement etc. (Brando et al. 2012).

The damages were also ranked based on severity. A numerical value was assigned to each damage based on severity. Damage scenarios were defined as none (0), minor damage (1) moderate damage (2), and high level of damage (3). The severe damages that were observed in the Christchurch CBD region are addressed in this paper. The associated damages are ranked based on the criteria set up by the structural consultants, as explained above (Brando et al. 2012).

i) **Colombo Street Bridge**

This bridge was built in the 1930's that crosses the Avon River from Kilmore Street to Oxford Terrace in North–South direction. It is a single-span bridge with a clear span of 16.8 m with an arch steel girder.

Earthquake Damages

It experienced severe damages at both the approaches due to lateral spreading, which was caused by liquefaction. Cracks were observed on both the abutments along the riverbank due to lateral displacement of the banks. North abutment pilasters rotated outwards due to the lateral spreading pressure enforced on the wing walls. The arch edge girder buckled on both upstream and downstream sides, as shown in Fig. 12. In addition to that, the cast-iron handrails also fractured and were not in a stable state. This bridge sustained severe damages; (ranked as level 3 damages) (Palermo et al. 2011).

ii) **Bridge of Remembrance**

This single-span stone-faced reinforced concrete arch bridge was constructed in 1924. This crosses the Avon river between Durham Street and Oxford Terrace to Cashel street. This bridge is supported on a shallow foundation (Palermo et al. 2011).

Earthquake Damages

This bridge showed moderate damages wherein the Triumphal arch was severely damaged. Signs of paving damages were evident in both approaches (Fig. 13a). Large cracks developed on the wing walls (Fig. 13b) and at the base along the entire length of the base. These cracks widened after the June 13th aftershock. Major damage was due to the settlement of approach fill, lateral spreading which initiated rotational displacement of wing walls. The small rotation on all four (4) wing walls caused cracks on stone facades. Cracks also appeared on concrete section behind the cracked stonework. This was a major issue since the wing walls were founded on a separate foundation. Overall, the chance for collapse

for this bridge is unlikely. This bridge sustained severe damages; ranked as level 3 damages (Palermo et al. 2011, 2012).

iii) **Antigua Street Footbridge**
Is a single span bridge that consists of steel arched trusses on the external side of the bridge, braced by Hot Rolled steel angle irons that longitudinally supports the timber stringers, and transverse timber deck. Shallow foundations are utilized to support the Concrete abutment walls.

Earthquake Damages
Liquefaction and lateral spreading resulted in crack formation along the riverbank. This soil displacement sheared the abutments linking to the top chord of the truss. Timber decking was pushed away from its original position at the approaches. There were no signs of top chord buckling due to the restraint provided by the decking in place. However, the bottom chord buckled due to no effective restraint. Back rotation of approximately 1–1.5° was evident at both the abutments (Fig. 1). Lack of reinforcement and insufficient piles was the drawback for the structural performance of this bridge. Vertical deflection and hogging resulted initiated due to the displacement of the abutment. The cross braces failed due to hogging and corrosion.

This bridge sustained severe damages; ranked as level 3 damages (Fig. 14a, d). The timber footbridge failed as a result of shear failure of the concrete wing walls (Fig. 14b, c) (Palermo et al. 2011).

iv) **Moorhouse Avenue Overpass**
This overbridge was built in 1964 and consisted of an eleven-span concrete structure separating the grades of Moorhouse and Colombo Street. Two-column bents support the T-beam superstructure which is then supported by 406 mm diameter octagonal concrete piles. This structure is linked with expansion joints

Fig. 9 Damages to residential houses as a result of lateral spreading causing foundation failure during the 2010 Darfield and 2011 Christchurch Earthquake (South Kaiapoi) *Source* (Yamada et al. 2011)

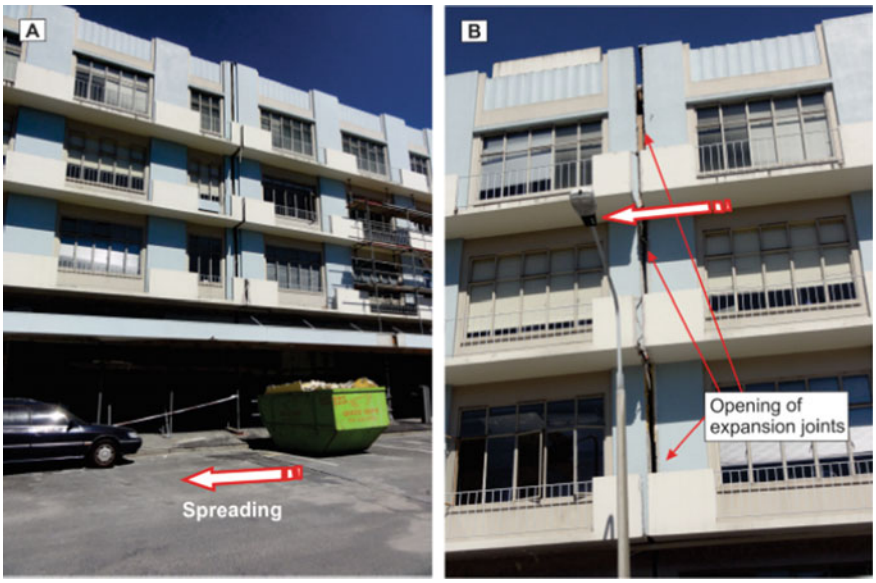

Fig. 10 **A** lateral spreading stretching the foundation & **B** Expansion joints opening the height of the structure of the CBD building *Source* (Cubrinovski et al. 2012b)

Fig. 11 Example of the longitudinal crack running along the crest of the leeve *Source* (Cubrinovski et al. 2012a)

(Fig. 15). The performance of this bridge during the 2011 Christchurch even was unacceptable.

Earthquake Damages

This bridge displayed brittle failures with extreme shear cracking and buckling of the piers. The performance of this bridge was unsatisfactory due to this failure, the

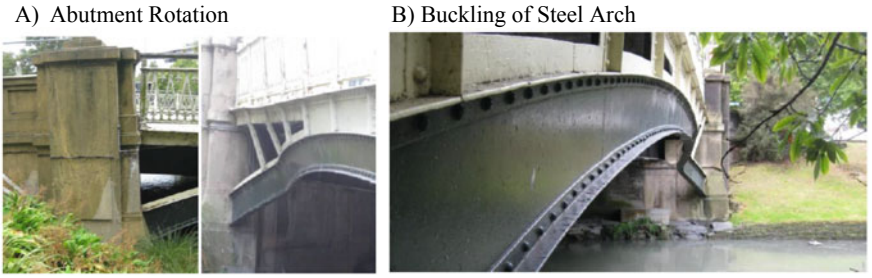

Fig. 12 **A** Rotation of Abutment and **B** Buckling of steel arch was observed at the Colombo Street Bridge *Source* (Palermo et al. 2011)

Fig. 13 **a** Damages to steps on western approach and **b** Damages to the wingwall on north-eastern wingwall *Source* (Palermo et al. 2011)

vertical load-carrying capacity together with the lateral load capacity depreciated. For this reason, the bridge was closed for five weeks, and strengthening was implemented.

One column near the north-east approach near the expansion joint was severely damaged. Irregularity in the transverse response was evident due to inserting the steel rod linkages at the expansion joints at one side only. High displacement demands on piers at the eastern expansion joint was noted. Unconfinement of transverse stirrups on the columns was a major reason for shear failure and brittle failures (Fig. 1a). Inspection after the 2011 Christchurch event displayed buckling of damaged columns transferring the load on the central span, which was predominant to collapse/failure (Fig. 1b). Extreme horizontal acceleration influenced flexure on columns which resulted in extensive column buckling (Palermo et al. 2011; Palermo and Brando 2013).

The influence of high displacement demand in the west-central part of the bridge caused the deck to pound against the south-west abutment. This caused significant spalling and reinforcement buckling. Ground motion in longitudinal direction pulled the deck away from the abutment wherein reinforcement bars yielded, and vertical cracks were displayed. Since the structure lost its load-carrying capacity (both in

A) Hogging underneath the bridge

B) Damages on north-east abutment (shear cracks)

C) End Support Failure (Timber beams)

D) Failure of cross-braces due to corrosion

Fig. 14 A, hogging of the underneath bridge structure. B, Shear cracks due to abutment rotation observed at the Antigua Street Footbridge *Source* (Palermo et al. 2011)

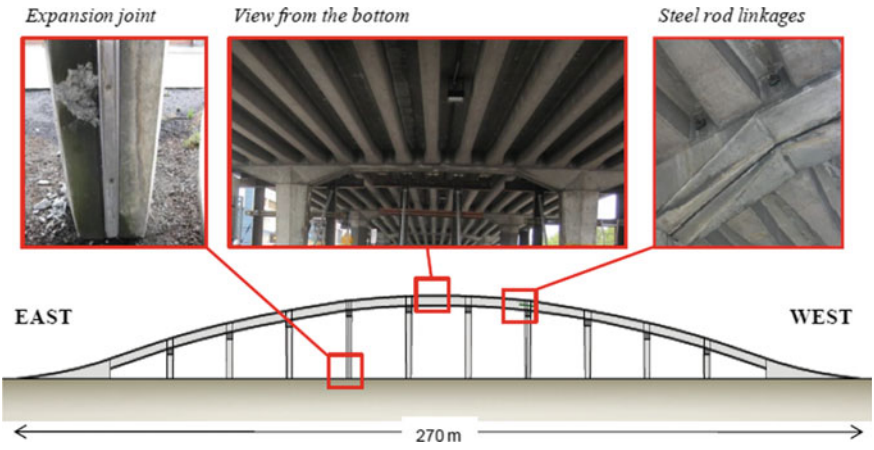

Fig. 15 The locations of the expansion joints and steel rod linkages are shown *Source* (Palermo et al. 2011)

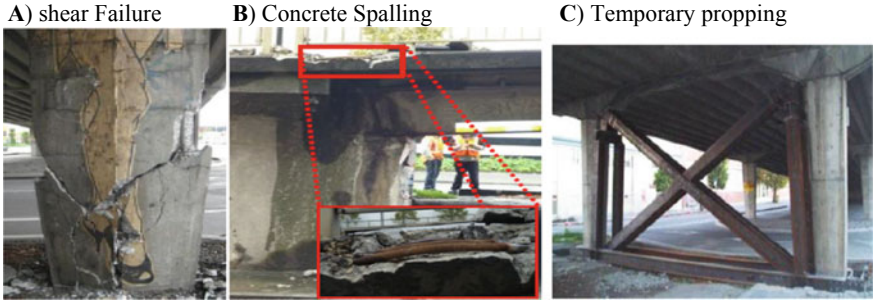

Fig. 16 **A** shear failure at expansion joints, **B** Concrete spalling and bar buckling at west side abutment. **C** Temporary propping was required due to reduced pier capacity to hold gravity load *Source* (Palermo et al. 2011)

vertical and lateral), Opus (WSP) provisioned a dual cross bracing to act as a prop to support the piers. This steel section was used diagonally to brace the piers (Fig. 16). This bridge sustained severe damages; ranked as level 3 damages (Brando et al. 2012; Palermo et al. 2012).

In addition, the damages identified outside the Christchurch CBD was mainly associated with bridge structures spanning over the Avon River. These were the bridges in the East and Southern Suburbs. Damages were mostly due to lateral spreading through liquefaction. Identified damages were the differential settlement due to ground vibration, large back rotations of abutments and piers due to spreading, which caused structural cracks and spalling.

The test results and analysis, together with site inspection, confirmed that the overall performance of the bridges during the 2011 Christchurch earthquake was good due to bridges mostly having short spans. However, just 4% of the bridges were accounted for severe damages. The 2011 event was marked as an event with a return period of 500 years and greater and a majority of the bridges mapped onto this design return period, and for bridges with a high importance level had no damages at all (Brando et al. 2012).

v) **Case study bridge performance**
Bridge: State Highway (SH) 74 Horotane Valley overpass
Description of the Bridge Configuration and Detail
The Horotane bridge was designed and constructed in 1963 and accounts for approximately 4800 vehicles per day consists of two bridges with each bridge having two (2) opposite lanes of State Highway 74 across Horotane Valley Road. The structural form of this bridge consists of a multi-span continuous concrete girder. The Horotane bridge overpass is situated of about 2 km west of the Christchurch portal to the Lyneelton Road tunnel. Both the bridges are identical. An exception is that bridge No. 2 carrying the westbound lanes widen towards its west end to provide room for an offramp. Both the 2 lane bridges have three simply supported spans. The deck is of reinforced concrete supported by prestressed concrete beams that stiffen the deck. The end spans are 13.9 m

Fig. 17 Overall side view of the Horortane Valley Overpass *Source* (Palermo et al. 2012)

with the central span having a length of 12.5 m (Palermo et al. 2011; Chapman and Lauder 2005) (Fig. 17).

The bridge deck is supported by the abutment and rectangular piers founded on a spread footing. The fixity of the spans to the abutment and piers are well supported by the hold-down dowels and linkage rods. The transverse load is resisted through the fabricated steel shear keys was installed at the abutments of the Overpass bridge. Each of the abutments consists of nine brackets which is fitted with a 30 mm diameter bolt into the bottom of the prestressed beams to provide additional longitudinal restraint in addition to the linkages provided. To robust the deck diaphragm action under transverse loading and to restrict unseating, additional linkage rods were installed between the outer beams and pier (Palermo et al. 2011; Brando et al. 2012; Palermo and Brando 2013) (Fig. 18).

Site Ground Motions and Bridge Response

The epicentre of the 2011 Christchurch was located at about 1.3 km from the Horotane Bridge Overpass. The peak ground motion was recorded by the closest strong-motion

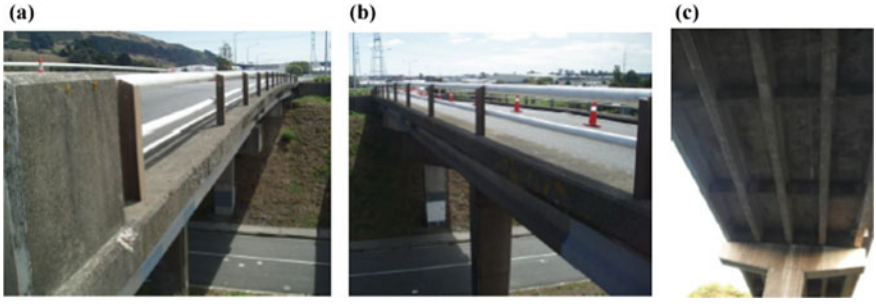

Fig. 18 **a-b** General view of the superstructure and **c** deck soffit of the bridge *Source* (Palermo et al. 2012)

station (HVSC) at 1.6 km from the bridges, which has a significant influence on the topographic effects. This bridge is close to the first (HVSC: a = 1.41 g) and second (LPCC: a = 0.92 g) strong motion record station, had a significant effect on the bridges structural system (Palermo and Brando 2013; Wotherspoon et al. 2011).

The bridge was relatively stiff in the longitudinal direction due to the large spread footings supporting the abutments. For this reason, the period of the structure was expected to be in between 0.3 to 0.5 s. The cantilevered tall piers allowed the bridge to have a flexible behavior in the transverse direction with the first mode of the periods ranging from 0.7 to 1 s with an assumption that the foundation pad is restricted to have a rocking behavior. For damping of 5%, the estimates of the response acceleration in both longitudinal and transverse directions were in a range of 1 to 0.5 g (Palermo and Brando 2013; Wotherspoon et al. 2011).

Observed Damages after the 2011 Christchurch Earthquake

A fine horizontal crack was observed on the lower half of the four piers following the 2011 Christchurch earthquake. The widths of these cracks were up to 0.2 mm, and the location of the cracks was about 500 to 2600 mm above the ground level. This means that the plastic hinges developed at the base. However, some hinges formed above the plastic hinge length. There was a shortening of distances between the bases of piers as the spacing had shorted by 200 mm for Bridge No: 1 and 260 mm for Bridge No: 2 (Palermo et al. 2011).

A severe vertical crack was observed at the junction between the abutment seating and abutment walls of both the bridges. This was due to the 100 mm horizontal displacement in a southward direction for the east end of bridge No: 2. Due to the displacements, minor spalling was observed at the beam ends (seating of beam on abutment). A transverse crack was developed on the north-west abutment back due to a rotation of 1° as shown in Fig. 19d. However, this crack was not continuous throughout the slope. A rotation of 3.4° occurred on the south-west abutment back with the initiation of transverse cracks at the bottom of the slope on the northeast side. Moreover, a significant transverse crack of 10 cm width and 60 cm depth opened at the top of the south-east slope and was continuous throughout the entire width of the bridge. Due to the displacement perpendicular to the bridge axis, cracks were developed, which extended through the abutment causing wider cracks and lateral movement of abutment and superstructure, as shown in Fig. 19b. (Wotherspoon et al. 2011).

The forward displacement of all four abutments by up to 20 mm was evident. This movement resulted in significant shear cracks on the back wall and shearing effect on the bolts of the new linkage brackets, which was loaded in shear at the west abutment of the No 1 bridge. The same bolt shearing effect was also observed on Bridge No 2, as shown in Fig. 19c. There was a 60 mm settlement of the west abutments. This was evident if viewed from the south side of the No 2 bridge. Separation gaps between the soil and abutment were seen at the east abutments signifying the down-slope movements as shown in Palermo et al. (2011); Palermo and Brando (2013).

Settlements were evident between approach pavement and abutments of both bridges. The roadway kerbs were damaged at several locations through compression

Fig. 19 Damage at the abutments: **a** Slope failure, **b** Flexural cracking, **c** Shearing bolt at the abutment retrofit, and **d** Transverse crack at the top of South-East slope *Source* (Palermo et al. 2011, 2012)

against abutments which was a result due to the forward movement of the backfill. Buckling of the guardrails together with the shearing of its bolts were also evident.

The bridge sustained minor damages following the 2010 Darfield Earthquake. The remarkable damage was that the abutment rods were loosened on both bridges where the slackness was monitored under the washer, which was about 5–10 mm.

The damages associated with the Horotane Overpass Bridge was not primarily associated with ground motion. The most vulnerable damages were due to the high stiffness, which generated a shorter fundamental time period of the bridge structure, which was observed to be in a range of 0.085–0.092 s. Slope failure was identified as the main cause of the damages and failures observed. Damage to pier diaphragm holding down and linkage bolts together with the flexural shear failure of pier footings was identified (Palermo and Brando 2013; Palermo et al. 2012) (Table 3).

Performance Evaluation of Horotane Valley Overpass

The abutment rod slackened which caused the abutment structures sliding towards the centre of the bridge. An allowance of 19 mm gaps filled with Flexcell was provisioned in the drawings. Most likely, these gaps could have widened about 5 mm during construction due to creep and shrinkage. Therefore, the abutments tended to slide forward, closing any creep and shrinkage and compressing the Flexcell to loosen the bolts (Wotherspoon et al. 2011).

Table 3 Summary of the level of damages observed during the site inspection after the Lyttelton Earthquake, 2011 *Source* (Palermo et al. 2012)

Deck	Null	**South-East Approach**	Null
Beams	Null	**North-West Approach**	Null
Piers	Minor	**Services**	Null
South-East Abutments	Minor	**Substructure**	Null
North-East Abutments	Minor	**Surrounds**	Null

The structure spans between two built up embarkments of approximately 9 m in height. The embarkments slope under the bridge was about at an angle of 34° degrees to horizontal (1.5 Hoz: 1 Vert), An assessment carried out in 2004 on the performance of this bridge under the influence of an earthquake predicted slope failure at ground acceleration above 0.12 g. This slope displacement had an influence on the pier spread footing movement towards the centre of the bridge that resulted in cracks in the piers (Palermo and Brando 2013; Palermo et al. 2012).

The schematic slope failure observed during the 2011 Christchurch earthquake performed better than what was expected. The transverse performance of this bridge was quite better since retrofitting tight linkages between the spans of such short bridge reduced the pier load by diaphragm action. Retrofitting functioned well in terms of protecting the structure although, 60% of the bolts between the attachment of prestressed beam and abutment sheared (Palermo and Brando 2013; Wotherspoon et al. 2011).

This bridge experienced huge abutment damages resulting from slope failure of its embarkments. The bolts connected to the soffit of the precast beams and abutment seat extensions suffered approximately 60% of the shearing effect. There was a high probability of collapse if the spans were not tied together and if the seats were not extended. Retrofitting proved to have functioned well as it prevented the onset damages to the beam diaphragm (Palermo and Brando 2013; Palermo et al. 2012).

4 Conclusion and Recommendation

Earthquake is lethal and destructive to human beings, physical structures and biological environment as experienced in the case studies of New Zealand. The south pacific islands are included in this hazard as well. It takes a precarious measure to understand the reality of loss by this dangerous phenomenon. However, this studies revealed the intricate needs of inculcating and mainstreaming building codes, structural codes and disaster risks analysis in construction of physical structures not only in New Zealand but in the South Pacific Islands as a whole.

References

Brando M, Lin SL, Giovinazzi S, Palermo A (2012) Observed and predicted bridge damage following the recent canterbury earthquakes: toward the calibration and refinement of damage and loss estimation tools

Chapman HE, Lauder MK (2005) Transit New Zealand (retired) C. Seismic assessment and retrofitting of New Zealand state highway bridges

Cubrinovski M, Robinson K, Taylor M, Hughes M, Orense R (2012b) Lateral spreading and its impacts in urban areas in the 2010–2011 Christchurch earthquakes. NZ J Geol Geophys 55(3):255–269. https://doi.org/10.1080/00288306.2012.699895

Cubrinovski M, Green R, Allen J, Ashford S, Bowman E, Bradley BA, Cox B, Hutchinson T, Kavazanjian E, Orense R, Pender, M, Wotherspoon L (2010) Geotechnical reconnaissance of the 2010 Darfield (New Zealand) earthquake. University of Canterbury. Civil and Natural Resources Engineering. http://hdl.handle.net/10092/5124

Cubrinovski M, Bradley B, Wotherspoon L, Green R, Bray J, Wood C, Pender, M, Allen J, Bradshaw A, Rix G, Taylor M, Wells D (2011) Geotechnical aspects of the 22 February 2011 Christchurch earthquake. http://hdl.handle.net/10092/6393

Cubrinovski M, Henderson D, Wood C, Winkley A, O'Rourke T, Rix G, Pender, M (2012a) Geotechnical aspects of the mw 6.2 2011 Christchurch, New Zealand, earthquake. In: GeoCongress 2012a, pp 1700–1709. https://doi.org/10.1061/9780784412121.175. http://ascelibrary.org/doi/abs/https://doi.org/10.1061/9780784412121.175

Mander JB, Dhakal RP, Mashiko N (2006) Incremental dynamic analysis applied to seismic risk assessment of bridges. Paper presented at the Retrieved from http://hdl.handle.net/10092/43

Palermo A (2010) Preliminary findings on performance of bridges in the 2010 Darfield earthquake. Bull New Zealand Soc Earthq Eng 43(4):412–420. https://doi.org/10.5459/bnzsee.43.4.412-420

Palermo A, Brando M (2013) Seismic assessment of New Zealand bridges in non-liquefiable soils during canterbury earthquake sequence. IABSE Symp Rep 99(17):982–989. https://doi.org/10.2749/222137813806501588

Palermo A, Wotherspoon L, Hogan L, Le Heux M, Camnasio E (2012) Seismic performance of concrete bridges during canterbury earthquakes. Struct Concr 13(1):14–26. https://doi.org/10.1002/suco.201100041

Palermo A, Wotherspoon L, Wood J, Chapman H, Scott A, Hogan L, Kivell A, Camnasio E, Yashinsky M, Bruneau M, Chouw N (2011) Lessons learnt from 2011 Christchurch earthquakes: Analysis and assessment of bridges

Palermo A, Liu R, Rais A, McHaffie B, Pampanin S, Gentile R, Nuzzo I, Granerio M, Loporcaro G, McGann CR, Wotherspoon LM, Andisheh K (2017) Performance of road bridges during the 14 November 2016 Kaikoura earthquake. http://hdl.handle.net/10092/15109

re3data.org (2018) Scholars' mine re3data.org - Registry of Research Data Repositories https://doi.org/10.17616/R31F8M

Smyrou E, Tasiopoulou P, Bal IE, Gazetas G, Vintzileou E (2011) Structural and geotechnical aspects of the Christchurch (2011) and Darfield (2010) earthquakes in New Zealand. https://doi.org/10.1002/eqe.2895

The bridge stock in the city of Christchurch suffered varying levels of damage as a result of the 2010-2011 Canterbury earthquake sequence. Detailed analyses, & damage observations for these bridges can be found in Palermo (2012). Performance of bridges in regions affected by liquefaction during the 2010–2011 canterbury earthquake sequence

Wotherspoon L, Bradshaw A, Green R, Wood C, Palermo A, Cubrinovski M, Bradley B (2011) Performance of bridges during the 2010 Darfield and 2011 Christchurch earthquakes. Seismol Res Lett 82(6):950–964. https://doi.org/10.1785/gssrl.82.6.950

Yamada S, Orense R, Cubrinovski M (2011) Earthquake news Geotechnical damage due to the 2011 Christchurch, New Zealand. http://hdl.handle.net/10092/5288

Wavelet Analysis of Near-Field Ground Motions from the M_W 7.8 2015 Gorkha Earthquake

Mohammed Ayub Ifan, Shalin Mathew, Jayaprakash Vemuri, and K. V. L. Subramaniam

Abstract The 2015 Nepal earthquake was one of the strongest quakes to strike the landlocked Himalayan country. The earthquake resulted in strong ground motions that severely affected various structures in the region. The unreinforced masonry structures were destroyed. Recorded ground motions from only five stations are available in the public domain. However, characterizing these ground motions in the time domain does not provide any information about the sequence of frequencies and amplitudes arriving at the station, which are key to understanding structural damage. The continuous wavelet transforms (CWT) are useful for such improved characterization of ground motions, as they provide a 3D view of time, frequency, and amplitude, thus enabling a comprehensive understanding of the damage potential of the ground motions. In this paper, recorded near-field ground motions from the earthquake are analyzed in the time and frequency domains. It is observed that the response spectra show a very wide acceleration sensitive region and some ground motions contain significant velocity pulses, both of which strongly influence structural damage. Further, it is observed that CWTs properly represent the critical characteristics of ground motions which can be correlated with the observed non-uniform damage to the built environment.

Keywords Strong ground motions · Frequency content · Fast fourier transforms · Continuous wavelet transforms · Time–Frequency analysis · 2015 Nepal earthquake

1 Introduction

The Himalayan belt is prone to high seismic hazards and is repeatedly struck by major earthquakes which cause significant structural damage. On 25th April 2015,

M. A. Ifan (✉) · S. Mathew · J. Vemuri
Mahindra University, Hyderabad, Telangana 500043, India
e-mail: ayubifan170119@mechyd.ac.in

K. V. L. Subramaniam
Indian Institute of Technology Hyderabad, Sangareddy, Telangana 502285, India

I. Pal et al. (eds.), *Proceedings of the 2nd International Symposium on Disaster Resilience and Sustainable Development*, Lecture Notes in Civil Engineering 294,
https://doi.org/10.1007/978-981-19-6297-4_6

the Mw 7.8 earthquake occurred in the Gorkha region of Nepal with a maximum felt intensity of IX on the Modified Mercalli Intensity (MMI) scale (Gautam and Chauglain 2016). The fault size was around 200 km in length and 150 km in width (Goda et al. 2015) with a focal depth of 15 km (United States Geological Survey 2015). The seismological characteristics of the earthquake have been investigated, and key features are described in detail by researchers (Parameswaran et al. 2015). There was extensive damage to 4,98,852 buildings and minor to moderate damage to 2,56,697 buildings (National Planning Commission 2015) causing 9,000 fatalities and injuries to 23,000 people (Whitney and Agrawal 2017). Nepal has a history of large earthquakes and has been reported (Gautam et al. 2018) to be repeatedly struck by major earthquakes since 1255 AD. Comprehensive records of the earthquakes of 1260, 1408, 1681, 1761, and 1810 do not exist. The 1833 earthquake was the first recorded earthquake and caused damage to 18,000 buildings (Ministry of Housing and Physical Planning 1994). The great Bihar-Nepal earthquake in 1934 damaged 2,07,248 buildings with a collapse of 80,893 buildings and in particular, the Kathmandu valley was severely affected with a collapse of 12,397 buildings and additional damage to 55,739 buildings (Rana 1935). Over 95% of the buildings in the Kathmandu valley were unreinforced masonry with mud mortar and did not meet seismic code provisions (Rana 1935). Reconnaissance surveys after the 2015 quake have reported non-uniform damage to masonry and reinforced concrete structures in and around the Kathmandu valley. Further, some reconnaissance surveys report that damage was confined to specific areas due to local soil characteristics and due to the sequence of earthquake waves (Goda et al. 2015). To understand this pattern, it is essential to understand the critical characteristics of recorded ground motions which can then be correlated to the observed non-uniform structural response (McGowan et al. 2017). This paper analyzes the characteristics of ground motions recorded at five stations in and around the Kathmandu valley in the time domain. Next, the frequency content is examined using Fourier Transforms. Finally, the frequency and time sequence are understood by decoupling them using the continuous wavelet transforms. However, since only a few recorded ground motions are available it is difficult to obtain a comprehensive view of the structural damage in the entire region.

2 Characteristics of Strong Ground Motions

Ground motion records are available from five stations in the Kathmandu valley. A strong ground motion was recorded by USGS at the station, KATNP (Dhakal 2016). Further, accelerometers were installed (Takai et al. 2016) at four sites: KTP, TVU, PTN, and THM. Figure 1 shows a map of Nepal (inset) and the locations of the five sites. The soil profiles of these stations are class-A (Hard rock) for KTP, and class-C (sedimentary) for the other four sites (KATNP, TVU, PTN, THM) situated on sedimentary soil. Figure 2 shows the response spectra and Table 1 lists the key characteristics.

Fig. 1 The epicenter and the stations. (1) KATNP, (2) KTP, (3) TVU, (4) PTN, (5) THM. The star (*) represents the epicenter of the earthquake

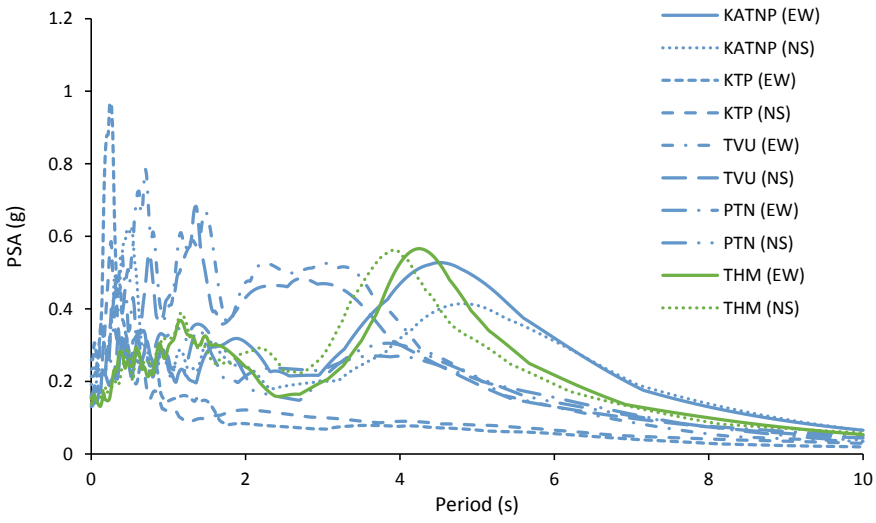

Fig. 2 Response spectra of ground motions

Table 1 Key characteristics of strong ground motions

S. No	Station	Direction	Distance (km)	PGA (cm/s^2)	PGV (cm/s)	V_{max}/A_{max} (s)	AI (m/s)	T_p (s)	T_m (s)
1	KATNP	EW	77	158.39	106.68	0.67	1.31	3.48	1.71
		NS		188.07	97.93	0.52	1.50	0.52	1.19
2	KTP	EW	76	254.78	33.36	0.13	0.87	0.26	0.39
		NS		153.58	36.47	0.24	0.59	0.26	0.47
3	TVU	EW	77	228.72	83.98	0.37	2.65	0.70	1.69
		NS		209.87	108.52	0.52	2.17	1.36	1.82
4	PTN	EW	79	150.69	69.08	0.46	1.05	0.44	1.17
		NS		128.13	60.89	0.48	0.87	1.38	1.46
5	THM	EW	84	134.00	77.33	0.58	1.43	1.16	2.14
		NS		150.49	73.22	0.49	1.73	3.48	2.82

From Fig. 2, it is observed that the response spectra of all recorded ground motions show a very wide acceleration sensitive region, and some ground motions contain significant velocity pulses. From Table 1, it is observed that the maximum recorded peak ground acceleration (PGA) was 254.78 cm/s^2, at KTP (class A) in the EW direction. The PGA of the NS component at this site was lower at 153.58 cm/s^2. Interestingly, the four sedimentary sites (Class C) had recorded slightly lower PGA results. The KATNP site, which is closest to the epicenter, recorded a PGA of 158.39 cm/s^2 (EW) and 188.07 cm/s^2 (NS). The TVU site experienced a higher PGA of 228.72 cm/s^2 (EW) and 209.87 cm/s^2 (NS). PTN has a lower PGA in both directions, i.e. 150.69 cm/s^2 (EW) and 128.13 cm/s^2 (NS). The THM site recorded PGA of 134 cm/s^2 (EW) and 150.49 cm/s^2 (NS). The highest peak ground velocity (PGV) of 108.52 cm/s was observed in the NS component at TVU, and the EW component at this site exhibited a PGV of 83.98 cm/s. The least PGV values were observed at the sites of KTP, where the recorded PGVs were 33.36 cm/s (EW) and 36.47 cm/s (NS). KATNP experienced a PGV of 106.68 cm/s (EW) and 97.93 cm/s (NS). PTN recorded PGV of 69.08 and 60.89 cm/s in the EW and NS directions respectively. The THM station had a PGV of 77.33 and 73.22 cm/s.

The predominant periods for the five accelerograms are also examined. The mean period (T_m) is the maximum for the ground motion recorded in the NS direction of the THM site having $T_m = 2.82$ and 2.14 s in the EW direction. The mean periods for the ground motions at the sites of KATNP in EW and NS directions are 1.71 and 1.19 s, respectively. The ground motions from the KTP rock site had the lowest mean period of 0.39 (EW) and 0.47 (NS). The ground motions from the TVU station had a mean period of 1.69 s (EW) and 1.82 s (NS). The PTN station exhibited a mean period of 1.17 s (EW) and 1.46 s (NS). The maximum V_{max}/A_{max} is seen for the KATNP site of 0.67 s (EW) and 0.52 s (NS). The minimum ratio is experienced in the hard rock site of KTP with 0.13 s (EW) and 0.24 s (NS). TVU has a V_{max}/A_{max} ratio of 0.37 (EW) and 0.52 (NS). EW and NS directions of the PTN site had V_{max}/A_{max} ratios of 0.46 and 0.48. THM site had a ratio of 0.58 and 0.49 in EW and NS directions respectively.

3 Fast Fourier Transforms

Figures 3, 4, 5, 6 and 7 show the Fast Fourier Transforms (FFTs). The frequencies lie in the range of 0–10 Hz, barring the KTP ground motions which exhibited frequency content till 20 Hz.

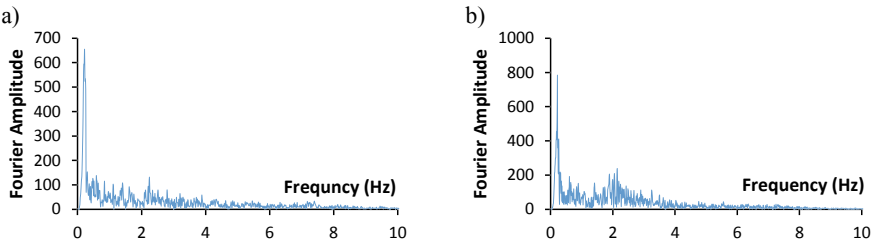

Fig. 3 FFT's of KATNP [**a** EW, **b** NS]

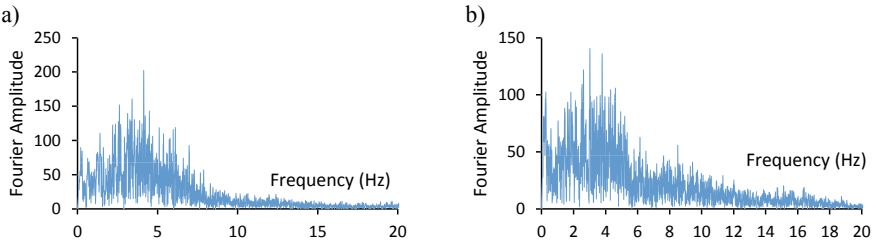

Fig. 4 FFT's of KTP [**a** EW, **b** NS]

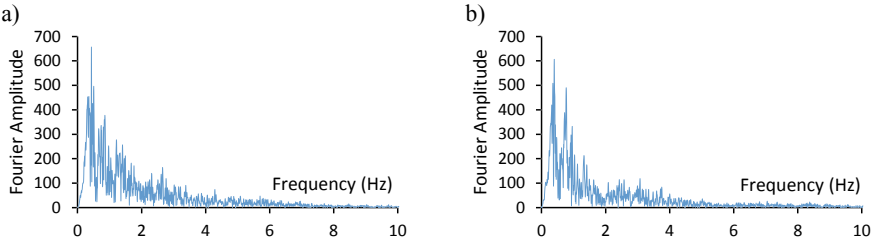

Fig. 5 FFT's of TVU [**a** EW, **b** NS]

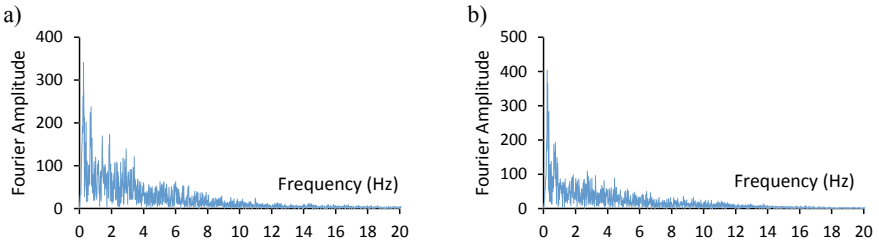

Fig. 6 FFT's of PTN [**a** EW, **b** NS]

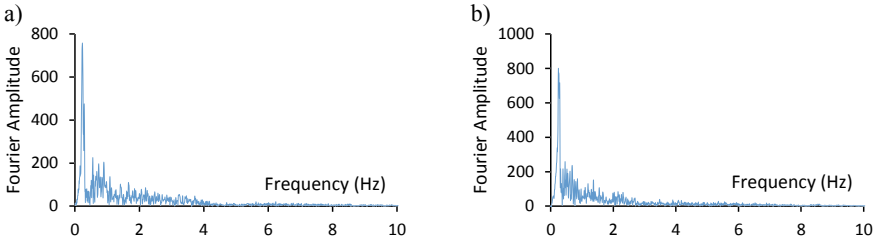

Fig. 7 FFT's of THM [**a** EW, **b** NS]

4 Continuous Wavelet Transforms

CWT is the more ideal candidate for signal or time series analysis due to its more fine-grained resolution. CWTs decompose a signal into wavelets and provide information on both the time and frequency content of non-stationary signals. The analytical Morse wavelet is employed in CWTs.

Figures 8, 9, 10, 11 and 12 present the CWT plots. Figure 8a shows that at the KATNP site, around a time of 45 to 55 s into the earthquake, a very high amplitude wave, corresponding to a magnitude of 60 units, arrived in the EW direction, and had a frequency corresponding to a period of 4–6 s. This indicates that tall structures in the region would have been severely affected due to the seismic wave. The observations from Fig. 8b for the NS component of the wave are similar with a slightly lower amplitude of the seismic wave. McGowan et al. (2017) assigned an intensity of VIII based on the damage to unreinforced masonry structures with timber near the KATNP station. URM structures and URM infills were damaged (McGowan et al. 2017). Based on the damage to mid-rise (4–7 storey) RC structures near the KATNP station, an intensity level of VII was assigned (McGowan et al. 2017). From Fig. 9a, it is observed that at the KTP site, around a time of 27–28 s into the earthquake, a very high amplitude wave, corresponding to a magnitude of 110–120 units, arrived in the EW direction, with periods ranging from 0.2–0.3 s. This indicates that the seismic waves would have damaged low-rise structures. The observations from Fig. 9b for the NS component of the wave are similar with a slightly lower magnitude of 50–60

units. It has been reported that at the KTP station, less than 1% of the structures were impacted and the majority were safe (McGowan et al. 2017).

From Fig. 10, it is observed that the TVU site had multiple high amplitude seismic waves at various time instants of the earthquake. Figure 10a shows that the first two high amplitude bursts in the EW component were noted at around 28 to 38 s into the earthquake, with a magnitude of 45–70 units, in the low-frequency region, i.e. causing damage to tall structures with a natural period of 2–4 s. Another high amplitude wave was observed at 43 s into the earthquake with a magnitude of 45–70 units: however, this wave had a higher frequency (period of 0.5–1.1 s). Figure 10b shows that similar effects were observed in the NS directions, about 26–35 s into the earthquake wave when seismic waves with periods corresponding to 2–4 s arrived with a magnitude of 45–65 units. In the NS direction, another high amplitude wave was observed at 27–40 s into the earthquake wave and medium amplitude waves at 42–55 s of the earthquake, corresponding to a period of 2–3 s were observed. At a later stage, i.e. 50 s into the earthquake wave, high amplitude waves (of 45 to 60 units) corresponding to periods of 0.9–1.1 s were observed. McGowan et al. (2017) assigned an intensity of VII based on the damage to unreinforced masonry structures with RC slabs near the TVU station. It has been reported that a few masonry buildings completely collapsed

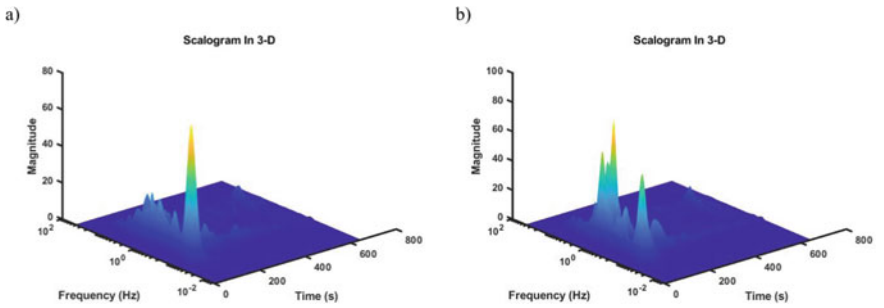

Fig. 8 CWT's of KATNP [**a** EW, **b** NS]

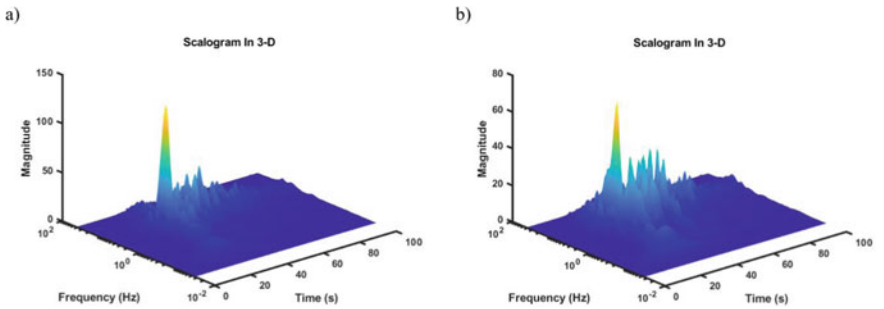

Fig. 9 CWT's of KTP [**a** EW, **b** NS]

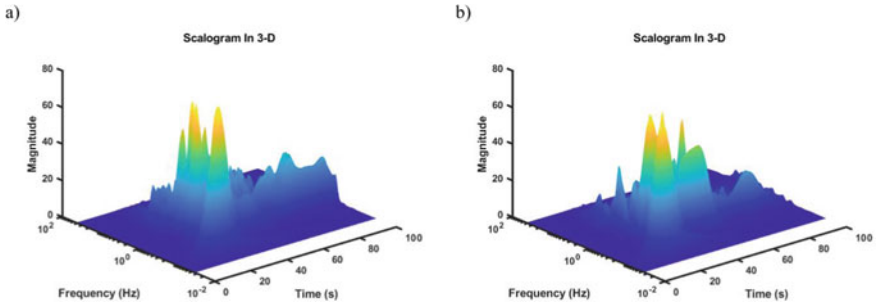

Fig. 10 CWT's of TVU [**a** EW, **b** NS]

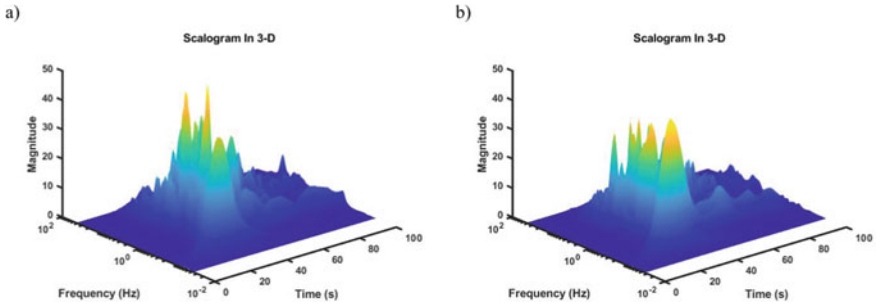

Fig. 11 CWT's of PTN [**a** EW, **b** NS]

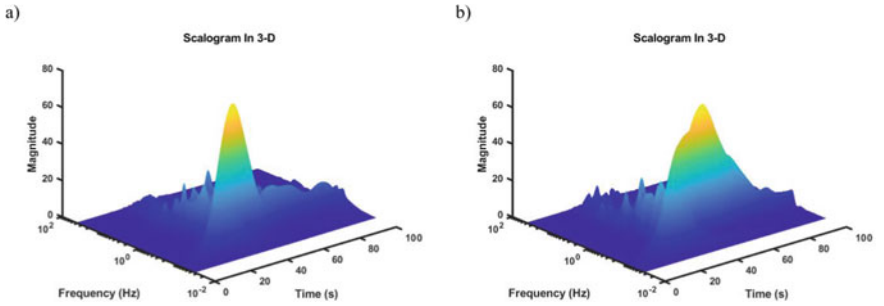

Fig. 12 CWT's of THM [**a** EW, **b** NS]

(McGowan et al. 2017). Similarly, an intensity level of VII was also assigned based on the damage to mid-rise (4–7 storey) RC structures near the TVU station.

Figure 11 shows that the PTN site also observed multiple high amplitude waves in both directions. From Fig. 11a it is observed that in the EW direction, at 25–35 s into the earthquake ground motion, smaller magnitude waves of 30–35 units with periods of 1.2–1.4 s arrived at the site and were followed by higher magnitude waves of 30–45 units having periods of 1 to 1.1 s. At 32–35 s into the earthquake

ground motion, higher frequency waves, corresponding to periods of 0.3–0.7 s, were observed. Around 37–40 s into the earthquake ground motion, high amplitude waves with periods of 0.2 to 0.5 s were observed. Finally, at 40–45 s into the earthquake, high amplitude waves with periods of 0.5–0.8 were observed. In the NS direction, at 25–35 s of the earthquake, damage to taller structures of a resonating period of 3–5 s could be observed with waves of the magnitude of 25–40 units. And at the same time instants, i.e. at 27–35 s high amplitude waves with periods corresponding to 1–1.1 s were observed. McGowan et al. (2017) assigned an intensity of VII based on the damage to unreinforced masonry structures with RC slabs near the TVU station. An intensity level of VII was assigned based on the damage to low rise (1–3 storey) structures near the TVU station. Similarly, an intensity level of VII was assigned based on the damage to mid-rise (4–7 storey) RC structures near the TVU station. However, an intensity of VIII was assigned based on the severe damage to unreinforced masonry structures with timber near the TVU station.

Figure 12 shows CWTs for THM sites, which is the farthest site at 84 km epicentral distance but had a considerably high amount of damage which appears to be due to the sedimentary nature of the soil at the site. From Fig. 12a, it is observed that at the time instants of 28–48 s of the earthquake, the EW components observed high amplitude seismic waves (45–70 units), corresponding to periods of 1.2–1.5 s, thus affecting taller structures. Between 48 to 52 s into the earthquake ground motion, medium to high amplitude waves (of 40–45 units) were observed with a period of 1.0 to 1.1 s. Figure 12b shows CWT plots for the NS component of the wave, which exhibits amplitudes of 45–65 units during the 30–70 s of the earthquake with periods of 1.2–1.4 s corresponding to taller structures. At this station, most RC structures were observed to be relatively safe with a low level of damage (McGowan et al. 2017).

5 Conclusions

The 2015 Nepal earthquake caused widespread destruction to old historical buildings and URM structures, in and around the Kathmandu valley. The earthquake also caused damage to RC structures in the Kathmandu valley, though comparatively, their performance was better than URM structures. It has been observed in reconnaissance surveys that damage was confined to specific areas due to local soil characteristics and due to the sequence of earthquake waves. Strong ground motions were recorded at five stations in the Kathmandu valley. In this study, these ground motions are analyzed both in the time domain and also in the frequency domain. From the time-domain analysis, key characteristics, such as PGA, PGV, Arias Intensity, and single parameter estimates of frequency, T_p, and T_m, of the seismic waves are obtained and tabulated. The frequency-domain analysis is performed using fast Fourier transforms (FFTs). From the FFTs, the true damage potential of the seismic waves is observed to be unclear. Results from the CWT analyses indicate that the primary

reason for structural damage is the presence of large-amplitude waves with frequencies that are similar to the fundamental period of buildings. Such high amplitude waves at frequencies close to tall structures were observed at the KATNP station. Further, the damage is pronounced if the frequencies are sustained in time or if the arrival of another frequency matches the altered frequency of a previously damaged structure. The CWTs of strong ground motions recorded from various sites in the Kathmandu valley substantiate the recorded structural damage observations available from various reconnaisance studies. However, since strong ground motion data is available only from five stations, the conclusions from this study are limited to examined regions only.

References

Gautam D, Chaulagain H (2016) Structural performance and associated lessons to be learned from world earthquakes in Nepal after 25 April 2015 (MW 7.8) Gorkha earthquake. Eng Fail Anal 68:222–243

Whitney R, Agrawal AK (2017) Ground motion characteristics of the 2015 Gorkha, Nepal, earthquake and its effects on a prototype unreinforced masonry building. J Struct Eng 143(4):04016220

Goda K et al (2015) The 2015 Gorkha Nepal earthquake: insights from earthquake damage survey. Front Built Environ 1:8

USGS (U.S. Geological Survey, 2015) M 7.8 East of Khudi, Nepal
https://earthquake.usgs.gov/earthquakes/eventpage/us20002926/executive

Parameswaran RM et al (2015) Seismotectonics of the April–May 2015 Nepal earthquakes: An assessment based on the aftershock patterns, surface effects and deformational characteristics. J Asian Earth Sci 111:161–174

Gautam D, Fabbrocino G, de Magistris FS (2018) Derive empirical fragility functions for Nepali residential buildings. Eng Struct 171:617–628

Building Code Development Project (1994) Seismic hazard mapping and risk assessment for Nepal; UNDP/UNCHS (Habitat) Subproject: NEP/88/054/21.03. Kathmandu: Ministry of Housing and Physical Planning

Rana BSJB (1935) The Great Earthquake of 1934 in Nepal. 2nd ed. Jorganesh Press, Kathmandu

National Planning Commission Nepal (NPC) (2015) Post disaster need assessment. Kathmandu: Government of Nepal

Dhakal YP, (2016) Analysis of strong ground motions and site effects at Kantipath, Kathmandu, from 2015 Mw 7.8 Gorkha, Nepal, earthquake and its aftershocks. Earth Planets Space 68(1):1–12

Takai N et al (2016) Strong ground motion in the Kathmandu Valley during the 2015 Gorkha, Nepal, earthquake. Earth Planets Space 68(1):1–8

McGowan SM, Jaiswal KS, Wald DJ (2017) Using structural damage statistics to derive macroseismic intensity within the Kathmandu valley for the 2015 M7. 8 Gorkha, Nepal Earthquake. Tectonophysics 714:158–172

Comparative Analysis of TANK and SimHyd Rainfall-Runoff Models in the Hemavathi Watershed, Cauvery Basin, India

Nagireddy Masthan Reddy, Subbarayan Saravanan, Leelambar Singh, and Devanantham Abijith

Abstract Water is one of the essential resources of a country, which controls human development activities and very much influences living things. Hydrologists had been interested in the discharge and runoff caused by precipitation. This study compares two daily conceptual models, TANK and SimHyd, using the Rainfall-Runoff Library (RRL) tool and suggests which model is suitable for the Hemavathi watershed. The daily rainfall and evapotranspiration were the inputs in the TANK and SimHyd to determine daily discharge. The daily streamflow was utilized to calibrate models from 1990 to 2006 and then validated for 2007 to 2015. These model parameters are optimized using the genetic algorithm technique. Model prediction effectiveness was assessed using Nash–Sutcliffe efficiency (NSE) and Correlation coefficient (C_C) values. NSE and C_C values during calibration was 0.71, 0.85 for TANK model, 0.66, 0.83 for SIMHYD model, and during verification was 0.64, 0.74 for TANK model, 0.62, 0.72 for SIMHYD model. From the obtained results, the TANK model performs satisfactorily in terms of NSE and C_C compared to the SimHyd model. This paper evaluates the model abilities in streamflow simulation, which policy makers can use.

Keywords Hemavathi watershed · TANK model · SimHyd · NSE · RRL

1 Introduction

Most hydrologists participating in rainfall-runoff modelling have the same goal to improve streamflow simulations. The most challenging task is determining an authentic connection between precipitation and runoff for a watershed. To develop or implement the necessary policies, stakeholders and policymakers need to assess, simulate, and anticipate rainfall and runoff. The complexity of hydrological models varies between simple and complex mathematical models. Rainfall-runoff models are used for many objectives, extending from calculating catchment water yield to estimating the effects of land use land cover (LULC) changes on streamflow

N. M. Reddy · S. Saravanan (✉) · L. Singh · D. Abijith
Department of Civil Engineering, National Institute of Technology, Tiruchirappalli, India
e-mail: ssaravanan@nitt.edu

I. Pal et al. (eds.), *Proceedings of the 2nd International Symposium on Disaster Resilience and Sustainable Development*, Lecture Notes in Civil Engineering 294,
https://doi.org/10.1007/978-981-19-6297-4_7

(Singh and Frevert 2002). Rainfall-runoff models are capable of replicating measured runoff, but determining appropriate model parameters to utilize for evaluating runoff in an ungauged watershed is complicated, and model regionalization is a term used to describe the process of relating calibrated model parameters to catchment characteristics (Blöschl and Zehe 2005; Sivapalan et al. 2003).

The most popular models are empirical or Blackbox (system theoretical) models, physically-based models, conceptual models or grey-box models (Chen and Adams 2006). Water resource modellers frequently use Blackbox models to simulate stream flows, such as regression analysis, ANN, fuzzy analysis and additional machine learning techniques (Shortridge et al. 2016). Conceptual models are based on actual empirical connections between different hydrological variables (Liu et al. 2017). They use first-order equations to approximate meteorological inputs and resemble the basin's hydrological processes (Orth et al. 2015). Constructing a qualitative model, establishing a mathematical relation among input data, processes, and outcomes, and implementing a computation model that solves the model equations are all steps in the process, with some parameter values calibration in between (Fenicia et al. 2014). Various conceptual studies have been presented in the literature to provide accurate daily streamflow forecasts at the watershed level, such as GR4J (Perrin et al. 2003) and the TUW model (Parajka et al. 2007). Physically-based models, also known as white-box or mechanistic models, solve a set of differential equations that explain the laws of physics such as mass, energy, and momentum conservation for various hydrological activities in a catchment (Devia et al. 2015; Liu et al. 2017).

Among the widely used physically based models are the HEC-HMS (Scharffenberg and Fleming 2006) and SWAT (Singh et al. 2022; Singh and Saravanan 2022; Arnold et al. 2012). A brief description of the growth of hydrological models and their current situation and prospects for the future was provided by a few people (Devia et al. 2015; Todini 2007). The quality of the data input used for the model impacts the results, and conceptual models depend exclusively on actual observations. The results of conceptual models are mainly dependent on real observations, and the quality of the data input used in the model determines the model's outcome. In the earlier years, several conceptual or grey-box models have been developed, which include the Sacramento model (Brazil and Hudlow 1981), Nash model (Nash 1957), The HBV model (Bergstrom 1992; Bergström 1995), HYMOD (Moore 1985), The TANK model (Sugawara et al. 1984), Boughton model (Boughton 2004), Xinanjiang model (Zhao et al. 1995), The ARNO rainfall-runoff model (Todini 1996), etc.

Local, regional, and watershed scales, the Cauvery basin has water management issues. The growing rivalry to meet rural and urban water requirements, which cut across administration borders, poses considerable challenges for combined water resources management in the watershed. There are still significant gaps in our scientific understanding of Peninsular Indian hydrology, making it more challenging to meet these problems (Horan et al. 2021). Many of Cauvery's catchment areas have already been simulated using the SWAT model (Singh and Saravanan 2022; Gosain et al. 2006), GWAVA (Horan et al. 2021), the Water Evaluation and Planning System (WEAP) model (Bhave et al. 2018), remote sensing methods (Ramachandra et al. 2014), ANN, SCS-CN model (Geetha et al. 2008) and VIC-mHM (Raje et al. 2014).

Sugawara, a Japanese hydrologist, developed a tank model to explain water flow concepts in a drainage basin (Sugawara et al. 1984) and takes advantage of the capabilities of conceptual models (Ekenberg 2016). Results that predict the streamflow on ungauged watershed using rainfall-runoff models largely depends on a small portion of parameters being transferred (Patil and Stieglitz 2014). The simplicity of conceptualizing hydrological responses, obtaining satisfactory results, and requiring minimal data are reasons for hydrologic modellers to consider lumped models as effective platforms, mainly when resources are scarce (Amiri et al. 2019; Goodarzi et al. 2018). Comparison of two conceptual lumped models TANK and AWBM using RRL toolkit with physically distributed model SWAT for Tandula basin, India which has an area of 827 km^2 and compared NSE values for the best model and concluded TANK models performs better as compared to AWBM and SWAT (Jaiswal et al. 2020). One more study has shown that the TANK model performs better than AWBM for a region located in Balod district, Chhattisgarh region of India and takes major assessment criteria are NSE, Correlation coefficient, etc. (Ali et al. 2019). TANK model and its applicability challenges, particularly in the Province of Aceh, which is located in Indonesia and finally suggested how the simulation of tank model results can be improved (Basri et al. 2013). SimHyd model runoff from four bases, i.e., direct surface runoff from impervious areas, infiltration excess runoff, interflow, and baseflow from groundwater storage. Additional technical details can be found in Chiew et al. (2002), the RRL toolkit user guide (Podger 2003). SIMHYD was applied to approximately 300 catchments over Australia (Chiew and Siriwardena 2005).

The main objective of this study is to evaluate the model performance of conceptual rainfall-runoff models, i.e., TANK and SimHyd, to simulate streamflow for the Hemavathi sub-watershed. The suitability of the models was compared and discussed in terms of various error statics. The developed model can be used for climate change, i.e., change in temperature, precipitation and LULC, etc., on future streamflow changes in the catchments.

2 Description of the Study Area

The study area Hemavathi subwatershed is in the Cauvery basin, India, and it is extending from 75°29′ to 75°51′ E longitude and 12°55′ to 13°11′ N latitude having an area of 617 km^2 shown in Fig. 1. The Hemavathi River is the most important tributary of the Cauvery River, an interstate river. The study area is in the Malnad region, on the hills of the Western Ghats, a biodiversity hotspot. It has a temperate climate with a maximum temperature of 27.4 ºC and a minimum temperature of 18 ºC, and it is surrounded by lofty green hills covered in cardamom, pepper, coffee, and areca plantations. The catchment area's head reaches are in the Western Ghats,

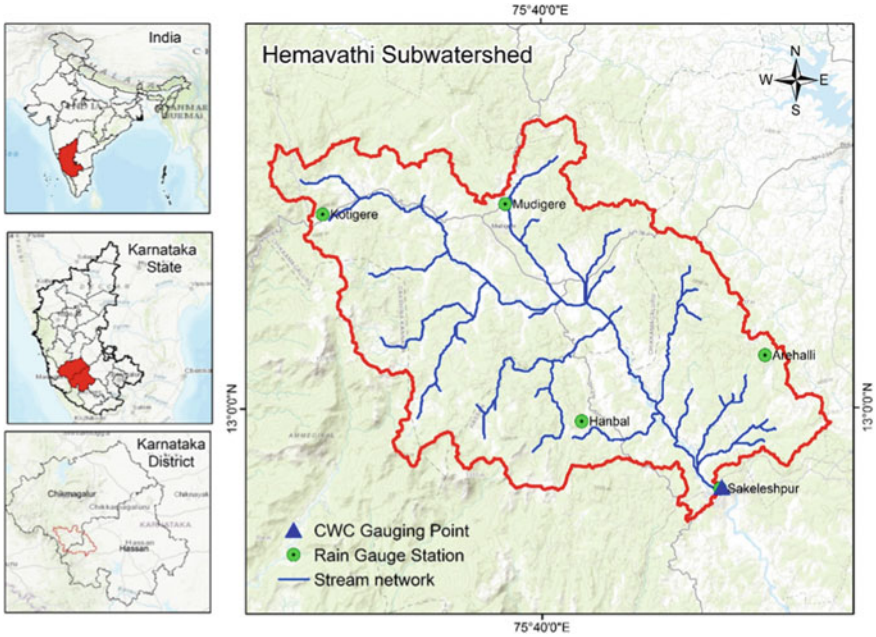

Fig. 1 The study area geographic location is depicted on this map

and most of the rain falls between June and September. And the river will be flooded during this time when nearly the entire yield is received. The highest rainfall in the sub-basin is received during the southwest monsoon, with an annual average rainfall of almost 1534.2 mm shown in Fig. 2. The altitude ranges between 889 m above MSL and 1423 m above MSL. The PET varies from 2 to 5 mm/day depending on several climate factors. The stream outlet gauge is located at Sakleshpur. The study area's land use primarily consists of the vegetation and forest. Peninsular gneiss dominates the geology of the study area, and red loamy and clay sandy soils are found there which is shown in Fig. 2.

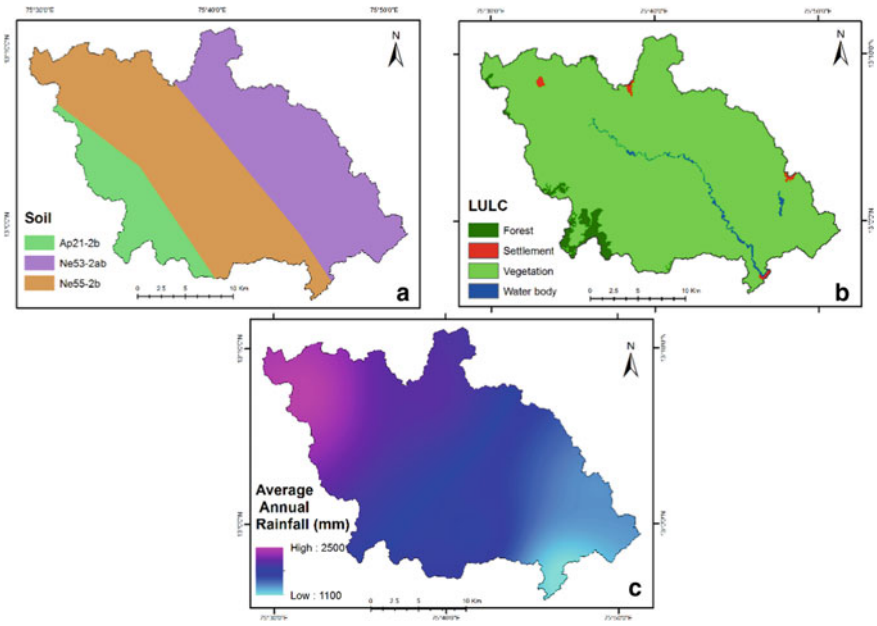

Fig. 2 Soil **A**, LULC **B** and Average annual rainfall (in mm) **C** map of the study area

3 Materials and Methods

3.1 Data Used

The daily stream gauge level from 1990 to 2015 has been used for the catchment has been collected from CWC department recorded at Sakleshpur gauging station. The rainfall and climatic data of Sakleshpur have been used, collected from Karnataka state PWD at five rainfall stations shown in Fig. 1. Thiessen polygon method has been used to estimate average precipitation over the study area. The Sakleshpur climatic station's climatic data have been used in rainfall-runoff modelling to calculate PET using the Hamon equation. Data from the Landsat-8 satellite, which is atmospheric correction was performed later. Anderson's Level 1 classification was used to classify using the supervised classification technique. The layers used in this study are 30*30 m spatial resolution. Table 1 shows various data sources such as precipitation, LULC, Soil data, etc.

Table 1 Data source table

Parameters	Data source	Source location
Discharge	Central Water Commission, (CWC) Water Resources Information System (WRIS)	http://www.cwc.gov.in/water-resources-information-system-wris
Landuse and Landcover	Landsat 8 OLI/ Date Acquired: 2015/12/22 Path: 145 Row: 051	https://earthexplorer.usgs.gov/
Precipitation, Temperature	Karnataka Public works department (KPWD)	https://kpwd.karnataka.gov.in/english
Soil	National Bureau of Soil Survey and Land Use Planning (NBSS and LUP)	https://www.nbsslup.in/

3.2 TANK Model

A tank model (Sugawara and Funiyuki 1956) consisting of four tanks stacked straight up in a row, as illustrated in Fig. 3, is a straightforward model. Rainfall is collected in the topmost tank, and evaporation is gradually lowered. When each tank has been depleted, the evaporation deficiency has been removed from the next bottom tank until every tank has been emptied. The calculated runoffs are discharged from the side outlets. Surface runoff is considered as the topmost tank output, intermediate runoff is regarded as the second tank output, sub-base runoff is considered as the third tank output, and baseflow is considered as the fourth tank output. Even though this is a simple concept, the TANK model behaviour is not so straightforward. Each store's content has a significant impact on the model's behaviour. The runoff generated by the same precipitation and different storage volumes varies dramatically. The tank model is used to simulate daily streamflow based on daily rainfall and evapotranspiration inputs. The phenomenon of preliminary precipitation loss is unnecessary because its impact is accounted for in the tank model's non-linear structure.

The sum of the runoffs from each tank is used to calculate the total runoff. Each tank's runoff is calculated as below

$$q = \sum_{x=1}^{4} \sum_{y=1}^{nx} (C_x - H_{xy}) a_{xy} \tag{1}$$

where "q" is the depth of runoff in mm is shown in Eq. 1, C_x is the water level in the "x" tank, H_{xy} is the height at the outlet, and a_{xy} is the coefficient of runoff for the tank outlet in question. Suppose the water level is located lower the outlet, discharge won't take place. The Beken's formula used for evapotranspiration,

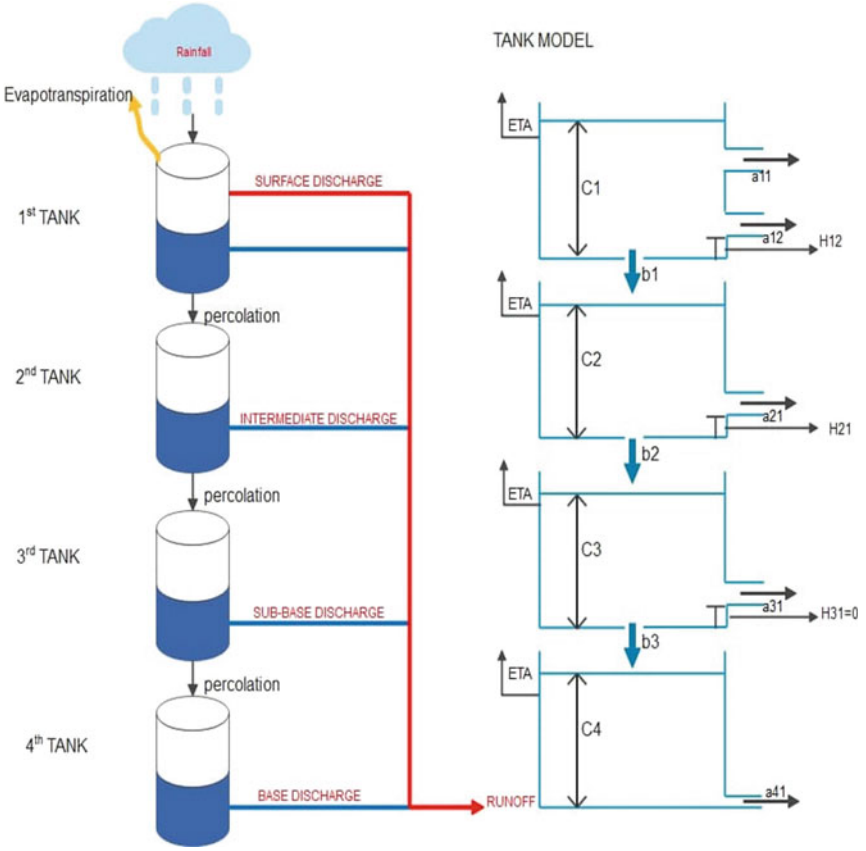

Fig. 3 TANK model structure in RRL

$$ETa = ETp * (1 - \exp(-\alpha \sum_{x=1}^{4} C_x)) \tag{2}$$

where ETa is referred to as evapotranspiration in mm is represented in Eq. 2, α referred to as a coefficient of evapotranspiration (0.1). Each tank's infiltration is calculated using the following Eq. 3 and referred to as I_x (in mm), and B_x is referred to as the coefficient of infiltration in tank x.

$$I_x = C_x B_x \tag{3}$$

For each model parameter, the RRL is configured with default values. These default settings define the beginning parameter value, as well as the parameter's minimum and maximum values. Default values for the SimHyd model are listed in Table 2.

Table 2 Parameter values by default for the Tank model

Parameter	Minimum	Default value	Maximum
First outlet height of the first tank (H_{11}) (in mm)	0	0	500
Second outlet height of first tank (H_{12}) (in mm)	0	0	300
First outlet height of second, third, and fourth tanks (H_{21}, $H_{31,}$ and H_{41}) (in mm)	0	0	100
Coefficient of runoff from various tanks outlets (a_{11}, a_{12}, a_{21}, $a_{31,}$ and a_{41})	0	0.2	1
Coefficient of Evaporation (α)	0	0.1	1
Coefficient of infiltration in tanks 1,2, and 3 (b_1, $b_{2,}$ and b_3)	0	0.2	1
Tanks water level (C_1, C_2, $C_{3,}$ and C_4) (in mm)	0	20	100

3.3 SimHyd Model

SIMHYD model (Chiew et al. 2002) based on each day precipitation and potential evapotranspiration (PET) data using this data predicts daily discharge at the gauging site. SIMHYD is a simplified HYDROLOG model developed in 1972 in a daily conceptual rainfall-runoff model (Porter and McMahon 1975) and MODHYDROLOG (Chiew and McMahon 1994). This model has 7 parameters, contrasted to seventeen for HYDROLOG and nineteen for MODHYDROLOG. Figure 4 describes SIMHYD as a simple daily rainfall-runoff conceptual framework. The interception store is first filled with daily precipitation in SIMHYD, which is then emptied every day. Excess precipitation is then carried out by a function to determine infiltration capacity. Surplus rainfall that surpasses infiltration capacity is referred to as infiltration excess runoff.

Infiltrated moisture is applied by a function that is diverted to a stream as interflow, groundwater as a soil moisture store and recharge. The interflow is first calculated as a linear function of soil moisture. As a result, the interflow simulation equation attempts to simulate both the interflow and saturation excess runoff activities. The recharge of groundwater is then calculated the same interflow, which is a linear function of soil moistness. Existing moisture is absorbed by the soil moisture store. The rate of areal PET as a linear function of soil moistness, the soil moisture store is computed. However, it cannot be greater than the atmospherically controlled rate. The capacity of the soil moisture store is limited, and it spills to meet the groundwater reservoir. Infiltration excess runoff, interflow, and baseflow are the three sources of runoff estimated by the model.

For each model parameter, the RRL (Podger 2003) is configured with default values. These default settings define the beginning parameter value, as well as the parameter's minimum and maximum values. Default values for the SimHyd model are listed in Table 3.

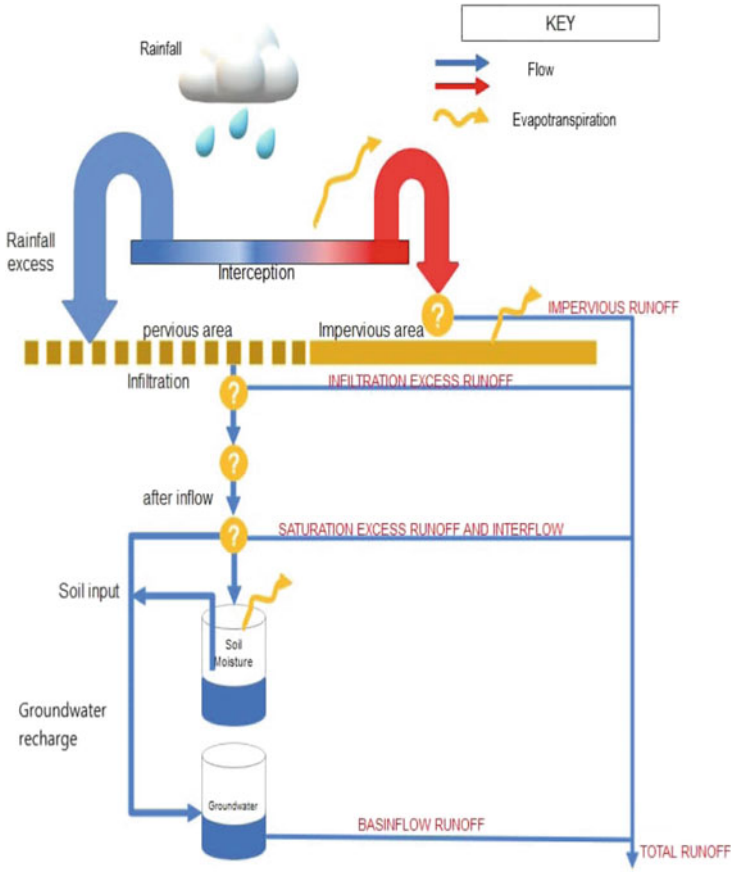

Fig. 4 SimHyd model structure in RRL

Table 3 Default SimHyd model parameter values

Parameter	Minimum	Default value	Maximum
Coefficient of baseflow	0.0	0.3	1.0
Impervious Threshold	0	1	5
Coefficient of Infiltration	0	200	400
Infiltration Shape	0	3	10
Coefficient of Interflow	0.0	0.1	1.0
Pervious Fraction	0.0	0.9	1.0
Rainfall Interception Store Capacity	0.0	1.5	5.0
Coefficient of recharge	0.0	0.2	1.0
Soil Moisture Store Capacity	1	320	500

3.4 Model Assessment Criteria

Statistical fitness parameters can be employed to assess the model performance. Two criteria, NSE and C_c were used in this study. Nash and Sutcliffe formulated the NSE in 1970. It calculates the ratios of variance of something like the observed data for the model and is widely used for hydrology. The Nash–Sutcliffe efficiency coefficients vary from $-\infty$ to 1. If NSE is 1 it represents actual and simulated values are perfectly aligned. Similarly, an NSE of 0 means that the simulation results are just like the mean of the actual dataset. If NSE is in between 0.75 to 1, model performance is very good. If it lies between 0.65 to 0.75 and 0.5 to 0.65, model performance is good and satisfactory, and If NSE is less than 0.5, model is unsatisfactory (Moriasi et al. 2007). The following Eq. 4 used to calculate the NSE

$$NSE = 1 - \frac{\sum_{T=1}^{n} (Q_S^T - Q_A^T)^2}{\sum_{T=1}^{n} (Q_A^T - \overline{Q}_A)^2} \tag{4}$$

where $\overline{Q}_A$ is mean of actual discharges, $\overline{Q}_S$ is mean of simulated discharges, Q_S^T is simulated discharge and Q_A^T is actual discharge at 'T' time. The second statistical parameter is the C_c evaluates the extent of similarity between actual and forecasted data and indicates the amount of variation explained between actual and simulated values. C_c is zero for actual and simulated data entirely independent. C_c is calculated using Eq. 5 shown below

$$C_C = \frac{\sum_{T=1}^{n} \{(Q_A^T - \overline{Q}_A)(Q_S^T - \overline{Q}_S)\}}{\sqrt{\sum_{T=1}^{n} (Q_A^T - \overline{Q}_A)^2} \sqrt{\sum_{T=1}^{n} (Q_S^T - \overline{Q}_S)^2}} \tag{5}$$

4 Results and Discussion

Whether simple or complex, the effectiveness of models is defined by their potential to reproduce the system response. NSE and the C_C were utilized as the best fit criterion for choosing a suitable model. For the Sakleshpur basin, the RRL library (Podger 2003) was used to create conceptual models such as the TANK model and SimHyd model. Daily rainfall, PET, and stream discharge for the Sakleshpur basin over 26 years from 1990 to 2015 were used as input to the models before modelling. The TANK and SimHyd model's results are shown below. The genetic algorithm (GA) is used in this work to optimize the parameters (Holland 1984).

In a population of observations, the genetic algorithm queries and operates instead of the parameter values themselves by coding the parameter set. The transition rules are probabilistic. A genetic algorithm is used for the study area to carry out parameter optimization with the optimizer parameters values given as maximum iterations 50, Prob. Mutation 0.01, Nb. Points 40, and Trapezoidal PDF as 2.

4.1 TANK Model

Daily rainfall was collected from a nearby rain gauge station, and evapotranspiration was determined using the Thornthwaite equation. The model used data from 1990–1994 for warm-up, 1995–2006 for calibration, and 2007–2015 for verification. The model parameters were optimized using GA to process the values of the parameters. Figure 5 provides a schematic interpretation of observed and calculated streamflow runoff for the TANK model. Table 4 represents the enhanced parameters for the TANK model in the RRL toolkit. During calibration and validation, the model NSE was 0.71 and 0.64, respectively, which is a good match (Moriasi et al. 2007). During calibration and verification, the TANK model's Correlation values were 0.85 and 0.74, respectively. In both calibration and validation, the NSE value was observed to be more than 0.6 for daily streamflow values. The monthly streamflow NSE values were observed to be more than 0.8 during calibration and validation, which resembles a good simulation. Perfect results were achieved when the NSE value is 1 and the Correlation coefficient is best when it reaches 1. TANK model achieved the best results in terms of NSE and C_c.

4.2 SimHyd Model

The model was warmed, calibrated, and validated for 1990–1994, 1995–2006, and 2007–2015, respectively. The SimHyd Model's parameters were calibrated using a genetic algorithm to optimize the parameters. Figure 6 shows the real and calculated runoff from the optimized SIMHYD model, with a good match discovered during calibration. Table 5 represents the optimized parameters for the SimHyd model in the RRL toolkit. The model's Nash–Sutcliffe efficiency was calculated to be 0.66 and 0.62. In which NSE values are quite unsatisfactory during validation. During calibration and validation, the SimHyd model's Correlation values were 0.83 and 0.73. In both calibration and validation, the NSE value was observed to be more than 0.6 for daily streamflow values. The monthly streamflow NSE values were observed to be more than 0.75 during calibration and validation, which resembles better simulation.

Two conceptual TANK and SIMHYD models were used in this study. These models each have their own set of parameters as well as the same optimization technique. These models performance has been tested using certain basic fitness

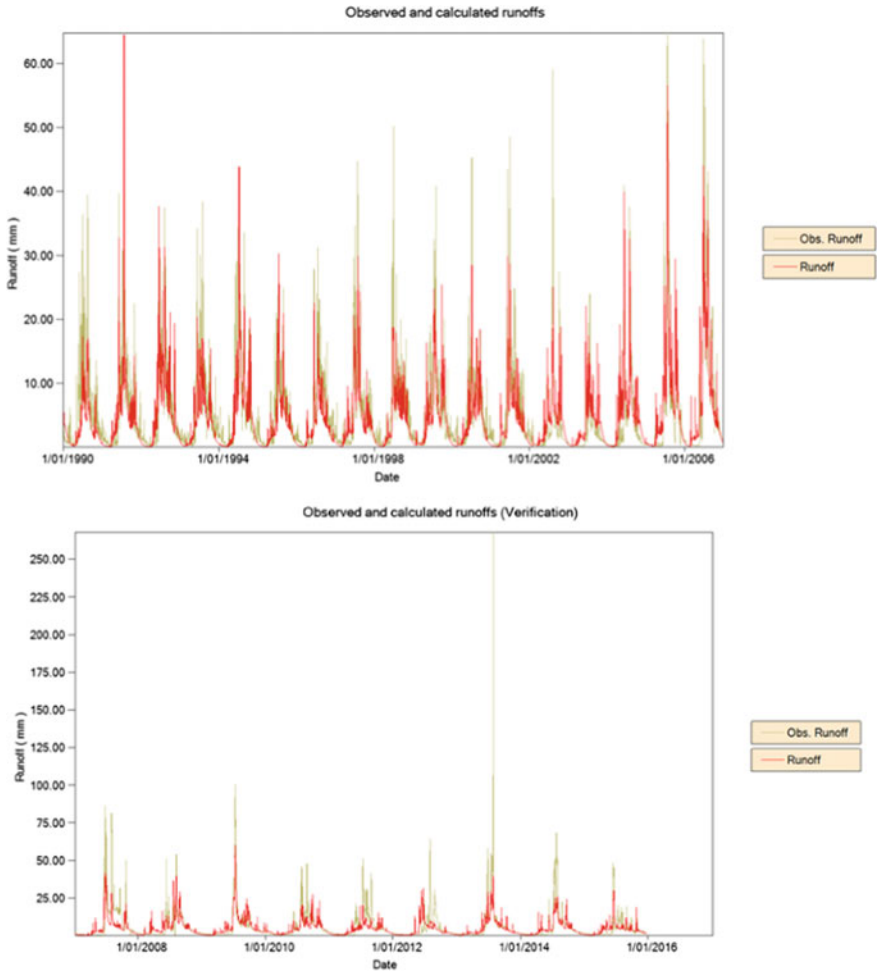

Fig. 5 Observed vs Calculated runoff during **a**. Calibration, **b**. Validation for TANK model

criteria, such as the C_c and NSE. TANK model is most sensitive to the parameters such as Height of outlets at different tanks (H_{11}, H_{12}, H_{21}, H_{31}), Coefficient of runoff from various tanks at the outlet (a_{12}, a_{21}, a_{31}, a_{41}), coefficient of infiltration in tanks (b_1, b_2, and b_3) and model is insensitive for the parameters such as coefficient of evaporation (α) and tank water levels (C_1, C_2, C_3, and C_4). Similarly, the SimHyd model is most sensitive to Baseflow coefficient, Infiltration coefficient, Pervious fraction, RISC, SMSC parameters, and it is insensitive to Infiltration shape, Interflow coefficient, Recharge coefficient. The minimal number of parameters present in the SimHyd model results faster than the TANK model in both calibration and validation. Table 6 shows the best-fit criterion for calibration and verification of various models. The efficiency criteria for the different models revealed that the TANK model used

Table 4 Optimized parameters for the TANK model obtained from RRL toolkit

Parameter	Optimized value	Parameter Range
a_{11}	0.188	0–1
a_{12}	0.137	0–1
a_{21}	0.156	0–1
a_{31}	0.584	0–1
a_{41}	0.058	0–1
Alpha	0.588	0–1
b_1	0.960	0–1
b_2	0.113	0–1
b_3	0.117	0–1
C_1	98.82	0–100
C_2	93.33	0–100
C_3	4.705	0–100
C_4	75.29	0–100
H_{11}	194.11	0–500
H_{12} ($<H_{11}$)	0	0–194.11
H_{21}	29.705	0–100
H_{31}	97.25	0–100
H_{41}	53.33	0–100

for the study was satisfactory during calibration and validation. According to the analysis results, the RRL TANK model outperformed the SimHyd model in both calibration and verification.

Due to the simplicity of conceptual models and complexity of distributed models in India, most of the works carried out based on conceptual, distributed, and comparisons, but conceptual models are easy to understand and interpret results with minimal data such as daily streamflow runoff, daily rainfall, and potential PET and catchment characteristic such as area rather than LULC, soil type, Digital elevation model (DEM) and climate parameters which are used in semi-distributed and distributed models like VIC, SWAT, etc. Conceptual models give only output at a streamflow location, and these models are unfit to find out water balance terms such as baseflow, soil moisture, etc. Jaiswal et al., 2020 conclude that RRL TANK outperformed AWBM and the physically distributed SWAT models in terms of NSE with 0.84 and 0.81 during calibration and validation. Conceptual models were pretty superfast compared to distributed and semi-distributed models due to their data inputs and fewer parameters. A study conducted by Horan et al. 2021 in the upper Cauvery basin has concluded that the ensembled model is most stable for the upper Cauvery basin compared to physically distributed models such as V-VIC V-SWAT, and GWAVA. A study conducted in the Tandula catchment, which is in the Balod district of the Chhattisgarh region of India has concluded that the TANK model performs well

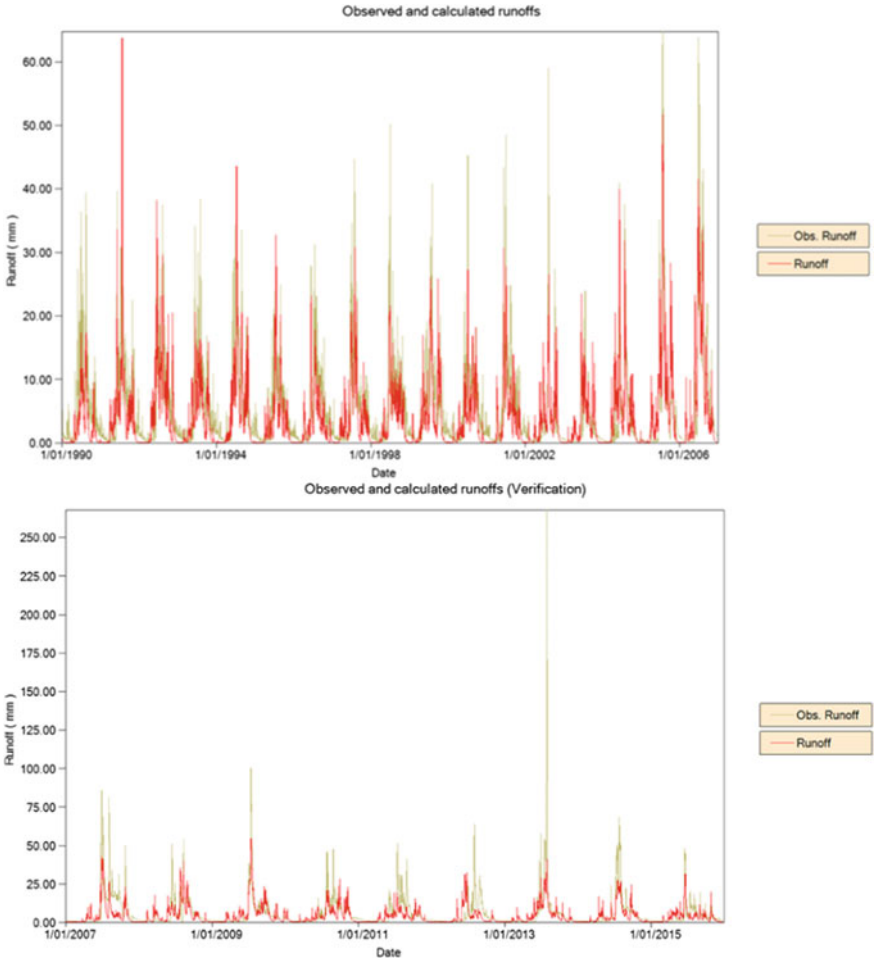

Fig. 6 Observed vs Calculated runoff during **a**. Calibration, **b**. Validation for SimHyd model

compared to AWBM (Ali et al. 2019). A study conducted for the upper Godavari basin concluded that GR4J slightly performs better than AWBM and Sacramento in terms of NSE, C_c and PBIAS (Kunnath-Poovakka and Eldho 2019).

Conceptual models like TANK and SimHyd models are well applicable for the given area, and they may be suitable for most Indian sub-continent parts. TANK model captures medium flows accurately as compared to extreme flows. This may be due to data uncertainty in the basin. Especially during the validation period, there are more extreme events than calibration periods because conceptual models work based on input–output data. This may be the possible reason for low NSE and correlation values during the validation period. But overall, TANK and SimHyd models simulate better results for the selected study area.

Table 5 Optimized parameters for the SimHyd model obtained from the RRL toolkit

Parameter	Optimized value	Range
Coefficient of baseflow	0.125	0–1.0
Impervious threshold	0	0–5
Coefficient of infiltration	345.09	0–400
Infiltration shape	8.98	0–10
Coefficient of interflow	0.815	0–1.0
Pervious fraction	0.831	0–1.0
Rainfall interception store capacity	0	0–5.0
Coefficient of recharge	0.968	0–1.0
Soil moisture store capacity	1	1–500

Table 6 Best-fit criterion for calibration and validation of various models

Method	NSE		C_C	
	Calibration	Verification	Calibration	Verification
TANK model	0.71	0.64	0.85	0.74
SimHyd model	0.66	0.62	0.83	0.72

5 Conclusions

The TANK and SimHyd models in the Hemavathi watershed were compared in this study. Conceptual models are getting popular for many hydrological models being applied in watershed modelling across the world due to their simple structure and excellent performance. On the other hand, hydrologists face a significant challenge in selecting the best model for assessing water resources in a specific region. This difficulty is addressed by modelling systems such as the eWater RRL toolkit, which combines all the data to manage water resources and model in one platform. This research was used to determine which of the two conceptual models included in the RRL framework, TANK and SimHyd, was the most appropriate. The NSE, as the objective function, performs daily calibration at the Source calibration framework. The TANK is suggested as the best model based on NSE shows 0.71 during calibration, which offers good performance and 0.64 during validation which resembles a satisfactory model. SimHyd model given satisfactory performance during both calibration with NSE 0.66 and validation with NSE 0.62. TANK and SimHyd models have shown better performance in terms of C_C values during calibration and validation. TANK model produced C_C value of around 0.85 during calibration and 0.74 during validation. SimHyd model had correlation coefficient values of 0.83 during calibration and 0.72 during validation. TANK captures flow events better than SimHyd, especially the medium streamflow discovered. TANK and SimHyd both models were applicable for the study area, and it may apply to Cauvery Basin and some Indian sub-continent parts. This analysis demonstrates a good relationship

between the predicted and observed runoff. This can be used to predict long-term runoff. SimHyd model is a simple conceptual model which consists of three stores and has seven parameters to optimize parameters during calibration and validation as compared to the TANK model. In terms of NSE and correlation coefficient, the TANK model was far superior for the study area.

References

Ali S, Jaiswal RK, Bharti B, Kumari C (2019) Comparative analysis of conceptual rainfall-runoff modeling. Int J Adv Innov Res 6(2):20–28

Amiri BJ, Gao J, Fohrer N et al (2019) Examining lag time using the landscape, pedoscape and lithoscape metrics of catchments. Ecol Indic 105:36–46. https://doi.org/10.1016/j.ecolind.2019.03.050

Arnold JG, Moriasi DN, Gassman PW et al (2012) SWAT: model use, calibration, and validation. Trans ASABE 55:1491–1508

Basri H (2013) Development of rainfall-runoff model using tank model: problems and challenges in Province of Aceh, Indonesia. Aceh Int J Sci and Technol 2(1):26–36

Bergstrom S (1992) The HBV model-its structure and applications

Bergström S (1995) The HBV model. Computer models of watershed hydrology

Bhave AG, Conway D, Dessai S, Stainforth DA (2018) Water resource planning under future climate and socioeconomic uncertainty in the Cauvery River Basin in Karnataka, India. Water Resour Res 54:708–728. https://doi.org/10.1002/2017WR020970

Blöschl G, Zehe E (2005) On hydrological predictability. Hydrol Process 19:3923–3929. https://doi.org/10.1002/hyp.6075

Boughton W (2004) The Australian water balance model. Environ Model Softw 19:943–956. https://doi.org/10.1016/j.envsoft.2003.10.007

Brazil LE, Hudlow MD (1981) Calibration procedures used with the national weather service river forecast system. In: IFAC Proceedings Volumes. IFAC by Pergamon Press, pp 457–466

Chen J, Adams BJ (2006) Integration of artificial neural networks with conceptual models in rainfall-runoff modeling. J Hydrol 318:232–249. https://doi.org/10.1016/j.jhydrol.2005.06.017

Chiew F, McMahon T (1994) Application of the daily rainfall-runoff model MODHYDROLOG to 28 Australian catchments. J Hydrol 153:383–416. https://doi.org/10.1016/0022-1694(94)90200-3

Chiew FHS, Peel MC, Western AW (2002) Application and testing of the simple rainfall-runoff model SIMHYD. Math Models Small Watershed Hydrol Appl 335–367

Chiew FHS, Siriwardena L (2005) Estimation of SIMHYD parameter values for application in ungauged catchments. In: MODSIM05–International Congress on Modelling and Simulation: Advances and Applications for Management and Decision Making, Proceedings, pp 2883–2889

Devia GK, Ganasri BP, Dwarakish GS (2015) A review on hydrological models. Aquat Procedia 4:1001–1007. https://doi.org/10.1016/j.aqpro.2015.02.126

Ekenberg M (2016) Using a lumped conceptual hydrological model for five different catchments in Sweden

Fenicia F, Kavetski D, Savenije HHG et al (2014) Catchment properties, function, and conceptual model representation: is there a correspondence? Hydrol Process 28:2451–2467

Geetha K, Mishra SK, Eldho TI et al (2008) SCS-CN-based continuous simulation model for hydrologic forecasting. Water Resour Manag 22:165–190. https://doi.org/10.1007/s11269-006-9149-5

Goodarzi MS, Amiri BJ, Navardi S (2018) Investigating the optimization strategies on performance of rainfall-runoff modeling 3:827–817. https://doi.org/10.29007/66vq

Gosain AK, Rao S, Basuray D (2006) Climate change impact assessment on hydrology of Indian river basins. Curr Sci 90:346–353

Holland JH (1984) Genetic algorithms and adaptation. In: Selfridge OG, Rissland EL, Arbib MA (eds) Adaptive Control of Ill-Defined Systems. NATO Conference Series, vol 16, pp 317–333. Springer, Boston, MA. https://doi.org/10.1007/978-1-4684-8941-5_21

Horan R, Gowri R, Wable PS et al (2021) A comparative assessment of hydrological models in the upper cauvery catchment. Water (switzerland) 13:1–25. https://doi.org/10.3390/w13020151

Jaiswal RK, Ali S, Bharti B (2020) Comparative evaluation of conceptual and physical rainfall–runoff models. Appl Water Sci 10:1–14. https://doi.org/10.1007/s13201-019-1122-6

Kunnath-Poovakka A, Eldho TI (2019) A comparative study of conceptual rainfall-runoff models GR4J, AWBM and Sacramento at catchments in the upper Godavari river basin, India. J Earth Syst Sci 128:1–15. https://doi.org/10.1007/s12040-018-1055-8

Liu Z, Wang Y, Xu Z, Duan Q (2017) Conceptual hydrological models. In: Duan Q, Pappenberger F, Thielen J, Wood, A, Cloke H, Schaake J (eds) Handbook of Hydrometeorological Ensemble Forecasting, pp 1–23. Springer, Berlin, Heidelberg. https://doi.org/10.1007/978-3-642-40457-3_22-1

Moore RJ (1985) The probability-distributed principle and runoff production at point and basin scales. Hydrol Sci J 30:273–297. https://doi.org/10.1080/02626668509490989

Moriasi DN, Arnold JG, Van Liew WM et al (2007) Model evaluation guidelines for systematic quantification of accuracy in watershed simulations. Trans ASABE 50:885–900. https://doi.org/10.13031/2013.23153

Nash JE (1957) The form of the instantaneous unit hydrograph. Int Assoc Hydrol Gen Assem Toronto Ontario 3:114–121

Orth R, Staudinger M, Seneviratne SI, et al (2015) Does model performance improve with complexity? A case study with three hydrological models. J Hydrol 523:147–159. https://doi.org/10.1016/J.JHYDROL.2015.01.044

Parajka J, Merz R, Blöschl G (2007) Uncertainty and multiple objective calibration in regional water balance modelling: case study in 320 Austrian catchments. Hydrol Process 21:435–446. https://doi.org/10.1002/hyp.6253

Patil S, Stieglitz M (2014) Modelling daily streamflow at ungauged catchments: what information is necessary? Hydrol Process 28:1159–1169. https://doi.org/10.1002/hyp.9660

Perrin C, Michel C, Andréassian V (2003) Improvement of a parsimonious model for streamflow simulation. J Hydrol 279:275–289. https://doi.org/10.1016/S0022-1694(03)00225-7

Podger G (2003): http://www.toolkit.net.au/rrl

Porter JW, McMahon TA (1975) Application of a catchment model in South Eastern Australia. J Hydrol 24:121–134. https://doi.org/10.1016/0022-1694(75)90146-8

Raje D, Priya P, Krishnan R (2014) Macroscale hydrological modelling approach for study of large scale hydrologic impacts under climate change in Indian river basins. Hydrol Process 28:1874–1889. https://doi.org/10.1002/hyp.9731

Ramachandra TV, Bharath S, Bharath A (2014) Spatio-temporal dynamics along the terrain gradient of diverse landscape. J Environ Eng Landsc Manag 22:50–63. https://doi.org/10.3846/16486897.2013.808639

Scharffenberg WA, Fleming MJ (2006) Hydrologic modeling system HEC-HMS: user's manual. US Army Corps of Engineers, Hydrologic Engineering Center

Shortridge JE, Guikema SD, Zaitchik BF (2016) Machine learning methods for empirical streamflow simulation: a comparison of model accuracy, interpretability, and uncertainty in seasonal watersheds. Hydrol Earth Syst Sci 20:2611–2628. https://doi.org/10.5194/hess-20-2611-2016

Singh VP, Frevert DK (2002) Mathematical models of large watershed hydrology. Water Resources Publication

Sivapalan M, Takeuchi K, Franks SW et al (2003) IAHS decade on predictions in ungauged basins (PUB), 2003–2012: shaping an exciting future for the hydrological sciences. Hydrol Sci J 48:857–880. https://doi.org/10.1623/hysj.48.6.857.51421

Sugawara M, Funiyuki M (1956) A method of revision of the river discharge by means of a rainfall model. Collection Res Pap Forecast Hydrologic Variables 14–18

Sugawara M, Watanabe I, Ozaki E, Katsugama Y (1984) Tank model with snow component. Research Notes of the National Research Center for Disaster Prevention No. 65. Sci Technolgoy, Ibaraki-Ken, Japan

Todini E (1996) The ARNO rainfall-runoff model. J Hydrol 175:339–382. https://doi.org/10.1016/S0022-1694(96)80016-3

Todini E (2007) Hydrological catchment modelling: past, present and future. Hydrol Earth Syst Sci 11:468–482. https://doi.org/10.5194/hess-11-468-2007

Zhao RJ et al (1995) The Xinanjiang model. Comput Model Watershed Hydrol 215–232

Singh L, Subbarayan S, Jacinth Jennifer J, Abhijith D, Sankriti R (2022) Assessment of impact of spatial distribution of rainfall on streamflow modelling using Arcswat in the noyyal river catchment Tamil Nadu, India. In: Hydrological Modeling, pp. 517–526. Springer, Cham

Singh L, Saravanan S (2022) Assessing streamflow modeling using single and multi-site calibration approach on Bharathpuzha catchment, India: a case study. Model Earth Syst Environ 1–14

Singh L, Saravanan S (2022) Evaluation of blue and green water using combine stream flow and soil moisture simulation in Wunna Watershed, India. Water Conserv Sci Eng 1–15

Stability Analysis of a Failure Slope After Treatment as Considering Influence of Rainfall

Tuan-Nghia Do, Lan Chau Nguyen, and Nguyen Trung Kien

Abstract This study investigates stability of a failure slope, which locates at km 34 of the Halong-Vandon highway (Northeast area of Vietnam). The slope was orignially designed with 4 stages and average 40 m height. The concrete plates were employed to cover the slope surface and protect the infiltration of the rainfall herein. Failure took place from May to June 2019 after heavy rainfalls, causing the 1-m-subsidence at crown and the 40-cm-heave at the 1st stage of the slope. The concrete plates were destroyed throughout the failure surface. A 30-m-high MSE wall with 4 stages has been constructed as a retaining structure of the slope. In order to analyze the slope stability considering the influence of rainfall during May and June 2019, the c-phi reduction method coupled with flow analysis in Plaxis software was employed. Results showed that the factor of safety of the slope was closed to 1.0 before treatment, which agreed well with observations, and greater than 1.3 after treatment, which indicated that the slope was stable.

Keywords Slope stability · Plaxis · Rainfall · Finite element method · Strength reduction technique

1 Introduction

Landslides are one of the most common disasters that often take place in mountaneous areas, especially, along road, where cut slopes are popular. Once landslides occur, they will cause economic and human losses. In order to estimate stability of slopes, the limit equilibrium methods are usually adopted by Bishop (1955), Spencer (1967), Morgenstern and Price (1965), etc. In principle, these methods firstly assume the failure surface of slopes and then calculate the ratio between the resisting forces to the driving forces. The factor of safety is defined as the minimum ratio and the corresponding failure surface is the critical one. Since these methods are quite simple, they have been used by many researchers and pratical engineers.

T.-N. Do (✉) · L. C. Nguyen · N. T. Kien
Thuyloi University, No. 75 Tayson, Dongda, Hanoi, Vietnam
e-mail: dotuannghia@tlu.edu.vn

I. Pal et al. (eds.), *Proceedings of the 2nd International Symposium on Disaster Resilience and Sustainable Development*, Lecture Notes in Civil Engineering 294,
https://doi.org/10.1007/978-981-19-6297-4_8

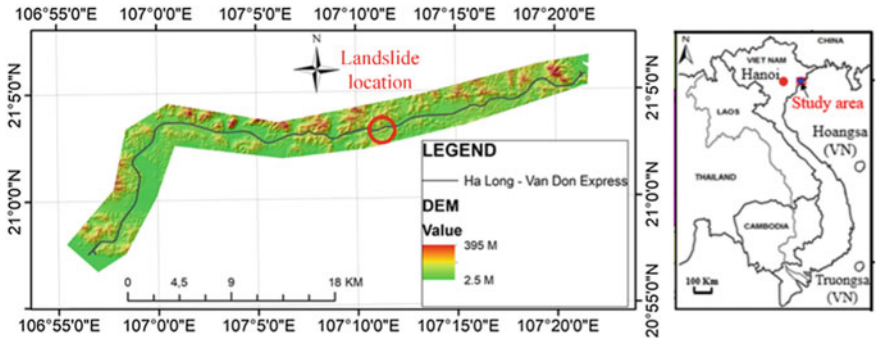

Fig. 1 Location of the investigated area

Due to the fact that most of Vietnam area is mountaineous terrain, it is vulnerable to the risk of landslides (Nguyen et al. 2020). Many highways have been constructed in recent years, which also trigger the occurrence of numerous landslides. Among them the Halong-Vandon highway is a representative case. During the construction of this road, there have been about 80 landslides. One of them is a landslide at km 34, which took place on June, 1, 2019 in Hoabinh commune, Hoanh Bo district, Quang Ninh province. The landslide site is located at 21°3′13.87″N and 107°11′12.74″E as shown in Fig. 1. The landslide occurred on a cut slope, which has been stabilized using the retaining wall at the slope toe and concrete plates along the slope. There are some observations by road managers that the landslide was triggered by rainfall from May 10 to June 1, 2019. However, so far there are no researches to demonstrate that.

The aim of this study is to investigate the effect of rainfall on the landslide at km 34. Based on that the road managers can have more understanding on the failure mechanism of landslide and put forward appropriate measurements.

2 Landslide at km 34

2.1 Regional Settings

The investigated area is located at northeast of Halong city. Most of the topography is hilly with low-relief mountains with an average altitude from 150 to 250 m and slope angles from 15 to 25°. The landslide at km 34 lies on the Hon Gai and Bac Son formations with limestone, sandstone, siltstone, conglomerates, gritstones, shale, and thin lenses of coal. In this area, the climate has two separate seasons, including summer (from May to October) and winter (from November to April) with heavy rainfall occurs continuously for 2–3 days.

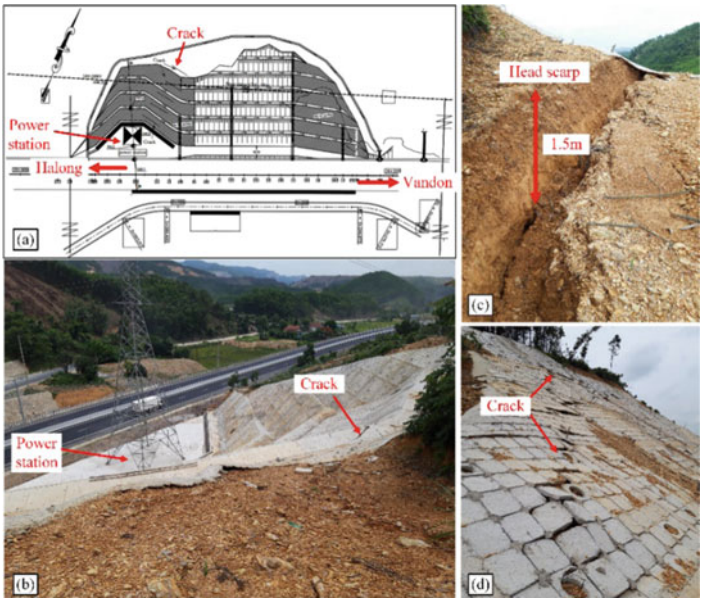

Fig. 2 Field photos of landslide

2.2 Landslide Characteristics

Figure 2 presents an overview of the landslide at km 34 and its geological features. The slope was composed of four stages and located on north-south direction (Fig. 2a). This was a deep-seated slump type. The head scarp was observed at 1.5 m height. Cracks took place from the 1st to 4th stages of the slope as shown in Figs. 2a, 2b, and 2d. Although the retaining wall and concrete plates has been adopted, the slope remained unstable. The development of cracks along the concrete plates could be observed in Fig. 2d. In the past, the power staion was constructed on the top of slope. Due to the occurrence of previous cracks during the construction of the road, it has been moved to the toe of slope. However, landslide still occurred toward it.

2.3 Geological Drilling and Soil Properties

Layout of boreholes is presented in Fig. 3a, including HK1, HK2, HK3, and HK4. It can be seen that all the four boreholes was located nearby the power station and the landslide. The drilling deph was 15 m at each of the boreholes. Fig. 3b illustrated the geological cross section A-A'. In this area, the slope strata consists of three layers. The 1st layer is soft yellow sandy clay mixed with small gravel. This layer appears in boreholes HK1, HK3, and HK4 with thickness from 3.7 to 4.7 m. The N_{spt} value

Table 1 Geotechnical properties of soil samples

Properties	Sample (from the bore holes at different elevations)											
	HK1			HK2			HK3			HK4		
	UD1 (1.8–2.0 m)	UD3 (5.8–6.0 m)	UD6 (11.8–12.0 m)	UD1 (1.8–2.0 m)	UD3 (5.8–6.0 m)	UD4 (7.8–8.0 m)	UD1 (2.0–2.2 m)	UD2 (4.0–4.2 m)	UD3 (5.8–6.0 m)	UD1 (1.8–2.0 m)	UD2 (3.8–4.0 m)	UD3 (5.8–6.0 m)
W (%)	23.65	19.20	10.35	19.42	19.32	18.20	23.60	25.13	18.20	25.10	24.40	18.80
γ (kN/m^3)	19.4	19.6	19.6	19.7	19.7	19.6	19.4	19.4	19.7	19.4	19.4	19.6
γ_d (kN/m^3)	15.7	16.4	16.3	16.5	16.5	16.6	15.7	15.5	16.7	15.5	15.6	16.5
Δ (kN/m^3)	26.9	26.8	26.9	26.9	26.9	26.9	26.9	26.9	26.8	26.9	26.9	26.8
n (%)	41.62	38.80	39.39	38.65	38.65	38.27	41.62	42.36	37.69	42.36	42.00	38.42
e	0.713	0.634	0.650	0.630	0.630	0.620	0.713	0.735	0.605	0.735	0.724	0.624
S (%)	89.23	81.16	84.22	82.92	82.49	78.96	89.04	91.97	80.62	91.86	90.66	80.74
LL (%)	34.62	33.20	4.16	33.15	31.15	32.52	34.76	35.72	32.15	35.76	35.39	32.51
PL (%)	18.21	17.45	18.68	17.45	17.32	16.24	18.16	19.46	16.2	20.05	18.75	16.63
Pl (%)	16.41	15.75	15.48	15.70	13.83	16.28	16.60	16.26	15.95	15.71	16.64	15.88
LI (%)	0.33	0.11	0.11	0.13	0.14	0.12	0.33	0.35	0.13	0.32	0.34	0.14
c (kPa)	24.5	26.5	27.1	26.4	26.7	27.3	24.3	24.8	27.5	24.3	24.8	26.8
ϕ (°)	17.52	20.45	19.08	21.05	20.35	19.75	17.60	16.80	19.75	16.42	17.18	20.42

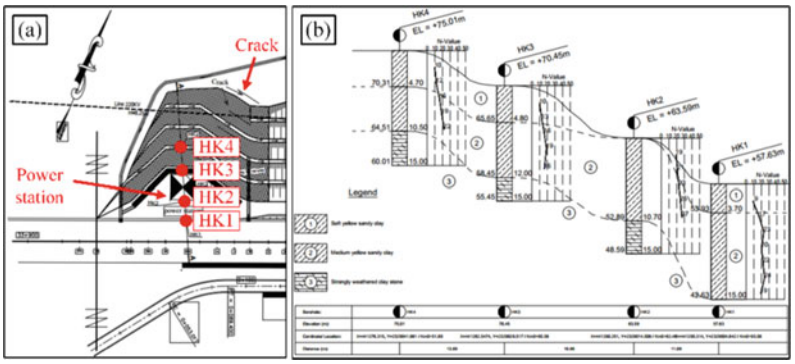

Fig. 3 Layout of boreholes and geological cross section

is from 9 to 13. The 2nd layer is medium yellow sandy clay with N_{spt} value from 19 to 24. This layer is very thick. At the borehole HK1, it is more than 11.3 m thick. The 3rd layer is strongly weathered clay stone sometimes mixed with coal. This is the final layer.

Samples for laboratory tests, including UD1, UD3, and UD6 from HK1; UD1, UD3, and UD4 from HK2; UD1, UD2, and UD3 from HK3; UD1, UD2, and UD3 from HK4, were obtained from different layers of boreholes to measure soil properties as summarized in Table 1. Note that the friction angle and cohesion of soil were determined from direct shear test. In addition, to model the effect of rainfall on stability of the slope, samples at the main soil layers were tested to determine soil-water characteristic curves. Figure 4 shows the tested curves for the air entry vaules of 21 and 17 kPa corresponding to the samples at the 1st and 2nd soil layers, respectively.

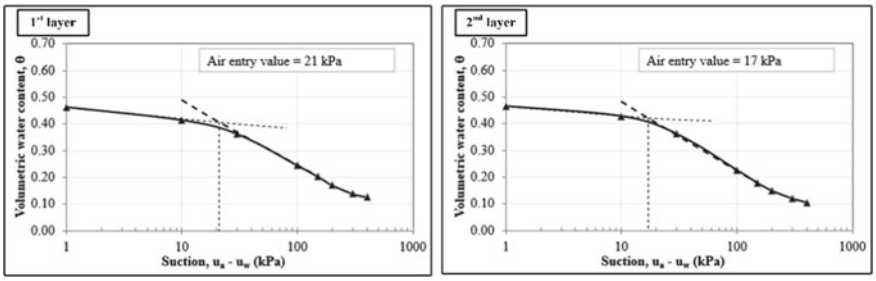

Fig. 4 Soil–water characteristic curve

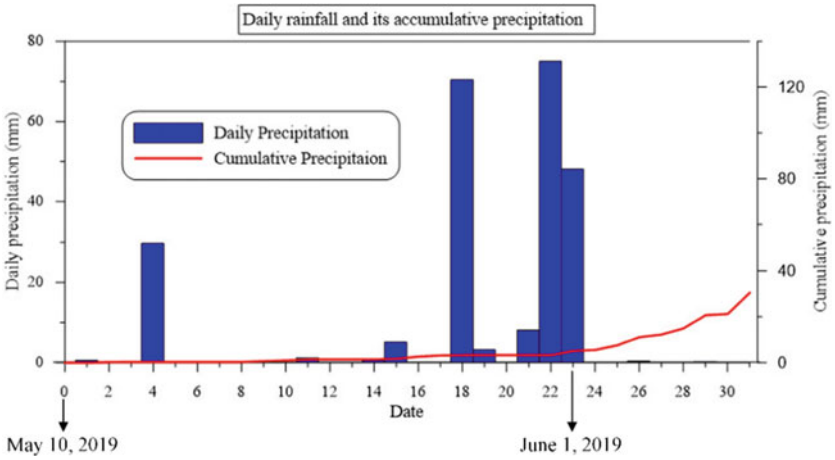

Fig. 5 Daily rainfall and its accumulative precipitation in May and June 2019

2.4 Geological Drilling and Soil Properties

Figure 5 shows the rainfall data before and after the landslide occurrences, which was recorded at the Baichay station. It can be observed that rainfall with moderate intensity happened discontinously during May and June 2019. However, from May 10 to June 1, 2019, the frequency of rainfall is quite high. The greatest rainfall was about 80 mm on June 1, 2019, which corresponded to the occurrence of landslide.

3 Stability Analysis

This study adopted the Seep/W module in Geostudio to predict the change of ground water table and influence of rainfall on the ground surface through transient analysis. The rainfall event from May 10 to June 1, 2019 was taken into account, which was simulated through the water unit flux and time. Due to the fact that the ground water table data corresponding to May 10, 2019 was not recorded, it was assumed that the downstream and upstream levels located at the retaining wall and the top of the 3rd soi layer, respectively. Figure 6 presents the change of ground water tables with time. The infiltration of rainfall could be observed on the ground surface. It can be seen that the ground water table rises clearly during the rainfall event.

The stability analysis was performed using the Slope/W module in Geostudio, at which stability of slope corresponds to rainfall at May 10 and June 1, 2019 was analyzed. As shown in Fig. 7, the factor of safety is 1.034 at May 10, 2019 and 0.968 at June 1, 2019. It is clear that the rainfall event has caused the reduction of factor of safety of the slope. The slope becomes unstable at June 1, 2019 with the

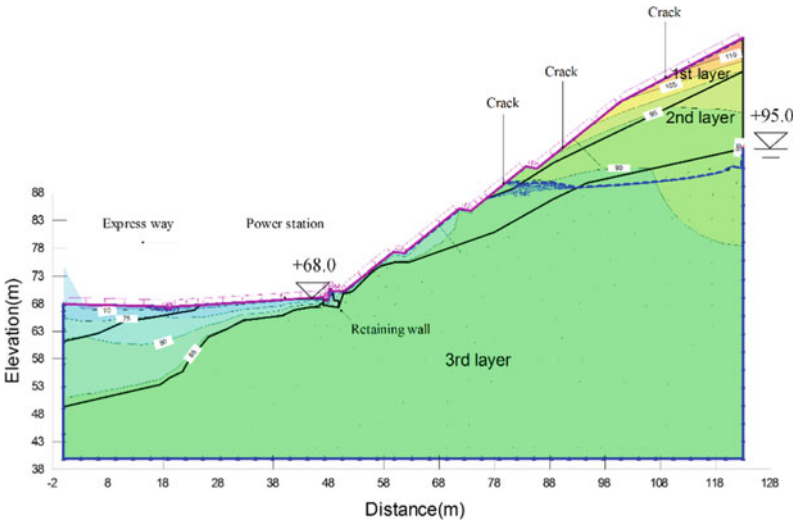

Fig. 6 Total head plot and ground water tables in transient analysis

critical failure surface ranging from the 1st to 4th stages, which agrees well with the observation data.

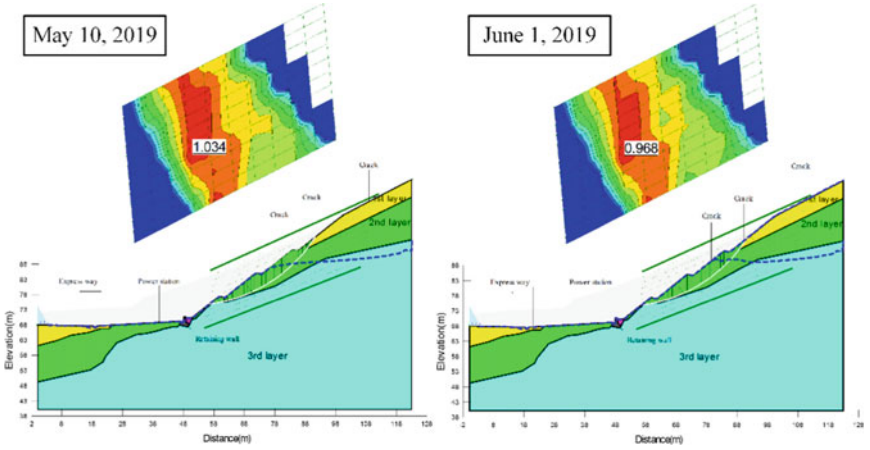

Fig. 7 Slope stability on May 10 and June 1, 2019

4 Conclusions

Based on results of this study, it can be concluded that the failure of slope at km 34 of the Halong-Vandon highway is due to the rainfall from May 10 to June 1, 2019. In principle, the rainfall causes the increase of ground water table, which leads the decrease in effective stress of soil and factor of safety of whole slope. Therefore, besides the structural measurement, it is important to install the drainage system into slope, which can control the ground water table of slope.

References

Bishop AW (1955) The use of the slip circle in the stability analysis of slopes. Geotechnique 5(1):7–17

Morgenstern NR, Price VE (1965) The analysis of the stability of general slip surfaces. Geotechnique 15(1):79–93

Nguyen LC, Pham VT, Do TN (2020) Deep-seated rainfall-induced landslides on a new expressway: a case study in Vietnam. J Landslides 17:395–407

Spencer E (1967) A method of analysis of the stability of embankments assuming parallel inter-slice forces. Geotechnique 17(1):11–26

DRR, Geopgysical and Engineering Perspective

A Study on Seismic Behavior of Hyperbolic Cooling Tower with V and X Columns

C. L. Mahesh Kumar, K. G. Shwetha, B. C. Shanthappa, and K. Manjunatha

Abstract In this day and age, innovative construction technology has improved to a great extent. Cooling tower construction is one of the components of the construction that is still in the process of being improved. Some research is being done to improve the cooling tower's efficiency by changing its structure and design. Evaporative coolers, such as cooling towers, are used to chill water or other working media to temperatures close to the ambient wet-bulb air temperature. Cooling towers eject heat from activities like cooling circulating water in oil refineries and power plants by evaporating water. The cooling tower may now be seen in many thermal power stations. As a result, keeping a structure is an attempt to protect the cooling tower from dangerous earthquakes. Natural draught cooling towers (NDCT) are less in Karnataka. As a result, two natural draft cooling tower models are developed in this article, one with Raker Columns and the other with Meridional Columns, utilizing SAP2000 software, which is a Finite element program. Models are analyzed for seismic loads and responses are determined in terms of Time period, Lateral Deformation, Base Shear, and Axial force for Zone-II. The Meridional columns supported cooling towers have more seismic resistance than raker columns supported cooling towers.

C. L. M. Kumar (✉)
Department of Civil Engineering-VTU RRC, Jnana Sangama, VTU, Belagavi 590018, India
e-mail: Maheshkumar.cl@nmit.ac.in

C. L. M. Kumar · K. G. Shwetha
Department of Civil Engineering, Nitte Meenakshi Institute of Technology, Yelahanka, Bengaluru 560064, India
e-mail: Shwetha.kg@nmit.ac.in

Present Address:
B. C. Shanthappa
SJM Institute of Technology, NH-4 Bypass, PB No 73, Chitradurga 577501, India
e-mail: shanthappa2204@yahoo.com

K. Manjunatha
Department of Studies in Civil Engineering, U B D T College of Engineering, Hadadi Road, Davangere 577004, India
e-mail: drkmanjunatha@gmail.com

I. Pal et al. (eds.), *Proceedings of the 2nd International Symposium on Disaster Resilience and Sustainable Development*, Lecture Notes in Civil Engineering 294,
https://doi.org/10.1007/978-981-19-6297-4_9

Keywords Cooling tower · Seismic loads · Thermal power plants · Meridional columns · Raker columns

1 Introduction

According to the most recent census, India is the world's fifth-largest electricity producer. We find that the thermal power stations contribute roughly 65% of the total power. Six thermal power stations have been developed in Karnataka, with a per-capita production of 5975.91 MW (Kumar et al. 2021a).Coooling tower is also called as hyperbolic cooling tower. The hyperbolic cooling tower is very important and essential component in thermal and nuclear power plants (Naghshineh et al. 2012, Murali et.al 2012).

The cooling tower may now be seen in many thermal power stations. As a result, keeping this structure is an attempt to protect the cooling tower from potentially dangerous earthquakes. A minor earthquake measuring 3.9 on the Richter Scale struck the Dakshin Kannad region of Karnataka, (Kumar et al. 2021b) but the atmospheric and environmental changes necessitate seismic analysis of all structures in and out of Karnataka, particularly important structures such as thermal power stations, where we come across various segments, one of which is the "COOLING TOWER."Natural draft cooling towers are exceptional structures in view their sheer size and complexities (Prabhakar et.al 1990).

A cooling tower is a structure that takes heat from water and releases it into the atmosphere to cool a water stream. Cooling towers can drop water temperatures more effectively than devices that merely use air to evacuate heat, such as a car's radiator, and are thus more cost-effective and energy-efficient.

2 Literature Review

Zhang et al (2011) studied the effect of latitude wind pressure Distribution on the load effects of hyperboloid Cooling tower shells. In this paper, they focused on Internal and external Wind Pressure Distribution, Excited vibration, and instability induced by the wind and predicted the results in terms of base shear or Base force, Meridional forces, Latitude force, Latitude moment, and Base moment under wind excitation. Busch et al. (2002) demonstrated the optimization of a 200 m height natural draught cooling tower by varying the height of throat and inclination of meridian in reducing the stress due to wind load.

Chiranjit Mishra (2015) presented the net pressures, expressed in non-dimensional form as pressure coefficients concerning the velocity at the top of the structure would be governing the circumferential design stresses in the Cooling towers.

For the interference case, the highest net pressure coefficient is obtained as 1.436 at the front stagnation point when the wind incidence angle is about 0°. The minimum

value of Cp is found to be about −0.934 when the wind incidence angle is about 330° and occurs at 105° angle in azimuth concerning the wind. The magnitude of this minimum Cp is well within the current design practice. Overall, there is about a 3% increase in Cp, max, and about 11% increase in Cp, min due to the interference of the surround.

2.1 Objectives of Study

In this paper, an attempt is made to study the seismic response of cooling towers so the objectives of the study are,

- To model the Cooling tower using SAP 2000 Software.
- To find the time period and mode shape of the cooling tower.
- To find the response at top of the cooling tower for seismic forces.

3 Methodology

In this paper two Natural Draft Cooling tower models with raker columns and with X-Columns are considered for three different cases. Gravity load analysis and lateral load analysis is carried out as per the seismic IS code 1893 (Part I): 2002 for both Natural draft Cooling tower models and an effort is made to study the effect of seismic load on them. The Natural draft Cooling tower consists of a hyperboloidal Wall, Top Ring Beam, Bottom Ring Beam, Raker columns. Shell elements are used to model hyperboloidal walls. The top and bottom columns and curving beams are treated as frame elements. The joints between the beam and the column are presumed to be rigid.

Natural Draft Cooling Towers are modelled in two different forms here, namely MODEL I-Raker Columns Natural Draft Cooling Tower.

MODEL II-X-Column Natural Draft Cooling Tower.

Model I is Natural Draft Cooling Tower with Raker(Inclined) Columns in which Shell elements are used to model hyperboloidal walls and Each of the 40 columns has a radial distance of 45° and a length of 5 m. Connectivity between the columns and the hyperboloidal Shell is given by a bottom ring beam.

Model II is Natural Draft Cooling Tower with X-Columns (Meridional) in which Shell elements are used to model hyperboloidal walls and Each of the 72 columns has a radial distance of 45° and a length of 5 m. Connectivity between the columns and the hyperboloidal Shell is given by a bottom ring beam (Fig. 1).

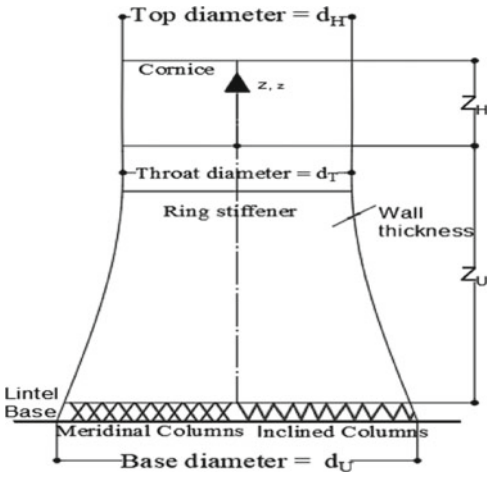

Fig. 1 Geometry of cooling tower

3.1 Geometrical Dimensions of Cooling Tower

Model Dimensions:

1. Top diameter $d_H = 35$ m
2. Distance from top to throat level, $Z_H = 18$ m
3. Distance from throat to Raker column level, $Z_U = 57$ m.
4. Total height of tower $H = 80$ m
5. Base diameter $d_U = 55$ m
6. Throat diameter $d_T = 38$ m
7. Column height = 5 m

4 Results and Discussions

Static analysis is carried out with the help of the equivalent-static method and Dynamic analysis is carried out with response spectrum method to obtain the results. Results obtained in the study are (a) Time Period & Natural frequencies (b) Mode shapes (c) Lateral deformation (d) Base shear (e) Axial force in columns and Time period. frequency results are presented in Tables 1 and 2:

Table 1 Time Period of Cooling Tower obtained from code analysis and Software analysis

Model type	Gravity load (sec)		Seismic Load					
			1.2(DL + IL + EL) (sec)		1.5(DL + EL) (sec)		0.9DL + 1.5EL (sec)	
	Codal	Analytical	Codal	Analytical	Codal	Analytical	Codal	Analytical
Model I	0.965	0.704	0.965	0.704	0.965	0.704	0.965	0.704
Model II	0.965	0.684	0.965	0.684	0.965	0.684	0.965	0.684

Table 2 Time period and frequency for natural draft cooling tower Model-I & Model-II

Mode number	Model-I		Model-II	
	Time period (Sec)	Frequency (Cyc/sec)	Time Period (Sec)	Frequency (Cyc/sec)
1	0.7036	1.4211	0.6832	1.4636
2	0.7036	1.4211	0.6832	1.4636
3	0.6490	1.5407	0.6436	1.5535
4	0.6490	1.5407	0.6436	1.5535
5	0.6002	1.6659	0.5947	1.6813
6	0.6002	1.6659	0.5947	1.6813
7	0.5225	1.9139	0.5162	1.937
8	0.5225	1.9139	0.5162	1.937
9	0.5006	1.9973	0.4879	2.0492
10	0.5006	1.9973	0.4879	2.0492
11	0.4951	2.0197	0.4718	2.1194
12	0.4951	2.0197	0.4718	2.1194

4.1 Time Period & Natural frequencies

From the above Table 2, it is notified that the Time period is decreasing as mode number increases and frequency increases as mode number increases for Model-I and Model-II.

4.2 Lateral Deformation

Lateral deformation values for two different models of loading combination are shown in Table 3, 4 and 5 and a plot of height versus lateral deformation is presented in Fig. 2, 3 and 4.

Table 3 Lateral deformation of Model I and Model II for loading 1.5(DL + TL)

	Model type	Gravity		
		Height of natural draft cooling tower (m)		
		5	*62*	*80*
Lateral Deformation (mm)	I	3	9.7	10.9
	II	3	9.9	10.1

Table 4 Lateral deformation for the loading combination 1.2(DL + TL + EQX) & 1.2(DL + TL + RSX)

Height of natural draft cooling tower (m)	Lateral deformation (mm)			
	Model I		Model II	
	EQX	RSX	EQX	RSX
5	8.8	0.988	9.3	2.4
62	13.5	5.0	42.2	32.5
80	11.4	7.9	52.2	46.9

Table 5 Lateral deformation for the loading combination 1.2 (DL + TL + EQY) & 1.2 (DL + TL + RSY)

Height of natural draft cooling tower (m)	Lateral deformation (mm)			
	Model I		Model II	
	EQY	RSY	EQY	RSY
5	0.3975	0.1567	1.4	1.2
62	5.7	1.7	32.5	11.54
80	8.5	2.6	41.7	26.82

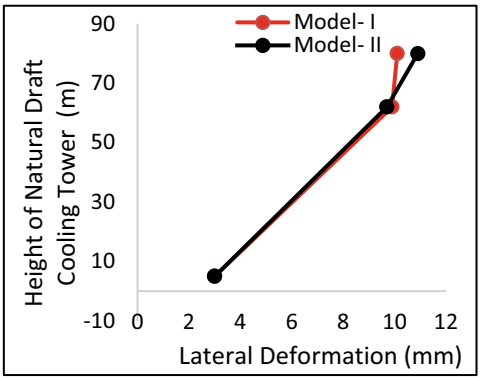

Fig. 2 Lateral deformation of Model I and Model II for loading 1.5(DL + TL)

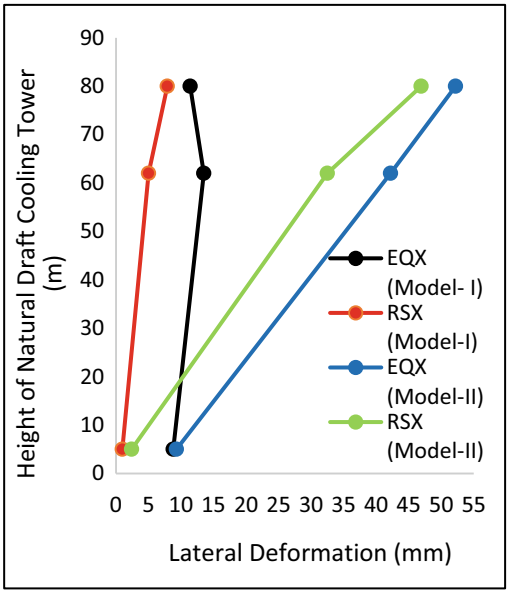

Fig. 3 Lateral deformation of Model I and Model II for loading 1.2(DL + TL + EQX) & 1.2(DL + TL + RSX)

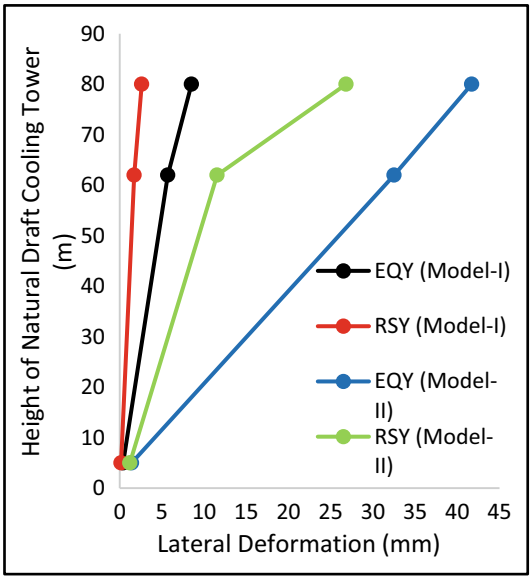

Fig. 4 Lateral deformation of Model I & Model II for loading 1.2(DL + TL + EQY) & 1.2(DL + TL + RSY)

Table 6 Base Shear and scaling Factors for loading combination 1.2 (DL + TL + EQX) in X Direction

Model type	Equivalent static method (kN)	Response spectrum method (kN)	Scale factor
I	4707.134	3875.809	1.2
II	4300.211	3500.130	1.22

Table 7 Base Shear and scaling factors for loading combination 1.2(DL + TL + EQY) in Y direction

Model type	Equivalent static method (kN)	Response spectrum method (kN)	Scale factor
I	4707.134	3318.52	1.41
II	5346.03	4544.12	1.17

4.3 Base Shear

The base shear results for two models of Cooling Towers has been showin in Table 6 and 7.

4.4 Axial Forces on Columns

The axial forces results for two models of cooling towers in x and y direction has been shown in Table 8 and 9respectively.

Table 8 Axial force on columns for Seismic loading combination in the X direction

	1.2(DL + TL + EQY) (kN)	1.5(DL + EQY) (kN)	0.9DL + 1.5EQY (kN)
Model I	2196.34	2563.72	1536.79
Model II	1835.44	1174.68	1047.144

Table 9 Axial force on columns for seismic loading combination in the Y direction

	1.2(DL + TL + EQY) (kN)	1.5(DL + EQY) (kN)	0.9DL + 1.5EQY (kN)
Model I	2529.52	2100.52	1608.35
Model II	1278.67	1306.48	1627.44

5 Conclusions

The seismic response of the Hyperbolic cooling tower is determined in the form of the natural time period, Lateral Deformation, base shear, axial forces on columns were analyzed and compared.

- Natural Time Period was analyzed using IS code 1893 (Part 4): 2005 as well as by using finite element package SAP 2000. Empirical expression is the same for all types of Hyperbolic cooling towers but this is not true in all conditions. It also depends on the configuration of the structure. In this paper, it is found that the time period is greater for the natural draft cooling tower supported on Raker columns than Meridional columns.
- Lateral deformation due to seismic forces for Natural draft cooling towers supported on Raker columns is more compared to the Meridional columns. The lateral deformation increases from bottom to the top of the cooling tower and maximum deformation for Meridional column supported Cooling Tower is less than deformation for Raker column supported the cooling tower.
- Base Shear increases with an increase in mass and stiffness. Natural draft cooling tower with Meridional columns experiences high Base Shear than cooling tower with raker columns.
- Axial Forces on columns of Natural draft cooling tower supported on raker Columns found more compared to the Natural Draft Cooling Tower supported on Meridional columns.
- The Meridional columns supported cooling towers have more seismic resistance than raker columns supported cooling towers.

References

Naghshineh A, Alavi E, Rezaee MR (2012) Seismic behavior of column-supported and innovative fixed-base cooling towers with ring beam. In: Proceedings of the 15th World Conference on Earthquake Engineering, NITK

Chiranjit M, Ranjith A, Sanjith J, Kiran BM (2015) Wind induced interference effects on natural draught cooling tower. Int J Prog Civ Eng IJPCE 2(1):6–12

Zhang, JF, Ge YJ, Zhao L (2011) Effect of latitude wind pressure distribution on the load effects of hyperboloidal cooling tower shell. In: The 13th International Conference on Wind Engineering. Amsterdam, Netherlands, vol. 201, pp 326–341

Murali G, Vardhan CMV, Prasanth Kumar Reddy BV (2012) Response of cooling towers to wind loads. ARPN J Eng Appl Sci 7(1):114–120

Kumar CLM, Shanthappa BC, Manjunatha K (2021a) A study on dynamic response of hyperbolic cooling tower for fixed base condition. In: Sitharam T, Pallepati RR, Kolathayar S (eds) Seismic Design and Performance. LNCE, vol 120, pp 269–275. Springer, Singapore. ISBN 978-981-334-4004-6. https://doi.org/10.1007/978-981-33-4005-3_22

Kumar CLM, Shwetha KG, Shanthappa BC, Manjunatha K (2021b) A study on dynamic behavior of natural draft cooling tower considering the effect of soil-structure interaction. Civ Environ Eng Rep 31(4):17–32. https://doi.org/10.2478/ceer-2021-0047

IS:11504 (1985), Criteria for Structural Design of reinforced Concrete Natural Draught Cooling Towers, Bureau of Indian Standards, New Delhi, 1985

IS 1893(Part 4): (2005) Criteria for Earthquake resistant design of structures, Bureau of Indian Standards, New Delhi, 2005

N Prabhakar, Structural design aspects of hyperbolic cooling towers, National Seminar on Cooling towers, (1990) 65-72.

Busch D, Harte R, Krätzig WB, Montag U (2002) New natural draft cooling tower of 200 m of height. Eng Struct 24(12):1509–1521, S0141029602000822. https://doi.org/10.1016/S0141-0296(02)00082-2

Evaluate the Durability of RC Bridge Under the Impact of Climate Change in Vietnam

Trong-Ha Nguyen, Ngoc-Long Tran, and Duy-Thuan Phan

Abstract Climate change has increased worldwide and has adversely affected almost all areas, including construction. This study wants to mention was that the Climate change of construction deteriorate more quickly. Due to climate change, the air environment has changed greatly in a direction is was harmful to constructions. This has caused a high level of erosion and has a strong impact on the durability of constructions, especially those near the sea. surveyed data on the impacts of the compromised environment on the quality and longevity of RC Bridges in the coastal area. The actual survey data at some reinforced concrete bridges in Vietnam showed that: compressive strength, C25/30, after 30 years of using the durability decreased by 13%, and compressive strength, C30/37, after 25 years of use, the durability decreased by 3.6%. The results of this study have evaluated the current durability and predicted lifespan of RC Bridges affected by environmental erosion caused by climate change.

Keywords Climate change · Climate change · Construction · RC bridges · Compressive strength

1 Introduction

The climate change phenomenon that has taken place has become more and more serious in recent years (ADB 2013; Schmidt-Thome et al. 2015; Thuc et al. 2016). The consequences of climate change have made the air components change significantly, the concentration of chloride, acid and sulfate increases, especially in coastal areas and industrial zones. This has accelerated the corrosion of materials, especially reinforced concrete in buildings (Gao and Wang 2017, Mahindrakar 2017, Medeiros-Junior 2018).

T.-H. Nguyen · N.-L. Tran (✉) · D.-T. Phan
Department of Civil Engineering, Vinh University, Vinh 461010, Vietnam
e-mail: longtn@vinhuni.edu.vn

D.-T. Phan
National University of Civil Engineering, 55-Giai Phong, Ha Noi, Vietnam

I. Pal et al. (eds.), *Proceedings of the 2nd International Symposium on Disaster Resilience and Sustainable Development*, Lecture Notes in Civil Engineering 294,
https://doi.org/10.1007/978-981-19-6297-4_10

There are many different types of corrosion, such as: chemical corrosive, corrosive to physical, corrosive to chloride, corrosive to Acid, corrosive to Sunfar. Chemical corrosion is the result of the chemical reactions of the environment with the minerals of cement and aggregate; As the chemical reactions that cause the destruction of the concrete structure gradually occur, it reduces the strength of the concrete and ultimately destroys the building structure. Physical corrosion of concrete takes place under the influence of internal and external forces, which is caused by the effect of the service load, the volume expansion of frozen water in holes in the concrete, permeability.

There are many studies of corrosion on concrete and steel structures with all of the above types of corrosion. V. L'Hostis*, A. Millard, S. Perrin, E. Burger, D. Neff and P. Dillmann have been studies on "Modelling the corrosion-induced cracking of reinforced concrete structures exposed to the atmosphere". This study predicted corrosion cracking of concrete under carbon atmospheric conditions. This is the main problem in assessing) the durability of the structure, from which to make a choice for the maintenance of the building (L'Hostis et al. 2011). Another research team including: Gilles Pijaudier-Cabot, Khalil Haidar, Ahmed Loukili, Mirvat Omar, carried out the research project on "Ageing and durability of concrete structures" (Pijaudier-Cabot et al. 2004). The team investigated the chemotherapeutic damage caused by calcium leaching. The characteristics of the crack, namely its length on the inside of the structures that continuously grow with aging, were studied by the team. This statement is confirmed by experiments on similar material models. This study came to the conclusion of a number of concrete creep experiments that were carried out to investigate the related influence between creep and cracking (Pijaudier-Cabot et al. 2004, Balafas and Burgoyne 2010, Gjørv 2011, Pakkala et al. 2014). A number of other research projects have been carried out with regard to environmental corrosion, (Petkar 2014, Poteraş et al. 2014, Van den Heede et al. 2014, Bastidas-Arteaga and Stewart 2015, de Medeiros-Junior et al. 2015, Gao and Wang 2017, Wang et al. 2018).

2 Chemical Corrosion

According to (Gaidis 2004; Lukovits et al. 2001), the interaction with different salts in the environment is very different due to the multi-mineralization of cement. Can be divided into basic types of concrete corrosion.

2.1 Concrete Corrosion is Due to the Solubility of the Cement Hydration Products

This type of corrosion has occurred due to solubility from cement hydration products. Mainly dissolved calcium hydroxide ($Ca(OH)_2$) and hydrated calcium aluminate $CaO.Al_2O_3.nH_2O$) dissolved, especially the most powerful dissolved calcium hydroxyt (takes place when under the influence of relatively pure water). There is always an amount of CO_2 and H_2O is converted with. This amount of CO_2, H_2O will be reacted with $Ca(OH)_2$ (produced by cracked or vandalized concrete) and $CaCO_3$ is created. This type of corrosion is also known as concrete desalination (concrete whitening), it causes a decrease in the pH concentration in the concrete and also promotes the corrosion of the reinforcement.

2.2 Corrosive to Concrete Due to the Reaction of the Cement with the Environment

This type of corrosion is caused by exchange reactions between water with aggressive chemicals (acids, salts) and cement components. The resulting products of these reactions are dissolved and carried away by water, or separated into porous amorphous masses. Among these corrosive agents, acids are considered to be the most powerful, followed by acid salts and compounds capable of interacting with the hydration products of cement with strong activity.

Carbonic acid corrosion is indicated by the reaction of CO_2 in water with $Ca(OH)_2$. Initially $CaCO_3$ limestone is created, it will adhere to the concrete outer surface and thus temporarily increase the strength of the concrete. However, $CaCO_3$ continues to react with CO_2 and H_2O to form Ca $(HCO_3)_2$, which is highly soluble. The reactions that have occurred when carbonic acid corrodes concrete are as follows:

$$CO_2 + Ca(OH)_2 \rightarrow CaCO_3 + H2O \quad (1)$$

$$CaCO_3 + CO_2 + H2O \rightarrow Ca(HCO_3)_2 \quad (2)$$

Corrosion from other acids like HCl, H_2SO_4, HNO_3 and organic acids such as lactic acid, acetic acid is similar. Presented below are the dissolving reactions of Ca $(OH)_2$:

$$Ca(OH)_2 + 2HCl = CaCl_2 + 2H_2O \quad (3)$$

$$Ca(OH)_2 + H_2SO_4 = CaSO_4 + 2H_2O \quad (4)$$

$$Ca(OH)_2 + 2HNO_3 = Ca(NO_3)_2 + 2H_2O \quad (5)$$

$CaCl_2$, $Ca(NO_3)_2$ are salts with very high solubility. $CaSO_4$ will react with 3CaO.Al2O3.6H2O to produce ettringite, which is a substance that increases the volume of cement and disrupts the structure of cement stone. Corrosive due to magnesium-containing compounds, such as MgSO4 and MgCl2, it will react with Ca $(OH)_2$ as follows:

$$MgSO_4 + Ca(OH)_2 + 2H_2O = CaSO_4.2H_2O + Mg(OH)_2 \quad (6)$$

$$MgCl_2 + Ca(OH)_2 = CaCl_2 + Mg(OH)_2 \quad (7)$$

2.3 Cloride Corrision

Arcoding to (Ann and Song 2007; Hope and Ip 1987) Corrosive chloride is usually concentrated in a small area, forming a small hole surrounded by uncorroded reinforcement. This corrosion process is illustrated in Fig. 1. This can lead to a rapid decrease in cross-sectional area, resulting in a decrease in the load-carrying capacity of reinforced concrete structural members. Deterioration of the load-bearing capacity of a structure can be significantly developed before the deterioration in the surface is increased.

During the corrosion cycle, Fe ions become readily combined with chloride ions to form compounds such as ferric chloride (FeCl2). The hydrolysis of these products is time dependent, chloride ions will be released and lead to a decrease in pH at

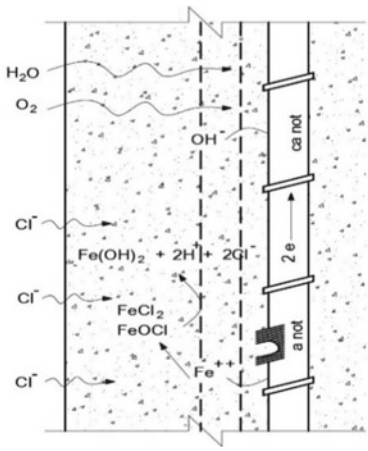

Fig. 1 Concrete surface pitting corrosion process

the anode. Corrosion rates increase because Fe oxidation is encouraged under acidic conditions. The regenerated chloride ions exacerbate the problem. An influencing parameter is the chloride/hydroxyl ion ratio at the reinforcement.

2.4 Sunfar Corrision

The deterioration in the quality of the concrete is due to the penetration of salt. Salts are chemical compounds usually formed by reactions between acids and bases and dissociated into water to form ionic molecules. Rebar corrosion problems associated with sodium chloride have been noted, but degradation of concrete can also be generated through exposure to sulfate salts. The word 'sulphate corrosion' is commonly associated with durability deterioration through destructive expansion of concrete in contact with sulfate-containing soils or groundwater. There are three phenomena related to sulfate and concrete interactions that can be distinguished by chemical or time-dependent properties:

- 'classic' sulfate corrosion,
- sulfate thaumasite corrosion,
- Delay formation ettringite.

The European standard EN 206–1 presents sufate corrosion as a subset of many chemical corrosion phenomena. This standard covers three exposure categories for minor, moderate and major chemical corrosion - based on common chemical composition in the environment.

2.5 Acid Corrision

It is known that an acidic environment dissociates hydrogen ions into solution. The rate of attack on concrete depends on the amount of hydrogen ions that have been formed. This will be dependent on the acidic nature (strong or weak) and the concentration of the acids in the solution (concentrated or diluted). Strong acids, e.g. hydrochloric (HCl) and sulfuric acid (H2SO4), have a high degree of dissociation while weak acids do not, e.g. acetic acid (CH3COOH) (De Waard and Milliams 1975).

The external acids react with the constituents of the concrete to form a salt made up of calcium and water. The salts are soluble and thus the solid product is gradually lost. For example, the reaction of calcium hydroxide with hydrochloric and sulfuric acids is as follows:

$$Ca(OH)_2 + 2HCl \rightarrow CaCl_2 + 2H_2O \quad (8)$$

Fig. 2 Damaged images at Rao and Duc Nghia bridges in Quang Binh Province

Fig. 3 Damaged images at Rac and Ho Do bridges in Ha Tinh Province

$$Ca(OH)_2 + H_2SO_4 \rightarrow CaSO_4.2H_2O \quad (9)$$

3 The Survey of RC Bridge Corrosion Situation

The current situation has shown that the construction project near the sea is heavily and increasingly corroded. The sea area of central Vietnam has a fairly high salt and acid concentration, so that the constructions here have been damaged by the frequent erosion. Some construction projects have been investigated in Nghe An, Ha Tinh and Quang Binh provinces. The survey results are shown in Figs. 2 and 3 and Table 1.

Corrosion of reinforced concrete structures is easily encountered in heavily aggressive environments. he most noticeable is the phenomenon of concrete cracking, peeling, leaching, rusted reinforcement, broken (Duc Nghia, Rac Bridge). Structural parts that are in direct contact with the external environment, which are constantly changing wet, dry and wet, are very susceptible to corrosion damage.

4 Evaluate the Durability of RC Bridges

The data analysis Tables 1 and 2 has shown that Duc Nghia Bridge's Pillar has a decrease in strength of 2.8%, a decrease concrete cover thickness of 7.1%, and Ho Do Pillar has 2, respectively, 7 and 3.8%. This is the largest reduction of the surveyed

Table 1 Survey data on construction in Nghe An, Ha Tinh, Quang Binh provinces

Name of Project	Year	Number of years	Compressive strength (Mpa)		Concrete cover thickness (cm)		Rebars	
			Designed	Surveyed	Designed	Surveyed	Designed (mm)	Surveyed (mm)
1. Rao bridge	2015	15	25				25 D	25 D
No1				24,65	8	7,86	25 D	25 D
No2				24,87	8	7,88	25 D	25 D
2. Duc Nghia Bridge	1990	30	25					
No1				24,3	7	6,5	25 D	25 D
No2				24,7	7	6,6	25 D	25 D
3. Nhat Le Bridge	2004		30					
No1				29,6	10	9,5	32 D	32 D
No2				28,9	10	9,88	32 D	32 D
4. Rac Bridge	2010	10	30					
No1				29,7	8	7,92	28 D	28 D
No2				29,5	8	7,88	28 D	28 D
No3				29,7	8	7,87	28 D	28 D
5. Ho do Bridge	1995	25	30					
No1				29,2	8	7,87	28 D	28 D
No2				29,3	8	7,95	28 D	28 D
No3				29,6	8	7,98	28 D	28 D
6. Thach Son Bridge	2010	10	30					
No1				29,92	8	7,90	28 D	28 D
No2				29,96	8	7,87	28 D	28 D
No3				29,98	8	7,89	28 D	28 D
7. LamGiang Bridge	2010	10	25					
No1				24,83	7	6,94	25 D	25 D
No2				24,88	7	6,93	25 D	25 D
No3				24,87	7	6,92	25 D	25 D

Bridges and the sharp reduction is compared with the area of normal cavitation. The data table and chart above have shown that for high strength concrete, the degree of compressive strength degradation is lower. For concrete C25/30 after 30 years, the bearing capacity has decreased by 13%, C30/37 after 25 years, the bearing capacity has decreased by 3.6%.

The diagrams in Figs. 4, 5, and 6 show that the closer the building is to the sea or in an area with a high salinity and greater erosion, the greater the loss of quality. At the same time, it is also shown that when the age of the building is large, the rate of deterioration of construction quality is greater and the rate of corrosion is faster. This has reduced the life span of the building. Also from the data table (Tables 1 and 2) and the above figures, it is shown that Duc Nghia Bridge in Quang Binh and Ho Do Bridge in Ha Tinh are the oldest constructions, and they are located closer to the sea. Therefore, the rate of corrosion and erosion of the environment is higher than that of the remaining bridges.

Table 2 Comparative results of measurement and calculation results according to standards

Constructions	Years	Load bearing capacity (kN)			Compressive strength			Concrete cover (cm)		
		Design	Surveyed	The degree of reduction (%)	Design	Surveyed	The degree of reduction (%)	Design	Surveyed	The degree of reduction (%)
1. Rao bridge	15	485,130,0	480,622,5	0,9	25	24,65	1,4	8	7,86	1,8
2. Duc Nghia Bridge	30	71,654,6	62,521,0	13	25	24,3	2,8	7	6,74	3,7
3. Nhat Le Bridge	15	3,95E + 05	3,86E + 05	2,4	30	29,6	1,3	10	9,5	5,0
4. Rac Bridge	10	3,76E + 05	3,66E + 05	2,7	30	29,5	1,7	8	7,87	1,6
5. Thach Son Bridge	10	2,31E + 05	2,27E + 05	1,3	30	29,92	0,3	8	7,87	1,6
6. Ho do Bridge	25	3,76E + 05	3,63E + 05	3,6	30	29,2	2,7	8	7,7	3,8
7. LamGiang Bridge)	10	1,50E + 05	1,47E + 05	2,1	25	24,83	0,7	7	6,92	1,1

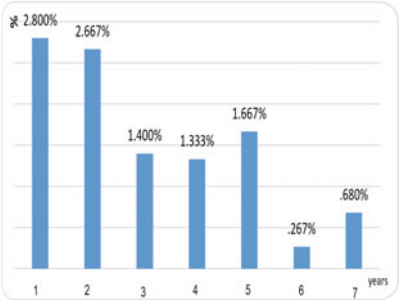

Fig. 4 Decreasing compressive strength of concrete bridge pillars

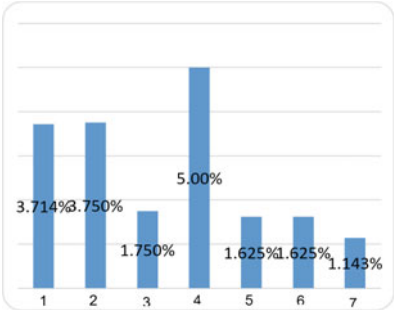

Fig. 5 The concrete cover thicknessr is reduced

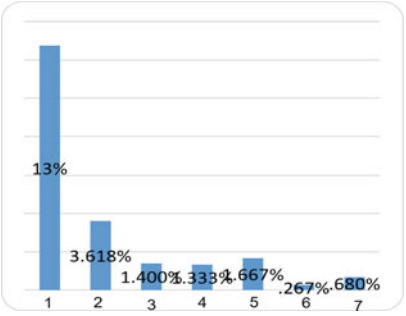

Fig. 6 Load bearing capacity of reinforced concrete bridge pillars is reduced

5 Conclusions

Some conclusions are drawn for reinforced concrete structures:

The quality of concrete is rapidly declining, which has strong effects of climate change. The lifespan of the construction has been reduced significantly in highly aggressive environments. For structures near the sea (high salinity) and affected areas with severe climate change, there will be a high level of erosion, so that it has been shown that the deterioration in the quality of construction in these areas is faster than for structures in less aggressive areas.

The degree of rapid or slow deterioration depends on the level of environmental erosion and the durability of the concrete. Structures with a high degree of strength have better resistance to environmental erosion than those with a smaller lateral level. Therefore, it is necessary to develop high-strength concrete for reinforced concrete structures in a strongly aggressive environment.

References

ADB (2013) Viet Nam: Environment and climate change assessment. Asian Development Bank Manila

Ann KY, Song H-W (2007) Chloride threshold level for corrosion of steel in concrete. Corros Sci 49:4113–4133

Balafas I, Burgoyne C (2010) Environmental effects on cover cracking due to corrosion. Cem Concr Res 40:1429–1440

Bastidas-Arteaga E, Stewart MG (2015) Damage risks and economic assessment of climate adaptation strategies for design of new concrete structures subject to chloride-induced corrosion. Struct Saf 52:40–53

De Medeiros-Junior RA, de Lima MG, de Brito PC, de Medeiros MHF (2015) Chloride penetration into concrete in an offshore platform-analysis of exposure conditions. Ocean Eng 103:78–87

de Waard C, Milliams D (1975) Carbonic acid corrosion of steel. Corrosion 31:177–181

Gaidis JM (2004) Chemistry of corrosion inhibitors. Cem Concr Compos 26:181–189

Gao X-J, Wang X-Y (2017) Impacts of global warming and sea level rise on service life of chloride-exposed concrete structures. Sustainability 9:460

Gjørv OE (2011) Durability of concrete structures. Arab J Sci Eng 36:151–172

Hope BB, Ip AK (1987) Chloride corrosion threshold in concrete. Mater J 84:306–314

L'Hostis V, Millard A, Perrin S, Burger E, Neff D, Dillmann P (2011) Modelling the corrosion-induced cracking of reinforced concrete structures exposed to the atmosphere. Mater Corros 62:943–947

Lukovits I, Kalman E, Zucchi F (2001) Corrosion inhibitors—correlation between electronic structure and efficiency. Corrosion 57:3–8

Mahindrakar AB (2017) Impact of aggressive environment on concrete–a review. Technology 8:777–788

Medeiros-Junior RA (2018) Impact of climate change on the service life of concrete structures. In: Eco-Efficient Repair and Rehabilitation of Concrete Infrastructures. Elsevier

Pakkala TA, Köliö A, Lahdensivu J, Kiviste M (2014) Durability demands related to frost attack for Finnish concrete buildings in changing climate. Build Environ 82:27–41

Petkar S (2014) Environmental impact of construction materials and practices. PhD Thesis, National Institute of Construction Management and Research, Pune

Pijaudier-Cabot G, Haidar K, Loukili A, Omar M (2004) Ageing and durability of concrete structures. In: Darve F, Vardoulakis I (eds) Degradations and Instabilities in Geomaterials. International Centre for Mechanical Sciences, vol 461. Springer, Vienna. https://doi.org/10.1007/978-3-7091-2768-1_9

Poteraş G, Moncea MA, Panait AM (2014) Researches regarding marine environment corrosion on coastal structures. Turk J Fish Aquat Sci 14:965–971

Schmidt-Thome P, Nguyen TH, Pham TL, Jarva J, Nuottimäki K (2015) Climate change in Vietnam. In: Climate Change Adaptation Measures in Vietnam. SpringerBriefs in Earth Sciences. Springer, Cham. https://doi.org/10.1007/978-3-319-12346-2_2

Thuc T, Van Thang N, Huong HT, Van Khiem M, Hien NX, Phong DH (2016) Climate change and sea level rise scenarios for Vietnam. Ministry of Natural resources and Environment. Hanoi, Vietnam

van den Heede P, Maes M, de Belie N (2014) Influence of active crack width control on the chloride penetration resistance and global warming potential of slabs made with fly ash+ silica fume concrete. Constr Build Mater 67:74–80

Wang X-Y, Lee H, Kwon S (2018) Analysis of service life of cracked marine concrete considering global warming and Bruun rule

Mechanical Properties of Geopolymer Concrete Reinforced with Various Fibers: A Review

Divya Jat, Ronak Motiani, Sejal Dalal, and Ishan Thakar

Abstract Ever increasing environmental concern has led to find an alternative for steel reinforcement and ordinary Portland cement. Geopolymer primarily consists of fly ash, fine aggregates, coarse aggregates, and an alkaline activator. This review summarizes and discusses the recent developments in geopolymers with various fibers reinforcements like carbon fiber, basalt fiber, glass fiber, cotton fiber and polyvinyl alcohol (PVA) fiber. The review emphasizes mainly on the mechanical properties i.e., compressive strength, flexural strength, and split tensile strength of geopolymer with each fiber. It concludes with suggestions for the most suitable fiber reinforced geopolymer in comparison with other fibers.

Keywords Geopolymer · Mechanical behavior · Natural fiber · Basalt · Carbon · Glass fiber

1 Introduction

Alternatives for environmentally friendly materials in the construction industry have become a primary objective for researchers nowadays. One such alternative is geopolymer which was first developed by Davidovits in the late 1970s (Davidovits 1989).

In geopolymers, generally, low calcium fly ash (ASTM class F fly ash) is preferred over high calcium fly ash (ASTM class C fly ash), because a higher amount of calcium in fly ash alters the microstructure and inter polymerization process (van Deventer et al. 2007). The amount and type of fine aggregates and coarse aggregates generally depend on the mix design codal specifications. Alkaline activators that contain rich amounts of amorphous silica and alumina are used to achieve good binding in the

D. Jat · R. Motiani (✉) · I. Thakar
Department of Civil Engineering, School of Technology, Pandit Deendayal Energy University, Gandhinagar, Gujarat, India
e-mail: ronak.motiani@sot.pdpu.ac.in

S. Dalal
Department of Civil Engineering, Sardar Vallabhbhai Patel Institute of Technology, Vasad, Gujarat, India

I. Pal et al. (eds.), *Proceedings of the 2nd International Symposium on Disaster Resilience and Sustainable Development*, Lecture Notes in Civil Engineering 294,
https://doi.org/10.1007/978-981-19-6297-4_11

concrete, because sodium based activators may affect the compressive strength of the mix in a negative way. (Vora and Dave 2013),

The foremost effective way of strengthening and toughening geopolymer materials is through reinforcement (Alomayri et al. 2014a). The geopolymer having no fiber resulted in early crack development since it was unable to sustain load (Alomayri 2017). Naturally occurring fibers such as cotton, sisal, coir, and wool have not only environmental benefits but have resulted in a significant increase in strength when used with geopolymer composites. (Alomayri et al. 2013, 2014a, 2014b; Korniejenko et al. 2016). But, the most common inorganic fibers used as reinforcing materials are carbon and glass (Natali et al. 2011).

Fibers such as basalt, carbon, glass, basalt, PVA and cotton, have been popular in use amongst all other fibers mentioned above due to various reasons. Despite having been used in various fields, there has been very little application of basalt in the construction industry (Dhand et al. 2015). To enhance the mechanical properties of basalt fiber it is not necessary to add additives unlike in carbon and glass fiber (Kizilkanat et al. 2015).

Carbon fiber is inorganic fiber which is now widely been studied by researchers due to its high strength, high modulus, low thermal expansion, and good electrical properties. The addition of carbon fiber to geopolymer prevents catastrophic behavior and enhances the toughness of the matrix (Yan et al. 2016). Carbon fiber sheet geopolymer has good resistance to high temperatures (Samal et al. 2015; Timakul et al. 2016; Zhang et al. 2016) and it also slows down crack (Jiang et al. 2014). Carbon fiber geopolymer composites have shown pseudo plasticity behavior rather than brittle failure (Lin et al. 2008).

Several studies have shown that Glass fiber when used with geopolymer shows excellent strength. When compared with basalt fiber, it has shown greater flexural strength, and compressive strength (Kizilkanat et al. 2015). The optimum content of glass fiber is 2% (Thamer Alomayri 2017).

PVA fibers have been employed in geopolymers to improve the performance of the composite due to the micro bridging and pulling action which increases the flexural strength and flexural toughness leading to ductile failure. Fiber ratio and degree of temperature affect the strength of PVA fiber geopolymer composite (Tanyildizi and Yonar 2016). Fibers with a high aspect ratio have shown good chemical bonding with cement matrix. (Zheng and Feldman 1995).

It is clear from the above discussion that fibers alter the strength properties of geopolymers. The effect on compressive, flexural, and split tensile strength due to the addition of various fibers mentioned above is discussed at length in the next section.

2 Effect on Compressive Strength

The optimum PVA content is suggested as 1.2% (Al-mashhadani et al. 2018) to 2% (Tanyildizi and Yonar 2016) in mortar with fly ash and GGBS when cured at

60°C temperature to gain maximum compressive strength. Another similar study (Xu et al. 2017) shows that compressive strength increases in PVA fiber reinforced fly ash-geopolymer composites. Quite different results are observed by (Li and Xu 2009) where no remarkable improvement is seen in the dynamic compressive strength of basalt fiber, whereas when glass fiber is used, it shows an increase in compressive strength by 16% in comparison with the conventional geopolymer. Another study (Korniejenko et al. 2016) reported that by using natural fibers such as coconut, cotton and sisal fibers with 1% fiber content when heated at 75 °C, increases the compressive strength of the specimen as compared with the geopolymer without fiber. (Alomayri et al. 2014b) used cotton fabric of 30 × 7.5 cm in the composite with sodium hydroxide and sodium silicate as an activator, cured at temp 80 °C in an oven for 24 h. and found that fiber ratio, degree of high temperature affects the strength of geopolymer composite (Alomayri et al. 2014b; Tanyildizi and Yonar 2016). Furthermore, the molarity of the activator also plays a vital role in increasing the compressive strength (Patankar et al. 2014; Sathanandam et al. 2017).

The early strength gain of the specimen also depends upon the type of curing like thermal curing and ambient curing whereas a remarkable increase in strength is noticed when thermal curing is done when compared to ambient curing (Sathanandam et al. 2017; Singh et al. 2015). Since there's also a requirement of heat curing for the geopolymer composite, an alternative study reported that by using 10% OPC and 90% fly ash this limitation can be overcome (Vijai et al. 2012).

Carbon sheet up to 300 °C has good adhesive property (H. Zhang et al., 2016). However, a study (Alomayri et al. 2014a, b, c) used cotton fiber showed a decrease in strength after exposure to higher temperatures of 200–600 °C. In a study (Zhang et al. 2016) different layers of carbon fiber sheets on confined and unconfined cylinders with different elevated temperatures of 100, 200, 300 °C revealed that with an increase in the number of confining layers of carbon sheet higher strength and displacement were seen but the results were not up to expectation due to the slippage between geopolymer and carbon sheet.

Quite different results were obtained when basalt fiber is used as reinforcement. The addition of basalt fiber caused a 3.9% reduction of compressive strength when 0.5% wt. volume is added (Dias and Thaumaturgo 2005). (Jiang et al. 2014) stated that, in comparison to polypropylene fiber, basalt fiber shows a higher compressive strength with the same amount of fiber volume. Furthermore, the higher length of basalt fiber slightly increases compressive strength as stated by (Jiang et al. 2014). The compressive strength increases at an early stage and decreases with age (Branston et al. 2016). (Kizilkanat et al. 2015) reported that a slightly higher increase in compressive strength is seen in basalt fiber than in glass fiber geopolymer.

Table 1 and Figure summarize the various fibers used along with their compressive strength. After cotton and carbon fiber (Zhang et al. 2016), PVA fiber (Xu et al. 2017) showed higher compressive strength (Fig. 1).

Table 1 Summary of compressive strength

Sr. no	Experimental test	Type of fiber	Fiber content (%)	Compressive strength MPa	Specimen size (mm)	Type of test	Variables
1	(Korniejenko et al. 2016)	Cotton, coir, Raffia, sisal	1	13.66–31.36	50	EN—12,390–3	Type of natural fibers
2	(Alomayri 2017)	Glass	0,1,2,3	18–35	50	ASTM C39	Ambient curing
3	(Zhang et al. 2016)	Carbon	0.5	55.8–82.6	Ø150*300 cylinder	ASTM C	3 months ambient curing; Confined and unconfined specimen; High temperature
4	(Jiang et al. 2014)	Basalt Polypropylene	0,0.05,0.1,0.3,0.5	45.12–47.68 45.12–47.12	100Ø × 200 mm	AS1012.10–1999	Length of fiber; Volume fraction
5	(Kizilkanat et al. 2015)	Basalt Glass	0,0.25,0.5,0.75,1	67–63 62.6–67.5	150	EN 12,390–3	Volume of fiber
6	(Tanyildizi and Yonar 2016)	PVA	0,1,2	15–45	100	TS EN 12,390–3	Curing temp 60, 80,120 °C; Exposed temperature 20, 400, 600, 800 °C
7	(Alomayri et al. 2014b)	Cotton	0,4.5,6.2,8.3	20–90 (H) 20–60 (V)	100	ASTM C	Fabric orientation
8	(Al-mashhadani et al. 2018)	PVA	0,0.4,0.8,1.2	60.48–63.06	50	ASTM C 109	Type of fibers; Fly ash/GGBS; NaOH, Na_2SiO_3

(continued)

Table 1 (continued)

Sr. no	Experimental test	Type of fiber	Fiber content (%)	Compressive strength MPa	Specimen size (mm)	Type of test	Variables
9	(Xu et al. 2017)	PVA	0,0.5,1,1.5,2	49.18–84.95	100	ASTM C 109	Length of fiber (8, 12 mm); GBFS/binder ratio; Alkali activator dosage; Water/binder ratio; Modulus of sodium silicate
10	(Sathanandam et al. 2017)	Glass	0.1–0.5	24.8 max 22.8	150	EN–12,390–6	Type of curing; Concentration of NaOH
11	(Vijai et al. 2012)	Glass	0.01–0.03	32.08–4.73	150	IS	Ambient curing; 90% fly ash 10%OPC
12	(Branston et al. 2016)	Basalt	0.15,0.31,0.46,1,2	20.90–39.50	Ø100*200 cylinder	ASTM C39	Length of basalt fiber; Basalt bundled and minibars; Dosage of plain concrete
13	(Bhalchandra and Bhosle 2013)	Glass	0.01–0.04	36.33–43.67	100	IS	Fiber content
14	(Wongsa et al., 2020)	Sisal Coconut Glass	0.5,0.75,1	25–34.8	100	ASTM C39	Natural fiber; Fiber content
15	(Kizilkanat et al. 2015)	Basalt Glass	0.25, 0.50, 0.75, 1	63.4–66.6 63.4–67.6	150	EN 12,390–3	90% cement 10% fly ash
16	(Nematollahi et al. 2014)	PVA	2	59.8–63.7	50	ASTM C 109	Type of activator; Superplasticizer

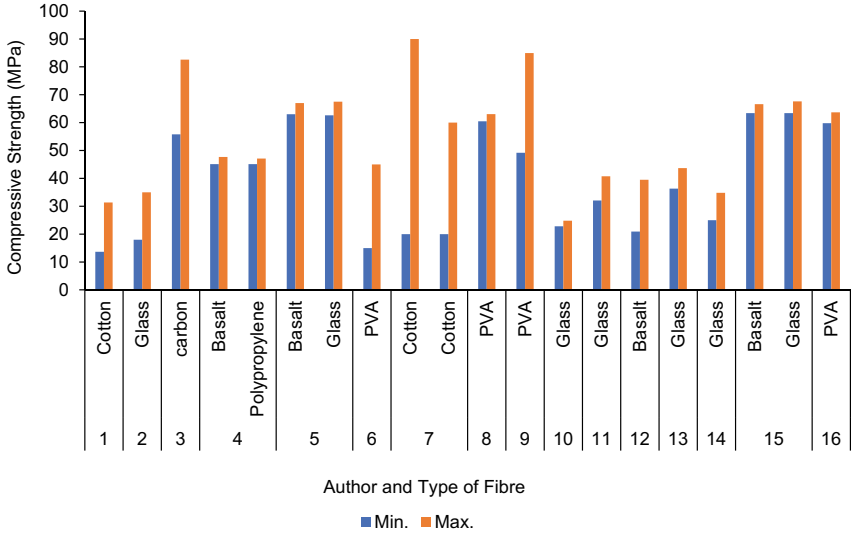

Fig. 1 Graphical representation of compressive strength as mentioned in Table 1

3 Effect on Flexural Strength

The main objective of adding fibers in geopolymer composites is to enhance the flexural and tensile strength. A study (Korniejenko et al. 2016) reported that the flexural strength is not significantly influenced by the addition of natural fibers (coir, cotton, sisal, and raffia fiber) as in carbon and glass fibers. While (Alomayri et al. 2013, 2014a) reported that with an increase in the fiber content up to 0.5%, the flexural strength increases but after 0.5% it decreases due to the formation of voids and fiber agglomeration, which is similar to (Lin et al. 2008) studies, but here instead of cotton, carbon fiber is used. (Alomayri et al. 2014b) also studied the effect of orientation of cotton fiber in horizontal as well as vertical directions and the results showed that the flexural strength of the composite is higher when kept in the horizontal layer than in the vertical layer.

The amount of fiber ratio and elevated temperature significantly affects the strength of the composite (Tanyildizi and Yonar 2016) (Bhalchandra and Bhosle 2013; Sathanandam et al. 2017), (Bhalchandra and Bhosle 2013; Vijai et al. 2012). Figure 2 adapted from (Vijai et al. 2012) shows the variation of different fiber content when ambient curing is done.

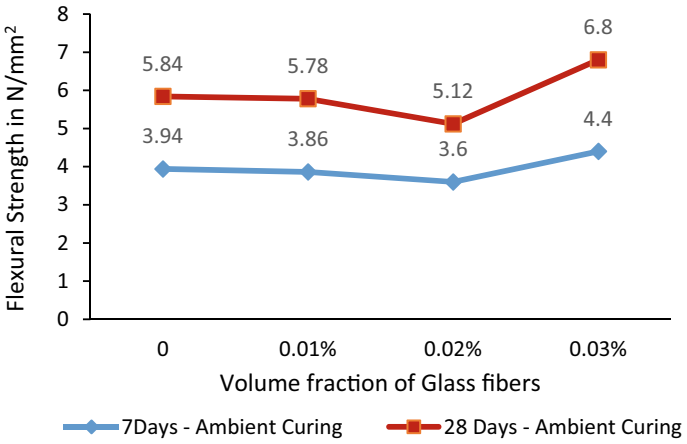

Fig. 2 Flexural strength of glass fiber reinforced geopolymer (Vijai et al. 2012)

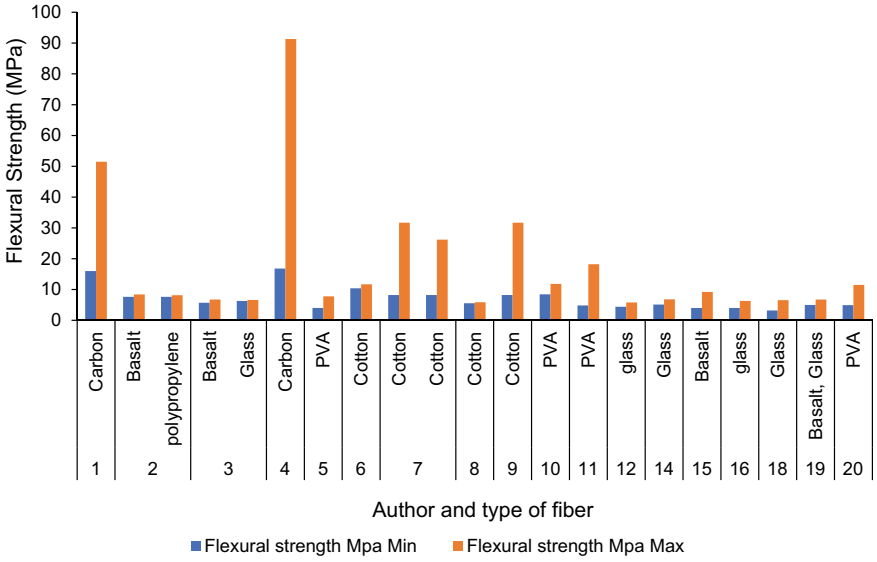

Fig. 3 Graphical representation of Flexural strength

(Lin et al. 2008, 2010; Tiesong et al. 2009) used potassium silicate solution and metakaolin powder to make a geopolymer resin with short carbon fiber forming a geopolymer composite bar that resulted in higher flexural strength and showed pseudo plasticity behavior rather than brittle failure. Another similar composition was investigated by (He et al. 2010) with heat curing. (Jiang et al. 2014) reported an increase in flexural strength of basalt fiber composite when compared to plain concrete. The strength is also affected by the length of fiber used, since longer

fiber shows a bridging effect and strong anchorage (Branston et al. 2016; Vairavan et al. 2013). An increase in strength is seen in the case of basalt fiber than glass fiber (Kizilkanat et al. 2015). Figure 3 and Table 2 summarize the flexural strength behavior due to the addition of different fibers as obtained by various research.

(Korniejenko et al. 2016) reported that natural fibers help in reducing the crack propagation compared to carbon and glass fibers in the composite. Figure 4 (Yan et al. 2016) shows the crack development and fiber pulling in geopolymer matrix with carbon fiber which contributed to the improved fracture toughness of composites. PVA fiber distributes uniformly in the matrix contributing to more strength (Xu et al. 2017). Disjointed crystals are seen in geopolymer with no fiber whereas, the geopolymer with glass fiber is seen with jointed crystals (Sathanandam et al. 2017).

4 Effects on Flexural Toughness

(Al-mashhadani et al. 2018) reported that the addition of fiber content has a greater influence on the toughness of the composite. In the case of PVA fiber, the toughness factor and mid-span deflection increased. (Xu et al. 2017) showed similar results of toughness that the more the fiber content the more will be the load and deflection. With the increase in the fiber content, there has been a significant increase in the flexural toughness due to the fiber pull out, fiber bridging, and fiber fracture, resulting in high ductility (Alomayri et al. 2014b; Kizilkanat et al. 2015; Yan et al. 2016) which was similar to the study (Alomayri 2017) in which glass microfibers with 2% wt. achieved the highest flexural toughness. However, basalt fiber inclusion when compared with glass fiber showed more crack resistance and ductility (Kizilkanat et al. 2015). Basalt fiber with 22 mm length shows the finest toughness improvement capacity (Jiang et al. 2014). The load displacement curve Fig. 5 with 0.2–1% carbon fiber showed pseudo plasticity behavior rather than catastrophic behavior resulting in a more ductile behavior of the composite. With increase in the fiber content the amount of fiber pulling from the fracture surface increases which ultimately prevented the catastrophic behavior of the composite (Yan et al. 2016).

Figure 6 shows the curve where the bridging effect improves toughness and ductility when compared to plain which showed brittle failure. However, a decrease is seen with a higher fiber content of cotton fiber due to poor dispersion of cotton in the matrix (Zhang et al. 2016). Optimum mechanical properties of cotton fiber geopolymer can be achieved with 0.5% fiber content (Alomayri et al. 2013). Table 3 summarizes the flexural toughness of various types of fiber whereas Fig. 7 shows its graphical presentation.

Table 2 Summary of flexural strength

Sr. no	Experimental test	Type of fiber	Fiber content (%)	Flexural strength MPa	Specimen (mm)	Type of test	Curing temp.
1	(Yan et al. 2016)	Carbon	0,2.5,4,5,5.5	16–51.5	4*3*36	TPB	60 °C for 7d
2	(Jiang et al. 2014)	Basalt polypropylene	0,0.05,0.1,0.3,05 0,0,05,0.1,0.3	7.62–8.41 7.62–8.15	75*75* 305	ASTMC 1609	20 °C covered by PP film
3	(Kizilkanat et al. 2015)	Basalt Glass	0,0.25,0.5,0.75,1	5.7–6.75 6.3–6.6	100*100*350	JCI-S-002	24 h
4	(Lin et al. 2008)	Carbon	3.5	16.8–91.3	4*3*36	TPB	80 °C for 48 h
5	(Tanyildizi and Yonar 2016)	PVA	0,1,2	4–7.8	75*75*300	TS EN 12,390–5	60, 80, 120 °C
6	(Alomayri et al. 2013)	Cotton	0.3–1	10.4–11.7	80 *20 *10	TPB	105 °C for 3 h
7	(Alomayri et al. 2014b)	Cotton	0,4.5,6.2,8.3	8.2–31.7 H 8.2–26.2 V	80*20*20	ASTMC 348	80 °C for 24 h
8	(Korniejenko et al. 2016)	Cotton, coir, Raffia, sisal	1	3.05–5.90	200*50*50	EN 12,390–5	75 °C for 24 h
9	(Alomayri et al. 2014a)	Cotton	0,3.6,4.5,6.2,8.3	8.2–31.7	60*20*20	ASTMC 348	80 °C for 24 h
10	(Al-mashhadani et al. 2018)	PVA	0,0.4,0.8,1.2	8.45–11.82	40*40* 160 prisms	ASTMC 348	80 °C for 24 h
11	(Xu et al. 2017)	PVA	0,0.5,1,1.5,2	4.81–18.19	75*75* 300	ASTMC 348	20 °C room with 90% humidity
12	(Sathanandam et al., 2017)	Glass	0.1–0.5	4.4–5.8 max	100*100*500	EN 12,390–5	100 °Cfor 24 h

(continued)

Table 2 (continued)

Sr. no	Experimental test	Type of fiber	Fiber content (%)	Flexural strength MPa	Specimen (mm)	Type of test	Curing temp.
13	(Tiesong et al. 2009)	Carbon	0,3.5,4.5,6,7.5	42–96.6	4*3*36	TPB	120 °C for 24 h
14	(Vijai et al. 2012)	Glass	0.01–0.03	5.12–6.8	100*100*500	IS Code	Ambient curing
15	(Branston et al. 2016)	Basalt	0.15,0.31,0.46,1,2	4.01–9.22	610*152*152	ASTM C1609	28 days curing
16	(Bhalchandra and Bhosle 2013)	glass	0,0.01–0.04	4–6.28	100*100*500	IS Code	90 °C for 8 h
17	(He et al. 2010)	Carbon	3.5	54.6–234.2	4*3*36	TPB	1100 to 1300 °C
18	(Wongsa et al. 2020)	Sisal Coconut Glass	0.5,0.75,1	3.2–6.56	40*40*160	ASTM C78	60 °C oven for 24 h
19	(Kizilkanat et al. 2015)	Basalt Glass	0.25, 0.50, 0.75, 1	5–6.75	100*100 _*350	JCI-S-002	Ambient curing
20	(Nematollahi et al. 2014)	PVA	2	4.92–11.5	60*60*280	ASRMC 348	60 °C oven for 24 h

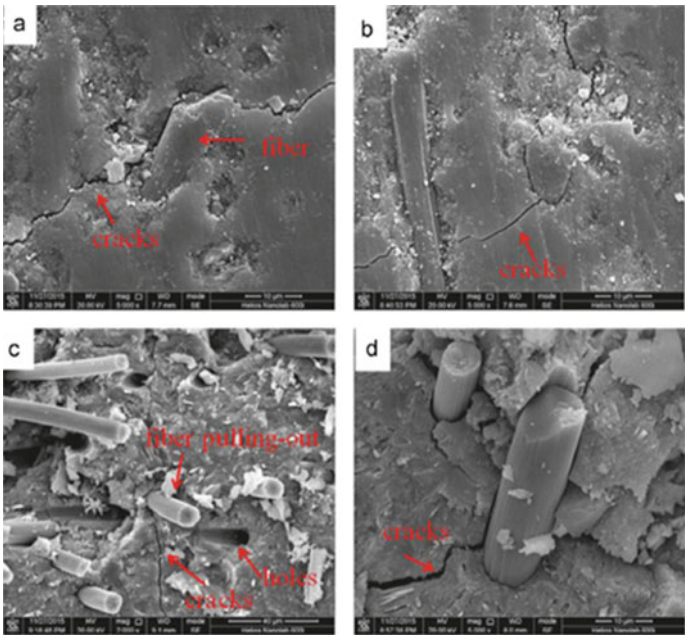

Fig. 4 Detailed microstructure observation of carbon fiber geopolymer **a, b** surface **c, d** fracture surface (Yan et al. 2016)

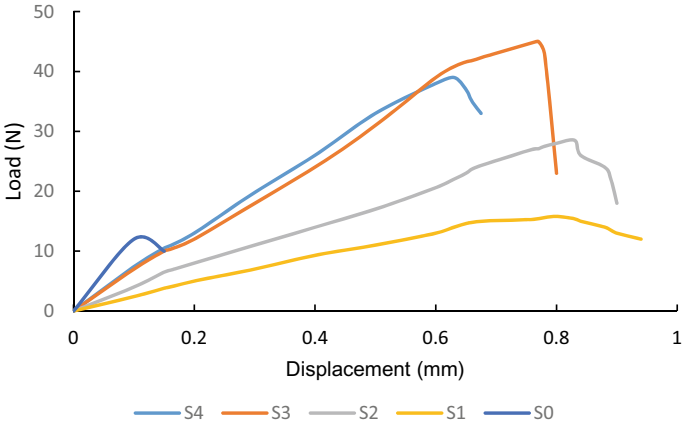

Fig. 5 Load displacement curve for carbon fiber geopolymer composites with fiber content (0,2.5,4,5,5.5%) (Yan et al. 2016)

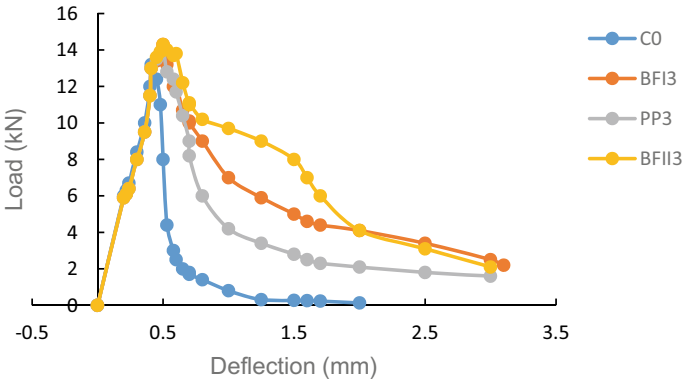

Fig. 6 Load vs deflection curve for polypropylene fiber, basalt. (Jiang et al. 2014)

Table 3 Summary of flexural toughness

Sr. no	Exp test	Type of fiber	Fiber content (%)	Flexural toughness factor	Method
1	(Yan et al. 2016)	Carbon	0,2.5,4,5,5.5	0.31–1.27 MPa m $^{1/2}$	SENB
2	(Alomayri 2017)	Glass	0,1,2,3	0.65–1.23 MPa m $^{1/2}$	TPB
3	(Kizilkanat et al. 2015)	Basalt Glass	0,0.25,0.5,0.75,1	17.5–27.5 MPa/mm^2 17–25 MPa/mm^2	TPB
4	(Alomayri et al. 2013)	Cotton	0.3–1	0.7–1.12 MPa m$^{1/2}$	JSCE SF4
5	(Alomayri et al. 2014b)	Cotton	0,4.5,6.2,8.3	0.6–1.8 MPa m$^{1/2}$ (H) 0.6–1.4 MPa m ^{½}(V)	JSCE SF4
6	(Alomayri et al. 2014a)	Cotton	0,3.6,4.5,6.2,8.3	0.6–1.8 MPa m$^{1/2}$	JSCE-SF4
7	(Al-mashhadani et al. 2018)	PVA	0,0.4,0.8,1.2	0.58–3.92 N/mm^2	JSCE-SF4
8	(Xu et al. 2017)	PVA	0,0.5,1,1.5,2	0.22–3.28 N/mm^2	JSCE-SF4
9	(Nematollahi et al. 2014)	PVA	2	0.086–0.59 N/mm^2	ASRMC 348

5 Effect on Split—Tensile Strength

A study (Xu et al. 2017), reported that tensile strength is influenced mainly by the alkali activator dosage. The tensile strength will be more with an increase in the fiber volume of the specimen (Jiang et al., 2014). Quite an opposite result is seen in the case of (Tiesong et al. 2009) study where short carbon fiber shows a greater toughening and strengthening effect for low volume percentage of fibers. Similarly, in the case of glass fiber, it is reported that 0.5% fiber content attains a maximum tensile strength when it is thermally cured (Sathanandam et al. 2017). Furthermore, there's a slight

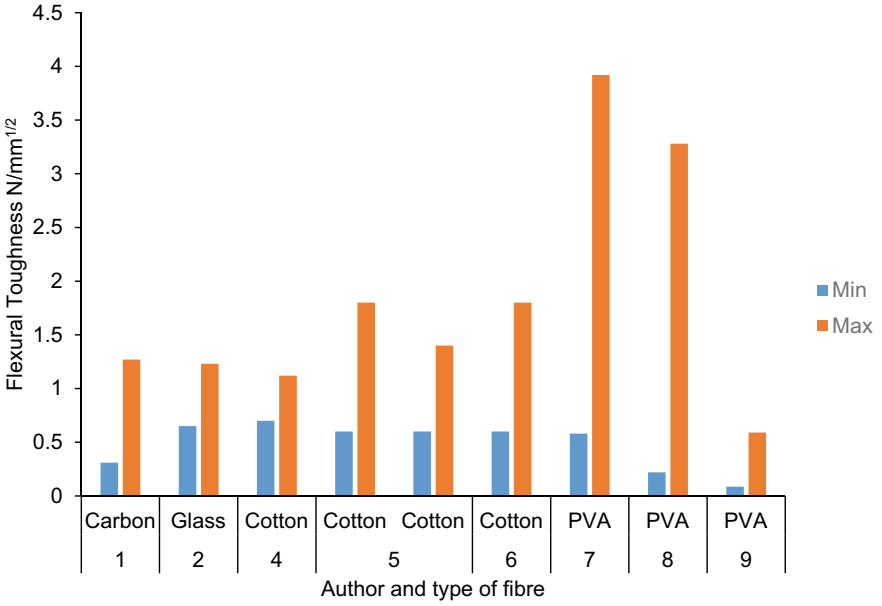

Fig. 7 Graphical representation of flexural toughness

difference in tensile strength when ambient curing is done while (Vijai et al. 2012) used 10% OPC with 90% flyash mixed glass fiber showing a slight increase in the strength with 0.03% as seen in Fig. 8.

(Jiang et al. 2014; Wongsa et al. 2020) reported that with an increase in fiber content, the split tensile strength of basalt fiber increases which can also be seen in Fig. 9 by (Kizilkanat et al. 2015). Figure 11 Basalt fiber shows elastic behavior in

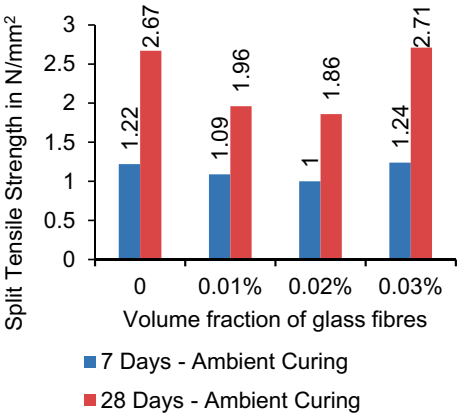

Fig. 8 Split tensile strength of glass reinforced adopted from (Vijai et al. 2012)

tension and a linear stress strain behavior until brittle failure (Dias and Thaumaturgo 2005; Vas et al. 2007). There is an increase in tensile strength in the case of basalt fibers (Phua et al. 2010; Vairavan et al. 2013). In Fig. 10 it can be seen that basalt fiber possesses higher stiffness when compared with carbon and glass fiber as well as high strength and ductility.

.

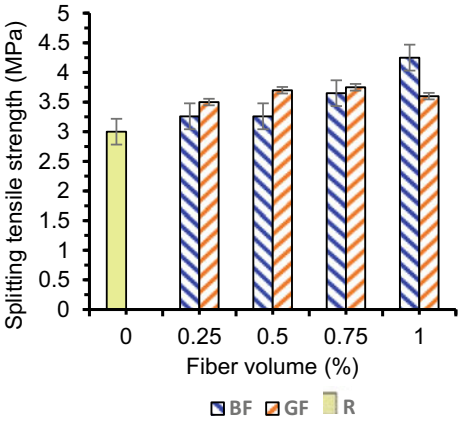

Fig. 9 Split tensile strength of glass and basalt reinforced concrete (Kizilkanat et al. 2015)

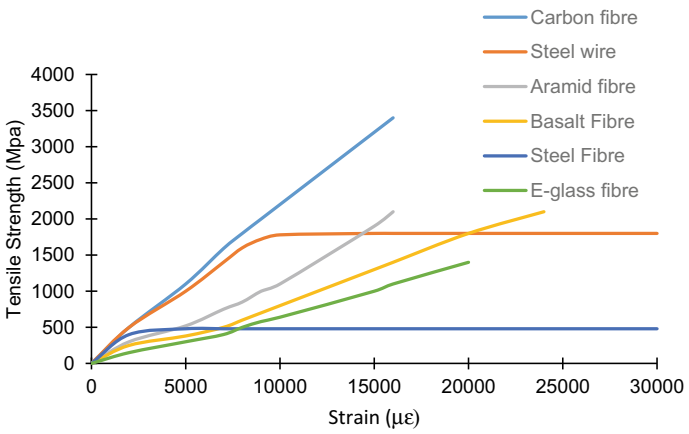

Fig. 10 Tensile strength vs. strain of different Geopolymer fibers compared with basalt fibre (Raj et al. 2017; Wu et al. 2012)

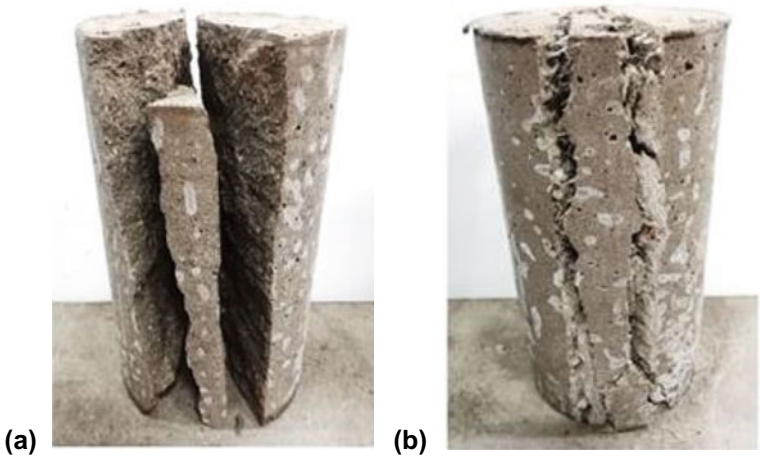

Fig. 11 The ductile failure mode of Composite with glass fiber **b** Vs. brittle failure of geopolymer without fiber **a** after splitting tensile strength test (Wongsa et al. 2020)

6 Conclusion

In this review, the research trends for using various fibers as reinforcement for geopolymer composites have shown that fiber can be used in the construction industry. Almost all the fibers have shown significant changes in their mechanical behavior as compared to the conventional OPC as well as geopolymer composite without fiber. Presently, carbon as well as glass fibers are being used for column confinement and retrofitting due to high flexural and tensile strength. Natural fibers like cotton, and coconut has shown the most compressive strength among other natural fiber like sisal. Based on the result of the mechanical behavior of different fibers from different studies following conclusions can be made-

- Irrespective of the fiber content and types, significant improvements in mechanical strength are seen in 28 days period.
- Geopolymer with fiber content exhibits higher fracture toughness than conventional OPC.
- In general, the larger the molarity of the alkaline solution, such as sodium hydroxide, the higher the strength. However, more research is needed as it is dependent on other factors such as the water to binder ratio.
- Although increased fiber content improves mechanical properties, flexural and compressive strength decreases after reaching a certain limit of fiber content.
- The presence of fibers in the geopolymer composite prevented catastrophic failures. Due to fiber pull out, fiber bridging, crack propagation, and matrix fracture, different morphologies in the fracture surface of the composite are visible with each type of fiber used.

- Basalt fiber, as well as glass fiber, have shown greater compressive, tensile, and flexural strength followed by carbon fiber. However, Carbon fiber when used at elevated temperatures up to 1100°C has shown remarkable strength.

Despite numerous studies that have been conducted to obtain the optimum amount of fiber content to be added to geopolymer composites, further research is needed because the quantity to be added for maximum strength varies with the type of fiber used. When compared with Ordinary Portland cement, regardless of the type of fiber included in the geopolymer composites, there has been an increase in mechanical strength.

References

Al-mashhadani MM, Canpolat O, Aygörmez Y, Uysal M, Erdem S (2018) Mechanical and microstructural characterization of fiber reinforced fly ash based geopolymer composites. Constr Build Mater 167:505–513. https://doi.org/10.1016/j.conbuildmat.2018.02.061

Alomayri T, Shaikh FUA, Low IM (2013) Characterisation of cotton fibre-reinforced geopolymer composites. Compos B Eng 50:1–6. https://doi.org/10.1016/j.compositesb.2013.01.013

Alomayri T, Shaikh FUA, Low IM (2014a) Synthesis and mechanical properties of cotton fabric reinforced geopolymer composites. Compos B Eng 60:36–42. https://doi.org/10.1016/j.compositesb.2013.12.036

Alomayri T, Shaikh FUA, Low IM (2014b) Effect of fabric orientation on mechanical properties of cotton fabric reinforced geopolymer composites. Mater Des 57:360–365. https://doi.org/10.1016/j.matdes.2014.01.036

Alomayri T (2017) The microstructural and mechanical properties of geopolymer composites containing glass microfibres. Ceram Int 43(5):4576–4582. https://doi.org/10.1016/j.ceramint.2016.12.118

Alomayri T, Vickers L, Shaikh FUA, Low IM (2014c) Mechanical properties of cotton fabric reinforced geopolymer composites at 200–1000 °C. J Adv Ceram 3(3):184–193. https://doi.org/10.1007/s40145-014-0109-x

Bhalchandra SA, Bhosle AY (2013) Properties of glass fibre reinforced geopolymer concrete. Int J Mod Eng Res (IJMER) 3(4):2007–2010

Branston J, Das S, Kenno SY, Taylor C (2016) Mechanical behaviour of basalt fibre reinforced concrete. Constr Build Mater 124:878–886. https://doi.org/10.1016/j.conbuildmat.2016.08.009

Davidovits J (1989) Geopolymers and geopolymeric materials. J Therm Anal 35(2):429–441. https://doi.org/10.1007/BF01904446

Dhand V, Mittal G, Rhee KY, Park SJ, Hui D (2015) A short review on basalt fiber reinforced polymer composites. Compos B Eng 73:166–180. https://doi.org/10.1016/j.compositesb.2014.12.011

Dias DP, Thaumaturgo C (2005) Fracture toughness of geopolymeric concretes reinforced with basalt fibers. Cement Concr Compos 27(1):49–54. https://doi.org/10.1016/j.cemconcomp.2004.02.044

He P, Jia D, Lin T, Wang M, Zhou Y (2010) Effects of high-temperature heat treatment on the mechanical properties of unidirectional carbon fiber reinforced geopolymer composites. Ceram Int 36(4):1447–1453. https://doi.org/10.1016/J.CERAMINT.2010.02.012

Jiang C, Fan K, Wu F, Chen D (2014) Experimental study on the mechanical properties and microstructure of chopped basalt fibre reinforced concrete. Mater Des 58:187–193. https://doi.org/10.1016/j.matdes.2014.01.056

Kizilkanat AB, Kabay N, Akyüncü V, Chowdhury S, Akça AH (2015) Mechanical properties and fracture behavior of basalt and glass fiber reinforced concrete: an experimental study. Constr Build Mater 100:218–224. https://doi.org/10.1016/j.conbuildmat.2015.10.006

Korniejenko K, Frączek E, Pytlak E, Adamski M (2016) Mechanical properties of geopolymer composites reinforced with natural fibers. Procedia Eng 151:388–393. https://doi.org/10.1016/j.proeng.2016.07.395

Li W, Xu J (2009) Mechanical properties of basalt fiber reinforced geopolymeric concrete under impact loading. Mater Sci Eng A 505(1–2):178–186. https://doi.org/10.1016/j.msea.2008.11.063

Lin T, Jia D, He P, Wang M (2010) In situ crack growth observation and fracture behavior of short carbon fiber reinforced geopolymer matrix composites. Mater Sci Eng A 527(9):2404–2407. https://doi.org/10.1016/j.msea.2009.12.004

Lin T, Jia D, He P, Wang M, Liang D (2008) Effects of fiber length on mechanical properties and fracture behavior of short carbon fiber reinforced geopolymer matrix composites. Mater Sci Eng A 497(1–2):181–185. https://doi.org/10.1016/j.msea.2008.06.040

Natali A, Manzi S, Bignozzi MC (2011) Novel fiber-reinforced composite materials based on sustainable geopolymer matrix. Procedia Eng 21:1124–1131. https://doi.org/10.1016/j.proeng.2011.11.2120

Nematollahi B, Sanjayan J, Shaikh FUA (2014) Comparative deflection hardening behavior of short fiber reinforced geopolymer composites. Constr Build Mater 70:54–64. https://doi.org/10.1016/J.CONBUILDMAT.2014.07.085

Patankar SV, Ghugal YM, Jamkar SS (2014) Effect of concentration of sodium hydroxide and degree of heat curing on fly ash-based geopolymer mortar. Indian J Mater Sci 2014:1–6. https://doi.org/10.1155/2014/938789

Phua YJ, Mohd Ishak ZA, Senawi R (2010) Injection molded short glass and carbon fibers reinforced polycarbonate hybrid composites: effects of fiber loading. J Reinf Plast Compos 29(17):2592–2603. https://doi.org/10.1177/0731684409358282

Raj S, Kumar VR, Kumar BHB, Iyer NR (2017) Basalt: structural insight as a construction material. Sādhanā 42(1):75–84. https://doi.org/10.1007/s12046-016-0573-9

Samal S, Phan Thanh N, Petríková I, Marvalová B, Vallons KAM, Lomov SV (2015) Correlation of microstructure and mechanical properties of various fabric reinforced geo-polymer composites after exposure to elevated temperature. Ceram Int 41(9):12115–12129. https://doi.org/10.1016/j.ceramint.2015.06.029

Sathanandam T, Awoyera PO, Vijayan V, Sathishkumar K (2017) Low carbon building: experimental insight on the use of fly ash and glass fibre for making geopolymer concrete. Sustain Environ Res 27:146–153. https://doi.org/10.1016/j.serj.2017.03.005

Singh B, Ishwarya G, Gupta M, Bhattacharyya SK (2015) Geopolymer concrete: a review of some recent developments. Constr Build Mater 85:78–90. https://doi.org/10.1016/j.conbuildmat.2015.03.036

Tanyildizi H, Yonar Y (2016) Mechanical properties of geopolymer concrete containing polyvinyl alcohol fiber exposed to high temperature. Constr Build Mater 126:381–387. https://doi.org/10.1016/j.conbuildmat.2016.09.001

Tiesong L, Dechang J, Meirong W, Peigang H, Defu L (2009) Effects of fibre content on mechanical properties and fracture behaviour of short carbon fibre reinforced geopolymer matrix composites. Bull Mater Sci 32(1):77–81. https://doi.org/10.1007/s12034-009-0011-2

Timakul P, Rattanaprasit W, Aungkavattana P (2016) Improving compressive strength of fly ash-based geopolymer composites by basalt fibers addition. Ceram Int 42(5):6288–6295. https://doi.org/10.1016/j.ceramint.2016.01.014

Vairavan M, Pandian A, Manikandan V, Jappes TW, Uthayakumar M (2013) Effect of fibre length and fibre content on mechanical properties of short basalt fibre reinforced polymer matrix composites. Mater Phys Mech 16(2013):107–117

van Deventer JSJ, Provis JL, Duxson P, Lukey GC (2007) Reaction mechanisms in the geopolymeric conversion of inorganic waste to useful products. J Hazard Mater 139(3):506–513. https://doi.org/10.1016/j.jhazmat.2006.02.044

Vas LM, Poloskei K, Felhos D, Deak T, Czigany T (2007) Theoretical and experimental study of the effect of fiber heads on the mechanical properties of non-continuous basalt fiber reinforced composites. Express Polym Lett 1(2):109–121. https://doi.org/10.3144/expresspolymlett.2007.19

Vijai K, Kumutha R, Vishnuram BG (2012) Properties of glass fibre reinforced geopolymer concrete composites. Asian J Civil Eng 13(4):511–520

Vora PR, Dave UV (2013) Parametric studies on compressive strength of geopolymer concrete. Procedia Eng 51:210–219. https://doi.org/10.1016/j.proeng.2013.01.030

Wongsa A, Kunthawatwong R, Naenudon S, Sata V, Chindaprasirt P (2020) Natural fiber reinforced high calcium fly ash geopolymer mortar. Constr Build Mater 241:118143. https://doi.org/10.1016/J.CONBUILDMAT.2020.118143

Wu Z, Wang X, Wu G (2012). Advancement of structural safety and sustainability with basalt fiber reinforced polymers. In: Proceedings of the 6th international conference on FRP composites in civil engineering, CICE 2012

Xu F, Deng X, Peng C, Zhu J, Chen J (2017) Mix design and flexural toughness of PVA fiber reinforced fly ash-geopolymer composites. Constr Build Mater 150:179–189. https://doi.org/10.1016/j.conbuildmat.2017.05.172

Yan S, He P, Jia D, Yang Z, Duan X, Wang S, Zhou Y (2016) Effect of fiber content on the microstructure and mechanical properties of carbon fiber felt reinforced geopolymer composites. Ceram Int 42(6):7837–7843. https://doi.org/10.1016/j.ceramint.2016.01.197

Zhang H, Hao X, Fan W (2016) Experimental study on high temperature properties of carbon fiber sheets strengthened concrete cylinders using geopolymer as adhesive. Procedia Eng 135:47–55. https://doi.org/10.1016/j.proeng.2016.01.078

Zheng Z, Feldman D (1995) Synthetic fibre-reinforced concrete. Progr Polym Sci 20(2):185–210. https://doi.org/10.1016/0079-6700(94)00030-6

Performance Prediction of Axially Loaded Square Reinforced Concrete Column with Additional Transverse Reinforcements in the Form of (1) Master Ties, (2) Diamond Ties, and (3) Open Ties under Close-in Blast

S. M. Anas, Mehtab Alam, and Mohammad Umair

Abstract Compression members in a building structural system called columns are the most important elements since they support other structural elements. Columns of many building structures with stilt floors for parking are exposed and therefore vulnerable to blast loading. Damage to the columns may be hazardous to the structure and its users. Such loadings may destabilize the entire building leading to even catastrophic collapse causing an enormous economic loss of property and human lives. Conventional structural design does not include loading from explosion events. Thus few buildings are designed with the requisite resistance against blast loading. Exceptions to this are buildings in petrochemical facilities where explosion hazards exist and high profile buildings such as embassies. One single explosion may damage not only a number of the load-carrying members of the same structure but adjoining structure too. Therefore, the response of the column under short-duration/high-magnitude blast loads from accidental and intentional explosions is of concern. In this study, a three-dimensional finite element model of 3000 mm long reinforced concrete (RC), 300 $\times$ 300 mm, square column provided with ductile reinforcement is developed using a general finite element software package, ABAQUS/Explicit-v.6.15. The developed model is subjected to an axial working load of 950 kN and a high explosive load of 100 kg ANFO ($\approx$82 kg TNT) at a scaled distance of 1.00 m/kg$^{1/3}$. The blast load is modelled as a pressure function of the stand-off distance and the equivalent mass of TNT. The so-called Concrete Damage Plasticity (CDP) model including the strain rate effect is used to model the concrete material behavior against blast loading.

S. M. Anas (✉) · M. Umair
Department of Civil Engineering, Faculty of Engineering and Technology, Jamia Millia Islamia (A Central University), New Delhi 110 025, Delhi, India
e-mail: mohdanas43@gmail.com

M. Umair
e-mail: mumair@jmi.ac.in

M. Alam
Department of Civil Engineering, Netaji Subhas University of Technology, 110073 New Delhi, India
e-mail: mehtab.alam@nsut.ac.in

I. Pal et al. (eds.), *Proceedings of the 2nd International Symposium on Disaster Resilience and Sustainable Development*, Lecture Notes in Civil Engineering 294,
https://doi.org/10.1007/978-981-19-6297-4_12

The nonlinear behavior of the longitudinal and transverse reinforcements is taken into account. By comparing the finite element (FE) results with the available experimental results in the open literature, the accuracy of the FE model is verified. To enhance the blast performance of the column, analysis has been extended to investigate the effect of additional transverse reinforcements in the form of (1) master ties, (2) diamond ties, and (3) open ties at key locations of the column and their role has been highlighted in the study. Dynamic responses including maximum displacement, stresses, damage dissipation energy, and crack/damage patterns have been evaluated and discussed. Localized damage in the form of concrete crushing on the explosion face over the confining regions and the spallation on the rear surface along with predominant flexure-shear cracks are observed. The study undertaken provides insight into the role played by the additional transverse reinforcements used in the RC columns and predicts improved blast performance in reducing the risk generated by chemical explosive-induced loadings.

Keywords Blast loading · RC columns · Numerical simulation · CDP model · Damage dissipation energy · Concrete cracking

1 Introduction

Explosions, whether accidental or planned, can cause significant damage to the built infrastructure and result in fatalities to occupants of buildings in close proximity to the centre of explosion. In a structural system, the load-bearing columns are one of the most important and vulnerable structural members. The columns damaged by blast loading may initiate the progressive collapse of the structure, resulting in tremendous casualties and major economic loss, as exemplified by the accidental detonation of 2,750 tons of Ammonium Nitrate in the Beirut City of Lebanon (Anas et al. 2021c, 2022, 2022a; Rajkumar et al. 2019; Ahmadi et al. 2021; Ul Ain et al. 2021). Progressive collapse of a building is typically initiated by an abrupt failure of one or more of the load-bearing structural components, such as columns (Jacques et al. 2015; Zhang et al. 2015). Therefore, the endurance of columns and similar other load-bearing elements in a structure under severe short-duration/high-magnitude blast loads is important to comprehend (IS 1968; Jayasooriya et al. 2014; Jacques et al. 2015; Kyei and Braimah 2017). With the aim of preventing catastrophic consequences of the possible blast events, understanding of the behavior of RC members under blast load is very crucial for not only the designing stages but also retrofitting possibilities thereafter. The blast waves generated from an explosion exert a transient dynamic load on structures. The short duration impulsive load and resulting inertial forces generated due to the acceleration of the structure are resisted by internally generated strain energy. The present work study the blast performance insight on account of the additional transverse reinforcement in the axially loaded seismically designed RC column using the ABAQUS/Explicit, a high-fidelity commercial software program (Anas and Alam (2021j); Rigby et al. (2020)). ABAQUS is one of the powerful finite

element codes, and its applications are widely used by engineers and researchers to model and analyze several automobile, aerospace, civil, and mechanical engineering problems and complexities.

The study of the blast resistance of conventionally designed structures has become significantly important in recent years in light of the increase in global terrorism. A number of papers have been published on the performance of the RC columns under blast loading in recent years (Fujikake and Aemlaor 2013; Jayasooriya et al. 2014; Li and Hao 2014; Burrell et al. 2015; Cui et al. 2015; Jacques et al. 2015; Zhang et al. 2015; Zhang et al. 2016; Hu et al. 2018; Wang et al. 2018; Rajkumar et al. 2019; Alsendi and Eamon 2020). Many researchers have identified failure of RC columns under blast loading as a potential precursor to progressive collapse. (Fujikake and Aemlaor 2013) experimentally investigated the effect of concrete strength and steel ratio on the blast performance of the 1200 × 180 × 180 mm RC columns of the building that was scheduled to be demolished. Obvious conclusions were drawn with regards to concrete strength and steel ratio such as an increase in the load-carrying capacity of the column with an increase of the concrete strength and steel ratio. (Jayasooriya et al. 2014) examined the damage resistance of 1000 × 1000 mm axially loaded concrete-steel-composite (CSC), and reinforced concrete (RC) columns subjected to different explosive loads (between 50 and 500 kg TNT) at standoff distances ranging from 0.63 to 1.36 m/kg$^{1/3}$. It was concluded that the CSC column gives superior performance against the blast loading with regards to load carrying capacity and cracking. (Li and Hao 2014) proposed various numerical models to predict concrete spall damage in the RC columns under different combinations of the explosive charges and standoff distances. (Cui et al. 2015) numerically investigated the effect of the column's dimension and steel ratio on the behavior of the RC column subjected to close-in explosion loading using the LS-DYNA software. Results showed that increasing the column's dimension and reinforcement ratio can improve the blast resistance capacity of the column. (Zhang et al. 2016) experimentally and numerically examined the behavior of square concrete-filled-double-skin-steel-tube (CFDST) columns with steel-fiber reinforced concrete subjected to explosive loads of 35 and 50 kg TNT at a standoff distance of 1.50 m. Results revealed that the CFDST column can withstand the explosive load of 50 kg TNT detonated at a height of 1 m from the ground. No concrete crushing and yielding of reinforcement were observed. (Hu et al. 2018) numerically studied the effect of charge shape and configuration on the blast response of the RC column using AUTODYN software. It was reported that the peak overpressure generated by cylindrical-shaped TNT charge is 2 times larger than that of the spherical one. The objectives of the research work reported in this paper are, primarily: To investigate the effect of seismic detailing (transverse reinforcement spacing) of RC columns carrying axial compression, in accordance to CSA A23.3, on their response to blast loading. To investigate the effect of additional transverse reinforcements (master tie/ diamond tie) and number of longitudinal steel bars on the blast resistance of the column.

2 Modeling of RC Column under Blast Loading

A high-fidelity professional software, ABAQUS/CAE version 6.15 has been employed in this study to investigate the effect of the additional transverse reinforcements used in design practice on the air-blast response of the axially loaded RC column experimentally tested by (Kyei and Braimah 2017) under a high explosive load of 100 kg ANFO (≈82 kg TNT). The charge was assumed to be 1.50 m high from the ground surface. The ductile detailing of the columns has been provided following the guidelines of CSA A23.3–04 (R2010) (CSA 2010) and IS 13920:2016 (IS 1968). The column tested was not designed against seismic loading and was assumed to be part of the seismic force-resisting system (SFRS) of the building with sufficient ductility to undergo lateral deformation (Kyei and Braimah 2017). Different approaches for investigating the response of RC columns under different blast loading conditions draw interest from many researchers. The most common numerical technique, Finite Element Method (FEM), is employed by many researchers to analyze structures under various types of dynamic loading conditions such as blast, impact, and wind. Therefore, the FEM investigations performed by researchers are presented herein.

2.1 General Description

A total of fourteen number of FE models of the RC columns with seismic reinforcement have been developed, Figs. 1 and 2. In the first model, the column is reinforced with 4 bars of 25 mm diameter and provided with the confining reinforcement in the form of 10 mm diameter master ties of grade Fe500 at a spacing of 75 mm c/c over a length of 600 mm at each end of the column, Fig. 1(a). In the second model, the confining reinforcement has been doubled i.e., with two master ties over the confining regions, Fig. 1(b). In the third model, the double master ties are provided over a length of 600 mm at the mid-height level of the column, while the top and bottom regions are with single master ties, Fig. 1(c). The fourth model has been obtained by providing an additional master tie over the mid-height region in the second model, Fig. 1(d). It is worth mentioning that the double master ties are with no spacing between them i.e., they are together. To investigate the effect of the number of bars on blast performance of the column without changing the longitudinal reinforcement ratio, 4–25 mm bars have been replaced with 4–16 and 4–20 mm diameter bars having 20 mm bars at the corners in the fifth model maintaining the transverse reinforcement as that in the first model, Fig. 1(e). Models no. 6, 7, and 8 have the longitudinal reinforcement layout of model no. 5 and having the provision of transverse reinforcement of models 2, 3, and 4, respectively, Fig. 1(f–h). Diamond ties being very popular with structural designers, models no. 9, 10, and 11 are the same as the models no. 6, 7, and 8, but with a difference that the additional master ties are replaced by the diamond ties of the same diameter, Fig. 1(i-k). Diamond ties used in models no. 9, 10, and 11 have

been replaced by two open ties of the same diameter to obtain models no. 12, 13, and 14, Fig. 1(l–n). All the columns are 300 × 300 mm in size. The span of the column is 3000 mm. The columns are subjected to an axial working gravity load of 950 kN and blast pressure of 8.60 MPa generated from the 100 kg ANFO charge.

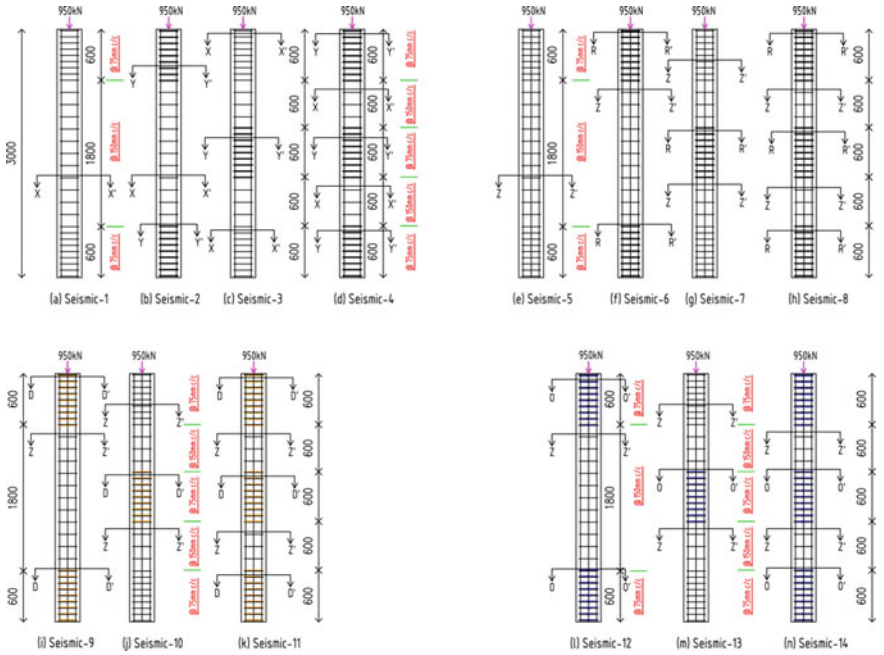

Fig. 1 Reinforcement details for seismic columns

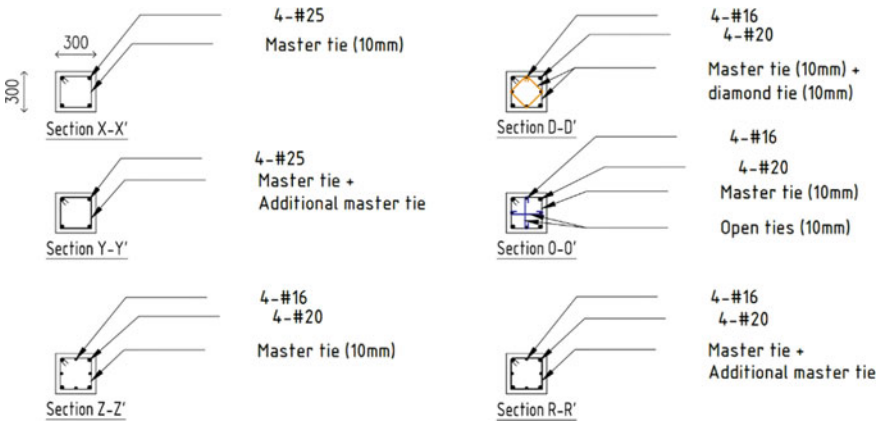

Fig. 2 Section details for seismic columns

2.2 Element Mesh, Material Properties, and Boundary Conditions

Selection of appropriate element types is essential for accurate modelling in the finite element method (FEM). The columns are discretized with 8-node linear brick explicit elements (C3D8R) with reduced integration and hourglass control (ABAQUS 2017) (ABAQUS User Assistance Guide, 2017). A mesh size of 10 mm has been adopted following the convergence test conducted at a scaled distance of 1.00 m/kg$^{1/3}$. The final mesh was automatically generated by ABAQUS, and is rather refined. The compressive strength, tensile strength, Young's modulus, and Poisson's ratio of the concrete taken from (Kyei and Braimah 2017) are 30 MPa, 3.00 MPa, 26.60 GPa, and 0.20, respectively. The mass density, ultimate tensile strength, yield strength, Young's modulus, and Poisson's ratio of the steel are 7850 kg/m^3, 545 MPa, 500 MPa, 210 GPa, and 0.30, respectively. As per CEB-FIB code and UFC 3-340-02(2008), dynamic increase factors (DIF) are applied to the material properties to incorporate the strain rate effect (Anas and Alam 2022c; Anas and Alam 2022d; Anas et al. 2022e; Anas et al. 2022f; Anas et al. 2022g; Anas et al. 2022h; Anas et al 2022i; Anas et al. 2022j; Anas et al. 2022k; Ahmadi et al. 2022; Shariq et al. 2022; Shariq et al. 2022a; Shariq et al. 2022b; Shariq et al. 2022c; Tahzeeb et al. 2022a; Tahzeeb et al. 2022b; Tahzeeb et al. 2022c; Ul Ain et al. 2021; Aamir et al 2022; Shariq et al. 2022d; Anas et al. 2022l; Anas and Alam 2022e; Anas et al. 2022m). The thickness of the concrete cover to the longitudinal steel bar is 40 mm. The re-bars are discretized with 2-node explicit linear 3-D truss elements (T3D2). The re-bars are embedded in the column using the EMBEDDED_REGION constraint command. This approach constrained translational degrees of freedom of the embedded reinforcement element nodes to the degrees of freedom of the surrounding concrete element nodes. Effects associated with the steel reinforcement–concrete interface, such as bond-slip, are modeled approximately by introducing some tension stiffening into the concrete modeling to simulate load transfer across cracks through the steel reinforcement. The axial load-carrying columns have been modeled with no translational degree-of-freedom restraint in the direction of the applied load (Kyei and Braimah 2017). However, the bottom of the columns is assumed fixed.

2.3 Material Modeling of Concrete

Concrete Damage Plasticity (CDP) model, a modification of the Drucker-Prager model put forward by (Lee and Fenves 1998), and (Lubliner et al. 1989), was developed to simulate the non-linear behavior of the materials such as concrete, masonry, etc., under quasi-static and extreme loadings. The evolution of the failure surface is controlled by two damage variables i.e., compression damage (D_c) and tension damage (D_t), which are connected to failure mechanisms of the material under compression and tension loadings (Hafezolghorani et al. 2017; Anas et al. 2022b;

Anas and Alam 2022c; Anas and Alam 2022d; Anas et al. 2022e; Anas et al. 2022f; Anas et al. 2022g; Anas et al. 2022h; Anas et al 2022i; Anas et al. 2022j; Anas et al. 2022k; Ahmadi et al. 2022; Shariq et al. 2022; Shariq et al. 2022a; Shariq et al. 2022b; Shariq et al. 2022c; Tahzeeb et al. 2022a; Tahzeeb et al. 2022b; Tahzeeb et al. 2022c; Ul Ain et al. 2021; Aamir et al 2022; Shariq et al. 2022d; Anas et al. 2022l; Anas and Alam 2022e; Anas et al. 2022m). It is assumed that the uniaxial stress–strain curves can be converted into stress versus inelastic-strain curves. This conversion is performed automatically by the ABAQUS/CAE program from the user-provided stress versus plastic strain data. The uniaxial compressive and tensile responses of the material with respect to the CDP model under compression and tension loadings are given as:

$$\sigma_c = (1 - D_c)E_0(\varepsilon_c - {\varepsilon_c}^{pl,h}) \tag{1}$$

$$\sigma_t = (1 - D_t)E_0(\varepsilon_t - {\varepsilon_t}^{pl,h}) \tag{2}$$

$$E_u = \left(1 - D_{i=c,t}\right)E_0 \tag{3}$$

Here, σ_c = nominal compressive stress; σ_t = nominal tensile stress; ε_c= compressive strain (${\varepsilon_c}^{pl,h}+{\varepsilon_c}^{el}$); ε_t = tensile strain (${\varepsilon_t}^{pl,h}+{\varepsilon_t}^{el}$); ${\varepsilon_c}^{pl,h}$ = plastic hardening compressive strain; ${\varepsilon_t}^{pl,h}$= plastic hardening tensile strain; ${\varepsilon_c}^{el}$ = elastic compressive strain; ${\varepsilon_t}^{el}$ = elastic tensile strain; E_0 = initial elasticity modulus of the material; D_c and D_t are compression and tension damage variables; and E_u = reduced elastic modulus of the material. Previous research has indicated that the CDP model can accurately predict damage/crack patterns under explosive-induced blast loading (Anas et al. 2020, 2021a, 2020b; Anas et al. 2021b, 2021c, 2021d, 2021fe, 2021gf, 2021g, 2021h; Anas and Alam 2021e; Valente and Milani 2016a, 2016b). The same is employed in this study using the mechanical properties of the concrete from (Hafezolghorani et al. 2017). A non-linear behavior is simulated for both the tension and compression regimes. An exponential softening is provided for the tension response. In compression, a hardening branch is assumed to be the post-peak response described by a parabolic softening law. These curves are represented in Ref. (Hafezolghorani et al. 2017) together with the corresponding parameters required as input. Note that the input for the CDP model in ABAQUS needs to be regularized aiming to guarantee mesh objectivity of the results. In this regard, it is assumed: a dilation angle of Ψ = 31 degrees; an eccentricity parameter e = 0.1; a ratio between the bidirectional and unidirectional compres sive strengths of masonry of $f_{b_0}/f_{c_0} = 1.16$; a stress ratio in the tensile meridian of k = 0.67; and a value for the viscosity parameter of 10 . The CDP model requires that the strain rate-dependent stress–strain curves belonging to the concrete for tension and compression are defined as tabular.

2.4 Blast Loading

Air-blast generates a shock wave of very high pressure accompanying high-temperature and supersonic expansion of hot gases (Goel and Matsagar 2014; Hao et al. 2016; IS 1968; TM 1990). The abrupt rise in the air pressure carried by the Mach stem can cause severe damage to the structure or structural elements. Figure 3(a) shows the systematic time variation of air-blast pressure, *P(t)*, which is determined by the blast wave arrival time, t_A, rising time, t_1, the peak overpressure, P_{OP}, positive blast phase duration, t_d, duration of the negative phase of the blast, t^-, and the maximum negative air-pressure, $P_S{}^-$ (Wu and Hao 2005). The peak value of the blast pressure (incident and reflected) is a function of the charge mass, standoff distance of the structure from centre of explosion, and the angle of incidence to the reflecting surface to the blast wave. Air-blast in the ABAQUS/CAE program can be simulated using different approaches (Anas and Alam 2022c; Anas and Alam 2022d; Anas et al. 2022e; Anas et al. 2022f; Anas et al. 2022g; Anas et al. 2022h; Anas et al 2022i; Anas et al. 2022j; Anas et al. 2022k; Ahmadi et al. 2022; Shariq et al. 2022; Shariq et al. 2022a; Shariq et al. 2022b; Shariq et al. 2022c; Tahzeeb et al. 2022a; Tahzeeb et al. 2022b; Tahzeeb et al. 2022c; Ul Ain et al. 2021; Aamir et al 2022; Shariq et al. 2022d; Anas et al. 2022l; Anas and Alam 2022e; Anas et al. 2022m). However, in the current study, empirical models based on experimental results available in the open literature have been used. Figure 3(b) shows the air-blast profile

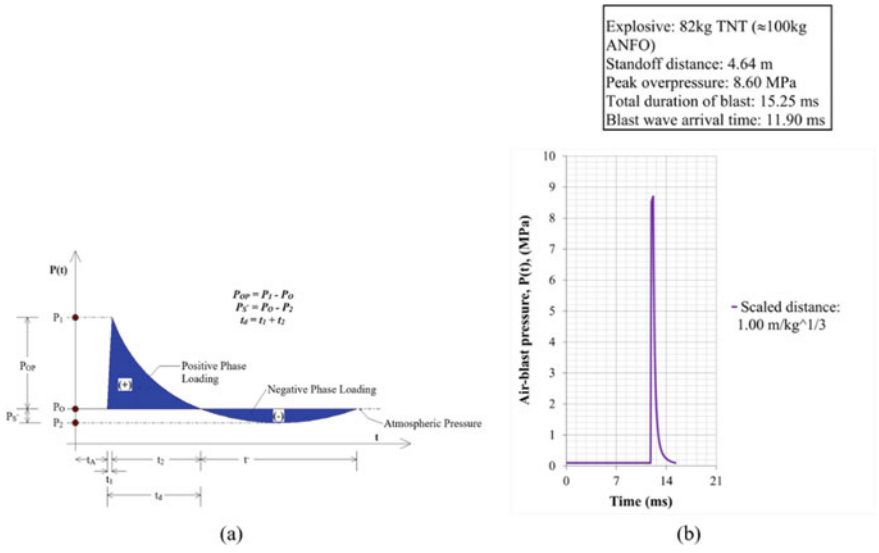

Fig. 3 **a** Time evolution of air-blast pressure due to an explosion acting on a target (Lubliner et al. 1989), and **b** Experimentally recorded air-blast history for a high explosive load of 100 kg ANFO (Hao et al. 2016)

for a scaled distance of 1.00 m/kg$^{1/3}$ in free air, experimentally recorded by (Kyei and Braimah 2017). The blast profile is modeled using the empirically-based model proposed by (Wu and Hao 2005). Referring to Fig. 3(b), the negative blast phase is neglected in this study following the guidelines of current blast design standards (Hao et al. 2016; IS 1968; TM 1990). The accuracy of the employed software and used numerical method to simulate the blast has been discussed in the previously published studies by the authors (Anas et al. 2020, 2021a, 2020b; Anas et al. 2021b, 2021c, 2021d, 2021fe, 2021gf, 2021g, 2021h; Anas and Alam 2021e). The air-blast pressure is defined as pressure versus time application and subsequently applied to the surface of the column facing the explosion using the explicit solver available in the ABAQUS/CAE program (Anas et al. 2020, 2021a, 2020b; Anas et al. 2021b, 2021c, 2021d, 2021fe, 2021gf, 2021g, 2021h; Anas and Alam 2021e). The explicit solver incrementally solves the equation of motion and updates the stiffness matrix at the end of each increment of load and displacement based on changes in geometry and material (Anas and Alam 2022c; Anas and Alam 2022d; Anas et al. 2022e; Anas et al. 2022f; Anas et al. 2022g; Anas et al. 2022h; Anas et al 2022i; Anas et al. 2022j; Anas et al. 2022k; Ahmadi et al. 2022; Shariq et al. 2022; Shariq et al. 2022a; Shariq et al. 2022b; Shariq et al. 2022c; Tahzeeb et al. 2022a; Tahzeeb et al. 2022b; Tahzeeb et al. 2022c; Ul Ain et al. 2021; Aamir et al 2022; Shariq et al. 2022d; Anas et al. 2022l; Anas and Alam 2022e; Anas et al. 2022m). It is worth noting that the loading on the RC column in the numerical simulations is accomplished in two phases. In the first phase, the axial loading is applied to the top surface nodes as linearly increasing load to the axial load level (ALR=1.0). The load is maintained for a few milliseconds until the internal stress stabilize at the stress corresponding to the ALR considered in the simulation. The static pressure is then maintained throughout the second phase of the loading which involves lateral blast loading (-Z direction) on the column.

3 Results and Discussions

3.1 Validation of the FE Model

The computed maximum transverse mid-height displacement (34.79 mm) of the reference column S–1, reinforced with 4 bars of 25 mm diameter and provided with the confining reinforcement in the form of 10 mm diameter master ties of grade Fe500 at a spacing of 75 mm c/c over a length of 600 mm at each end, is close to the maximum transverse mid-height displacement (36.00 mm) experimentally measured by (Kyei and Braimah 2017) with a percentage difference less than 4%. The crack patterns obtained on the side face of the column as depicted in Fig. 4 are closely matching with available test results, approve the application of the employed software to predicting the dynamic response of the column. The damage dissipation energy of the column S–1 subjected to a blast load of 100 kg ANFO is 731.15 J, Table 1. Maximum principal compressive and tensile stresses in the reinforcement of the

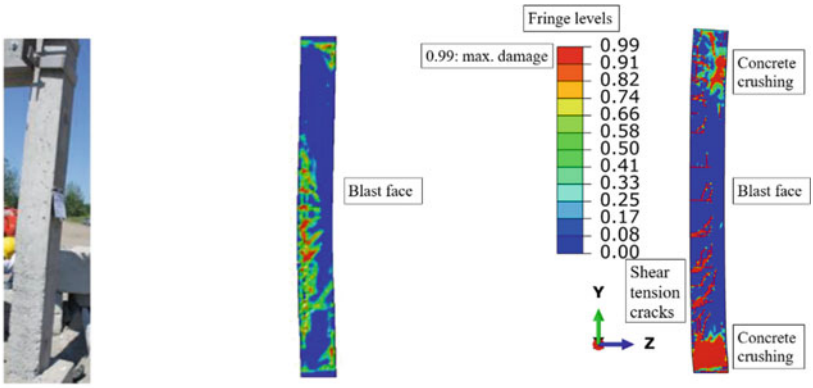

(a) Experimentally tested axially loaded RC column under 100 kg ANFO explosion (Kyei and Braimah, 2017)

(b) Tension Damage profile obtained using LS-DYNA under 100 kg ANFO explosion (Kyei and Braimah, 2017)

(c) Tension Damage profile obtained using ABAQUS/CAE under 100 kg ANFO explosion (Present study)

Fig. 4 Comparison of crack patterns on the side face of the reference S–1 column subjected to 82kg-TNT explosive load

Table 1 Summary of the displacement and damage dissipation energy

Column ID	Longitudinal steel bars	Maximum transverse mid-height displacement (mm) of the column	Maximum transverse displacement (mm) in the reinforcement of the column	Maxm. Damage dissipation energy (J)
S–1	4-25ϕ	34.79	34.53	731.15
S–2		32.60 (^{a}6)	32.39 (^{b}6)	672.65 (^{c}8)
S–3		30.43 (^{a}13)	30.31 (^{b}12)	669.02 (^{c}8)
S–4		28.42 (^{a}18)	28.34 (^{b}18)	548.36 (^{c}25)
S–5	4-20ϕ + 4-16ϕ	33.51 (^{a}4)	33.46 (^{b}3)	592.23 (^{c}19)
S–6		30.53 (^{a}12/ ^{d}9)	30.36 (^{b}12)	503.39 (^{c}31/ ^{e}15)
S–7		28.38 (^{a}18/ ^{d}15)	28.33 (^{b}18)	485.63 (^{c}34/ ^{e}18)
S–8		25.21 (^{a}28/ ^{d}25)	25.18 (^{b}27)	330.01 (^{c}55/ ^{e}44)
S–9	4-20ϕ + 4-16ϕ	33.09 (^{a}5/ ^{d}1)	33.03 (^{b}4)	621.48 (^{c}15/ ^{e}-5)
S–10		32.09 (^{a}8/ ^{d}4)	32.03 (^{b}7)	598.15 (^{c}18/ ^{e}-1)
S–11		31.01 (^{a}11/ ^{d}7)	30.96 (^{b}10)	588.57 (^{c}19/ ^{e}0)
S–12	4-20ϕ + 4-16ϕ	33.23 (^{a}4/ ^{d}1)	33.07 (^{b}4)	632.79 (^{c}14/ ^{e}-7)
S–13		32.22 (^{a}7/ ^{d}4)	32.18 (^{b}7)	579.61 (^{c}21/ ^{e}2)
S–14		31.04 (^{a}11/ ^{d}7)	30.97 (^{b}10)	608.99 (^{c}17/ ^{e}-3)

^{*a} percentage decrease (%) in displacement of the column with respect to reference S–1 column
^{*b} percentage decrease (%) in displacement of the reinforcements of the column with respect to S–1 column
^{*c} percentage decrease (%) in DDE with respect to S–1 column
^{*d} percentage decrease (%) in displacement of the column with respect to S–5 column
^{*e} percentage decrease (%) in DDE with respect to S–5 column

S–1 column are 200.00 and 237.60 MPa, respectively (Fig. 5). The concrete on the explosion face of the column experiences maximum principal compressive stress of 45.95 MPa which is approximately 1.50 times more than the compressive strength of the concrete (30 MPa) (Fig. 6). On the explosion face of the column, the damage is in the form of concrete crushing near the top and bottom, while the concrete spallation occurs on the rear surface more at the bottom than at top of the column along with predominant flexure-shear cracks with a maximum depth exceeding half of the size of the column (Figs. 7 and 8).

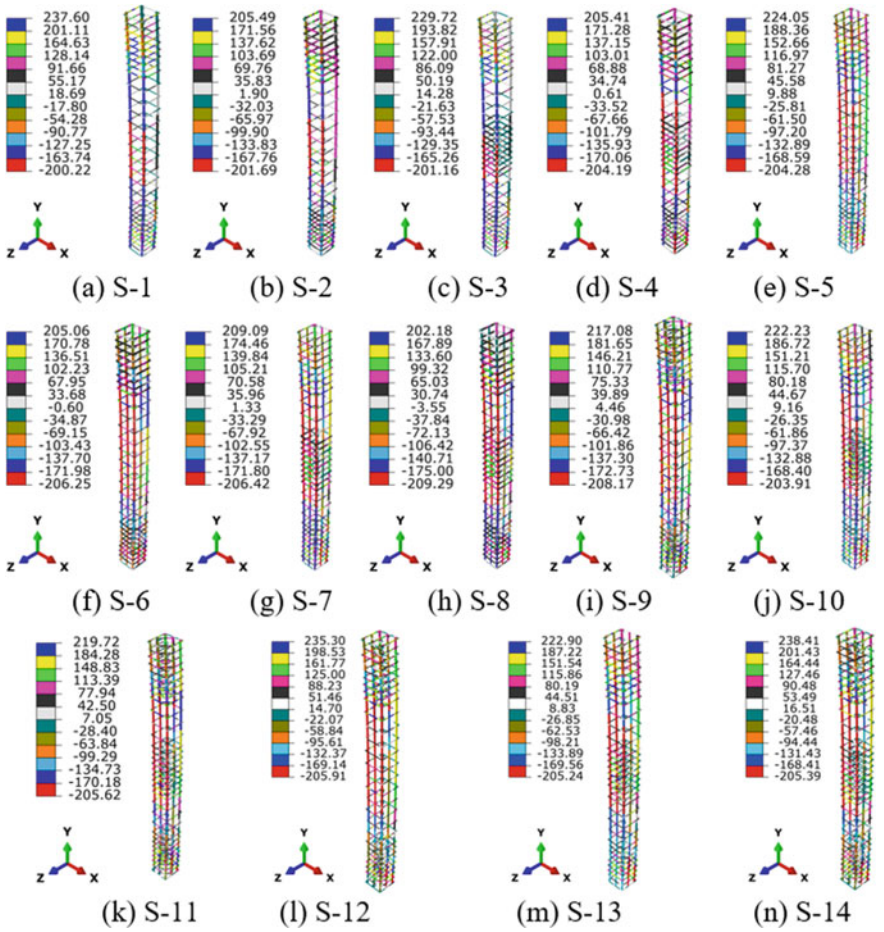

Fig. 5 Distribution of principal stresses (MPa) in the reinforcements of the seismic columns subjected to explosive load of 82kg-TNT (t = 15.25 ms)

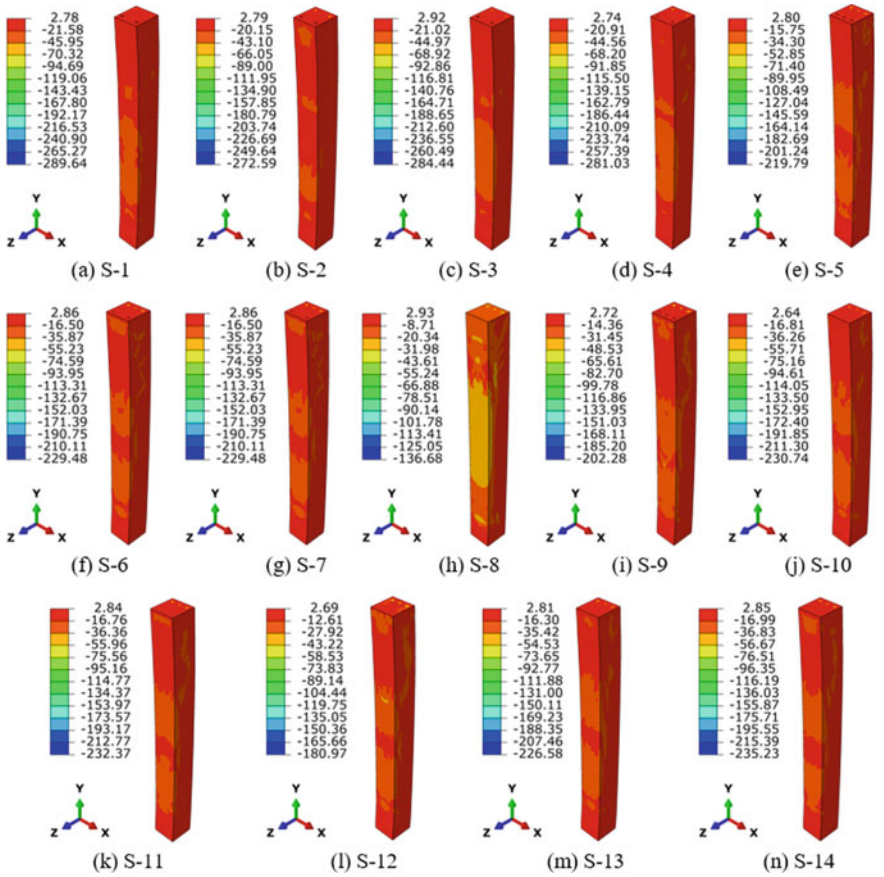

Fig. 6 Distribution of principal stresses (MPa) in the concrete columns subjected to explosive load of 82kg-TNT (t = 15.25 ms)

3.2 Effect of Additional Transverse Reinforcements and Number of Steel Reinforcing Bars

Table 1 summarizes the maximum displacement and damage dissipation energy of the seismic columns considered. The application of the additional master ties at each end of the column reduces the response by 14% or less with respect to control column S–1, i.e., the column with the single master ties at each of its end. Providing double master ties over a length of 600 mm at the mid-height region of the column (S–3) and single master ties at the top and bottom confining regions reduces the response almost as much as that of the column S–2, but the percentage reduction in maximum transverse mid-height displacement is more than twice of the reduction

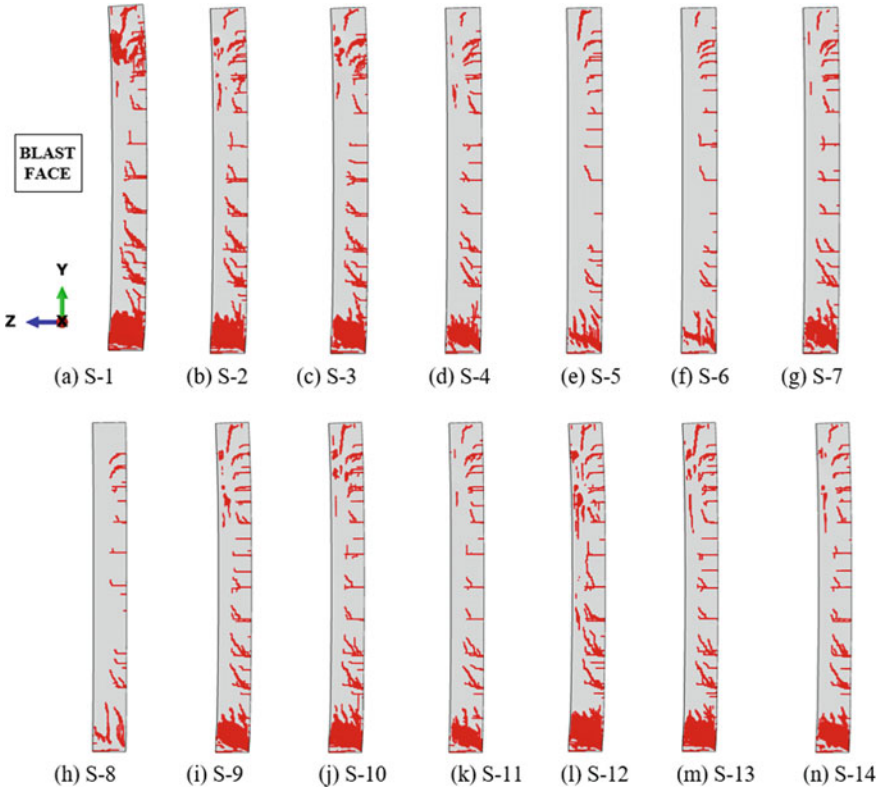

Fig. 7 Pattern of cracks developed on the side face of the seismic columns subjected to explosive load of 82kg-TNT (t = 15.25 ms)

in the column S–2. Additional transverse reinforcement over the mid-height region of the columns contributes more effectively than that at top and bottom confining regions with regards to maximum displacement and damage (DDE) by reducing the maximum tensile stress in longitudinal steel reinforcement (Table 1 & Figs. 5, 7, 8, 9 and 10). The use of the additional master tie over the mid-height, as well as the confining regions, decreases the maximum transverse mid-height displacement, damage dissipation energy, and maximum tensile stress in the reinforcement of the column S–4 by 18, 25, and 14%, respectively, with respect to the reference S–1 column (Table 1 & Fig. 5). It is evidenced from Fig. 5 that the maximum compressive stress in the concrete of the seismic columns S2-S4 is almost the same as that of column S–1.

Referring to Table 1, it is observed that the effect of the number of the longitudinal steel bars of the almost equal area of cross–section significantly reduces the damage (19%), however, the reduction in the transverse displacement is insignificant (4%) respectively, with respect to the column S–1. Comparing the analytical results of the

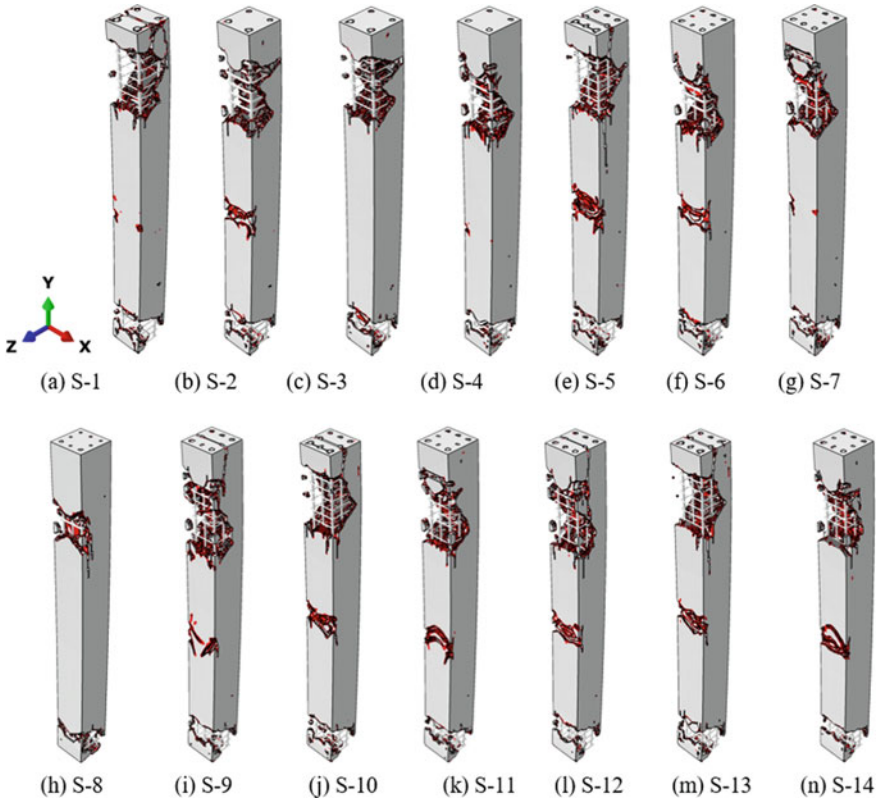

Fig. 8 Damage: Crushing of concrete of the seismic columns

columns S7 and S6 (Table 1), it is found that the provision of the additional master ties at the mid-height region of the column is more beneficial with regards to the damage (DDE) as well as maximum transverse displacement than the additional ties in the top and bottom confining regions of the column. More number of the longitudinal steel bars with the same area of the cross–section in combination with the additional master ties over the confining regions as well as the mid-height region of the column (S–8) is found to be the most effective to control the damage by more than 50% and maximum transverse displacement by more than 25% (Table 1).

Results obtained for the column S–9 show that the additional diamond ties at the top and bottom confining regions not only insignificantly contribute to control the maximum displacement but increase the damage too. The use of the additional diamond ties over the mid-height region of the column S–10 makes the blast response a bit better than the column S–9, but the contribution remains insignificant. Placement of the additional diamond ties over the confining regions as well as the mid-height region of the column (S–11) does not improve the performance of the column to

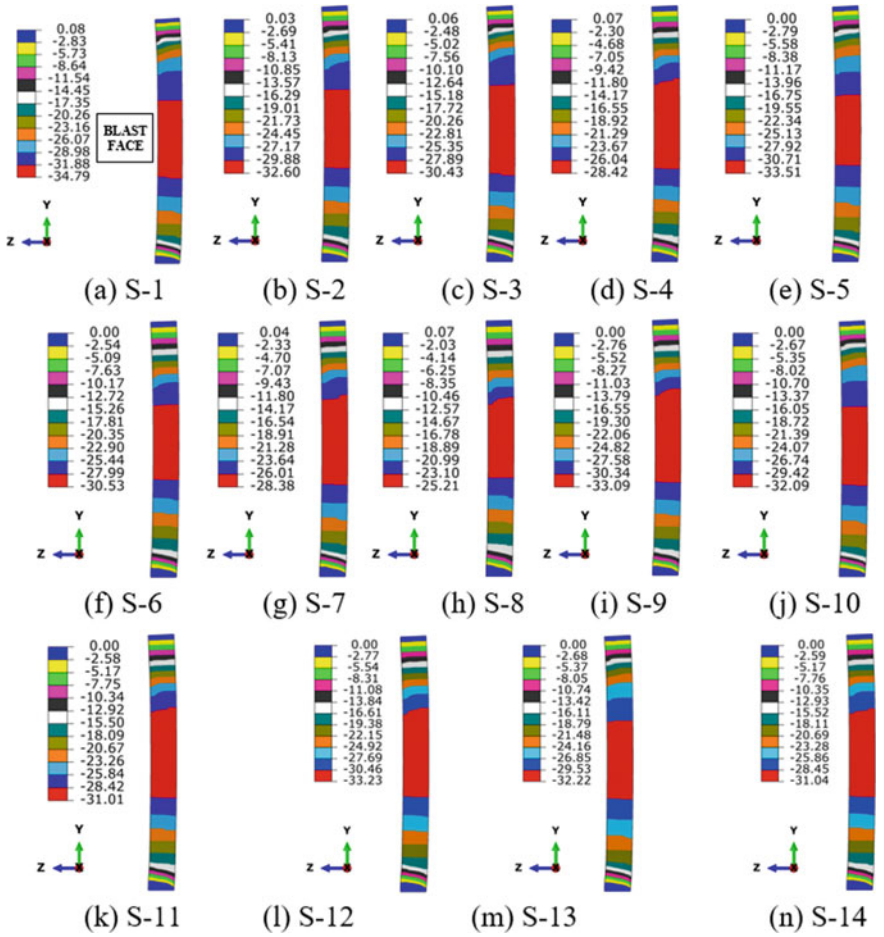

Fig. 9 Distribution of transverse Z-displacement (mm) for the seismic columns subjected to explosive load of 100 kg ANFO (t = 15.25 ms)

the acceptable level, therefore their application in the columns for blast performance point of view should be avoided. Responses of the additional open ties are found to be poorer than those of the additional diamond ties except their application over the mid-height level of the column (S–13) which gives better performance than the additional diamond ties over the same confining region with regards to the damage (DDE).

Figure 11 shows the distribution of principal stresses in the reinforcements of the column S–8 at different step times. At time $t = t_A$, i.e., when the blast wave hits the target column, maximum compressive stress carried by the steel bars facing the explosion is 107.19 MPa, while maximum tensile stress carried by the ties near the

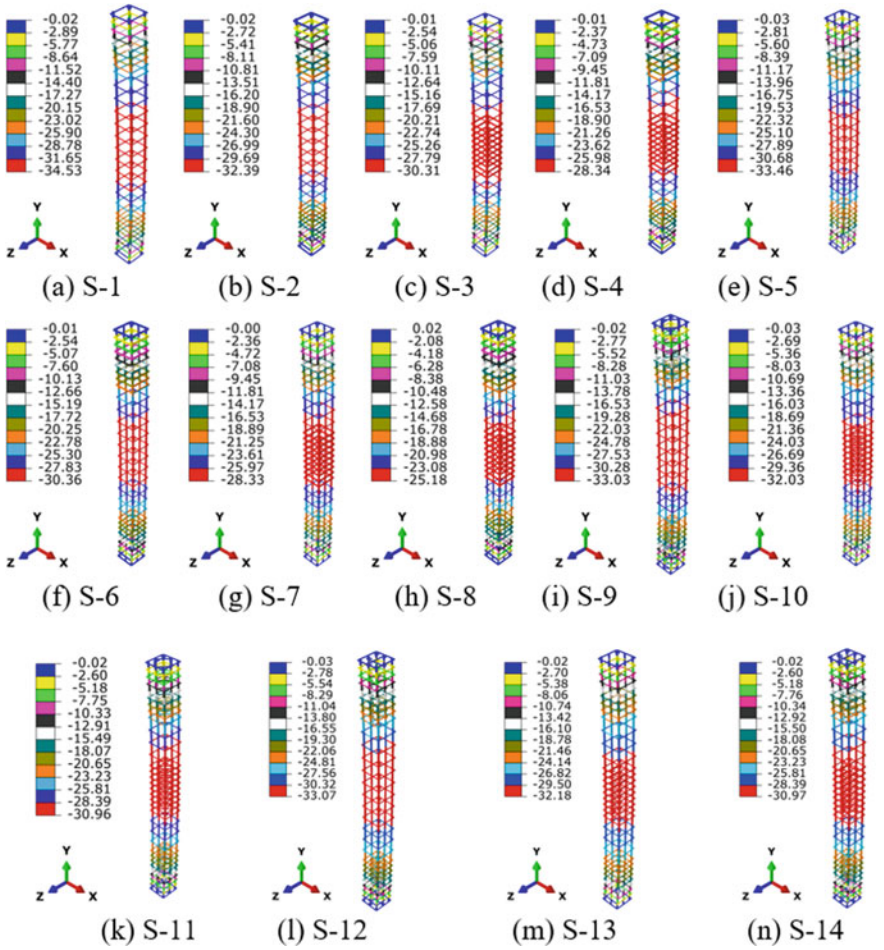

Fig. 10 Distribution of transverse Z-displacement (mm) in the reinforcements of the seismic columns subjected to explosive load of 100 kg ANFO (t = 15.25 ms)

mid-height level is 47.14 MPa. At time $t = t_1$, i.e., when the air-blast pressure reaches its peak value (8.60 MPa), the above compressive and tensile stresses increase by 30 and 41%, respectively. These stresses increase further for time $t > t_1$, but remain less than half of the yield stress of the steel (500 MPa), which shows that the steel reinforcement of the columns does not yield.

From the analytical results computed, shown in Table 1, it is concluded that the columns S–4, S–6, S–7, and S–8 give considerable blast performance. However, the performance of column S–8 is most superior.

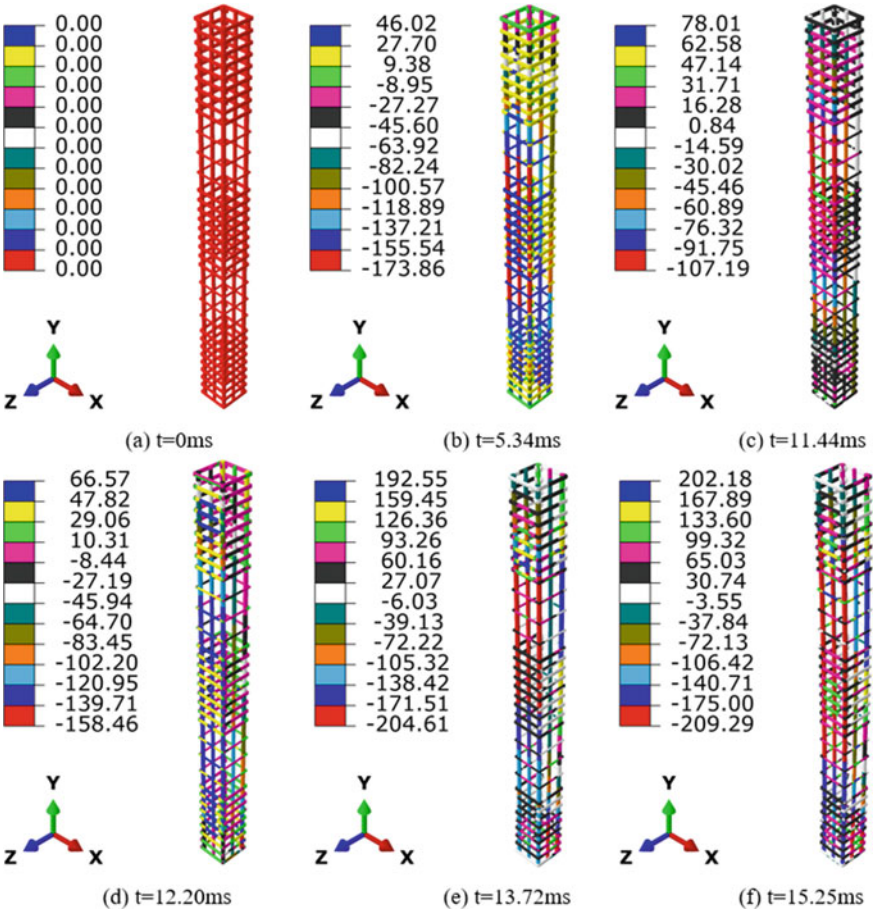

Fig. 11 Distribution of principal stresses (MPa) in the reinforcements of the column S–8 at different time steps (+ve values indicate tensile)

4 Conclusions

This study has performed finite element simulation of the 300 × 300 mm axially loaded, 3000 mm long, RC column subjected to a high explosive load of 100 kg ANFO using the ABAQUS/CAE program. The analytical results computed are verified with the available experimental ones. Following the blast response of the seismically reinforced column (S–1) with 4-25 mm diameter longitudinal steel bars and having confining reinforcement in the form of single master ties (10 mm diameter @75 mm c/c) over the top and bottom regions, the additional confining reinforcements have been considered over the confining regions, mid-height region only, and over the

confining regions as well as mid-height region. Changes in the configuration of the longitudinal steel reinforcement have also been made by increasing the number of steel bars from 4-#25 to 4-#20 + 4-#16 of approximately equal area. In the columns of the changed configuration of the longitudinal reinforcement, additional master ties, diamond ties, and open ties in the two directions have been considered and their blast performances are computed.

The following conclusions are drawn:

- Localized damage in the form of concrete crushing on the explosion face over the confining regions and the spallation on the rear surface along with predominant flexure-shear cracks are observed.
- Additional transverse reinforcement over the mid-height region of the columns reduces the maximum tensile stress in the longitudinal steel reinforcement and contributes more effectively than that over the confining regions with regards to maximum displacement and damage (DDE).
- The effect of the number of the longitudinal steel bars of almost equal area of the cross–section (column S–5) reduces the damage more significantly than the maximum transverse displacement with respect to the control column S–1.
- More number of the longitudinal steel bars with the same area of cross–section in combination with the additional master ties over the confining regions as well as the mid-height region (column S–8) is found to be the most effective combination to control the damage (DDE) by decreasing it to half and maximum transverse displacement to three-fourth of the column reference S–1.
- Additional diamond ties in place of the additional master ties are found not only ineffective to control the maximum displacement but increase the damage (columns S9-S12).
- Additional open ties in place of the additional master ties perform even worse than the additional diamond ties except for their use over the mid-height region where their contribution is marginally better than the diamond ties over the same region with regards to the damage (DDE).

The findings of the present research work are useful to structural engineers as well as the sectional committee for drafting the standard of blast-resistant design of the RC columns. This study also provides insight to mitigate the consequences of blast loading that may trigger progressive collapse risk out of accidental explosions or detonation of the high-yield explosives.

References

ABAQUS/CAE FEA program (2020) Concrete damage plasticity model, explicit solver, three dimensional solid element library. ABAQUS DS-SIMULIA User Manual

Alsendi A, Eamon DC (2020) Quantitative resistance assessment of sfrp-strengthened RC bridge columns subjected to blast loads. J Perform Constr Facil 34(4):1–9

Anas SM, Ansari MdI, Alam M (2020a) Performance of masonry heritage building under air-blast pressure without and with ground shock. Aust J Struct Eng 21(4):329–344

Anas SM, Alam M, Umair M (2021a) Performance of one-way concrete slabs reinforced with conventional and polymer re-bars under air-blast loading. In: Chandrasekaran S, Kumar S, Madhuri S (eds.) Recent Advances in Structural Engineering. Lecture Notes in Civil Engineering, April 2021a, vol 135, pp 179–191. https://doi.org/10.1007/978-981-33-6389-2_18

Anas SM, Alam M, Umair M (2020b) Performance of one-way composite reinforced concrete slabs under explosive-induced blast loading. In: 1st international conference on energetics, civil and agricultural engineering 2020b, ICECAE 2020b, Tashkent, Uzbekistan, vol 614. https://doi.org/10.1088/1755-1315/614/1/012094

Anas SM, Ansari MI, Alam M (2021) A study on existing masonry heritage building to explosive-induced blast loading and its response. Int J Struct Eng 11:387–412

Anas SM, Alam M, Umair M (2021c) Experimental and numerical investigations on performance of reinforced concrete slabs under explosive-induced air-blast loading: a state-of-the-art review. Structures 31:428–461

Anas SM, Alam M (2021d) Air-blast response of free-standing: (1) unreinforced brick masonry wall, (2) cavity RC wall, (3) RC walls with (i) bricks, (ii) sand, in the cavity: a macro-modeling approach. In: Marano GC, Chaudhuri S, Kartha GU, Kavitha PE, Prasad R, Achison RJ (eds) Proceedings of SECON 2021d. SECON 2021d. Lecture notes in civil engineering, vol 171. Springer, Cham, pp 921–930. https://doi.org/10.1007/978-3-030-80312-4_78

Anas SM, Alam M (2021e) Comparison of existing empirical equations for blast peak positive overpressure from spherical free air and hemispherical surface bursts. Iran J Sci Technol Trans Civil Eng 46:965–984

Anas SM, Alam M, Umair M (2021f) Performance of on-ground double-roof RCC shelter with energy absorption layers under close-in air-blast loading. Asian J Civil Eng 22:1525–1549

Anas SM, Alam M, Umair M (2021g) Air-blast and ground shockwave parameters, shallow underground blasting, on the ground and buried shallow underground blast-resistant shelters: a review. Int J Prot Struct 13:99–139

Anas SM, Alam M, Umair M (2021h) Out-of-plane response of clay brick unreinforced and strengthened masonry walls under explosive-induced air-blast loading. In: Kolathayar S, Ghosh C, Adhikari BR, Pal I, Mondal A (eds) Resilient Infrastructure, vol 202. Lecture Notes in Civil Engineering. Springer, Singapore, pp 477–491

Anas SM, Alam M, Umair M (2021h) Influence of charge locations on close-in air-blast response of pre-tensioned concrete u-girder. In: Kolathayar S, Ghosh C, Adhikari BR, Pal I, Mondal A (eds) Resilient Infrastructure, vol 202. Lecture Notes in Civil Engineering. Springer, Singapore, pp 513–527

Anas SM, Alam M (2021j) Performance of simply supported concrete beams reinforced with high-strength polymer re-bars under blast-induced impulsive loading. Int J Struct Eng 12:62–76

Burrell PR, Aoude H, Saatcioglu M (2015) Response of sfrc columns under blast loading. J Struct Eng 141(9):1–15

Cui J, Shi Y, Li XZ, Chen L (2015) Failure analysis and damage assessment of RC columns under close-in explosions. J Perf Constr Facil 29(5):B4015003

CSA A23.3–04 (2010) Design of Concrete Structures. Canadian Standards Association, Ontario

Fujikake K, Aemlaor P (2013) Damage of reinforced concrete columns under demolition blasting. Eng Struct 55:116–125

Goel DM, Matsagar AV (2014) Blast-resistant design of structures. Pract Per Struct Des Constr 19(2):1–9

Hao H, Hao Y, Li J, Chen W (2016) Review of the current practices in blast-resistant analysis and design of concrete structures. Adv Struct Eng 19(8):1193–1223

Hafezolghorani M, Hejazi F, Vaghei R, Jaafar BSM, Karimzade K (2017) Simplified damage plasticity model for concrete. Struct Eng Int 27(1):68–78

Hu Y, Chen L, Fang Q, Xiang H (2018) Blast loading model of the RC column under close-in explosion induced by the double-end-initiation explosive cylinder. Eng Struct 175:304–321

IS 13920 (1968) Indian Standard ductile detailing of reinforced concrete structures subjected to seismic forces – code of practice. Bureau of Indian Standards, New Delhi, India

IS 4991 (1968) Criteria for blast resistant design of structures for explosions above ground. Bureau of Indian Standards, New Delhi, India

Jayasooriya R, Thambiratnam PD, Perera JN (2014) Blast response and safety evaluation of a composite column for use as key element in structural systems. Eng Struct 61:31–43

Jacques E, Lloyd A, Imbeau P, Palermo D (2015) GFRP-retrofitted reinforced concrete columns subjected to simulated blast loading. J Struct Eng 141(11):1–13

Kyei C, Braimah A (2017) Effects of transverse reinforcement spacing on the response of reinforced concrete columns subjected to blast loading. Eng Struct 142:148–164

Li J, Hao H (2014) Numerical study of concrete spall damage to blast loads. Int J Impact Eng 68:41–55

Lee J, Fenves LG (1998) Plastic-damage model for cyclic loading of concrete structures. J Eng Mech 124(8):892–900

Lubliner J, Oliver J, Oller S, Onate E (1989) A plastic-damage model for concrete. Int J Solids Struct 25(3):299–326

TM 5–1300 (1990) Structures to resist the effects of accidental explosions. Technical Manual, Joint Department of the Army, the Navy, and the Air Force, US

Rajkumar D, Senthill R, Kumar MBB, Gomathi AK, Velan MS (2019) Numerical study on parametric analysis of reinforced concrete column under blast loading. J Perform Constr Facil 34(1):1–12

Rigby ES, Lodge JT, Alotaibi S, Barr DA, Clarke DS, Langdon SG, Tyas A (2020) Preliminary yield estimation of the 2020 Beirut explosion using video footage from social media. Shock Waves 30:671–675

Valente M, Milani G (2016a) Non-linear dynamic and static analyses on eight historical masonry towers in the north-east of Italy. Eng Struct 114(1):241–270

Valente M, Milani G (2016b) Seismic assessment of historical masonry towers by means of simplified approaches and standard FEM. Constr Build Mater 108(1):74–104

Wang W, Wu C, Li J (2018) Numerical simulation of hybrid frp-concrete-steel double-skin tubular columns under close-range blast loading. J Compos Constr 22(5):1–15

Wu C, Hao H (2005) Modeling of simultaneous ground shock and airblast pressure on nearby structures from surface explosions. Int J Impact Eng 31(6):699–717

Zhang F, Wu C, Zhao LX, Li XZ, Heidarpour A, Wang H (2015) Numerical modeling of concrete-filled double-skin steel square tubular columns under blast loading. J Perf Constr Facil 29(5):B4015002

Zhang F, Wu C, Zhao LX, Heidarpour A, Li Z (2016) Experimental and numerical study of blast resistance of square CFDST columns with steel-fibre reinforced concrete. Eng Struct 149:50–63

Anas SM, Shariq M, Alam M (2022) Performance of axially loaded square RC columns with single/double confinement layer(s) and strengthened with C-FRP wrapping under close-in blast. Mater Today Proc. https://doi.org/10.1016/j.matpr.2022.01.275

Anas SM, Alam M, Umair M (2022a) Strengthening of braced unreinforced brick masonry wall with (i) C-FRP wrapping, and (ii) steel angle-strip system under blast loading. Mater Today Proc. https://doi.org/10.1016/j.matpr.2022.01.335

Ahmadi E, Alam M, Anas SM (2021) Blast performance of RCC slab and influence of its design parameters. In: Kolathayar S, Ghosh C, Adhikari BR, Pal I, Mondal A (eds) Resilient Infrastructure, vol 202. Lecture Notes in Civil Engineering. Springer, Singapore, pp 389–402

Ul Ain Q, Alam M, Anas SM (2021) Behavior of ordinary load-bearing masonry structure under distant large explosion, beirut scenario. In: Kolathayar S, Ghosh C, Adhikari BR, Pal I, Mondal A (eds) Resilient Infrastructure, vol 202. Lecture Notes in Civil Engineering. Springer, Singapore, pp 239–253

Anas SM, Alam M, Umair M (2022b) Effect of design strength parameters of conventional two-way singly reinforced concrete slab under concentric impact loading. Mater Today Proc. https://doi.org/10.1016/j.matpr.2022.02.441

Anas SM, Alam M (2022c) Performance of brick-filled reinforced concrete composite wall strengthened with C-FRP laminate(s) under blast loading. Mater Today Proc 651–11. S2214785322014894. https://doi.org/10.1016/j.matpr.2022.03.162

Anas SM, Alam M (2022d) Role of shear reinforcements on the punching shear resistance of two-way RC slab subjected to impact loading. Mater Today Proc, Elsevier (in press)

Anas SM, Alam M, Umair M (2022e) Performance based strengthening with concrete protective coatings on braced unreinforced masonry wall subjected to close-in explosion. Mater Today Proc. 64:161–172. S2214785322023458 https://doi.org/10.1016/j.matpr.2022.04.206

Anas SM, Alam M, Shariq M (2022f) Damage response of conventionally reinforced two-way spanning concrete slab under eccentric impacting drop weight loading. Def Technol. S221491472200085X. https://doi.org/10.1016/j.dt.2022.04.011

Anas SM, Alam M, Umair M (2022g) Performance of (1) concrete-filled double-skin steel tube with and without core concrete, and (2) concrete-filled steel tubular axially loaded composite columns under close-in blast. Int. J Protective Struct. https://doi.org/10.1177/2F20414196221104143

Anas SM, Alam M, Shariq M (2022h) Behavior of two-way RC slab with different reinforcement orientation layouts of tension steel under drop load impact. Mater Today Proc, Elsevier (in press)

Anas SM, Alam M, Umair M (2022i) Air-blast response of axially loaded clay brick masonry walls with and without reinforced concrete core. In: Fonseca de Oliveira Correia JA, et al (eds) ASMA 2021, Advances in Structural Mechanic and Applications, STIN 19, pp 1–18, 2023

Anas SM, Alam M, Tahzeeb R (2022j) Impact response prediction of square RC slab of normal strength concrete strengthened with (1) laminates of (i) mild-steel and (ii) C-FRP and (2) strips of C-FRP under falling-weight load. Mater Today Proc. S2214785322049422. https://doi.org/10.1016/j.matpr.2022.07.324

Anas SM, Alam M, Umair M (2022k) Experimental studies on blast performance of unreinforced masonry (URM) walls of clay bricks and concrete blocks: a state-of-the-art review. Int J Mason Res Innov (in press). https://doi.org/10.1504/IJMRI.2022.10049719

Ahmadi E, Alam M, Anas SM (2022) Behavior of C-FRP laminate strengthened masonry and unreinforced masonry compound walls under blast loading, Afghanistan scenario. Int J Mason Res Innov (in press). https://doi.org/10.1504/IJMRI.2022.10049968

Shariq M, Alam M, Husain A, Anas SM (2022) Jacketing with steel angle sections and wide battens of RC columnand its influence on blast performance. Asian J Civil Eng 23(4):487–500. https://doi.org/10.1007/s42107-022-00437-9

Shariq M, Saifi F, Alam M, Anas SM (2022a) Effect of concrete strength on the dynamic behavior of axially loaded reinforced concrete column subjected to close-range explosive loading. Mater Today Proc. S2214785322049410. https://doi.org/10.1016/j.matpr.2022.07.313

Shariq M, Alam M, Husain A, Islam N (2022b) Response of strengthened unreinforced brick masonry wall with (1) mild steel wire mesh and (2) CFRP wrapping under close-in blast. Mater Today Proc 64:643–654. S2214785322034320. https://doi.org/10.1016/j.matpr.2022.05.153

Shariq M, Alam M, Husain A (2022c) Performance of RCC column retrofitted with CFRP wrappings and the wrappings with steel angle-batten jacketing under blast loading. In: Nandagiri L, Narasimhan MC, Marathe S (eds) Recent Advances in Civil Engineering, Lecture Notes in Civil Engineering, vol 256, Springer, Singapore. https://doi.org/10.1007/978-981-19-1862-9_21

Tahzeeb R, Alam M, Muddassir SM (2022a) A comparative performance of columns: reinforced concrete composite and composite with partial C-FRP wrapping under contact blast. Mater Today Proc 62:2191–2202. S2214785322017126. https://doi.org/10.1016/j.matpr.2022.03.367

Tahzeeb R, Alam M, Muddassir SM (2022b) Performance of composite and tubular columns under close-in blast loading: a comparative numerical study. Mater Today Proc 65:51–62. S221478532202750X. https://doi.org/10.1016/j.matpr.2022.04.587

Tahzeeb R, Alam M, Muddassir SM (2022c) Effect of transverse circular and helical reinforcements on the performance of circular RC column under high explosive loading. Mater Today Proc 64:315–324. S2214785322028383. https://doi.org/10.1016/j.matpr.2022.04.676

Ul Ain Q, Alam M, Anas SM (2022) Response of two-way RCC slab with unconventionally placed reinforcements under contact blast loading. In: Fonseca de Oliveira Correia JA, et al (eds) ASMA 2021, Advances in Structural Mechanics and Applications, STIN 19, pp 1–18, 2023 (in press). https://doi.org/10.1007/978-3-031-04793-0_17

Aamir M, Alam M, Anas SM (2022) Effect of blast location and explosive mass on the dynamic behavior of a bowstring steel highway girder bridge subjected to air-blast. Mater Today Proc. S2214785322054487. https://doi.org/10.1016/j.matpr.2022.08.275

Shariq M, Anas SM, Alam M (2022d) Blast resistance prediction of clay brick masonry wall strengthened with steel wire mesh, and C-FRP laminate under explosion loading: a finite element analysis. Int J Reliab Saf (in press)

Anas SM, Alam M, Umair M (2022l) Reinforced cement concrete (RCC) shelter and prediction of its blast loads capacity. Mater Today Proc, Elsevier (in press)

Anas SM, Alam M (2022e) Close-range blast response prediction of hollow circular concrete columns with varied hollowness ratio, arrangement of compression steel, and confining stirrups' spacing. Iran J Sci Technol Trans Civil Eng, Springer (in press)

Anas SM, Alam M, Umair M (2022m) Performance prediction of braced unreinforced and strengthened clay brick masonry walls under close-range explosion through numerical modeling. Int J Comput Mater Sci Surf Eng (in press).

Ultimate Bearing Capacity of Pipe Buried Near Sand Slopes

Sukanta Das

Abstract In hilly areas, the pipelines may be subjected to external forces due to slope topographic, which possibly might lead to leakage of hazardous liquid or gas into the environment. The slope angle may play a significant role to the soil-pipeline interaction. And many constrictions of commercial or industrial building is done above the pipe lines in hilly areas, which may lead damages of pipes within the slopes. The present research aims to study the ultimate bearing capacity of the pipelines buried in dry sand slopes. The two-dimensional finite element limit analysis (2D-FELA) is used for the present numerical analysis. The Mohr–Coulomb (MC) failure criterion with associate flow rule is assumed for the present FELA analysis. While the buried pipe is fully rigid with thickness of 120 mm. The ultimate bearing capacity of buried pipe corresponding to the internal friction angle of the soils is examined under vertical load. The effect of slope angles on bearing capacity of buried pipe and failure wedges formed beneath the buried pipe is also studied in the present work. The present FELA results concludes that the bearing capacity of buried pipe decreases as slope angle increases. Whereas, with the decrease of edge distance of pipe from crest of the slopes, the two-sided wedge failure beneath the buried pipe becomes one sided wedge failure.

Keywords Soil-pipeline interaction · Slope angle · 2D-FELA · Bearing capacity

1 Introduction

Buried pipelines are commonly used to transport and deliver the natural resources which is considered strategic infrastructure and often referred to as "lifeline" systems. leakage of these systems can have a major impact on the environment, and the economy as well as public safety. During the construction of buried pipelines, the pipelines may pass through or near the hilly slopes. The failure of pipelines can be observed under the gravitational load and due to instability of slopes. The ground

S. Das (✉)
Indian Institute of Technology Roorkee, Roorkee, Uttarakhand, India
e-mail: sdas@eq.iitr.ac.in

I. Pal et al. (eds.), *Proceedings of the 2nd International Symposium on Disaster Resilience and Sustainable Development*, Lecture Notes in Civil Engineering 294,
https://doi.org/10.1007/978-981-19-6297-4_13

deformation due to slope failure can have categorised as shallow and deep landslide which depends on the slope angle and geotechnical properties of the slopes (Chan and Wong 2004a, b). The moment of slope mass may have developed horizontal and inclined thrust in the pipe and the orientation of buried pipelines also influence the soil-pipe-interaction. The present focuses on estimating the bearing capacity of a pipe subjected to vertical load. Wu et al. (2017) reported that the slope failure was the reason of 13 percentage of European gas pipeline events during the years from 2004 to 2013.

In India many pipelines are failed due to ground movement, such as slope instability in Andaman and Nicobar Islands area, Chamoli and many places at the Himalayan side and northeaster part, Dash and Jain (2007). The external force exerted by the slope movements have a significant role in soil-pipe-interaction (Chan and Wong 2004a, b; Feng et al. 2015; Rammah et al. 2014), and found as the major problem to the pipeline operating. Moreover, the slope movement should be considered for the design of pipelines in hilly areas. And many roads, bridges and structures are constructed over the existing buried pipelines which may considered as surcharge load on pipelines. There might be possible of damage of pipelines due to the increases of surcharge loads which may refers as manmade deserter.

Di Prisco and Galli (2006) reported that the vertical and horizontal soil resistance have coupling effects. However, experimental work of the soil-pipeline interaction is carried out by pulling or pushing the pipeline horizontally in level grounds using wires or rigid shafts along a constant direction (Audibert and Nyman 1977; Trautmann and O'Rourke 1985; Paulin 1998; Calvetti et al. 2004; Liu et al. 2015; Sahdi et al. 2014; Almahakeri et al. 2013; Ono et al. 2017; Roy and Hawlader 2012; Zhang et al. 2002; Oliveira et al. 2009; Tian and Cassidy 2011). Ignoring the direction of the pipe movement might result in an underestimation of the loads that the soil can exert on the pipe (Calvetti et al. 2004).

Based on the results of small-scale experimental tests on buried pipeline pulled laterally under a flat soil surface, Audibert and Nyman (1977) suggested that the ultimate soil resistance (q_u) is expressed as follows:

$$q_u = \gamma D_p N_{uq} \tag{1}$$

where γ represents the soil unit weight; D_p is the buried pipe embedment depth (from the soil surface to the bottom of the pipe); N_{uq} is the ultimate bearing capacity factor proposed by Hansen (1961).

Moreover, much attentions are given by researchers for pipe located on horizontal ground surface and internal capacity of the pipe itself. As often structures are constructed above those pipe lines that may be in ground surface or hilly areas. The load carrying capacity of the pipe is also an important issues and it get more vulnerable when its placed in sloping ground. Therefore, the bearing capacity of a rigid pipe with varying slope angles and soil properties is considered and discussed in the present research.

2 FELA Modelling

The two-dimensional finite element limit analysis (2D-FELA) is used to investigate the effect of slope angles on soil-pipe-interaction (SPI). FELA method is most rigorous and takes less computation cost, which also provides advanced mesh adaptivity to define the failure surfaces. The detailed geometry of the FELA model, boundary conditions, mesh size and pipe dimension are presented in Fig. 1. The single faced ideal slopes ($\beta = 20$ and 30°) of constant height (h_s) of 5 m is considered in the present study. The lateral distance (w_1) of the FELA model is kept as 10 m from the crest, while 2 m from the toe (w_2) and the total height (H) of the model is 7 m. The rigid buried pipe of diameter 1 m is placed at varying distance (d) from the crest of the slopes. The depth of embedment of the buried pipe is define as D_p. To estimate the bearing capacity of pipe an external vertical load (q) is applied at the centre of the pipe. The present geometry is fixed after reviewing that the response of the SPI should not touches any of the FELA domain boundary. The boundary condition is considered in such a way that the base model fully fixed against any movement and the lateral sides are only free to move vertically. However, the slope surface is free to move any direction. The adaptive mesh is assigned for the present numerical analysis. The 15-noded gauss element is used for the present FELA analysis and the number of elements was decided based on the Mesh convergence study.

The Mohr–Coulomb (MC) failure criterion with associate flow rule ($\phi = \psi$) is assumed for the present FELA analysis. While the pipe is fully rigid with thickness

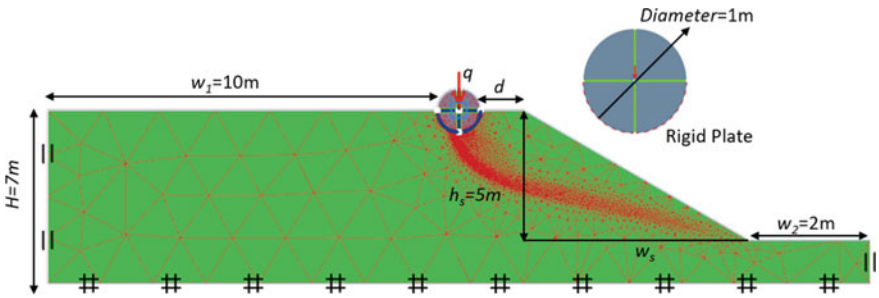

Fig. 1 Geometry and mashing of pipe buried near sand slopes

Table 1 Properties of soils and pipes are used in the FELA analysis

Properties	Soil	Pipe
Unit weight, γ (kN/m^3)	18	25
Young's modulus, E (MPa)	30	200,000
Poisson's ratio, ν	0.3	0.2
Angle of internal friction, ϕ (°)	5–45°	–
Dilation angle, ψ (°)	5–45°	–
Plate thickness, t (mm)	–	120

of 120 mm and embedded at a shallow depth (D_p = 0.5–1 m). The all material properties are used in the present FELA numerical analysis given in the Table 1.

3 FELA Result and Discussions

The bearing capacity of pipe buried in a shallow depth at flat and sloping ground is examined and discussed in the present study. The variation of bearing capacity with internal friction angle of soil for different slope angles is reported. The failure wedge developed beneath the buried pipe is also discussed after FELA analysis. The conventional two-sided wedge failure with well-defined three zones (I = Triangular wedge beneath the pipe, II = Radial shear zone and III = Passive zone) for flat ground has been presented in Fig. 2a. However, one sided wedge failure has been observed when pipe placed at the crest of the slopes as presented in Fig. 2b. The diameter of the pipe has been kept 1 m constant for all the analysis.

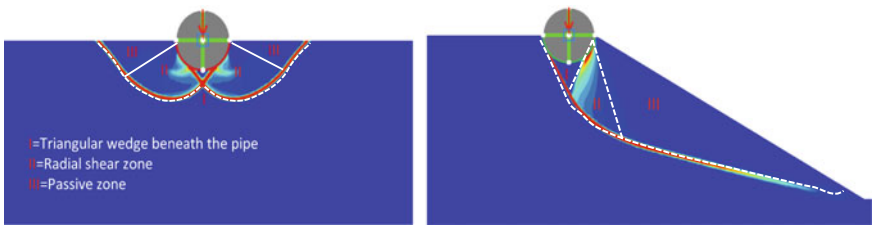

Fig. 2 Wedge of soil below the foundation pipe buried in **a** flat sand **b** sand slopes

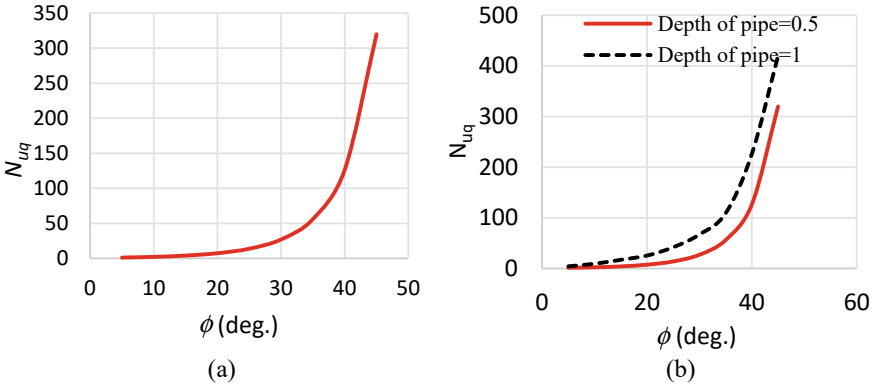

Fig. 3 Bearing capacity factor in flat ground for pipe diameter 1 m **a** $D_p = 0.5$ m **b** $D_p = 0.5$ and 1 m

3.1 *Effect of Internal Friction Angle of Soil*

The bearing capacity factor of the buried pipe for different angle of internal friction of soil and embedment depth of pipe for the flat ground has been given in Fig. 3. From Fig. 3a, for constant embedment of pipe $D_p = 0.5$ m, the bearing capacity factor increases with the increase in angle of internal friction. However, the rate of increase of bearing capacity factor at the initial ($\leq 20°$) value of ϕ is less compare to that of $\phi = 20$ to 45°.

After $\phi \geq 20^0$ the rate of increase in bearing capacity factor drastically increase. Similar trend with higher value of bearing capacity factor has been found for $D_p = 1$ m, which is expected as with embedment depth there is an increase in bearing capacity.

3.2 *Effect of Slope Angle*

The depth of embedment of buried pipe has been kept $D_p = 1$ m, to investigate the influence of slope angle on bearing capacity of shallow buried pipe. The buried pipe located at the different distance (d) from the crest of the slopes. The Fig. 4 depicts, the change of bearing capacity factor for different edge distance of buried pipe of pipes on slope angles 20 and 30° respectively. Due to presence of slope angle, the bearing capacity factor decrease compare to flat ground as given in Figs. 3 and 4. For slope 20°, the minimum bearing capacity has been found when the pipe located at the crest of the slopes, the bearing capacity increase as the edge distance increase which indicates that the effect of slope angle gets insignificant after a certain edge distance. In Fig. 4a, the bearing capacity vs. ϕ curves are overlapped at the edge distance d = 2, 3 and 4 m.

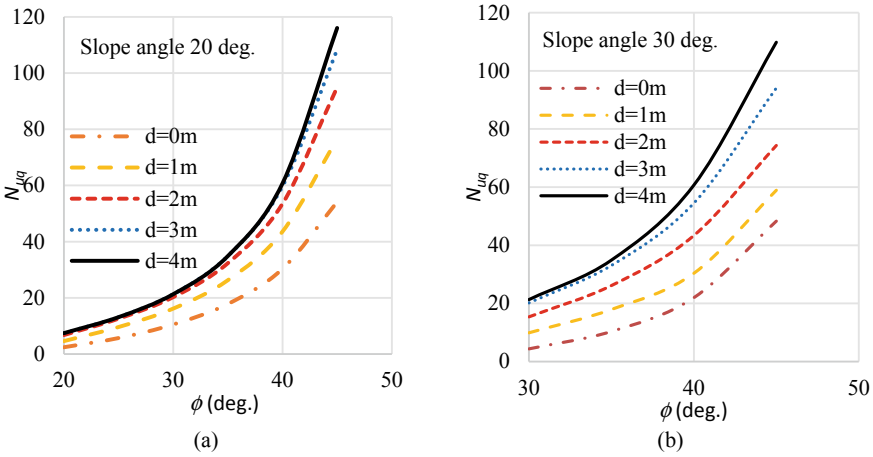

Fig. 4 The bearing capacity factor for different edge distance of buried pipe of pipes on slope angles for $D_p = 0.5$ m and radius $R = 1$ m **a** $\beta = 20°$ **b** $\beta = 30°$

However, after $\phi > 30°$ the curves for d = 2 m are not overlapped with d = 3 m. Similarly, from Fig. 4b, the maximum bearing cavity observed at the edge distance has been extended to 4 m and the minimum bearing capacity factor has been observed at the crest of the slopes. The reduction of bearing capacity factors has been for a constant embedment and angle of internal friction is given in Table 2. The reduction factor (i_β) has been determined using Eq. 2. The table also confirms that the reduction of bearing capacity decreases with the increase of slope angle at $d = 0$ m. And the reduction of bearing capacity decreases with the increase of edge distance. At the edge distance 4 m, the reduction of bearing capacity has been observed as 0.62 for slope angle 20 and 30° respectively.

$$i_\beta = \frac{\mathrm{N_{uq}}slopes}{\mathrm{N_{uq}flat}} \tag{2}$$

3.3 *Failure Mechanism*

The failure mechanism of buried pipes under a vertical load with constant pipe embedment depth has been presented in Fig. 5. The conventional two-sided wedge failure paten including triangular wedge, radial shear zone and passive zone has been observed beneath the pipe for flat ground as given in Fig. 5a. In Figs. 5b and c, the two-sided wedge failure paten has been observed beneath the pipe for slope 20° with d = 4 and 2 m respectively.

Table 2 Reduction of bearing capacity factor of pipe due to slope for $D_p = 0.5$ m and radius $R = 1$ m and $\beta = 35°$

Slope, β (°)	Edge distance, d (m)	Reduction of N_{uq}, i_β
20°	0	0.318013
	1	0.468909
	2	0.576912
	3	0.622075
	4	0.622183
30°	0	0.184563
	1	0.319636
	2	0.466125
	3	0.589498
	4	0.622173

Note $D_p = 0.5$ m and radius $R = 0.5$ m

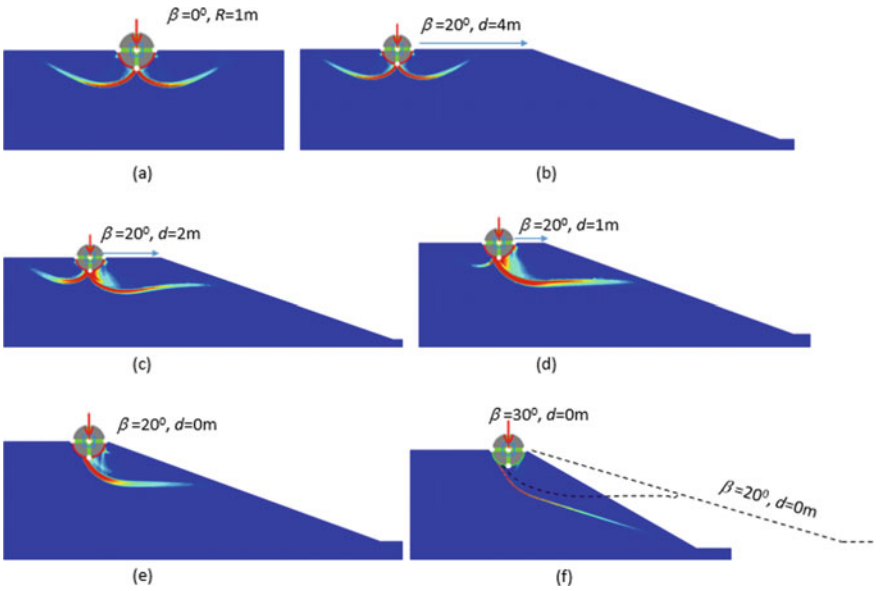

Fig. 5 Failure wedge of soil below the foundation pipe buried in sand slopes, for $D_f = 0.5$ m and radius R = 1 m **a** $\beta = 0°$ at Center **b** $\beta = 20°$ and $d = 4$ m **c** $\beta = 20°$ and $d = 2$ m **d** $\beta = 20°$ and $d = 1$ m **e** $\beta = 20°$ and $d = 0$ m **f** $\beta = 30°$ and $d = 0$ m

However, the maximum failure wedge zone has been observed at slope side for $d = 2$ m with reduced failure wedge zone to the other side of pipe. Further increase of failure wedge zone has been observed at slope side for $d = 1$ m, Fig. 5d, while complete one-sided failure has been found when pipes at the crest of the slopes as

shown in Fig. 5e. The comparison of failure surface of buried pipe on slopes 20 and 30° respectively in Fig. 5f. The failure surface moves toward toe as slope angle increases. However, these reduction of failure surfaces for different edge distance and slope angles has been observed with the cost of bearing capacity.

4 Conclusion

From the present 2D-FELA analysis of soil-pipe- interaction shows a significant effect of angle of internal friction of soils and slope angles. The following point can be drawn from the obtained results of the present study.

The bearing capacity increase as the angle of internal friction of soils and the depth of embedment of pipes increase which has been expected. However, the drastically increase of bearing capacity of pipe has been found at the range of $\phi > 20°$ which indicated the less bearing capacity at loose sand and high in dense sand.

For constant embedment of pipes and friction angle of soil, a reduction of the bearing capacity observed with the increase in sloe angle. And the edge distance has a significant role in of topographic-soil-pipe- interaction (TSPI), as the edge distance increases the bearing capacity increases and after a certain distance d > 4 m the effect of slopes diminished. The minimum bearing capacity has been found when pipe placed at the crest of the slopes.

The failure surface beneath the pipe strongly influenced by the slope angle and the edge distance of the pipe from the crest of the slopes. At the crest $d = 0$ m, the one-sided failure surface has been observed at the slope side. However, as the edge distance increase the two-sided failure surface has been reported for $d = 1$ and 2 m with lower failure wedge zone at the opposite side of the slopes. The fully two-sided failure envelop similar to flat ground has been observed after $d =$ 4 m.

The present study will be very much helpful for the development of pipeline infrastructures at hill areas which is still a challenging task for the geotechnical engineers. The proper design can only have made after having brief idea about soil-pipe-interaction in slopes.

Acknowledgements The author would like to thanks Optum computational engineering (Optum G2) for providing academic licence and sufficient example which is appraisable for present research work.

References

Dash SR, Jain SK (2007) Guidelines for seismic design of buried pipelines: provision with commentary and explanatory examples. In: IITK-GSDMA, National information centre of earthquake engineering, Kanpur, India, p 88. ISBN 81-904190-7-2

Chan PDS, Wong RCK (2004a) Performance evaluation of a buried steel pipe in a moving slope: a case study. Can Geotech J 41(5):894–907

Wu J, Zhou R, Xu S, Wu Z (2017) Probabilistic analysis of natural gas pipeline network accident based on Bayesian network. J Loss Prev Process Ind 46:126–136

Chan PDS, Wong RCK (2004b) Performance evaluation of a buried steel pipe in a moving slope: a case study. Can Geotech J 41:894–907

Feng W, Huang R, Liu J, Xu X, Luo M (2015) Large-scale field trial to explore landslide and pipeline interaction. Soils Found 55:1466–1473

Rammah KI, Oliveira JR, Almeida MC, Almeida MS, Borges RG (2014) Centrifuge modelling of a buried pipeline below an embankment. Int J Phys Model Geotech 14:116–127

Di Prisco C, Galli A (2006) Soil-pipe interaction under monotonic and cyclic loads: experimental and numerical modelling. In: Proceedings of the first euromediterranean symposium in advances on geomaterials and structures, Hammamet, Tunisia, pp 755–760

Audibert JM, Nyman KJ (1977) Soil restraint against horizontal motion of pipes. J Geotech Eng Div 103:1119–1142

Trautmann CH, O'rourke TD (1985) Lateral force-displacement response of buried pipe. J Geotech Eng 111:1077–1092

Paulin MJ (1998) An investigation into pipelines subjected to lateral soil loading. Doctoral dissertation, Memorial University of Newfoundland

Calvetti FD, Prisco C, Nova R (2004) Experimental and numerical analysis of soil–pipe interaction. J Geotech Geoenviron 130:1292–1299

Liu R, Guo S, Yan S (2015) Study on the lateral soil resistance acting on the buried pipeline. J Coast Res 73:391–398

Sahdi F, Gaudin C, White D, Boylan N, Randolph M (2014) Centrifuge modelling of active slide-pipeline loading in soft clay. Géotechnique 64:16–27

Almahakeri M, Fam A, Moore ID (2013) Experimental investigation of longitudinal bending of buried steel pipes pulled through dense sand. J Pipeline Syst. Eng. Pract. 5(2):04013014

Ono K, Yokota Y, Sawada Y, Kawabata T (2017) Lateral force–displacement prediction for buried pipe under different effective stress condition. Int J Geotech Eng, pp 1–9

Roy KS, Hawlader B (2012) Soil restraint against lateral and oblique motion of pipes buried in dense sand. In: 9th international pipeline conference, Calgary, 24–28 September 2012

Zhang J, Stewart DP, Randolph MF (2002) Modeling of shallowly embedded offshore pipelines in calcareous sand. J Geotech Geoenviron 128:363–371

Oliveira JR, Almeida MS, Almeida MC, Borges RG (2009) Physical modeling of lateral claypipe interaction. J Geotech Geoenviron 136:950–956

Tian Y, Cassidy MJ (2011) Pipe-soil interaction model incorporating large lateral displacements in calcareous sand. J Geotech Geoenviron 137:279–287

Hansen JB (1961) The ultimate resistance of rigid piles against transversal forces. Bulletin 12:5–9

Geopolymer Concrete – A Study of an Alternative Material for OPC

Ishan Thakar, Ronak Motiani, and Divya Jat

Abstract OPC is considered to be the most used cement in a concrete mix. While it may have been used for many years, its use increases the production of CO2 and provides for 7% of CO2 produced each year. Releasing of CO2 causes degradation in the atmosphere and results in air pollution. For the past two decades, an alternative for OPC, Geopolymer concrete is being tested. Geopolymer concrete is produced by recycling waste materials such as Fly Ash, Ground Granulated Blast Furnace Slag (GGBFS), and Rice Husk Ash. Geopolymer is required to be mixed with an activator as it does not hold all properties of cement. Alkaline activators such as sodium silicate, potassium silicate, sodium hydroxides, aluminosilicates have been used as activators. This paper deals with several combination activator solutions which can be used to increase the strength of geopolymer concrete. Tests are performed on different materials with different activators to find compressive test. Significant changes are observed in the strength of geopolymer concrete.

Keywords Geopolymer concrete · Alkaline activators · Ground Granulated Blast Furnace Slag (GGBFS) · Strength

1 Introduction

Science and technological advancements are a continuous process for improving infrastructure around the world. Each day, technological advances in the construction industry are developed which are safe, cost-effective, and environmentally friendly. Aside from water, concrete is by far the most widely utilized compound in the world. (Hardjito and Rangan 2005). Ordinary Portland cement (OPC) is commonly used as a primary binder in the preparation of concrete. The cement manufacturing process emits a lot of carbon dioxide into the atmosphere, polluting it. Waste generated from the thermal industry known as Flyash is dumped on the ground which occupies a lot of space. Also, the groundwater gets contaminated with the wastewater discharged

I. Thakar · R. Motiani (✉) · D. Jat
Department of Civil Engineering, School of Technology, Pandit Deendayal Energy University, Gandhinagar, Gujarat, India
e-mail: ronak.motiani@sot.pdpu.ac.in

I. Pal et al. (eds.), *Proceedings of the 2nd International Symposium on Disaster Resilience and Sustainable Development*, Lecture Notes in Civil Engineering 294,
https://doi.org/10.1007/978-981-19-6297-4_14

from the chemical industries. All of these concerns will be resolved by producing geopolymer concrete i.e. by using industrial waste fly ash along with wastewater from chemical industries (Aleem and Arumairaj 2012). It was observed that carbon dioxide is released at a one-to-one rate during OPC production, implying that for every kg of Ordinary Portland Cement is produced, the same quantity of Carbon dioxide is produced (Hardjito and Rangan 2005). Since there is no requirement of cement in geopolymer concrete, thus the production of cement will be significantly reduced causing less environmental pollution and therefore carbon dioxide emission can be minimized (Aleem and Arumairaj 2012).

In 1978, a French professor named Davidovits introduced the term "geopolymer" to describe a wide range of materials defined by inorganic molecular networks (Davidovits 1989). Aluminium (Al) and silicon (Si) are obtained from industrial waste such as fly ash or slag, as well as thermally activated natural minerals such as Meta Kaolinite. These Silicon and Aluminum are dissolved in an alkaline activating solution, where they ultimately polymerize into molecular chains and create the binder. Temperature plays a vital role during curing and according to the type of materials and the activating solution used, the heat is generated to facilitate polymerization however, there are some systems by which the composite can obtain desired strength by ambient curing (Davidovits 2008). The role of calcium in geopolymers generated from fly ash is important since its presence can result in flash setting, which must be carefully regulated (Rangan 2008).

(Manjunath et al. 2011) The effect of combined alkaline activator solution to fly ash ratio and NaOH molarities on compressive strength was examined of a geopolymer concrete composite. By changing the ratios of activator to fly ash the compressive strength significantly varies. (Pavithra et al. 2016) When the activator dose to fly ash ratio increases, the compressive strength of the geopolymer concrete reduces, similar to how the strength of Ordinary Portland cement decrease when the water to cement ratio increases. Moreover, curing temperature also affects geopolymer concrete's compressive strength (Guo et al. 2010; Yahya et al. 2015).

Some of the applications of geopolymer concrete can be to make precast structural elements as it there will be ease in handling and considering the higher curing temperature required for the geopolymer composite to gain its desirable strength. Geopolymer fiber composites can be used in structural retrofitting. Precast pavers and slabs for paving, bricks, and precast pipe can also be made with geopolymer.

From the various research work done to find an environmentally friendly material, it is now clear that geopolymer can be a substitute for ordinary Portland cement. The compressive strength test is performed on the geopolymer composite using various combinations of activators which are discussed in this paper.

2 Literature Review

Fly ash which is a waste material obtained from the coal-based thermal power station is nowadays being utilized as an alternative for cement concrete in the construction industry.

Pulverised fuel ash is a waste product created by the burning of coal or lignite in a thermal power plant's boiler, according to IS 3812: 2003. Fly ash, bottom ash, pond ash, and mound ash are all types of pulverised fuel ash. Fly ash is pulverised fuel ash that may be collected from combustion gases using any applicable method, such as cyclone separation or electrostatic precipitation. Bottom ash is pulverised fly ash obtained from the bottom of boilers in any feasible manner. Mound ash is produced when fly ash or bottom ash is brought in dry form and dumped dry.

2.1 Classification of Fly Ash

There are two grades of Fly Ash as per IS 3812-1981.

- Grade I and II fly ash, which is obtained from bituminous coal and lignite coal respectively.
- Grade I contains portion of SiO2 + Al2O3 + Fe2O3 greater than 70% whereas Grade II contains fraction above 50%.

Depending on the kind of coal and the chemical analysis, ASTM C618 divided fly ash into two categories: Class C and Class F.

Class C fly ash, which is often generated from the burning of lignite or sub-bituminous coals, has more than 10% CaO and has cementitious properties along with pozzolanic properties. Class F fly ash, which is generally formed from the burning of bituminous or anthracite coal, has pozzolanic properties and contains less than 10% CaO.

Based on the boiler operations, fly ash classification is divided into two categories: When the ignition temperature is less than 900 °C, low temperature (LT) fly ash is produced. Fly ash with a high temperature (HT) is created when the combustion temperature is less than 1000 °C.

2.2 Physical Properties

Fly ash is a fine-grained substance made up primarily of spherical, crystalline particles. Irregular or angled granules can also be seen in some ashes. The term "fly ash" refers to pulverised fuel ash collected from combustion byproducts using any approved process, such as cyclone separation or electrostatic precipitation.

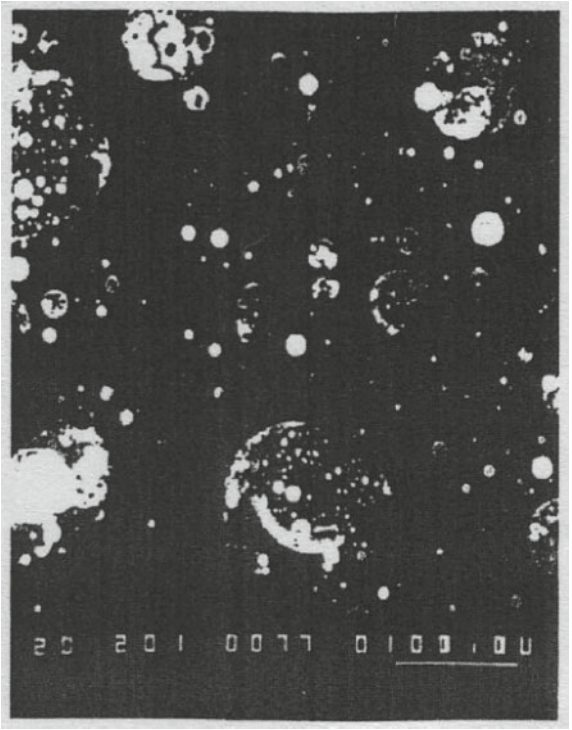

Fig. 1 SEM of polished sections of sub-bituminous fly ash particles

2.2.1 Shape and Size

Based on the source, the particulate size ranges. The texture of certain ashes is thinner than that of Ordinary Portland cement particles, while others are coarser. Fly ash is comprised of spherical sand sized particles ranging in size from 10 to 100 microns. Figure 1 shows scanning electron microscope (SEM) micrographs of refined sub-bituminous segments, whereas Fig. 2 shows SEM image of bituminous fly ash particles [Image source: Carette and Malhotra (1986)]. Some appear to be rigid, while others seems to be sections of slender, spherical particles holding a vast number of smaller particles.

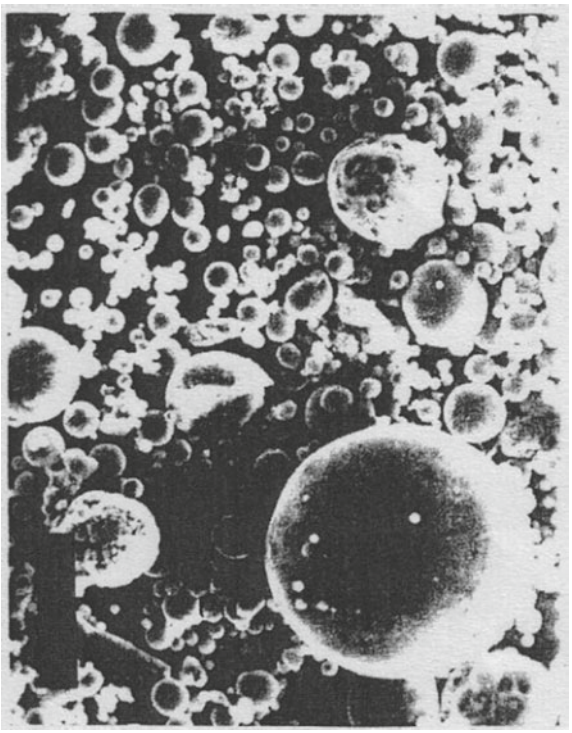

Fig. 2 SEM of polished sections of bituminous fly ash particles

2.2.2 Colour of Fly Ash

Depending on its chemical and mineral composition, fly ash can range in colour from tan to dark grey. High lime content is usually related to tan and light colors. The iron concentration is usually indicated by a brownish colour. Enhanced unburned content is usually linked to a hue ranges from dark grey to black. The colour of fly ash is usually relatively constant between power plants and coal sources.

2.3 Chemical Properties of Fly Ash

Since the chemical structure of fly ash varies depending on coal resources and boiler working circumstances, quality differs from one source to the next and even within a single source. Loss on Ignition is an indicator of carbon residue left in the ash when crushed coal as well as an adequate burning technique are utilised. Changes in the LOI can affect the air composition, demanding further in field analysis of air voids in concrete.

Table 1 Chemical and physical analysis of fly ash brought from Thermal Power Station, Gandhinagar

Sr.no	Parameter	Test method	Test result (%)
1	SiO2 content	I.S.712.1984/I.S.6932	51.40
2	Al2O3 Content	I.S.712.1984/I.S.6932	18.74
3	FE2O3 content	I.S.712.1984/I.S.6932	13.89
4	CAO content	I.S.712.1984/I.S.6932	4.35
5	MGO content	I.S.712.1984/I.S.6932	1.12
6	NA2O content	I.S.712.1984/I.S.6932	0.11
7	K2O content	I.S.712.1984/I.S.6932	2.32
8	SO3 content	I.S.712.1984/I.S.6932	0.65
9	LOI	I.S.712.1984/I.S.6932	7.28

THERMAL POWER STATION in Sector 28, Gandhinagar provides the fly ash utilised in the cement concrete replacement. Table 1 summarises the results of the chemical and physical analyses of fly ash. It has been found that it is Grade I Class F Low-Temperature Fly Ash as a result of the testing.

2.3.1 Activators

Fly ash has similar qualities to cement, however, due to a lack of silicate and calcium, appropriate reactions do not occur, resulting in poor hydration heat and a longer curing time. Alkaline activators are employed to balance the heat of hydration. Activators are used to improve the geopolymer chemical and mechanical properties. Sodium silicate, potassium silicate, sodium hydroxides, and alumina silicates have all been utilised as alkaline activators.

Sodium Hydroxide (NaOH) when used with higher molarity results in higher compressive strength of the composite (Rattanasak and Chindaprasirt 2009; Ryu et al. 2013). Studies reveal that potassium reacts with the reinforcement and can cause it to corrode, therefore sodium hydroxide and sodium silicate are by far the most cost-effective alternatives. To add to the fly ash mix, a 12 M NaOH solution was made by adding 480 g of sodium hydroxide pellets to make 1 L solution. The alkaline activator solution is made a day prior to the day of casting. As sodium silicate (Na_2SiO_3) is also a raw material for OPC, certain studies suggest that it forms a strong bond with sand, aggregate, and reinforcement. Because each activator aids in enhancing the strength of the design mix of fly ash, combining activators yields significantly more promising outcomes for geopolymer composite. Furthermore, the molarity of sodium hydroxide affects compressive strength considerably. A sodium hydroxide to binder ratio of 60–100% can offer adequate compressive strength values in a majority of construction practises (Assi et al. 2016). (Ng et al. 2018) When the molarity of sodium hydroxide is 12 M combined in a composite and the curing temperature was maintained at 70 °C for 24 h, an increase in the strength of geopolymer concrete is

seen. However, when a ratio of sodium silicate to sodium hydroxide is kept in between 2 to 2.5 in composite it was found to be more efficient as it has a high surface area which makes it easy to react and bind. As a combined activator, a solution of sodium hydroxide and sodium silicate is employed in this study.

During the chemical reaction that creates geopolymer concrete, water is released,while curing, the composite is subjected to heat which results in water vaporise (Hardjito and Rangan 2005). Due to pores containing little amount of water, the drying shrinkage is limited in hard specimens. The influence of curing conditions on the physical and mechanical qualities of geopolymer concrete has been studied using a set of methods (Perera et al. 2007). A similar study was carried out by (Kani and Allahverdi 2009) the change in compressive strength observed was depended largely upon the type of curing method opted (Heah et al. 2011). The curing temperatures for near-perfect geopolymerisation were found to be between 40 and 85 °C. The curing temperature greatly influenced the strength of geopolymer concrete combined with alkali activators (Singh et al. 2015). Mechanical strength was stronger in specimens exposed to higher curing temperatures than in those exposed to lower temperatures. This conclusion is consistent with those of (Nurruddin 2018). They also discovered that, while a longer curing duration increases strength, the increase is small if the curing time exceeds 24 h.

One of the most prominent research on geopolymer concrete strength about the type of curing was carried out by Yewale et al. 2016. The strength of geopolymer increases substantially as the temperature in steam curing rises, however the strength of geopolymer decreases after 28 days due to low temperature in water curing. The optimum strength for steam curing was attained at 80 °C. The addition of a small amount of OPC in the geopolymer concrete speeds up the hydration process when done by steam curing and hence its compressive strength increases Pangdaeng et al. (2014).Similar results have been reported in this literature when geopolymer concrete is combined with OPC.

Various research work has been done on obtaining the desired strength of geopolymer concrete when done by ambient curing Vijai et al. (2010). The compressive strength of fly ash mixed with activator at a ratio of 0.4 (solution to binder ratio) during a 5-day interval reveals that with ambient curing, the compressive strength improves with age. When done by oven curing, however, there has been less change in compressive strength with the age of the curing. When comparing the results of oven curing and ambient curing, the latter's strength development was low, suggesting that oven curing is more efficient.

3 Methodology

To examine the consistency of fly ash and cement, a consistency test was conducted. Fly ash has indeed been reported to have a consistency of 23% as compared to cement which has a consistency of 27%.

The slump test was used after the consistency test to examine the workability of various concrete mix proportions. It was discovered that the concrete mix had a 117 mm slump, indicating considerable workability. With 100% fly ash and NaOH solution as an activator, the slump was measured at 135 mm. 90% fly ash and 10% cement were used in geopolymer with NaOH as an activator where slump of 130 mm is produced. With Na2SiO3 as an activator, the slump was measured at 132 mm for 100% fly ash. A slump of 127 mm was achieved using a geopolymer with Na2SiO3 as an activator and 90% fly ash and 10% cement. A mixture of combine activators, sodium hydroxide and sodium silicate along with 100% fly ash were used to obtained slump at 125 mm. For geopolymer comprising mixed activators, 113 mm of the slump was produced in the case of 90% fly ash and 10% cement.

As per IS 3812, a mortar mix for fly ash is prepared. This mixture comprises fly ash taken from Gandhinagar thermal power plant. A ratio of 1:3 i.e. fly ash to aggregate was added in the composite. Fine aggregate was obtained by sieving with an IS sieve with a size of 1.18 mm and 600 microns. The fly ash was sieved using an IS Sieve of size 710 micron. According to recent research, the water binder ratio must be between 0.27 and 0.35 i.e. (water to fly ash ratio for higher strength. A ratio of 0.32 was chosen in this case for cube casting. The combined activator to fly ash ratio was adjusted to 0.45, meanwhile for cube casting, a sodium hydroxide to fly ash ratio of 0.13 and a sodium silicate to fly ash ratio of 0.32 have been used. The ratio of sodium silicate to sodium hydroxide ratio should be between 1.5 and 2.2. We've used a ratio of 2 in this scenario. The results of a consistency test for OPC grade 53 cement were 27%. Cement mortar cubes were also moulded as a reference for geopolymer strength. A total of 12 cubes measuring 7.05 × 7.05 × 7.05 cm were casted for compressive strength test over 7, 14, and 28 days. Geopolymer mortar cubes with NaOH, Na_2SiO_3 and a mixture of activators i.e. sodium silicate and sodium hydroxide were made (Fig. 3).

A batch of geopolymer mortar was cast and left to cure according to the process outlined above. The first batch was a failure because of an imbalanced water-to-activators ratio, and removing the cubes from the mould took more than 15 days. As a result, a new water and activator ratio was discovered by trial and error, resulting in an adequate curing time. Following that, in a ratio of 1:6 i.e. binder to sand ratio cement and geopolymer cubes with various activators were cast (Table 2).

After removing from the mould, unlike the first batch, this batch of mortar cubes retained its shape and did not deform. In order to decrease the amount of curing, some amount of cement was added to the mix. For the experiment, M25 concrete cubes 15 × 15 × 15 cm in size were utilized. The cubes were also cured using ambient curing. Geopolymer concrete cubes with different combinations of alkaline activators were cast as listed below:

Geopolymer with 100% Fly Ash using NaOH as an Activator
Geopolymer with 90% Fly Ash and 10% Cement using NaOH as an Activator
Geopolymer with 100% Fly Ash using Na_2SiO_3 as an Activator
Geopolymer with 90% Fly Ash and 10% Cement using Na_2SiO_3 as an Activator

(continued)

(continued)

Geopolymer with 100% Fly Ash using Combined Activators
Geopolymer with 90% Fly Ash and 10% Cement using Combined Activators

4 Observation and Result

4.1 Compressive Strength

The compressive strength of geopolymer mortar and concrete cubes was investigated using various combinations of alkaline activators. The results obtained in 7, 14, and 28 days is shown in Table 3. When used with a single activator either sodium hydroxide or sodium silicate, geopolymer does not yield much strength when compared to ordinary cement cubes. However, regardless of the ratio evaluated, the compressive strength of the composite is significantly increased when geopolymer is coupled with both activators, sodium silicate and sodium hydroxide. External heat influences both ultimate compressive strength and early compressive strength growth, according to (Assi et al. 2016). Geopolymer concrete cubes with different combinations of alkaline activators were cast (Fig 4) as listed below: Fig 5 provides a graphical representation of the compressive strength of the geopolymer mortar cubes, showing that after 28 days, the traditional OPC mortar cube has a compressive strength of 43 N/mm^2, while the geopolymer with combined activators has a compressive strength of 52.5 N/mm^2, nearly 1.7 times higher than the OPC.

Similarly, the compressive strength of geopolymer cubes with varied flyash content obtained in 7, 14, and 28 days is shown in Table 4. The compressive strength of geopolymer with combined activators containing 90% Fly Ash and 10% cement is the highest of all, at 43.9 N/mm^2. However, 41 N/mm^2 compressive strength of geopolymer with combined activators having 100% fly ash content is observed which is not less when compared with the former. Hence, a small quantity of cement will not alter the strength of the geopolymer composite if used which is similar to the observation by (Assi et al. 2016) where the compressive strength is improved by 82% after one day and 52% after 28 days in comparison with the free ordinary Portland cement geopolymer concrete while still providing acceptable workability.

As seen in Fig. 6, when geopolymer is combined with mixed activators, it has a compressive strength that is approximately 1.8 times that of a normal OPC.

From the above results, the following can be concluded:

- Combined activators provide more strength than single activators
- Geopolymer mixed with cement provides higher strength than Geopolymer made of fly ash

Although geopolymer is proven to be an ideal replacement for regular OPC it still has some challenges which make it quite difficult to be used on a regular basis

Fig. 3 Geopolymer cube casting

Table 2 Ratio considered while cube casting

Description	Binder to sand ratio
Cement concrete	1:6
Geopolymer with NaOH as an activator	1:6
Geopolymer with Na_2SiO_3 as an Activator	1:6
Geopolymer with combined activators	1:6

Table 3 Compressive strength of cement mortar cubes

Description	Compressive strength N/mm^2		
	7 days	14 days	28 days
Cement cube	23	38	43
Geopolymer with NaOH	14	18	27.5
Geopolymer with Na2SiO3	16	23	31.7
Geopolymer with combined activators	18	27	52.5

in the construction industries. The alkaline activators used in the composite are of higher cost also safety risk is involved in making the high molarity of activator to get the required solution. Furthermore, steam curing is not practically possible as of now to be used in a large-scale project which makes geopolymer unfit to use. Fly ash based geopolymer can be used in precast structures as of now as it requires elevated

Fig. 4 Mortar cube casting

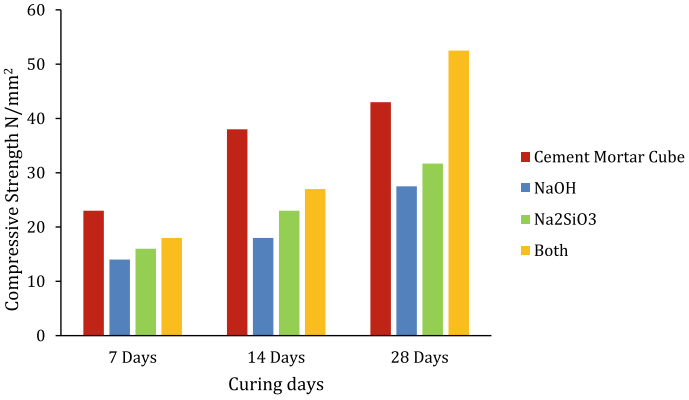

Fig. 5 Compressive strength of geopolymer and cement mortar cubes as in Table 3

temperature for curing (Ryu et al. 2013).Hence, further research work is to be done to overcome these challenges.

Table 4 Comparison of compressive strength test of geopolymer concrete cubes - M25

Description	Content of fly ash	Compressive strength (N/mm^2)		
		7 days	14 days	28 days
Cement concrete	0	17	22	24.8
Geopolymer with NaOH	100% Fly Ash	12.5	17	23
	90% Fly Ash and 10% cement	14	18.5	24.5
Geopolymer with Na2SiO3	100% Fly Ash	16	20	25
	90% Fly Ash and 10% cement	17.5	21.7	27.3
Geopolymer with combined activators	100% Fly Ash	19	28	41
	90% Fly Ash and 10% cement	19.5	30	43.9

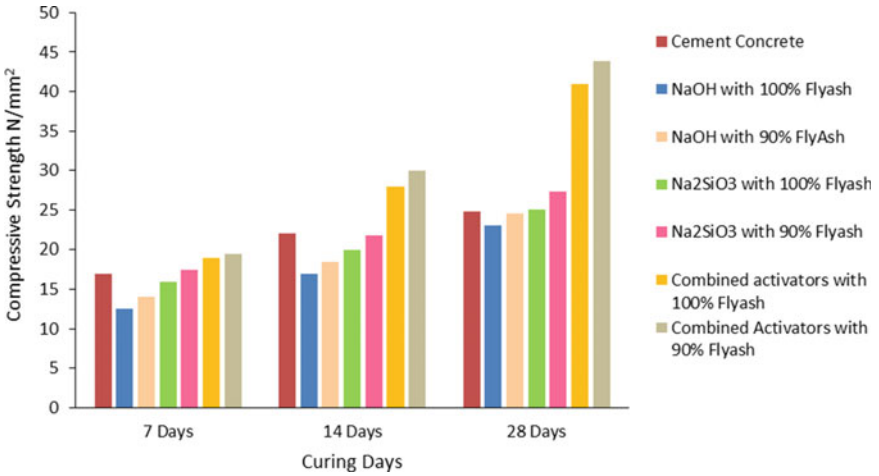

Fig. 6 Compressive strength of fly ash based geopolymer concrete cubes and cement concrete of grade M25 as in Table 4

5 Conclusion

The compressive strength of geopolymer cubes was examined. The ambient curing process was adopted. Even after ambient curing, it takes approximately 35 days before the first attempted mortar cubes could be tested due to the moist atmospheric conditions caused by the winter. When compressive strength was examined, it was shown that geopolymer cubes with single activators lack adequate strength in comparison to cement mortar. However, combined activators yielded promising results, suggesting that the compressive strength of fly ash based geopolymer with combined activators is 1.7 times that of cement mortar and 1.8 times more strength than that of cement concrete cubes. The higher the temperature, the faster will be the curing and more strength will be obtained. Although trial and error method is

required to decide water to activators ratio for which appropriate method is still needed. Further testing was to be done on a column for flexural strength but due to COVID-19, no further work could be done. There is no need for water curing since the geopolymer requires higher temperatures to cure. Curing under ambient temperatures, on the contrary, takes longer. As a result of the various experiments done, it can concluded that geopolymer delivers greater strength than Ordinary Portland cement and may be used as a cement substitute in the construction industry.

References

Aleem MIA, Arumairaj PD (2012) Geopolymer concrete- a review. Int J Eng Sci Emerg Technol 1(2):118–122. https://doi.org/10.7323/IJESET/V1_I2_14

Assi L et al (2016) Improvement of the early and final compressive strength of fly ash-based geopolymer concrete at ambient conditions. Constr Build Mater 123:806–813

Carette GG, Malhotra VM (1986) Characterization of Canadian fly ashes and their relative performance inconcrete. Canadian J Civil Eng 14(5):667–682. https://doi.org/10.1139/l87-097

Davidovits J (1989) Geopolymers and geopolymeric materials. J Therm Anal 35(2):429–441. https://doi.org/10.1007/BF01904446

Davidovits J (ed) (2008) 'Introduction', Geopolymer Chemistry and Applications, pp 3–22

Guo X, Shi H, Dick WA (2010) Compressive strength and microstructural characteristics of class C fly ash geopolymer. Cement Concr Compos 32(2):142–147. https://doi.org/10.1016/J.CEMCONCOMP.2009.11.003

Hardjito D, Rangan BV (2005) Development and properties of low-calcium fly ash-based geopolymer concrete. https://espace.curtin.edu.au/bitstream/20.500.11937/5594/2/19327_downloaded_stream_419.pdf, Accessed 22 Jan 2022

Ng C et al (2018) A review on microstructural study and compressive strength of geopolymer mortar, paste and concrete. Constr Build Mater 186:550–576. https://doi.org/10.1016/j.conbuildmat.2018.07.075

Nurruddin MF et al (2018) Methods of curing geopolymer concrete: a review. Int J Adv Appl Sci 5(1):31–36. https://doi.org/10.21833/IJAAS.2018.01.005

Pavithra P et al (2016) A mix design procedure for geopolymer concrete with fly ash. J Clean Prod 133:117–125. https://doi.org/10.1016/J.JCLEPRO.2016.05.041

Rattanasak U, Chindaprasirt P (2009) Influence of NaOH solution on the synthesis of fly ash geopolymer. Miner Eng 22(12):1073–1078. https://doi.org/10.1016/J.MINENG.2009.03.022

Ryu GS et al (2013) The mechanical properties of fly ash-based geopolymer concrete with alkaline activators. Constr Build Mater 47:409–418. https://doi.org/10.1016/J.CONBUILDMAT.2013.05.069

Yahya Z et al (2015) Effect of solids-to-liquids, Na2SiO3-to-NaOH and curing temperature on the palm oil boiler ash (Si + Ca) geopolymerisation system. Materials 8(5):2227–2242. https://doi.org/10.3390/MA8052227

Rangan, BV (2008) Low-Calcium, Fly-Ash-Based Geopolymer Concrete.' Concrete Construction Engineering Handbook. Taylor and Francis Group, Boca Raton

Manjunath GS, Radhakrishna GC, Jadhav M (2011) Compressive strength development in ambient cured geo-polymer mortar. Int J Earth Sci Eng 4(6):830–834

Perera DS, Uchida O, Vance E, Finnie K (2007) Influence of curing schedule on the integrity of Geopolymers. J Mater Sci 42(9):3099–3106

Kani EN, Allahverdi A (2009) Effects of curing time and temperature on strength development of inorganic polymeric binder based on natural Pozzolan. J Mater Sci 44(12):3088–3097

Heah CY, Kamarudin H, Al Bakri AM, Binhussain M, Luqman M, Nizar IK, Liew YM (2011) Effect of curing profile on kaolin-based geopolymers. Phys Procedia 22:305–311

Singh B, Ishwarya G, Gupta M, Bhattacharyya SK (2015) Geopolymer concrete: a review of some recent developments. Constr Build Mater 85:78–90

Yewale VV, Shirsath MN, Hake SL (2016) Evaluation of efficient type of curing for Geopolymer concrete. Evaluation 3(8):10–14

Pangdaeng S, Phoo-ngernkham T, Sata V, Chindaprasirt P (2014) Influence of curing conditions on properties of high calcium fly ash geopolymer containing Portland cement as additive. Mater Des 53:269–274

Vijai K, Kumutha R, Vishnuram B (2010) Effect of types of curing on strength of geopolymer concrete. Int J Phys Sci 5(9):1419–1423

Numerical Computation of Code Compliant Beam Column Joints Made with Low Strength Concrete

Muhammad Hamza Sabir, Qazi Samiullah, Shahid Ullah, and Shamsher Sadiq

Abstract Beam column assemblies made with reinforced concrete are weakest in the joint region. Studies show the failure of such portions to cause catastrophic brittle failure. In this study, low strength concrete, code compliant joint is simulated using Concrete Damaged Plasticity (CDP) model in ABAQUS. The biggest challenge in numerical studies is the selection of material models and to accurately replicate the experimental behavior. Therefore, In the present study an exterior RC joint under monotonic loading is selected from published data to check the reliability of numerical prediction. The compressive behavior is replicated using Hognestad's parabola and the tensile behavior is calculated using American Concrete Institute guidelines. Reinforcement is modelled discretely, and the concrete-steel interface is assumed to be rigid in connection. The comparison of numerical and experimental load deflection curve reveals a reasonable agreement with each other. The finding of present study provides a reference for the future parametric studies to investigate the RC joints progressive collapse behavior.

Keywords RC joints · Beam-column connections · Numerical simulation · ABAQUS · CDP

1 Introduction

The northern region of Pakistan lies on active faults (Umar et al. 2014). That is the reason, this region is not new to the concept of earthquakes and related catastrophes. These catastrophes require the structures to possess a resisting mechanism that counters their effects. This can either be done by redirection of load, or by damping of the incoming energy (Uma and Jain 2006). One of such techniques is the frame structure. The frame structure is designed to act as a damping mechanism. It counters

M. H. Sabir (✉) · Q. Samiullah · S. Ullah
University of Engineering and Technology, Peshawar, Pakistan
e-mail: mohammadhamza.sabir@gmail.com

S. Sadiq
Ghulam Ishaq Khan Institute of Engineering Sciences and Technology, Topi, Swabi, Pakistan

I. Pal et al. (eds.), *Proceedings of the 2nd International Symposium on Disaster Resilience and Sustainable Development*, Lecture Notes in Civil Engineering 294,
https://doi.org/10.1007/978-981-19-6297-4_15

the effects of earthquakes by deforming in the elastic region during mild earthquakes and in the plastic region in severe ones. Hence the design always ensures the safety of the life in the structure.

Studies show that the most vulnerable region of the frame structures are their joints (Behnam et al. 2018), (Del Vecchio et al. 2014). That is the reason, building codes (UBC 1997), (ACI 2008) suggest the use of confining reinforcements in the joints as well as the structural members. However, the critical portion still exists in the joint as has been verified by numerous studies (Omidi and Behnamfar 2015) (Sharma and Bansal 2019) (Del Vecchio et al. 2014), (Said and Nehdi, 2004). This claim has been supported by the numerical analysis as well. (Baji, Eslami and Ronagh, 2015). Luk et al. investigated the force transfer mechanism of wide beam column joints through FEA in ABAQUS. The material was regular reinforced concrete with the geometry being that of the exterior joints. The joint was divided into 4 triangles by means of cross shaped discrete cracks. It was concluded that the triangular regions rotate under the action of forces which when resisted by the concrete causes the production of shear stresses. Because of these, larger values of tensile stresses are produced in the reinforcements that result in the cracks to remain open. (Luk and Kuang 2017). Behnam et al. also studied exterior beam column connections through FEA in ABAQUS. They believed the damage parameters and angle of dilation were vital in predicting the correct behavior. The recommended dilation angle lied between 38 and 42°. Higher value causes ductile behavior, while a lower value shows brittle mode of failure. (Behnam et al. 2018).

Aside from that, Concrete Damaged Plasticity (CDP) model was used in slab modelling by (Genikomsou and Polak, 2015) and (Wosatko et al. 2015). Both studies emphasized on the sensitivity of mesh size, damage parameters, dilation angle and the tensile behavior of concrete. According to Genkimosu et al. the spine of the FEA is the mesh size. Wosatko et al. on the other hand pointed out that a continuum description should be combined with the CDP to combat the behavior of mesh size, localized deformation, and numerical instabilities. Both studies used Hillerborg (Hillerborg et al. 1976) fracture energy to substitute the slippage with the tensile behavior of concrete.

In the current study, a numerical simulation of an external beam column joint is carried out. The joint is modelled in a way to numerically predict the damage pattern of experimental results without prior definition of weak zones. Beside this, the concrete strength is taken as 2000 psi (13.8 MPa), which is very low as compared to aforementioned research as can be observed in the research of Phillip Francis (Francis 2018b) (Francis 2018a). The current research is based on the experimental work carried out by Yasir Irfan Badrashi (Badrashi 2016), whose research objective was to calculate the response modification factor of structures built in Pakistan. The shortcomings found in the building construction were considered in the form of 16 full scale joints including both: the controlled as well as the inadequate (deficient) models. The selected joint was a code compliant joint and was termed as EJ1A by the author.

2 Methodology

The CDP model in ABAQUS was used for the current study. The experimental data included the compressive behavior of concrete and yield strength of the reinforcements. Aside from that, no further data necessary for numerical simulation (Poisson's Ratio, ultimate tensile strength, and fracture energy) could be found. In the numerical analysis, Hognestad's parabola (Hognestad 1951) was used to define the material constitutive model for concrete in compression. The steel and concrete are Defined by separate elements with material specific modelling.

2.1 Material Models

2.1.1 Concrete

The compressive strength (f_c) of concrete was taken as 2000 psi. Elastic modulus (E_c) was equated using Eq. 1, and tensile strength (f_t) was calculated using Eq. 2 from the ACI building code (American Concrete Institute 2005).

$$E_c = 57000\sqrt{f_c} \tag{1}$$

$$f_t = 7.5\sqrt{f_c} \tag{2}$$

The built-in Damaged Plasticity Model was invoked for the modelling. The parameters are shown in Table 1.

2.1.1.1 Compression

The Hognestad's Parabola (Hognestad 1951) defined by Eq. 3 was used to represent the compressive hardening behavior of the concrete. The softening was defined by Eq. 4 in which the value of Z as defined by (Kent and Park 1971) was calculated to be 100 which can be observed in Fig. 1.

The compression damage was defined by Eq. 5 from Yu et al. (Yu et al. 2010) which is represented by Fig. 2.

$$\sigma_c = f_c\left(2\frac{\varepsilon_c}{\varepsilon_o} - \left(\frac{\varepsilon_c}{\varepsilon_o}\right)^2\right) \tag{3}$$

Table 1 Concrete damaged plasticity parameters

Dilation angle	E	fb/fc	K	Viscosity parameter
30,35,40	0.1	1.16	0.667	0.0001

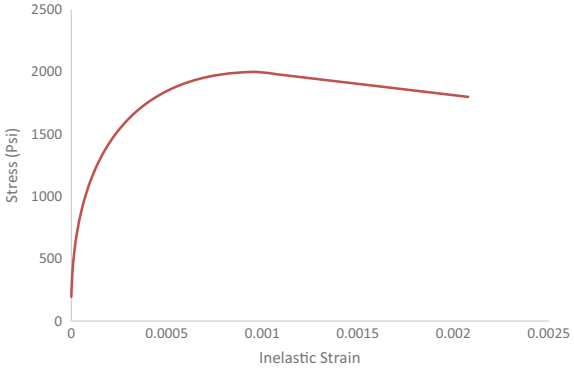

Fig. 1 Compressive behavior of concrete

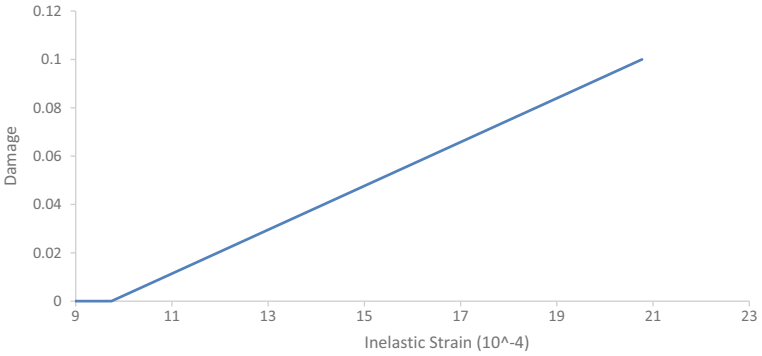

Fig. 2 Compression damage

$$\sigma_c = f_c(1 - 100(\varepsilon_c - \varepsilon_o)) \tag{4}$$

$$d_c = 1 - \frac{\sigma_c}{f_c} \tag{5}$$

2.1.1.2 Tension

The hardening behavior was assumed to be elastic until f_t as shown by Eq. 6. Softening behavior (Fig. 3) was as described by Eq. 7 from. (Wang and Hsu 2001). The compression damage (Fig. 4) was defined by Eq. 8 from (Yu et al., 2010)

$$\sigma_t = E_c \varepsilon_t \tag{6}$$

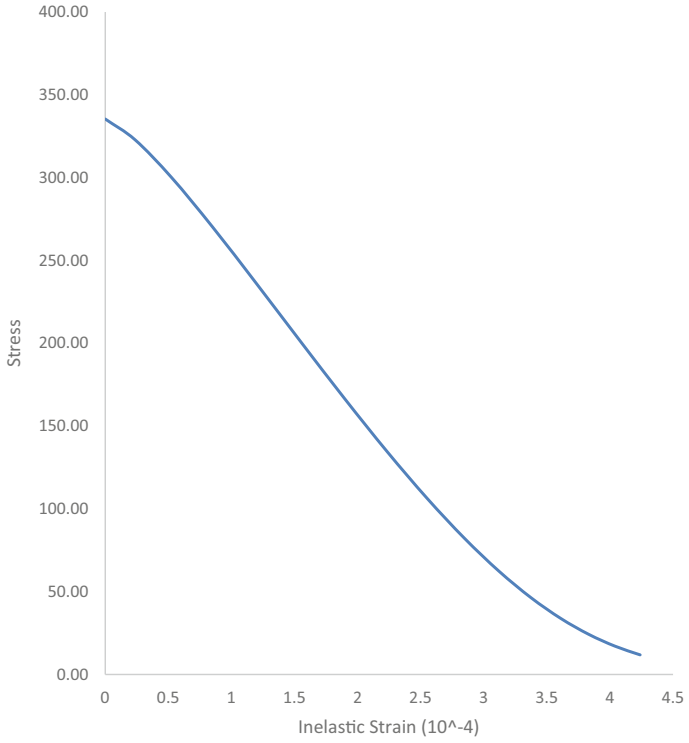

Fig. 3 Tension softening of concrete

$$\sigma_t = f_t \left(\frac{\varepsilon_{cr}}{\varepsilon_t} \right)^{0.4} \tag{7}$$

$$d_t = 1 - \frac{\sigma_t}{f_t} \tag{8}$$

2.1.2 Steel

Steel was assumed to be elastic-perfectly plastic. The elastic modulus was taken as 29,000 ksi as suggested by ACI code (American Concrete Institute 2005). The yield strength was reported to be 40 ksi by (Badrashi 2016) and the ultimate strength was taken as 60 ksi. The stress strain curve is shown in Fig. 6.

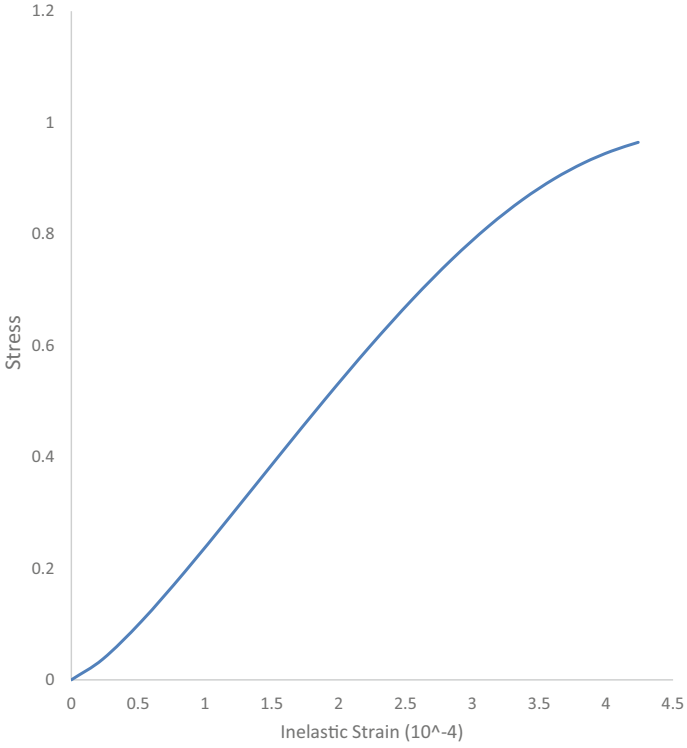

Fig. 4 Tension damage

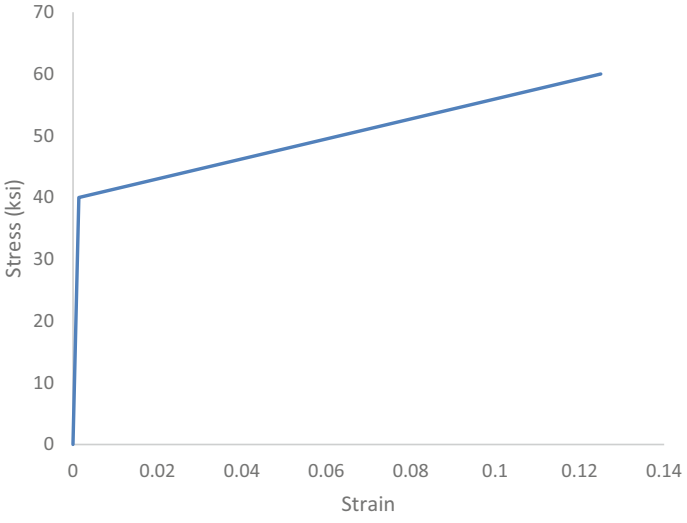

Fig. 5 Bilinear behavior of steel reinforcement

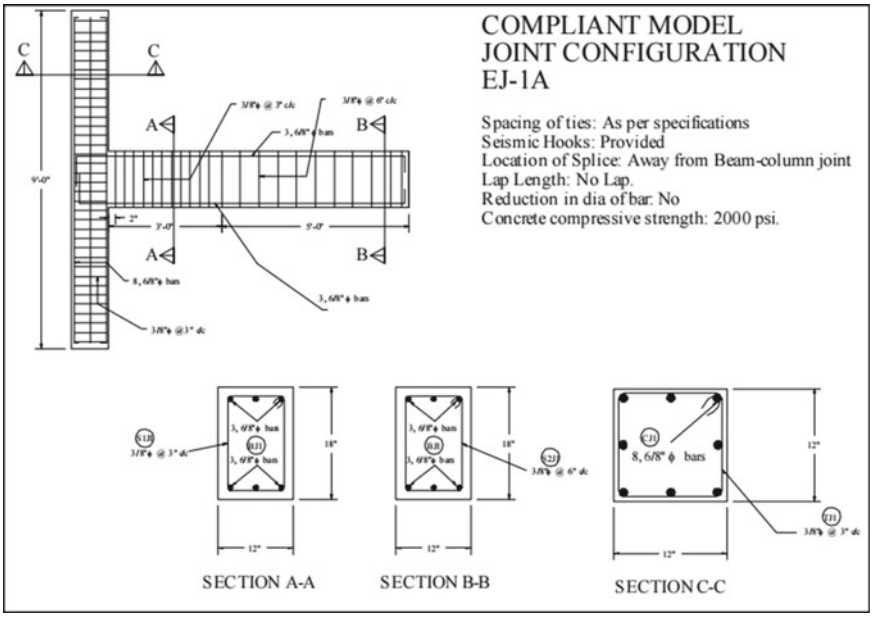

Fig. 6 Geometry of code compliant joint (Badrashi 2016)

2.2 FE Model

The detailing of the model is as shown in Fig. 6. Model was created in Abaqus CAE. The concrete portion was modeled as solid continuum element, while a truss element was used for representation of reinforcements (Figs. 7 and 8). Mesh size was variable and several trials with different meshes were carried out.

2.3 Boundary Conditions

Base of the column was restricted in x, y and z directions. The top of the column was free to move in y and z directions but restricted in x direction.

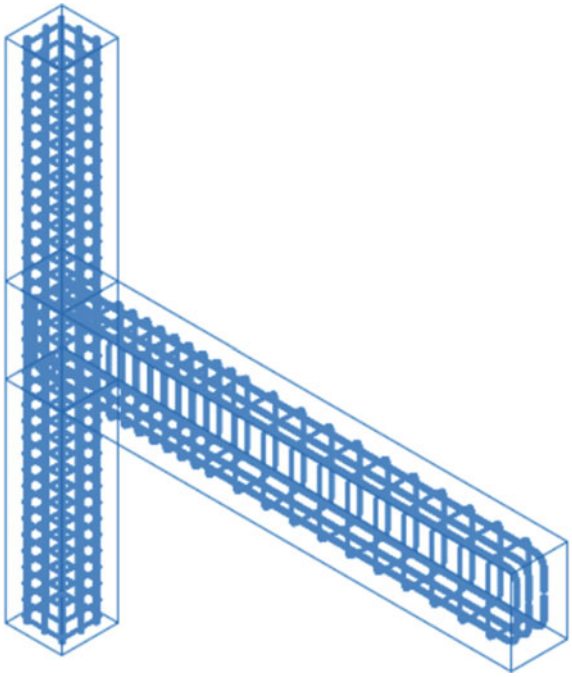

Fig. 7 ABAQUS model

The bond between concrete and reinforcement was assumed to be perfect. This implied that the strain in concrete was equal to that in steel, between any two nodes. The rebar slippage was incorporated in the form of tensile behavior of concrete.

3 Results and Discussion

Figure 9 shows the load vs deflection response for different dilation angles. Lesser value of the dilation angle causes the response to be less stiff and shows a gradual plastic response. The greater value shows greater initial stiffness and near flat plastic response. However, the results obtained in all case lie in the acceptable range. Furthermore, from Fig. 10, we observe that the mesh size also causes noticeable changes in the results. The coarser mesh gives a stiffer response. The coarser mesh also yields a more gradual and smooth plastic response with lesser deviation from original results. The deviation is in the damage. For a coarser mesh (Fig. 11), although the response is acceptable and the time is saved with a reduction in utilization of resources, the damage prediction is not accurate. Experimental procedure shows the failure in the joint region while the numerical result with coarser mesh fails in the beam region, hence the increasing plastic response. As the mesh size is reduced, more stress

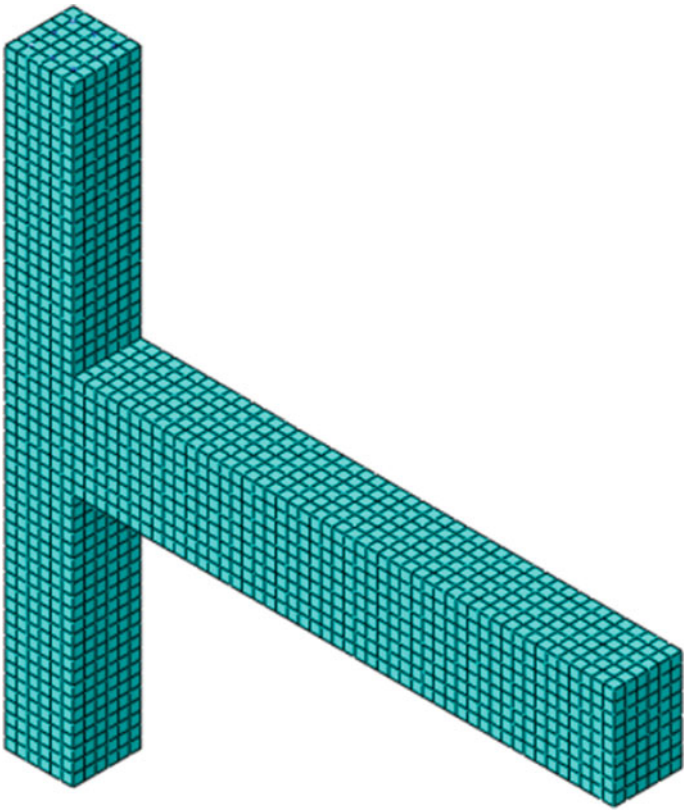

Fig. 8 Meshed model

concentrates in the joint and a realistic damage is simulated. For the mesh size of 2 × 2 in, the simulated damage is the closest to the experimental damage (Fig. 12).

It is worth mentioning here that the experimental procedure was loaded in a cyclic manner and the numerical result was simulated for monotonic loading. Therefore, the direction of damage in numerical result is in a diagonal pattern while the experimental pattern follows the "X" shape.

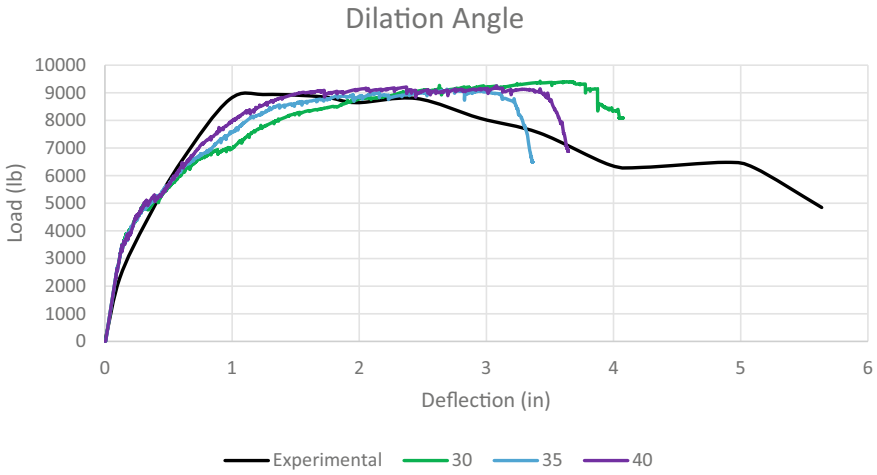

Fig. 9 Curves representing the variation of response with the dilation angle

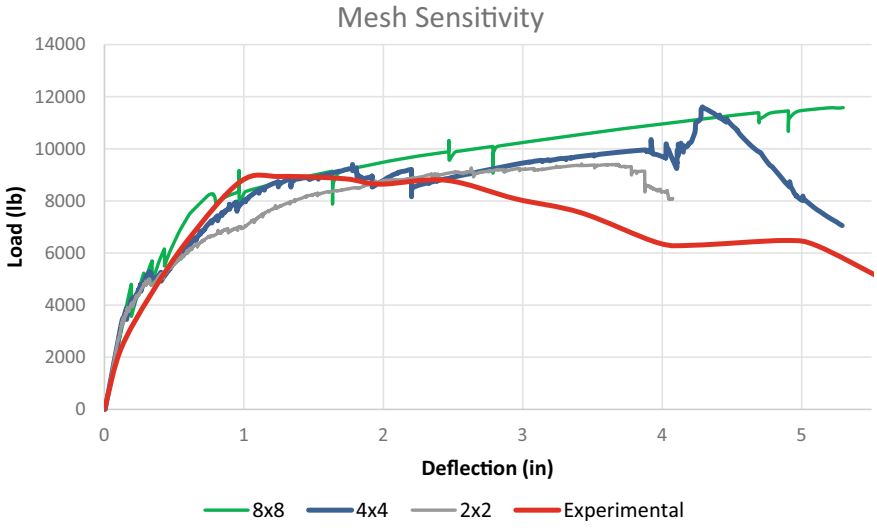

Fig. 10 Curves representing the variation of response with the change in mesh size

Although (Behnam et al. 2018) reported ductile behavior for increased values of dilation angle, the current results show a deviation from that conclusion. However, the results closest to the experimental procedure are obtained from the dilation angle

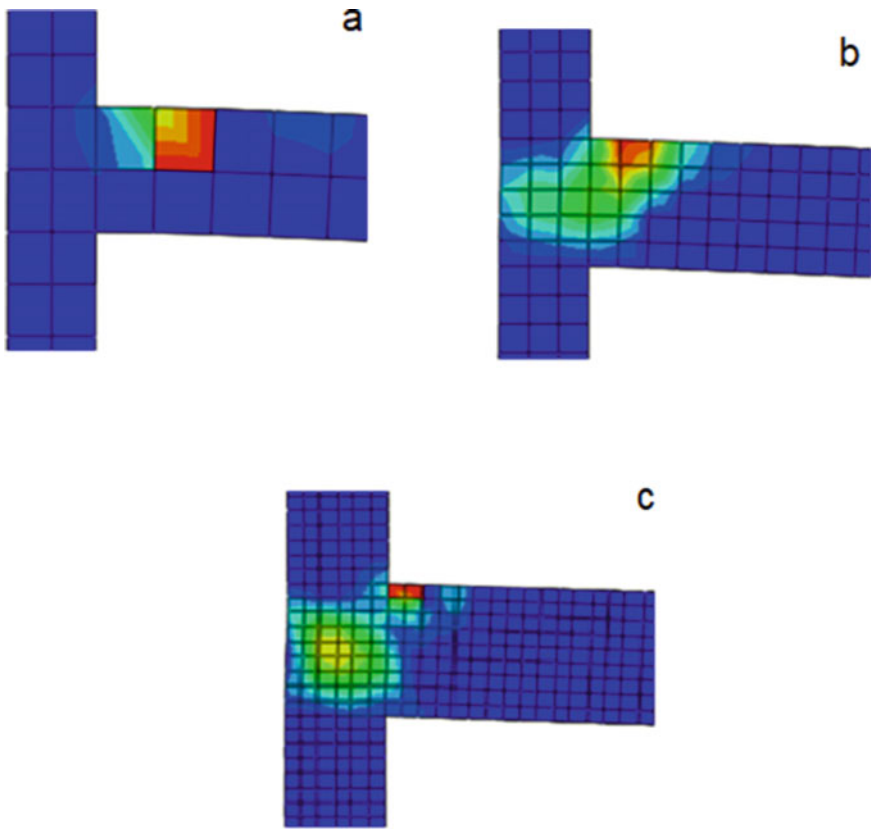

Fig. 11 Magnitude of plastic strain (PEMAG) for mesh size of **a** 8 × 8 in, **b** 4 × 4 in, and **c** 2 × 2 in

value of 40° reinforcing the claim of Behnam et al. this difference in behavior is possibly due to the fact that the concrete having low strength is usually more ductile compared to stronger concrete (ACI-318 2014).

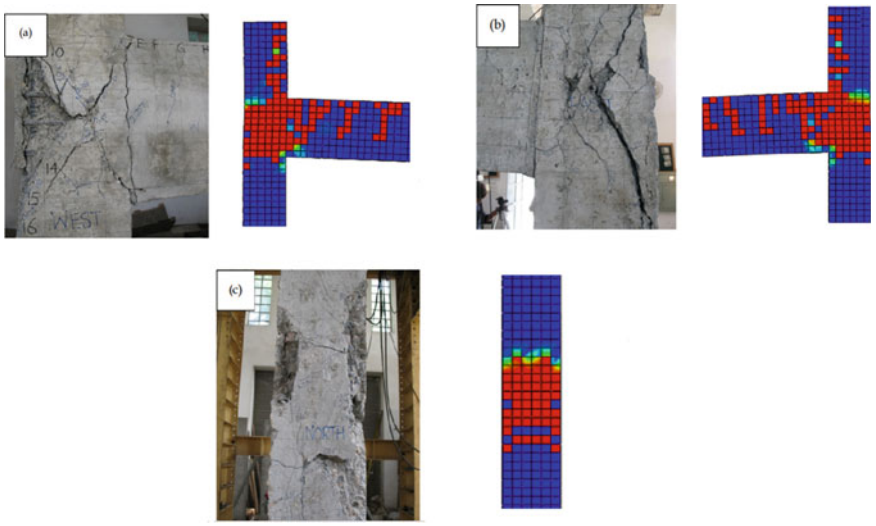

Fig. 12 Damage on **a** west, **b** east and **c** north faces

4 Conclusion

ABAQUS software has been employed with the damaged plasticity constitutive model in the current study to numerically simulate the experimental tests carried on code compliant joints. The bilinear elasto-plastic constitutive model has been used for steel. It can efficiently help in predicting the failure of reinforced concrete joints. The behavior of numerical model in terms of cracking and damage, is like the experimental model. This implies that the chosen material models and the material and geometrical approximations are suitable in predicting the experimental behavior of any such reinforced concrete joint. The dilation angle needs to be calibrated for individual models. The change may yield different results but the deviation from the original results is not so much as to be discarded entirely. Furthermore, the damage response must be compared along with the load vs deflection response. It is worth mentioning that the current research is carried out using only the values of concrete compressive strength and the yield strength of steel.

References

ACI-318 (2014) Building Code Requirements for Structural Concrete (ACI 318S-14) and Commentary (ACI 318SR-14), American Concrete Institute

ACI (2008) ACI Committee, & International Organisation for Standardization. (2008) Building code requirements for structural concrete (ACI 318M-08) and Commentary, American Concrete Institute

American Concrete Institute (2005) Building Code Requirements for Structural Concrete and Commentary (ACI 318M-05). American Concrete Institute, 2003, p 436

Badrashi YI (2016) Response modification factors for reinforced concrete buildings in Pakistan (Ph.D Thesis). University of Engineering and Technology, Peshawar. http://173.208.131.244:9060/xmlui/handle/123456789/5005

Baji H, Eslami A, Ronagh HR (2015) Development of a nonlinear FE modelling approach for FRP-strengthened RC beam-column connections. Structures 3:272–281. https://doi.org/10.1016/j.istruc.2015.06.003

Behnam H, Kuang JS, Samali B (2018) Parametric finite element analysis of RC wide beam-column connections. Comput Struct 205:28–44. https://doi.org/10.1016/j.compstruc.2018.04.004

Francis P (2018a) Concrete damaged plasticity tool. https://concretedamagedplasticity.com/

Francis P (2018b) The influence of shear connection strength and stiffness on the resistance of steel-concrete composite sandwich panels to out-of-plane forces. University of Surrey. http://epubs.surrey.ac.uk/848767/

Genikomsou AS, Polak MA (2015) Finite element analysis of punching shear of concrete slabs using damaged plasticity model in ABAQUS. Eng Struct 98:38–48. https://doi.org/10.1016/j.engstruct.2015.04.016

Hillerborg A, Modéer M, Petersson P-E (1976) Analysis of crack formation and crack growth in concrete by means of fracture mechanics and finite elements. Cem Concr Res 6(6):773–781. https://doi.org/10.1016/0008-8846(76)90007-7

Hognestad E (1951) A study of combined bending and axial load in reinforced concrete members; a report of an investigation conducted by the engineering experiment station. University Of Illinois, Under Auspices Of The Engineering Foundation, Through The Reinforced Concrete, in

Kent DC, Park R (1971) Flexural members with confined concrete. J Struct Div 97:1969–1990

Luk SH, Kuang JS (2017) Seismic performance and force transfer of wide beam-column joints in concrete buildings. Proc Inst Civil Eng Eng Comput Mech 170(2):71–88. https://doi.org/10.1680/jencm.15.00024

Omidi M, Behnamfar F (2015) A numerical model for simulation of RC beam-column connections. Eng Struct 88:51–73. https://doi.org/10.1016/j.engstruct.2015.01.025

Said AM, Nehdi ML (2004) Use of FRP for RC frames in seismic zones: part I. Evaluation of FRP beam-column joint rehabilitation techniques. Appl Compos Mater 11(4):205–226. https://doi.org/10.1023/B:ACMA.0000035462.41572.7a

Sharma R, Bansal PP (2019) Behavior of RC exterior beam column joint retrofitted using UHP-HFRC. Constr Build Mater 195:376–389. https://doi.org/10.1016/j.conbuildmat.2018.11.052

UBC I. C. of B. O. (1997) Uniform building code, In International conference of building officials, Whittier, CA

Uma SR, Jain SK (2006) Seismic design of beam-column joints in RC moment resisting frames - review of codes. Struct Eng Mech 23(5):579–597. https://doi.org/10.12989/sem.2006.23.5.579

Umar M et al (2014) Stratigraphic and sedimentological attributes in Hazara Basin Lesser Himalaya, North Pakistan: their role in deciphering minerals potential. Arab J Geosci 8:1653–1667. https://doi.org/10.1007/s12517-014-1322-1

Del Vecchio C et al (2014) Experimental investigation of exterior RC beam-column joints retrofitted with FRP systems. J Compos Constr 18(4):04014002. https://doi.org/10.1061/(asce)cc.1943-5614.0000459

Wang T, Hsu TTC (2001) Nonlinear finite element analysis of concrete structures using new constitutive models. Comput Struct 79(32):2781–2791. https://doi.org/10.1016/S0045-7949(01)00157-2

Wosatko A, Pamin J, Polak MA (2015) Application of damage-plasticity models in finite element analysis of punching shear. Comput Struct 151:73–85. https://doi.org/10.1016/j.compstruc.2015.01.008

Yu T et al (2010) Finite element modeling of confined concrete-II: plastic-damage model. Eng Struct 32(3):680–691. https://doi.org/10.1016/j.engstruct.2009.11.013

Seismic Behaviour of Pavements-An Approach Towards Seismic Resistance Design of Pavements

Sukanta Das and R. K. Burnwal

Abstract From past to date, earthquake road damages have been observed in India and worldwide. Road networks play a key role in natural and man-made disasters. Several researchers have been reported road, bridge, and tunnel damage due to earthquakes. However, very less literature and almost no guidelines have been established against seismic resistance design of pavements. In the present study, two-dimensional finite element analysis has been performed for seismic response of road under surcharge load as traffic loads. The three-layer road is modelled as three nodded triangular elements with an average element size of 1/10th of the seismic event wavelength. The seismic excitation is applied at the base of the model, and the model has been verified using the wave propagation theory. The lateral and vertical response of the road has been reported in terms of response spectra and displacement with depth. The result shows that road embanks are more vulnerable to seismic excitations, and significant aggravation of ground motion is observed at the top of pavements compared to free field conditions. A parametric study also has been reported in the present study.

Keywords Seismic-soil-pavement-interaction · 2D-FEA · Garber wavelet · Displacement

1 Introduction

Road networks are considered one of the most important transport systems since they play a critical role in attaining economic and social prosperity in the modern world. Moreover, the road lines play a major role during natural and man-made disasters for rescue and relief operations. Hence these roads should be working even in adverse weather conditions. Underground events which succeed each other during

S. Das · R. K. Burnwal (✉)
Indian Institute of Technology, Roorkee, Uttarakhand, India
e-mail: ravindra_b@ce.iitr.ac.in

S. Das
e-mail: sdas@eq.iitr.ac.in

I. Pal et al. (eds.), *Proceedings of the 2nd International Symposium on Disaster Resilience and Sustainable Development*, Lecture Notes in Civil Engineering 294,
https://doi.org/10.1007/978-981-19-6297-4_16

moderate or major shakes are believed to produce surface and above surface changes on local or regional scales. During the earthquakes, the failure of the road system has been reported worldwide. Nobuo et al. (2011) reported that during the Tohoku earthquake (11 March 2011), there was significant damage to National Route 45 and minor damages to National routes 4 and 6, and this quake has destroyed a total of 3546 areas along roads, 71 bridges and 26 ports. Further, Kazama and Noda (2012) reported that damage was caused to 20 stretches of expressway with a total length of 870 Km, maximum differential settlements of 2 cm or more at 174 locations.

A special report on the Baja earthquake (4 April 2010) by the Earthquake engineering Research Institute (EERI 2010) mentioned that Highway 2 and 5 were among the most damaged roads, and the significant damage to the roads in Mexico is either due to lateral spreading or displacement of the actual fault. From the Qinghai earthquake (14 April 2010), Tang et al. (2012) reported that the road leading to the airport was damaged. Named G214 and S308, two main highways have been damaged to different degrees and highway foundation split, and settlement damage was observed in the length of 875 Km everywhere with 87 landslides. DesRoches et al. (2011) on Haiti earthquake (12 January 2010) reported many road failures along the coast west of Carrefour, mainly due to settlement and localised creep. During the Chile earthquake (27 February 2010), as Elnashai et al. (2012) reported, four bridges crossing the Bio-Bio river near Concepcion were damaged. Llacolen bridge, built-in 2000, suffered deck unseating, Juan Pablo Iibridge, built in 1974, suffered lateral spreading at the approach. Route 160 In Lota along the coast was closed in both directions due to embankment slope failure.

Nepal earthquake (25 April 2015) has caused significant damage to life and infrastructures. Praksah et al. (2016) reported the dislocation of roads in the Kathmandu area also; a road in Sonitpur that was the epicenter of the earthquake has developed a crack following the impact of the earthquake, while several buildings and walls in the area suffered damage. Goda et al. (2016), during the Kumamoto earthquake (16 April 2016), reported that the Kyushu expressway was damaged, National road route 57, road 28 and road 175 (location 13), damaged and disconnected due to landslides. Alberto et al. (2018) reported that during the Puebla earthquake (19 September 2017), longitudinal cracks and cavities (up to 1 m depth) appeared in one lane of Tulyehualco-Xochimilco road. Krautwald et al. (2019), after the Indonesian Tsunami (28 September 2018), reported that the asphalt road between the shops and the coastline, a road connecting Makassar and Poso, was severely damaged, and the large cracks in the runway (maximum 500m) was reported.

During the Southcentral Alaska earthquake (30 November 2018), as reported by Liu et al. (2018) and Jibson et al. (2020), significant damage to the road, such as Glenn highway, ramp connecting Minnesota drive, Alaska railroad, was caused. However, Palmer-Wasilla Highway, Pittman Road, Point MacKenzie Road, and Vine Road were among the most damaged roads. West et al. (2019) also reported the road damages caused due to lateral spreading and sand boiling during the Southcentral Alaska earthquake. Figure 1, depicts typical road damages from the past earthquakes.

Fig. 1 Road damages due to past earthquakes **a** Chile earthquake, 2010 **b** Negros earthquake, 2012(UNDRR, 2012) **c** Alaska earthquake, 2018 (Structural Engineers Association of Alaska, 2018) **d** Sichuan earthquake, 2008 (Anbazhagan et al. 2012)

From the above studies, the damage to the road and bridges due to earthquakes is significant. However, despite these damages and losses, the literature on the seismic design of the pavement, as far as the Authors are aware, is not available. As a result, this paper aims to provide an assessment of seismic site amplification and its variations due to the presence of pavement layers; for that, the Finite element analysis has been carried out.

2 FEA Modelling of SSPI

The two-dimensional finite element analysis (2D-FEA) has been used to investigate the seismic behaviour of pavements which may be called as seismic soil pavement interaction (SSPI). The detailed geometry and boundary conditions of the FEA model has been presented in Fig. 2. A three-layered pavement situated on the homogeneous soil base layer of size 20 m height (H) and 200 m long (W) is considered in the study.

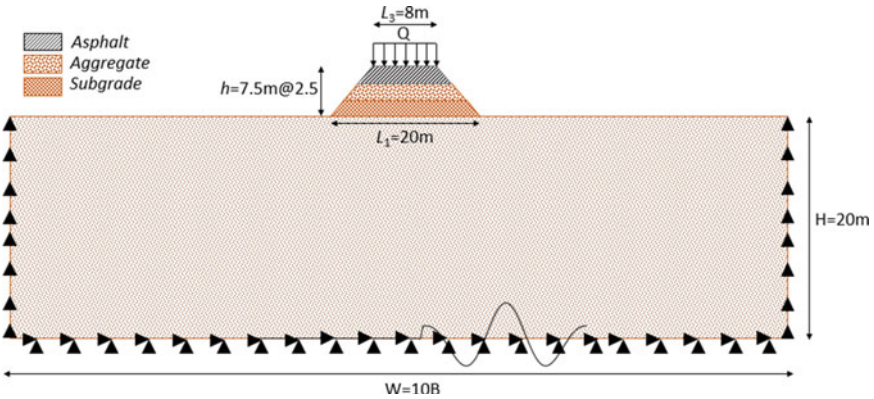

Fig. 2 Geometry and mashing of pipe buried near sand slopes

However, the FEA model has been varied for larger width of soil base and found as 200 m long width can produce the accurate seismic response of pavement. The three-layer pavement consisting of asphalt, aggregate and subgrade of total height (h) 7.5 m placed at the top center of the soil base. The asphalt layer of width (l3) 8 m has been placed over the base of 20 m (l1), and the other two layers have been placed at an interval of 2.5 m. Each pavement layer has been considered rigid compared to the soil base with different Young's modulus (E) values, and the elastic behaviour of the soil has been assumed in the present analysis. The effect of soil type has been investigated with varying E values; the soil and pavement material properties have been shown in Table 1. A Garber wavelet is applied in the horizontal direction at the base of the model with a peak ground velocity of 0.05m/s and a central frequency of 3Hz. The boundary condition has been applied at the lateral side so that the soil mass can move horizontal and fully restrain against the vertical direction. While the base of the FELA model has been fixed from any moment, the unit displacement has been allowed along with the movement of ground motion (horizontal direction). The average element size of the FEA model has been kept as 1/10th of the wavelength of the ground motion. The mesh density or element size has been kept minimum at the pavement layer and surrounding due to maximum stress concentration. A surcharge load has been applied at the top of the asphalt layer to simulate the seismic behaviour of pavements under traffic loads. All numerical FEA analysis has been carried out using commercial software Abaqus 2020. The seismic motion has been recorded at the Free Field condition and the presence of pavement.

Table 1 Material properties used in the SSPI analysis (Huang, 2004; Tang, 2011)

Pavement layer	Elastic modulus, kPa	Poisson's Ratio
Asphalt	1,800,000	0.30
Aggregate	40,000	0.35
Subgrade	15,000	0.45
Base	150,000	0.35

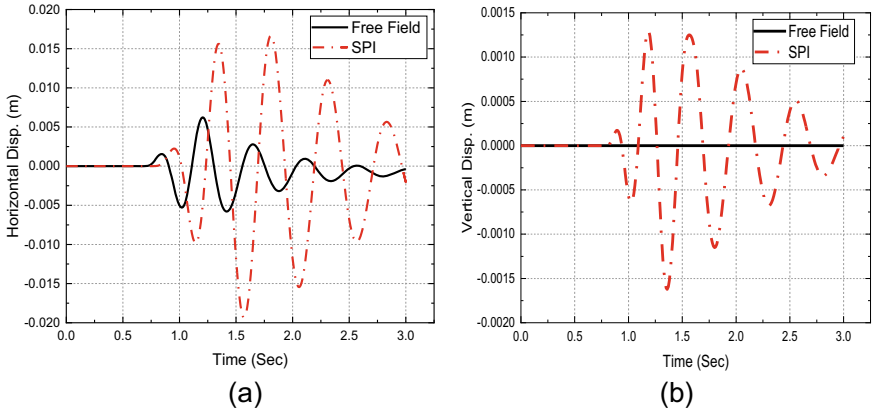

Fig. 3 Seismic displacement of pavement considering SPI and free field condition **a** horizontal displacement **b** vertical displacement

3 FEA Results and Discussions

To investigate the seismic response of pavements, initially, ground response analysis has been performed at free field condition and later, the three-layered pavement has been considered. The SV wave propagates from the base of the FEA model, and the response at the surface and the pavement has been recorded and presented in Fig. 3. Figure 3a and b represents the seismic displacement in the horizontal and vertical direction, respectively. The seismic response of pavement in horizontal has been observed maximum under SV wave propagation, as expected.

It can be observed from Fig. 3 that for both the cases with Soil Pavement Interaction (SPI), the amplification of the seismic wave is significant. While for the free field condition, there is a slight variation in horizontal displacement without the traffic load compared to SPI. However, the vertical displacement at free field condition has been found almost zero because of less amplitude of ground motion, while vertical displacement increases with the consideration of SPI because of inertial and kinematic interaction between the soil and pavement structure.

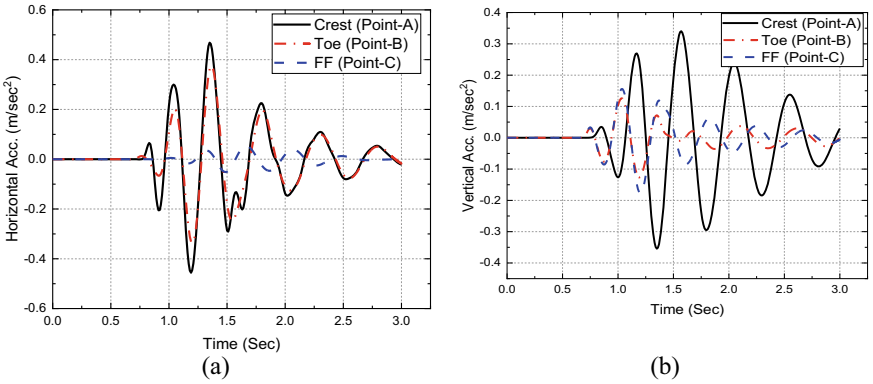

Fig. 4 Acceleration time history without traffic loading **a** Horizontal acceleration **b** Vertical acceleration

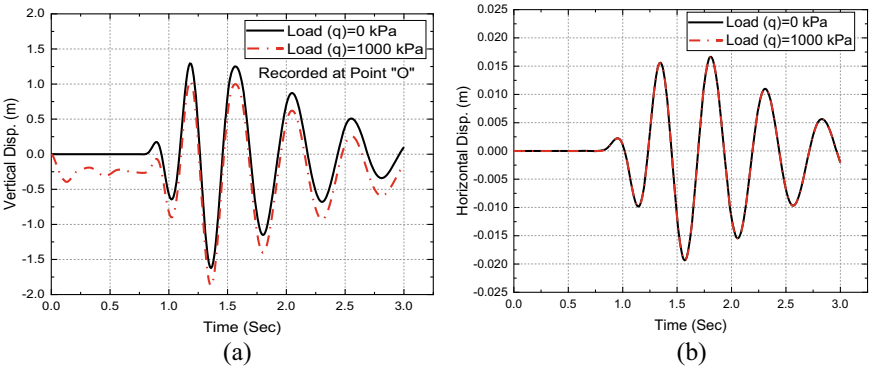

Fig. 5 Displacement time history with traffic loading **a** Horizontal displacement **b** Vertical displacement

Figure 4 shows the acceleration time history for the three different locations in the road embankment model, namely Crest, Toe and Far-field (Fig. 2), without considering the traffic loading. Both the horizontal and vertical acceleration is maximum at the Crest of the embankment, and the same amplitude has been found at the surface of the asphalt top layer.

The acceleration time history is minimum at far-field (Point-C) for case a, whereas, for case b, the acceleration with respect to time is minimum at the toe (Point-B) of the embankment. Moreover, in the vertical direction, the amplification at the Crest of the pavement is significant compared to other locations.

The seismic response of pavement under traffic load as surcharge loads has been examined and given in Fig. 5. No such effect has been observed on the seismic displacement of pavement in horizontal direction under surcharge loads 0 and 1000 kPa. However, in the case of vertical displacement, an initial displacement has been

observed under surcharge load 1000 kPa, and the vertical displacement increases with the time under loads 1000 kPa. All the seismic response has been recorded at the top surface of the asphalt layer.

Figure 6(a and b) shows the variation of horizontal and vertical acceleration with time. It can be observed that with the increase in the soil shear wave velocity, the amplification increases and the maximum amplification is observed in the case of $V_s = 200$ m/s and minimum at $v_s = 90$ m/s, which is because the resonance condition comes as the shear wave velocity of the soil increases. Moreover, the same trend was observed in the displacement time plot (See Fig. 6(c and d)).

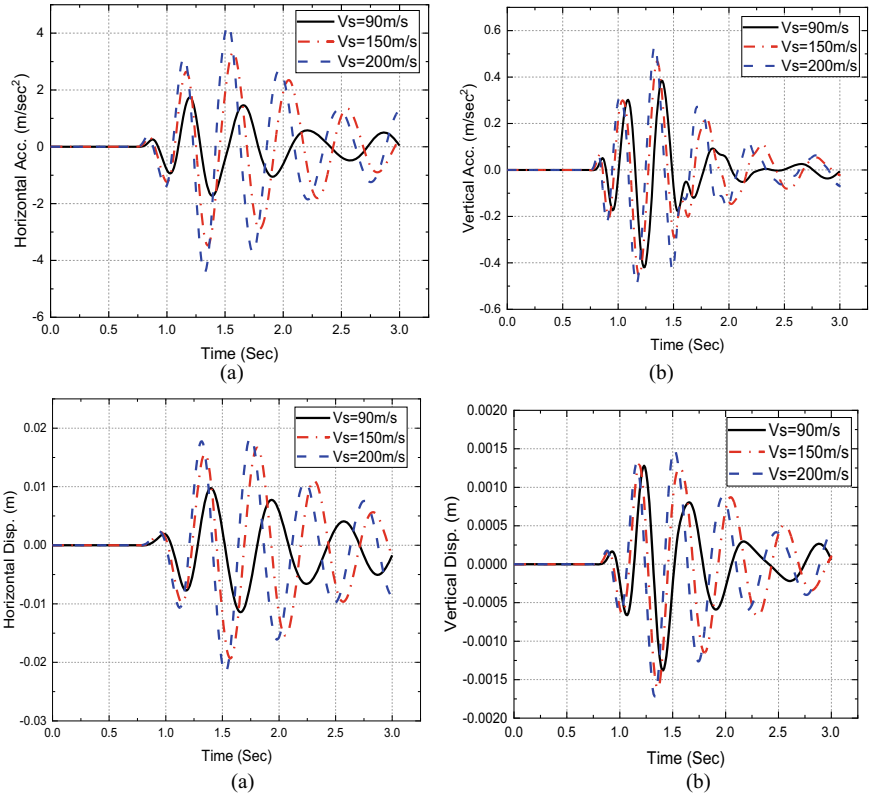

Fig. 6 Seismic response of pavements for different soil conditions, acceleration time history **a** Horizontal and **b** vertical direction and seismic displacement **c** Horizontal and **d** vertical direction

4 Conclusion

A sufficient numerical analysis has been carried out to examine the seismic behaviour of pavements. From the present 2D-FEA analysis of seismic-soil-pavement-interaction, the following conclusions can be drawn, as follows.

Based on extensive numerical analysis and obtained results, a significant amplification has been observed with the consideration of seismic soil pavement interaction; less amplification has been found due to less amplitude of the input ground motion. However, the response has been found maximum in the horizontal direction compared to the vertical direction due to the application of SV input motion. The seismic response at the top asphalt layer has been found maximum. As distance increases, the seismic response decreases. After a certain distance, it becomes similar, which has been found as that of free field conditions.

The traffic load as surcharge load significantly influences the seismic response of pavements in the vertical direction; as the intensity of surcharge load increases, the vertical displacement increases from the very beginning of time. However, the effect of surcharge loads on horizontal seismic displacement has been found insignificant.

The different soil type has also influenced the seismic response of pavements under traffic loads. From the present study, as the shear wave velocity of the soil increases, the acceleration and displacement increase that may be due to increase of natural frequency of the system, resonance occurred as the natural frequency of the system comes close to the predominant frequency of the input motion. Therefore at $v_s = 200$ m/s, the maximum seismic displacement has been observed.

References

Mimura N, Yasuhara K, Kawagoe S, Yokoki H, Kazama S (2011) Damage from the great east Japan earthquake and tsunami-a quick report. Mitig. Adapt. Strat. Glob. Change 16(7):803–818

Kazama M, Noda T (2012) Damage statistics (Summary of the 2011 off the pacific coast of Tohoku earthquake damage). Soils Found 52(5):780–792

Alberto Y, Otsubo M, Kyokawa H, Kiyota T, Towhata I (2018) Reconnaissance of the 2017 Puebla. Mexico Earthq Soils Found 58(5):1073–1092

Rodríguez-Pérez Q, Ottemöller L, Castro RR (2012) (2012) Stochastic finite-fault ground-motion simulation and source characterization of the 4 April 2010 Mw 7.2 El Mayor-Cucapahearthquake. Seismol Res Lett 83(2):235–249

Tang AP, Liu, YJ, Liu KT, Zhao AP (2012) Lifeline system earthquake damage in Yushu, Qinghai earthquake (ml= 7.1, 14th, April, 2010). In: The 15th world conference on earthquake engineering

DesRoches R, Comerio M, Eberhard M, Mooney W, Rix GJ (2011) Overview of the 2010 Haiti earthquake. Earthq Spectra 27(1_suppl1):1–21

Elnashai AS et al (2012) The Maule (Chile) earthquake of 27 February, 2010: development of hazard, site specific ground motions and back-analysis of structures. Soil Dyn Earthq Eng 42:229–245

Goda K et al (2016) The 2016 Kumamoto earthquakes: cascading geological hazards and compounding risks. Front Built Environ 2:19

Jibson RW, Grant AR, Allstadt RC, Allstadt KE, Thompson EM, Bender AM (2020) Ground failure from the Anchorage, Alaska, earthquake of 30 November 2018. Seismol Res Lett 91(1):19–32

Liu C, Lay T, Xie Z, Xiong X (2019) Intraslab deformation in the 30 November 2018 Anchorage, Alaska, MW 7.1 earthquake. Geophy Res Lett 46(5):2449–2457

Prakash R, Singh RK, Srivastava HN (2016) Nepal earthquake 25 April 2015: source parameters, precursory pattern and hazard assessment. Geomat Nat Haz Risk 7(6):1769–1784

Stolle J et al (2020) Engineering lessons from the 28 September 2018 Indonesian tsunami: debris loading. Can J Civ Eng 47(1):1–12

West ME et al (2020) The 30 November 2018 M w 7.1 anchorage earthquake. Seismol Res Lett 91(1):66–84

Anbazhagan P, Srinivas S, Chandran D (2012) Classification of road damage due to earthquakes. Nat Hazards. 60(2):425–460. https://doi.org/10.1007/s11069-011-0025-0

Anchorage Earthquake (2018) Reports & Information, *Structural Engineers Association of Alaska*, VoR (2018). https://seaak.net/2018-anchorage-earthquake

Tsunami alert system tried and tested by Philippines earthquake, *United Nations Office for Disaster Risk Reduction*, VoR (2012). https://www.undrr.org/news/tsunami-alert-system-tried-and-tested-philippines-earthquake

The Mw 7.2 El Mayor Cucapah (Baja California) Earthquake of April 4, 2010, VoR (2010). https://www.eeri.org/site/images/eeri_newsletter/2010_pdf/Baja_CA_EQRpt.pdf

DRR, Socio-Economic and Cross Cutting Issue

Policy Ecosystem of Social Entrepreneurship for Sustainable and Resilient Development: A Doctrinal Review

Apoorva Patel and Nageswara Rao Ambati

Abstract Growing as a global movement, social entrepreneurship has acclaimed attention from policymakers, development practitioners, researchers, communities, and academia. Social entrepreneurship is considered a potential solution for the economy and addresses risks emerging from climate change and humanitarian crises by integrating sustainability across models, initiatives, and strategies. It has also been deemed necessary to progress towards the global agenda 2030 by providing innovative social development responses to persisting and evolving social issues. India has also witnessed a surge in public discourse and programs related to social entrepreneurship, mainly reflected through its national flagship programs and proactive initiatives taken up by some of the states. The study investigates the dynamic ecosystem of entrepreneurship, especially the legal framework and policies concerns social entrepreneurship in India, using an inductive method and exploratory design. The research expands on the growing notion of a social entrepreneurial ecosystem for resilient and long-term development, with a focus on India. The findings of this doctrinal analysis show that the policy environment has a critical role in leveraging or opposing social entrepreneurship's long-term viability and resilience.

Keywords Policy initiatives · Policy ecosystem · Resilience · Social entrepreneurship · Sustainability

1 Introduction

The growth of social entrepreneurship (hereafter "SE") as a global movement and its escalated acceptance as a tool for achieving progress towards the global agenda 2030 and sustainable development has enabled better understanding and attention of the phenomenon. The context of SE and its ecosystem is interpreted differently

A. Patel (✉) · N. R. Ambati
Gujarat National Law University, Gandhinagar, Gujarat, India
e-mail: apoorva.tiss@gmail.com; apatel@gnlu.ac.in

N. R. Ambati
e-mail: anrao@gnlu.ac.in

I. Pal et al. (eds.), *Proceedings of the 2nd International Symposium on Disaster Resilience and Sustainable Development*, Lecture Notes in Civil Engineering 294,
https://doi.org/10.1007/978-981-19-6297-4_17

in different countries and regions. It reflects the diversity in areas, people, unique local challenges, and opportunities by historical, contextual, socio-demographic, economic, and political factors. Across many countries, the move to globalisation, privatisation, and a market economy has also instigated social differentiation and exclusion. This resulted in livelihood insecurity or marginalisation from the labour market and the multi-faceted risk of differentiation and exclusion arising from barriers to access to justice, inequity in healthcare, food and nutrition insecurity, poverty, and low levels of education.

This has enthused the non-profits and civil society enterprises and unlocked new ways towards social entrepreneurial endeavours. SE has emerged as one of the vital sectors of the national economies of various countries. It is also recognised as contributing to the social economy, which is considered a hybrid of the private and public sectors that strives to provide pivotal social facilities & services for needy communities and individuals. The rise of circular economic and cooperative processes in policy discourse and business activity also emanated from the transformative initiatives of SE and other players in the social economy (Commission Expert Group on Social Entrepreneurship 2016). SE is positioned to eliminate institutional and societal bottlenecks that inhibit their growth and functioning (Hogenstijn et al. 2018).

SE has been acknowledged as a driver of employment generation, livelihood creation, innovation, and inclusive growth driving local and national economies. It also gained traction as a possible solution to social, economic, and environmental issues.

Gradually this also resulted at the beginning of legal institutionalisation of social enterprises at various stages.

The need to address the emerging social, economic, and environmental issues and bring about a transformation have emanated from the state and businesses and non-profits. The non-profits are often clubbed as third sector organisations outside the state and the markets. They are given rise by the situations wherein the state or the market might not perceive a prospect for intervention or as a result of a market or a state failure and is usually identified by the third sector or a sector that identifies this as a "social" issue which needs to be resolved, rather than as a business opportunity. There is a predominance of social objective, hybrid or mixed financial resources, recognition of differences in support schemes, differences in the level of national recognition, differences in legal frameworks, and differences in the entrepreneurial process.

With the evident growth and attention, the SE sector has continually been confronted with significant differences in needs and challenges in terms of competitiveness, finance, skilled human resources, technology, formalisation, marketing, access to knowledge services, etc. To overcome these challenges and promote social entrepreneurship, a supportive entrepreneurial ecosystem comprising attitudes, resources, infrastructure, integration of new technologies, partnerships, individual characteristics (agency), etc., is vital. This synthesis of conducive endogenous and exogenous factors comprises the 'entrepreneurial ecosystem'.

A critical analysis of the ecosystem, primarily the law and policy environment, provides a significant departure for the researcher's consideration to understand the policy paradigm in social entrepreneurship for sustainable and resilient development. In their study, Avery and Bergsteiner emphasised the need of improving business performance and resilience.

This is undoubtedly an entrepreneurial challenge: "the choice to adopt a more sustainable strategy, one that research and practice show leads to higher resilience and performance over the long term, remains in the hands of each executive team" (Avery and Bergsteiner 2011).

This is also where policy, governance, institutions, and planned arrangements come into the picture and are discussed at domestic and international forums. If SE is to be successful and sustainable, it is necessary to critically analyse pertinent challenges and opportunities and identify and address practical impediments to SE.

As a result of structural and systemic changes in the recent past, SE has strongly emerged as the critical field, with immense scope of growth and potential of bringing in sustainability and resiliency through social innovation. Pathak and Ahmad (2018) provide that to achieve sustainability and resilience, the need is to pay attention to inter-departmental coordination, management of available resources, transparency in the action plans, etc. The recent trends indicate that resilience can be considered a novel form of sustainability. The ultimate aim of sustainability and resilience is to converge resources to prepare for future challenges. Hence, SE strives to achieve both resilience and sustainability, and both these concepts should be a priority of policymakers while formulating better policies.

In the context of this paper, the focus is on how the policy frameworks in place may accelerate or inhibit the active engagement or the uptake of social entrepreneurship.

Constraints relating to initial investments are pressing challenges at the early stage of SE. In addition, restricting legal and regulatory frameworks and other barriers (for example, equating access to technology (the digital divide)) due to social exclusion and differentiation aggravates disparities across geographies.

Following a brief conceptual introduction, this paper, through a survey/review of extant literature, investigates the international legal framework and provides a critical analysis of the impact of the legislative ecosystem, which reveals the limits of law as a driver of SE expansion and consolidation. The paper then examines the evolutionary and current trends such as government schemes, policy framework, and entrepreneurial ecosystem in the context of the Indian state.

2 Methodology and Research Aim/Objectives

The paper adopts an inductive approach and exploratory design to review policy ecosystems around social entrepreneurship by incorporating the doctrinal methodology. This approach is widely applied in doctrinal research in the legislative field. Policy review (analysis of individual provisions of legislative acts, policy documents, reports, and scientific works) is conducted of extant literature between the

period 2011–2020 in the domain of social entrepreneurship policy/legal framework with the following objectives:

i. To review and appraise the existing policy ecosystem of social entrepreneurship for sustainable and resilient development;
ii. To draw a conceptual framework from policy paradigm influencing the social entrepreneurship landscape in India; and
iii. To pave the future scope of research and policy advocacy.

The research questions

- What is the state of policy and legal ecosystem for social entrepreneurship globally?
- How do the policy measures contribute (accelerate or inhibit) to SE as a pathway to Sustainable and Resilient Development (with particular reference to the Indian context)?

The policies and laws formulated between 2011 and 2020 are collected and sourced from various secondary sources. Government websites, online portals, working papers, international and national reports and journals relevant to SE were accessed. Legislation and policy documents (acts, schemes, programs, and interventions) in the context of India promoting social entrepreneurship and social innovation were sourced from the websites of the Ministry of Skill Development and Entrepreneurship (MoSDE); the Ministry of Micro, Small and Medium Enterprises (MoMSME); and the Ministry of Finance (MoF).

The relevant literature is obtained and analysed in terms of factors and frequently used words, "policy ecosystem", "Social Entrepreneurship", "sustainability", "resilience", etc." combined with an "AND" and an "OR". The paper utilises theoretical data for content review to facilitate a unified understanding and draw intertwined linkages with sustainable and resilient development.

This methodology can be distinguished from the systematic literature review approach. It integrates perspectives and insights from diverse fields to create a new conceptual framework or theory. Below is the literature review structured into How, Why and What to unravel the key concepts.

3 Understanding the How–Concept of Social Entrepreneurship (SE) and Its Ecosystem

Whilst there is no uniform etymological, epistemological understanding around the concept of social entrepreneurship, it could be said that it is a multi-dimensional concept. "It involves analysing people and their actions together with how they interact with their environments, be these social, economic, or political, and the institutional, policy, and legal frameworks that help define and legitimise human activities" (Blackburn 2011). Various definitions exist, and a wide variety of ontological meanings and organisational forms are adopted by social enterprises worldwide.

3.1 Operational Definition of Social Entrepreneurship

The word social entrepreneurship (SE) defines sustainable ventures as the ones that integrate "business principles with a passion for social impact" (Wolk 2008, p.1). Social entrepreneurs use business ideas to support their operations so that they may focus on creating social impact as their primary goal (Weerawardena and Sullivan Mort 2001).

SE is an all-embracing nomenclature used for portraying a rational process of enterprise creation and sustenance, bringing about transformative societal change on a significant and impactful scale compared to a traditional not-for-profit or non-governmental organisation. SE refers to the innovation and sustainable utilisation of prospects to create public goods or create societal and economic value on a sustainable basis. SE is embodied under the third sector and social economy. The 'UN World Youth Report' (2020) defines social entrepreneurship as an entrepreneurial action that addresses societal problems.

To ascertain the phenomenon of SE by overcoming the country-specific definitions and variations in legal status, the Global Entrepreneurship Monitor (GEM) surveys entrepreneurs on the predominance of the social mission, their innovativeness, and revenue model. For the same, GEM had developed a dataset in 2009 on social entrepreneurial activities in 49 countries. This paper will use the broader definition of SE espoused by GEM and further operationalised through the abovementioned criteria, like social, economic, etc.

3.2 Concept of Ecosystem

James More was the first to coin the term "entrepreneurial ecosystem" to describe the logical nature of how businesses interact (Hechavarria and Ingram 2014). Furthermore, according to their analysis, the ecosystem approach encompasses both changes in entrepreneurial processes or structure as well as policies that address the various issues that entrepreneurs encounter. The entrepreneurial ecosystem hypothesis lays forth a comprehensive knowledge of the many settings that benefit businesses when they cluster (Mason and Brown 2014).

With the emergence of SE as a movement and surge in research and policy on social entrepreneurship, the term 'ecosystem' has also evolved as a catchword and calls for investigation (Pratono and Sutanti 2016). Prior studies on the SE ecosystem points to macro-level factors comprising economic opportunities, good governance, abilities and resources, performance-based and socially supportive culture (Thai and Turkina 2014). Since SE is still a contested concept (Chandra 2015), studies on the SE ecosystem. The gaps from the research also highlight the need to determine how is the SE ecosystem (market, value chains, networks, operation field, etc.) is different

from other business models. Soto-Rodríguez (2014) states that the strong interactions amongst institutions lessen the risk associated with entrepreneurial initiatives, particularly when the payoff approach of policy may not suffice.

Lumpkin et al. (2011) state that multiple stakeholders distinguish the SE ecosystem regarding the social context within which SE operates. Social entrepreneurs transform the equilibrium by building partnerships and involving stakeholders in the existing ecosystem. For example, as per Martin and Osberg (2015), the advocacy and changes in the economic policies and shifts in the power balance can be brought in by customer empowerment.

3.3 Policy Paradigm

In 1962, Thomas Kuhn put forth the concept of paradigm. He posited that science never develops gradually towards truth. Every science paradigm shifts when extant theories fail to explain certain phenomena and someone proposes a new approach. This observation is pivotal for social sciences and policymaking. Hall (1993) applied the concept of a policy paradigm to emphasise certain beliefs that determine the choice and nature of policy instruments.

The concepts of episteme and dispositif are pivotal and emphasise the heterogeneous aspects of policy content and facilitate coherence, which is the core of the analysis. The researchers should use the heuristic concept of a policy statement as it helps treat coherence and not as a fact. Formulating a policy proposal statement and its implementation is a convoluted process, and it involves a lot of intricacies. The policy evolves because of counter-arguments and gets redefined by new actors who provide vital inputs (Hogan et al. 2015).

4 Understanding the Why–Sustainability and Resilience

According to the United Nations Sustainable Development Goals (SDGs) and the International Labour Organization's latest work narratives (ILO 2018), striving towards sustainability is critical for all types of businesses (ILO 2018). The 17 Sustainable Development Goals (SDGs) of the United Nations Agenda express far-reaching and yet highly categorical effects linked to our society, environment, and development with distributive justice rather than just growth (Rawls 1971).

Resilience implies "the ability of a system, community or society exposed to hazards to resist, absorb, accommodate, adapt to, transform and recover from the effects of a hazard in a timely and efficient manner, including through the preservation and restoration of its essential basic structures and functions through risk management" (UNDRR). There has been significant growth in the acknowledgement of SE as an essential structure for sustainable development to address social needs and ensure adherence to SDGs.

Iva Konda, Jasmina Starc, and Barbara Rodica (2015) argue that the connection between sustainable growth and social innovation is a must-have in today's economy.

The findings outline a strong association between SE and sustainable development in the study area (Slovenia). It is significant in several fields, particularly social integration, social inclusion, employment, health care, education, finance, demographic changes, and political structures. However, they also state that the growth of social entrepreneurship is hindered due to scattered and distinct support mechanisms that lack the suitable attraction for social enterprise creation and expansion.

Malak Bou Diab's (2019) paper examines SE as an operative tool in determining social hitches, perceiving that SE examination can retort sustainable development challenges. It was discovered that social entrepreneurship may help alleviate poverty, ensure employment, financial success, environmental fairness, and a pollution-free environment, among other things.

This can lead to prospects to accomplish SDGs in Lebanon. Lastly, he concludes that social business models advance an elementary reach, backing-up social entrepreneurs to contribute pro-actively to sustainable development.

Social entrepreneurship and long-term development are influenced by socio-cultural and economic issues (Voegel et al. 2020). The hypothesis of the impact of social entrepreneurship on sustainable development was expressed by Luke A. Voegel and Jacob A. Voegel (2020). They offered a framework for ambitious social entrepreneurs to create a venture that focuses on long-term development.

This model emphasises that the social entrepreneurial process has two steps that lead to social value creation. They are 1) the generation of good notions; and; 2) the progress of the promising ideas into unique opportunities. Hence, they propose that this method will lead to sustainable human development in a linked, just, comprehensive, informed, and secure manner. Government backing, qualified personnel, public awareness, making a livelihood, increasing momentum, and access to financing are among the six criteria for growth and support of social entrepreneurship in the Thomson Reuters Foundation report, which ranks 45 nations.

5 Understanding the What–Review of Policy Ecosystem

5.1 Analyzing Policy Implications and Designing a Conceptual Model

Governments across the globe have felt the need and initiated efforts to standardise the process, regulation, etc., in entrepreneurship. The numerous policy initiatives have facilitated the mushrooming of many micro and small ventures contributing to the economy. The paradigm of entrepreneurship development has been gradually shifting from financial assistance to 'skill development' for fostering sustainable and resilient expansion. The entrepreneurship sector has also been observed to have undergone unusual dynamism, focusing mainly on economic development, digitalisation, access

to finance and the market, etc. Efforts have also been made to link various policy initiatives and measures relating to entrepreneurship development with global goals and national priority issues to leverage the transformative potential of the SE sector.

It has been found that the entrepreneurial ecosystem in the context of SE differs from for-profit institutions. An in-depth understanding of social entrepreneurship processes, initiatives, and their impact is needed for the policymakers to address the specific requirements or fill the existing gaps, promote resilience, sustainability, effectiveness, and efficiency within the SE sector. There is still a need to discuss/identify the 'social' in national policies for entrepreneurship. Public policy can be a critical medium restricting social entrepreneurship's 'social context'.

5.2 Overview of International Policy Initiatives in the Domain of Social Entrepreneurship

A comprehensive overview of the legal frameworks of SE, basically of the last decade, i.e., policies and laws formulated between 2011 and 2020, collected from various reports, policy papers, etc., relevant to this subject has been taken into consideration for this paper. In pursuit of exploring 'the policy and legal framework of SE', prospects and problems associated with this phenomenon with particular reference to SE in the Indian state, the researcher has reviewed available pieces of literature and has categorised it in undermentioned sections-

- Overview of International Policy framework of SE
- Overview of National Policy Initiatives/Legal framework supporting SE

The entrepreneurial ecosystem differs significantly across and within countries but generally includes key supportive and building blocks and scaffolds. It includes support mechanisms such as financial products and services, entrepreneurial education and training, financial literacy education, economic, regulatory frameworks, innovation systems, business regulatory environment, various support networks ranging from peer connections and mentoring schemes to incubators and accelerators, and public awareness of social entrepreneurship as a sector that can help to leverage sustainable development in general and to advance social entrepreneurship in particular.

The following might be inferred based on an analysis of some of the most recent governmental efforts aimed at boosting entrepreneurship in various nations:

(i) United Kingdom (Government Policy for Social Enterprise 2013–the Social Value Act), United States (Act on L3Cs), South Korea (Social Enterprise Promotion Act, Accreditation Schemes, Young Social Entrepreneur Program), etc., have a national strategy or policy for SEs with an extensive range of tools and programs to support, certification at the level of Ministry of Employment and Labour and thus can be categorised as states with '**mature policy framework'.**

(ii) SE rules and laws exist in Canada (only in British Columbia and Nova Scotia–Community Interest Companies (CIC) Act, Community Contribution Company (C3) Regulation), Poland, Italy, Chile, Malaysia, Thailand, and other countries. At the same time, on April 26, 2016, Chile's Ministry of Economy, Development, and Tourism stated that a legislation project to build a legal framework for SEs will be sent to Congress. As a result, they might be classified as states with a 'Growing policy framework.'

(iii) Spain, Greece (having Law on Limited Liability Social Co-operatives), France (having Law on Social and Solidarity Economy), Slovenia (having Act on Social Entrepreneurship), Denmark (having Law on Registered Social Enterprise), India (having central flagship policy on skill development and entrepreneurship and also policies to support SEs or social innovation Small- and medium-sized enterprise), Egypt (having Youth Social Entrepreneurship program of the Ministry of Communications and Innovation Technology), Colombia, etc. They can be thus categorised as the states with **'emerging policy framework.'**

(iv) Kenya, South Africa, etc., which witnessed a significant overhaul of South African company law, partly in response to the emergence of new hybrid forms of the enterprise (Companies Act of 2008) and the Non-Profit Organizations Act of 1997 governs NGOs and CSOs. Thus, there are no policies or regulations for SEs but policies for small- and medium-sized enterprises. This can be categorised as states with an **'early-stage policy framework.'**

5.3 Indian Policy Initiatives in the Domain of Social Entrepreneurship

In recent decades, India has witnessed considerable growth in SE. It has emerged as a robust potential solution for society and the economy and even addresses growing risks arising from climate change and humanitarian crises. The supporting ecosystem aids social enterprises in a variety of ways, including direct, indirect, financial, and advisory support. With increasing awareness, support, mentorship, training, and workshops available for social entrepreneurs and social enterprise leaders from policymakers, development practitioners, researchers, communities, and academia, the integration of sustainability across models, initiatives, and strategies is constantly evolving.

It is also pertinent to mention the crucial 'legislative' changes during COVID-19, such as revising the definition of Micro, Small and Medium Enterprises (MSMEs) and up-scaling or widening the scope of existing schemes and financial assistance promote youth for SE. This is also in furtherance to the PM's call to become Atmanirbhar (self-reliant), which inherently promotes the idea of entrepreneurship and social entrepreneurship in particular.

To address important concerns, the Indian government is aggressively promoting entrepreneurial culture and activities across a variety of priority and impact

sectors through enabling laws, financial allocations, special committees, schemes, programmes, and indirect incentives.

The Government has introduced a bulk of skill-building, self-employment, and self-enabling schemes to provide avenues for gainful and sustainable employment, cater to skill and entrepreneurship needs across the country, improve employment outcomes, and support the citizens in their journey towards self-reliance. The policies promoting self-employment and entrepreneurship are directed at self-employment generation for creating "necessity entrepreneurs" and "opportunity entrepreneurs" (NITI Ayog). Entrepreneurship policy emphasises facilitating required training, building an enabling environment for entrepreneurs, providing mentorship and nurturing through incubators and accelerators, and improving access to finance by making available the risk capital needed by the entrepreneurs.

An overview of Indian entrepreneurship policy initiatives at a glance gives information on some of the helpful programmes and schemes offered by a variety of government ministries and agencies in India. Some of the most prominent initiatives include Startup India Seed Fund Scheme (SISFS), 2021; National Policy on Skill Development and Entrepreneurship, 2015; Upgrading the Skills and Training in Traditional Arts/Crafts for Development (USTTAD), 2015; NewGen Innovation and Entrepreneurship Development Centre (NewGen IEDC); Start-up India, 2016; etc.

On aspects of sustainability and resilience, the inferences drawn from the reviewed schemes/policy analysis are as enlisted hereunder:

i. Promote sustainability by incentivizing the use of certifications such as ZED (Zero Effect, Zero Defect)
ii. Expected to have a multiplier effect on the economy, making India more resilient
iii. Facilitating scaling up to a level where funding can be sought from angel investors, venture capital firms, banks, and other financial institutions
iv. An enabling regulatory environment with a minimal compliance burden imposed on the enterprises, social entrepreneurs, and investors is envisaged
v. Incentivize youths for cooperative business ventures
vi. Promote entrepreneurship culture, facilitating innovative business solutions
vii. Emphasize fostering social entrepreneurship through grassroots innovations
viii. Imparting skills for self-reliance and self-sustenance among minority women
ix. Endeavours to inculcate the spirit of innovation and entrepreneurship among the Indian youth
x. Promotes a healthy ecosystem for the growth of innovation and startups, which will lead to long-term economic growth and large-scale job creation.
xi. For enabling scalable and sustainable enterprises building
xii. Encourage a culture of entrepreneurship and innovation.
xiii. Enhance credit facilities and boost the growth of small businesses in rural areas
xiv. Provision of financial sustainability
xv. Suitable assistance by way of term loan/working capital

xvi. Provide financing to small enterprises within the MSME sector
xvii. Recognizes the operational and financial challenges faced by the startups
xviii. Agenda of inclusive development - one of the thrust areas of XII five-year plan (2012–2017) is the key focus
xix. Sustainable employment generation opportunities by establishing microenterprises in the non-farm sector.

6 Discussion and Conclusion

The enabling policies are key in fostering the social entrepreneurial ecosystem in sustainable and resilient development. The ease of doing business is essential for entrepreneurial organisations to grow in scale, sustain, and create social value and impact. The formalisation of the SE sector facilitates social entrepreneurial organisations to draw a tailored structure and approaches. This encompasses a unique identity that adopts and affects the ecosystem.

Sustainability is presumed to complement resilience. With the concept of entrepreneurship, sustainability is an embedded phenomenon. And thus, the policies, programs, or schemes aimed towards fostering or creating a supportive ecosystem for SE embrace the concept of sustainability and, if effectively implemented, can build or lead to resilience in the longer term. The literature, policy documents, reports, etc., concerning SE, examining the role of the policy ecosystem, has certain limitations. It is mainly coupled with social-ecological systems but is much dispersed, less quantified, and challenging to be relied on for evidence-based policymaking. A good empirical approach(s) to the concept of resilience in the context of SE could facilitate better assess the contribution to sustainability and resilience.

This implies a greater need for testing the practical approaches with accurate data and integrating the concept of resilience for policymaking, policy implementation, policy analysis, and policy revisions.

If we analyse the policy ecosystem in the context of its ultimate contribution to SDGs, the indicators used to reflect the concept of resilience requires improvisation to reflect the elements of resilience effectively. For example, in the case of SE, this would include the ability to navigate through, consider adaptation, integrate social and environmental dimensions, evaluate systems-level tradeoffs, innovate for social aims, create socio-economic value, create social impact, etc. The paradigm shift through SE would be a unique empirical approach toward pragmatic sustainability and resilience challenges. This model can be better applicable in the emerging world of big data, gig economy, digital divide, and Industry 4.0.

7 Scope of Future Research

Building upon the doctrinal analysis and drawing upon the intertwined linkages, this paper paves the way for further empirical work to study in-depth the specific phenomena of social entrepreneurship and policy/legal challenges as a pathway and propose strategies for the resilience of SE. Given the global discussions and efforts towards accomplishing the Global Agendas 2030, it is imperative to make efforts to measure and quantify resilience and look to its relationship to common sustainability challenges.

8 Theoretical and Practical Implications

The great interest in entrepreneurship promotion for social, economic, and sustainable development on legislators, governments, and scientific communities makes social entrepreneurship practically an exciting and contemporary significant area of investigation.

The paper provides the much-needed research for social entrepreneurs, policymakers, leaders, investors, and incubators to further discuss, explore and pursue avenues in social entrepreneurship as a new way to address old problems. This paper contributes by identifying policy factors/determinants (accelerating/inhibiting) as a solid ecosystem for proposing pathways that can advance the legitimacy of social entrepreneurship and highlight its emancipatory transformation potential and role in contributing to resilient and sustainable development.

References

Aspire–A Scheme for Promotion of Innovation, Rural Industries and Entrepreneurship. https://www.startupindia.gov.in/content/sih/en/government-schemes/aspire-scheme-promotion-innovation-entrepreneurship-and-agro-industry.html

Atal Innovation Mission. Atal Innovation Mission. https://aim.gov.in/. Accessed 9 Dec 2021

Avery GC, Bergsteiner H (2011) Sustainable leadership practices for enhancing business resilience and performance. Strateg Leadersh 39(3):5–15. https://doi.org/10.1108/10878571111128766

Blackburn R (2011) Foreword. In: Dana LP (ed), World Encyclopaedia of Entrepreneurship. Edward Elgar Publishing Limited., Cheltenham, UK

Cabinet Office (2013) Significant boost to social enterprises as the Social Value Act comes into force, 31 January 2013. GOV.UK. https://www.gov.uk/government/news/significant-boost-to-social-enterprises-as-the-social-value-act-comes-into-force

Chandra Y (2015) The Darkside, myths, and reality of social enterprises: a social accounting view. Paper presented at 5th EMES International Research Conference on Social Enterprise, Helsinki, Finland

Commission Expert Group on Social Entrepreneurship (2016) Social Enterprises and the Social Economy Going Forward: A Call for Action from the Commission Expert Group on Social Entrepreneurship (GECES). European Commission. http://gsgii.org/reports/social-enterprises-and-the-social-economy-going-forward/

Dana L (2021) World Encyclopaedia of Entrepreneurship, 2nd edn. Edward Elgar Publishing, Cheltenham

Department of Economic and Social Affairs of the United Nations Secretariat (2020) The World Youth Report: Youth Social Entrepreneurship and the 2030 Agenda. United Nations. https://www.un.org/development/desa/youth/wp-content/uploads/sites/21/2020/07/2020-World-Youth-Report-FULL-FINAL.pdf

Diab MB (2019) Towards social entrepreneurship and sustainable development in Lebanon. In: Proceedings of the International Conference on Business Excellence, vol 13, no 1, pp 56–70. https://doi.org/10.2478/picbe-2019-0007

Entrepreneurship & Business Statistics GEDI. Entrepreneurship and Development Index. https://thegedi.org/global-entrepreneurship-and-development-index/

Galindo-Martín M-A, Castaño-Martínez M-S, Méndez-Picazo M-T (2020) The relationship between green innovation, social entrepreneurship, and sustainable development. Sustainability 12(11):446–479. https://doi.org/10.3390/su12114467

Hall P (1993) Policy paradigms, social learning, and the state: the case of economic policymaking in Britain. Comp Polit 25(3):275. https://doi.org/10.2307/422246

Hogan J, Howlett M (2015) Policy paradigms in theory and practice. Discourses, ideas and anomalies in public policy dynamics. Palgrave Macmillan, New York. https://www.researchgate.net/publication/279845482_Policy_Paradigms_in_Theory_and_Practice_Discourses_Ideas_and_Anomalies_in_Public_Policy_Dynamics

Hogenstijn M, Meerman M, Zinsmeister J (2018) Developing stereotypes to facilitate dialogue between social entrepreneurs and local Government. J Innov Entrep 7(1):213–228. https://doi.org/10.1186/s13731-018-0084-5

Hulgård L, Chodorkoff L (2019) Social enterprises and their ecosystems in Europe. European Commission. Luxembourg: Publications Office of the European Union. https://europa.eu/!Qq64ny

Ingram A, Hechavarria DM (2015) A review of the entrepreneurial ecosystem and the entrepreneurial society in the United States: an exploration with the global entrepreneurship monitor dataset. J Bus Entrep. Fall 2014 (Special)

Konda I, Starc J, Rodica B (2015) Social challenges are opportunities for sustainable development: tracing impacts of social entrepreneurship through innovations and value creation. Econ Themes 53(2):211–229. https://doi.org/10.1515/ethemes-2015-0012

Lumpkin GT, Moss TW, Gras DM, Kato S, Amezcua AS (2011) Entrepreneurial processes in social contexts: how are they different, if at all? Small Bus Econ 40(3):761–783. https://doi.org/10.1007/s11187-011-9399-3

Mason C, Brown R (2014) Entrepreneurial ecosystems and growth oriented entrepreneurship, background paper prepared for the workshop organised by the OECD LEED. https://www.oecd.org/cfe/leed/Entrepreneurial-ecosystems.pdf

Ministry of Commerce and Industry. Startup India Seed Fund Scheme (India). https://seedfund.startupindia.gov.in/

Ministry of Minority Affairs (2018) USTTAD (Upgrading the Skills and Training in Traditional Arts/ Crafts for Development). Government of India, January 2018. https://www.minorityaffairs.gov.in/sites/default/files/USTTAD%20English%20Guidelines.pdf

Ministry of Skill Development and Entrepreneurship (2015) National Policy for Skill Development and Entrepreneurship 2015. https://msde.gov.in/sites/default/files/2019.09/National%20Policy%20on%20Skill%20Development%20and%20Entreprenurship%20Final.pdf

National Cooperative Development Corporation (NCDC) new scheme 'Yuva Sahakar', launched in November 2018, gives young entrepreneurs in cooperatives:–Radha Mohan Singh (pib.gov.in)

NewGen Innovation and Entrepreneurship Development Centre: Startup India. https://www.startupindia.gov.in/content/sih/en/government-schemes/newgen-innovation-and-entrepreneurship-development-centre.html. Accessed 9 Dec 2021

OECD LEED Programme and the Dutch Ministry of Economic Affairs (2014) Entrepreneurial Ecosystems and Growth-oriented Entrepreneurship. OECD LEED, January 2014. https://www.oecd.org/cfe/leed/Entrepreneurial-ecosystems.pdf

OECD/European Union (2013) Policy Brief on Social Entrepreneurship Entrepreneurial Activities in Europe. https://www.oecd.org/cfe/leed/Social%20entrepreneurship%20policy%20brief%20EN_FINAL.pdf

Osberg SR, Martin RL (2015) Two keys to sustainable social enterprise. Harv Bus Rev. https://hbr.org/2015/05/two-keys-to-sustainable-social-enterprise

Pathak S, Ahmad MM (2018) Role of Government in flood disaster recovery for SMEs in Pathumthani province, Thailand. J Int Soc Prev Mitig Nat Hazards 93(2):957–966. https://doi.org/10.1007/s11069-018-3335-7

Pratono A, Sutanti A (2016) The ecosystem of social enterprise: social culture, legal framework, and policy review in Indonesia. Pac Sci Rev B Humanit Soc Sci. https://doi.org/10.1016/j.psrb.2016.09.020

Promoting Innovations in Individuals, Startups and MSMEs (PRISM), December 2021. Startup India. https://www.startupindia.gov.in/content/sih/en/government-schemes/promoting-innovations-MSME.html

Reinhart C (2011) Low-profit limited liability companies or L3CS. OLR Research Report. https://www.cga.ct.gov/2011/rpt/2011-R-0344.htm

Slovenia: Art. 2 of the Social Entrepreneurship Act. http://www.mddsz.gov.si/fileadmin/mddsz.gov.si/pageuploads/dokumenti__pdf/zaposlovanje/Act_SE_rev_clear.pdf

Social Investment Tax Relief: call for evidence, 5 December 2019. GOV.UK. https://www.gov.uk/government/consultations/social-investment-tax-relief-call-for-evidence/social-investment-tax-relief-call-for-evidence

Soto-Rodriguez E (2014) Entrepreneurial ecosystems as a pathway towards competitiveness: the case of Puerto Rico. Compet Forum 12(3):31–40. https://doi.org/10.1043/s11167-011-9398-3

Sustainable Finance Scheme. Startup India. https://www.startupindia.gov.in/content/sih/en/government-schemes/sustainable-finance-scheme.html. Accessed 9 Dec 2021

Thai MTT, Turkina E (2014) Macro-level determinants of formal entrepreneurship versus informal entrepreneurship. J Bus Ventur 29(4):490–510. https://doi.org/10.1016/j.jbusvent.2013.07.005

UK: Part 2 of the Companies (Audit, Investigations and Community Enterprise) Act (2004). https://www.legislation.gov.uk/ukpga/2004/27/part/2

United Nations Office for Disaster Risk Reduction. (n.d.). Resilience. https://www.undrr.org/terminology/resilience. Accessed 9 Dec 2021

Voegel LA, Voegel JA (2020) Social entrepreneurship and sustainability: how social entrepreneurship can lead to sustainable development. J Appl Bus Econ 22(11):341–362. https://doi.org/10.33423/jabe.v22i11.3736

Weerawardena J, Sullivan-mort G (2001) Learning, innovation and competitive advantage in not-for-profit aged care marketing: a conceptual model and research propositions. J Nonprofit Public Sect Mark 9(3):53–73. https://doi.org/10.1300/j054v09n03_04

Wolk AM (2008) Advancing Social Entrepreneurship: Recommendations for Policy Makers and Government Agencies: The Aspen Institute. https://rootcause.org/wp-content/uploads/2019/05/Advancing_Social_Entrepreneurship.pdf

Indigenous Knowledge of Chepang in Disaster Risk Reduction

Ganesh Dhungana, Indrajit Pal, and Prakash C. Bhattarai

Abstract The Chepang community of Nepal has been knowingly and unknowing utilizing their indigenous knowledge in Disaster Risk Reduction (DRR) in the form of societal functioning and cultural rituals. The study outlines best practices from indigenous knowledge interlinked with scientific knowledge and its contribution to DRR. Chepang community has developed mitigation and preparedness knowledge within their context, based on knowledge passed down from previous generations. The indigenous knowledge of Chepang has worked as the practiced indigenous solution to minimize the risk of natural hazards. Those applied skills can be documented as traditional innovation and technology. The study shows that the proper incorporation of positive aspects of indigenous knowledge of Chepang in the development plan will be a win–win for the indigenous Chapang community and local government. However, due to a lack of social innovation and handover approaches, indigenous knowledge of Chepang has not transformed adequately to the present generation. Furthermore, the younger generation's lack of commitment and learning attitude is a significant threat in preserving that knowledge and skills.

Keywords Indigenous knowledge · Chepang · Nepal · Disaster risk reduction

1 Introduction

Fifty-nine indigenous communities are living in Nepal. They have been categorized into five groups; endangered, highly marginalized, marginalized, disadvantaged, and advantaged. Chepang is listed in a highly marginalized group (Khanal 2014) Chepangs reside in the remotest areas of the Mahabharat mountain range in Nepal. This

G. Dhungana (✉) · I. Pal
Disaster Preparedness Mitigation and Management, Asian Institute of Technology, Khlong Nueng, Thailand
e-mail: gan.dhungana@gmail.com

P. C. Bhattarai
Department of Development Education, Kathmandu University School of Education, Patan, Nepal

I. Pal et al. (eds.), *Proceedings of the 2nd International Symposium on Disaster Resilience and Sustainable Development*, Lecture Notes in Civil Engineering 294,
https://doi.org/10.1007/978-981-19-6297-4_18

Tibeto-Burman ethnic group remained in isolation for decades following their primitive ways of survival. Chepangs are mostly found in the fragile slopes of Chitwan, Dhading, Gorkha, Lamjung, Makwanpur, and Tanahun (Beine 2012). Several myths can be found regarding the origin of Chepang. According to Khanal (2014), the first myth can be drawn from the language. Chepang calls themselves "Chyobang". The meaning of Chyo is "on top" and bang means "Stone". Chepang believed that their forefather lived in caves, and that is the initial of their originality. Another myth says that in the Chepang language, "Che" means dog, and "pang" means arrow. It is also believed that Chepang used to hunt wild animals for their living with the help of dogs and arrows, and ultimately, they were named Chepang Khanal (2014).

The total population of Chepang is 68,399. In the Dhading district, Chepang settlement is found in the upper belt of Madevesthan, Dhusha, and Jogimara villages with a total population of 14,492, which is 4.3% of the total population of the district (Central Bureau of Statistics 2011). In the earliest days, Chepangs moved from one place to another, lived in the caves, and practiced the shifting cultivation for food (Khanal 2014; Mukul and Byg 2020; Piya et al. 2011; Sharma 2012). They also hunted animals and birds and gathered wild roots and shoots to ensure adequate food for their families. Slowly they began life as a forager by settling down at a place and doing seasonal agriculture at the same place. They follow animism and strongly believe in the power of nature and spirit. During the field visit for this study, it was observed that the Chepang community has a profound relation with forests and nature. Chepangs have lived a forager life, depending on the forests and their products, and it has helped them have an enormous knowledge of large plant species (Rijal 2008).

Joshi et al. (2008) has discussed that indigenous knowledge has significant boundaries to know and accompaniment technical knowledge. However, classifying and detailing local experiences is challenging and intensive. The real issue is channeling this through community-based disaster risk reduction strategies. With specific to Nepal, Tuladhar (2012) focused on DRR knowledge of local people in Nepal and has highlighted that the DRR education initiatives implemented in Nepal are not enough. Further, Tuladhar (2012) has also pointed out that there is a limited publication to understand DRR practices in Nepal and has provided essential recommendations to government and international organizations to modify DRR and management programs targeted towards local communities. Similarly, Dhungel (2011) has investigated the indigenous knowledge and some strategies practiced by indigenous communities in DRR. Focusing on the Tharu community residing in Bardiya, Nepal, Dhungel (2011) has shown that the community people have limited knowledge regarding hazards, and they lack to showcase their knowledge in mitigation and management of those hazards. One of the critical concerns raised by Dhungel (2011) is the lack of incorporation of modern technology and traditional perception and practices and has reflected that indigenous knowledge is not enough to cope with climatic hazards, and integrating scientific knowledge with indigenous knowledge could be a sustainable solution.

Limited studies in the academic domain have investigated Chepang communities and their indigenous knowledge and practices in disaster management. The

vulnerability assessment conducted by Thapa and Upadhyaya (2018) to identify the potential threats posed by climate change to indigenous peoples in Kailali, Chitwan, and Rautahat revealed that the Chepang community has a higher adaptive capacity than the Tharu and Musahar communities. The study has also suggested that the indigenous knowledge of Chepang could be helpful in developing resilient livelihood programs. Similarly, Piya et al. (2013) also share that Chepang communities have been using their indigenous knowledge to cope with climate change extremes. The Chepang have been engaging in conservation practices like terracing, constructing walls, and planting hedgerows. These practices have been helping the community in soil conservation, which is essential as geographically fragile Mid-Hills are prone to landslides. Another considerable fact is that Chepangs are very knowledgeable in using wild plants for various purposes. A study by Rijal (2008) shows that indigenous knowledge of the Chepang about different kinds of plants and their medical purpose can significantly contribute to scientific research.

For decades, community-based knowledge has kept communities safe from natural hazards. This knowledge, accumulated through generations of observation, has improved people's ability to understand the behavior patterns of natural hazards specific to their local environment (Silva et al. 2021). Over centuries, indigenous people have developed skills and knowledge that have been tested and proven effective in reducing disaster risks and managing hazards (Cuaton and Su 2020). In this context, the study aims to explore the indigenous knowledge of Chepang community and their practices in DRR in their natural setting. Other communities residing in similar topography can adopt the knowledge and practice shared in the study.

The study has been divided into different subsections to systematically investigate indigenous knowledge practiced by the Chepang communities. The following section of the study defines the methodology used in the study and provides information about the study area. The study then delves into the indigenous knowledge practiced by the Chepang Community. Following that, the study's insight and discussion section examine the indigenous practices of Chepang in conjunction with scientific knowledge to support the study's argument. Finally, the study concludes with the key recommendations.

2 Ethnographic Field Work

Ethnography allows a researcher to observe and study the community that drives a particular pattern of behavior (Hulst et al. 2020). During the field visit, I (first author) observed daily activities, rituals, and surroundings of the Chepang and had conversations with them to have insight information about those activities and rituals. Observation, conversation, interview, and archival research were used to gather information. Fourteens Chepang people from different Chepang settlements located in Benighat Rorang Rural Municipality were interviewed for this study. The participants were selected based on their profession, community involvement, and recommendations

Fig. 1 Landscape of Thakthali Village. (*Courtesy* Ganesh Dhungana)

of community members. In addition, a reference check with local government officials was carried out to ensure that they had enough relevant information demanded by the study.

2.1 Study Area: Benighat Rorang Rural Municipality, Dhading

Dhading is one of the Nepal Earthquake 2015—affected districts. Benight Rorang Rural Municipality is a local administrative unit located in the district's southwest corner. Benighat Rorang has sloping terrain with elevations ranging from 292 to 1770 m above sea level (Khanal 2014). The Rural Municipality's geographical area is 207.1 square kilometers. A total of 71% of this area is covered by forest. The total population of the Rural Municipality is 33,029; among them, 7,761 are Chepang. 1484 of the 5854 households in the Rural Municipality belong to Chepang (Benighat Rorang Rural Municipality 2017). The settlement of the Chepang community and their experiences in disaster management were the main reasons for choosing Benighat Rorang Rural Municipality for the study.

3 Indigenous Technique of House Construction in Chepang

Chepang settlements are located over the hill, and close relatives usually live in a settlement. Chepang houses are a type of traditional house found in Nepal's mountain region. These houses are built with stone, mud, and other locally available materials. These houses are climate-resilient as they maintain the heat during winter and cold during the summer. The oven in a traditional Chepang house is built inside the house with the help of mud, stone, and an iron tripod for cooking and keeping the house warm. They primarily store their harvest upstairs or make bundles and hang them from the string attached to the roof (Karmacharya 2015). The traditional Chepang house differs from other houses in its composition. Chepang's traditional houses are easily identified. Chaitish, one of the settlements of Kosrang village in Benighat Rural Municipality of Dhading, has five such houses and is located on rocky land. All these houses belong to brothers of the same family. For their regular livelihood, among five brothers, three are engaged in agriculture, one of them is a mason, and the remaining one is working as a contractor to supply fruits and vegetables from the community to market.

Madan Kumar Chepang (pseudo name), recalling his childhood memories, shared that the structure of their house was completely different. Their house had only one room, which was round and was constructed of wood. He spent his entire childhood with his mother and other brothers in the same room. His father used to work for a master living in another village as a bonded labor. His father had to construct houses, cattle shades, and paddy field boundary walls for his master. After the master migrated to Chitwan, his father was sent back home. Since then, they have been living together. He and his brothers started working with his father to construct houses for others. Their father initially taught them construction skills, and later on, while working with his father and other senior community members, Madan Kumar and his brothers learned the necessary skills. When asked about their experiences with the earthquake of 2015, he stated that, despite the traumatic shaking, not a single house in their settlement was damaged. Pointing towards their houses, with a happy face, he said to me,

"Our house had just a few cracks."

I further asked him a question regarding the resilience of their houses; then, he shared the history of their house. According to Madan Kumar, they constructed their house sixteen years back. The house was built by themselves using their skills under the guidance and supervision of their father.

While sharing his stories, Madan Kumar was a bit emotional as he looked at his old father, struggling to get dressed. His father was mentally and physically unwell but seemed interested in looking at us. He proudly told us that his house was safer than that of the cemented house. According to him, they had used their unique technique to construct that house. To understand more about that unique technique acclaimed by him, I asked him. He then explained their way of the construction method.

"Firstly, we have to mix the mud with the water. Then we have to keep the stone over it, making an equal adjoining. All walls have to be connected, and stones should overlap each other. That will help each portion get connected to another, making it interlocked. During an earthquake, the entire building shakes but does not fall apart due to the interlocking."

He further added.

"We have not received any formal training for this. We learned it from our father and other elders."

In between my conversation with Madan Kumar, his younger brother Dipendra Chapang (pseudo name) joined our conversation and added.

"It will be stronger if the add connection is overlapped. To overlap the add connection, we must first cut the stone, which should be between one and two meters long. It's better if it's longer. When we compare this type of house to a cemented house, the cemented house may fall apart, but our house won't. I am confident in this."

After seeing his confidence, I was interested in some of their works. Then Dipendra shared that they had constructed houses in Ghalchowk, Gorkha, and none were damaged during the earthquake in 2015. He further stated that he could guarantee that houses constructed by the Chepang community using their technique would not fall apart for a hundred years. He also added that comparatively, the house construction technique of the Chepang community is a bit expensive and time-consuming but will be more durable. According to him, houses constructed by their method will last longer than the cemented modern buildings.

Then Madan Kumar added to our conversation,

"Many engineers have failed, compared to our skills. Engineers just go to school, and they lack practice. Just going to school cannot teach us everything. We did not go to school. However, we have skills. We did not have to spend a single rupee to learn this skill. A few skills were taught to me by my father and others I learned while working with my elders. We use our minds to internalize the concept said by others to construct the houses. Look at our settlements; none of these houses we constructed were destroyed by the earthquake in 2015. Not even a single house. However, toilets were destroyed. Because we had used cement to construct it."

Chepang takes advice from Pande (their religious leader) before the construction of their house. Pande is responsible for selecting and worshiping the land to construct the house and perform certain rituals. The ritual's compulsion is that Pande must verify that no evil soul is living nearby stones and rivers that may harm the family. Chepangs are more conscious of selecting the land to construct houses (Adhikari 2010). They prefer to construct houses on rocky landscapes. They collect big slates of rock and make a proper cut having a minimum size from one meter to two meters. Afterward, they select the mud and mix it with water and locally available grass. While mixing the mud, they ensure that they maintain the proper air pressure to stay longer. Then, they construct the wall adjoin those stones making them overlap.

Based on the information provided by Madan Kumar and Dipendra regarding the indigenous Chepang technique of construction of houses, I talked with other community members. They validated that they had been constructing the houses

Fig. 2 Traditional Chepang houses in Chaitisha. (*Courtesy* Ganesh Dhungana)

for years, and their houses were not affected by the 2015 earthquake. As a social science researcher, I have limited technical knowledge regarding the engineering aspects of housing construction. However, this study has provided a ground to explore further the Chepang community's indigenous technique of housing construction. The proper scientific testing of the indigenous techniques and their validation through the engineering domain could significantly contribute to resilient housing construction, which could considerably contribute to constructing resilient housing in the mid-hills of Nepal, where the earthquake is a prime threat.

4 Soil Erosion Mitigation Through Bio–Fencing

During the field visit, I had noticed that some Chepang families had *Kutmiro* (Litsea) and *Tanki* (Bauhinia purpurea) in their land. Besides being a feeder for their domestic animals, these plants also protected the area from soil erosion. Alongside, dead leaves served as fertilizers, topping on the manure of livestock for vegetables and seasonal crops. As the history of Chepang is associated with nomads, they have good knowledge about the trees and forests. Instead of big trees, they have preferences for small trees, shrubs, and grass to feed their domestic animals; cows, ox, goats, and buffalo. My field observation showed that having small shrubs and grass have been mitigating soil erosion and landslide in their settlement during heavy rainfall. My observation from the field is in line with the finding of a study by Piya et al. (2013), which has stated that the Chepang communities have been helping in soil conservation by practicing terracing, constructing walls and planting hedgerows. Chepangs of Kosrang village shared that they have been growing small trees and

Fig. 3 Soil erosion from the newly constructed rural road in Kosrang. (*Courtesy* Ganesh Dhungana)

shrubs in their land to feed their domestic animals; however, none of them had any idea about the role of those plants in controlling soil erosion. The indigenous practice of planting small trees and shrubs in their land is, in fact, working as the bio fencing, mitigating hazards such as landslides and soil erosion. Likewise, in Kosrang, Chepangs living in other places are also doing the same.

Knowing or unknowingly, Chepang, through their regular activities, somehow contributes to the mitigation of soil erosion. However, the contrast is that the local government's initiative to provide access to rural roads to communities has induced soil erosion and landslides in Kosrang and Thakthali communities of Chepang. During the field visit, I had noticed that the random use of excavators has made the land fragile and has inclined the risk of natural hazards. The random decision of the local government of Nepal regarding rural road construction and poor engineering designs used has created severe problems for local communities. The height cutting, retaining wall construction, and drainage construction in rural road construction of Nepal have already demonstrated that a lack of proper knowledge about road construction has accelerated massive soil degradation and impacted environmental resources (Linkha et al. 2020). Similar is the condition of the Chepang community of Benighat Rorang. The incorporation of the indigenous knowledge and practices of

local communities and their meaningful participation in designing the development plan of their community can be a suitable approach in addressing issues induced by development activities. The bio fencing practice of Chepang can be adapted in mitigating soil erosion and the risk of landslides in the excavated elevation of the rural roads.

5 Ecological Adaption Through Shifting Cultivation

One of the significant contributions of the Chepang community in nature-based solutions to natural hazards is shifting cultivation. Indigenous knowledge and practices of Chepang people have constantly endorsed the practice of shifting cultivation, which is an excellent ecological adaptation for the environment (Sharma 2012). In shifting cultivation, the land for cultivation is used only for two years, and then the farmers change to another area (Dhakal 1970). Shifting cultivation is considered an integral part of the Chepang community for their livelihood. During the ancient period, the Chepang community has mainly practiced hunting and slash and burn cultivation while living in caves and forests. They started modern agriculture about 120 years ago (Gurung 1970). As Chepang was a part of the Kipat system, they had practiced shifting cultivation. They cultivated maize and millet. This shifting cultivation supports nature for rebirth and controls the land's overuse, ultimately protecting biodiversity. Though the land use policy of Nepal does not promote shifting cultivation, however, scientific studies based on Chepang practice of shifting cultivation have significantly acknowledged the contribution of shifting cultivation in preserving the biodiversity of nature and mitigating soil erosion and landslide (Sharma 2012). During the field visit, though, I could not find any ongoing practice of the shifting cultivation besides hearing some stories from elderly people. However, reviewing Dhakal (1970); and Sharma (2012), significant evidence can be taken to argue the role of shifting cultivation in maintaining ecological diversity.

There is an ongoing debate that unsustainable shifting cultivation has many inverse effects. Deforestation, forest degradation, forest product depletion, soil erosion, and downstream effects are some environmental impacts (Rahman et al. 2012). However, the case of the Chepang community and their indigenous practice cannot be generalized in the global debate. As Rijal (2008) has found that Chepangs are well-versed in the use of various plants and have used a total of 219 plant parts from 115 species for medicinal purposes. Seventy-five of these had 118 new medicinal uses, and 18 of them had not been reported as medicinal plants in any previous Nepalese documents. Instead, they have been contributing to protecting those plants. Indigenous knowledge of Chepang poses to manage the forest is environmentally friendly (Rijal 2010), but when population pressure on the forest increased, these traditions broke down. Therefore, comprehensive solutions to environmental management demand the incorporation of indigenous knowledge. On a similar note, the study argues that the proper investigation of the indigenous knowledge about the shifting cultivation

and its incorporation in the policy will significantly contribute to ecological management. Shifting cultivation is an integral part of Chepangs' traditional ways of life, and their traditional right to continue this practice should be recognized in government policy (Mukul and Byg 2020). The proper incorporation of positive aspects of shifting cultivation knowledge of Chepang in the development plan will be a win–win for the indigenous community, local government, and, most importantly, ecological diversity.

6 Indigenous Knowledge in Forest Protection and Drought Stress Management

Khoriya land is the identity of Chepang (Sharma 2012). Some Chepang families residing in the Kosrang still don't have land ownership, as they used to farm *Khoriya* in the middle of the forest. Afterward, with the nationalization of the forest as state's property, these indigenous people had no longer claim ownership of the forest. (Luni et al. 2011). The Chepang have been utilizing the Khoriya land from the ancient period. However, they do not have ownership (legal certificate) of the land they have been using. Sujan Chepang (pseudo name), the first person to have a master's degree from the Chepang community, shared that besides their food production, *Khoriya* land is also connected with spiritual and religious beliefs. The Chepang believes that their forefather preserved those land, and their god lives there.

Chepang has always contributed to maintaining and protecting those areas in the Khoriya system. Not just in the forest, listening to the stories from elderly community members of Kosrang that they have also done Khoriya in the barren community land. The Forest Act of 1961, the Forest Protection Special Act of 1968, and the Forest Products (Sales and Distribution) rules of 1971 were all enacted to keep the general public out of the forests and protect the environment. However, these acts did not recognize that people had long-standing rights to forests (Luni et al. 2011). Moreover, the lack of incorporation of indigenous knowledge and negligence from government agencies in recognizing the participation of the indigenous community in the policy formulation created a problem in the exploitation of the forest in Nepal. Thus, the study argues that all the context of forest management should not be generalized; instead, acknowledging the contribution of Chepang and their interrelation with forest may work better in the form of a locally induced model for forest management and protection.

Chepangs, through hundreds of years of experience and continuous search for solutions for their survival, have developed solutions to emerging crises. However, such innovations of the Chepang have been neglected by Nepal's research, education, and extension systems (Khatiwada et al. 2012). Their initiatives and activities have been helping in maintaining greenery in their surroundings. Most importantly, making production in barren land is one of the ways to reduce the agriculture drought. Plants have a variety of drought-resistance mechanisms, including reduced water

loss through increased diffusive resistance, increased water uptake through prolific and profound root systems, and smaller and succulent leaves to reduce transpiration loss. Plant drought stress can be managed by growing plants that are drought resistant (Farooq et al. 2012). Similarly, indigenous farming knowledge of Chepang has contributed to plant resistance mechanisms and management strategies for dealing with drought stress. Khatiwada et al. (2012) share that Chepang adapts to water scarcity by using sustainable soil management and crops with low water requirements through their indigenous ways of farming. The Chepang are aware of the changing environment and use traditional methods to adapt. These techniques include water storage, reusing wastewater, re-sowing seeds, using high-yielding seed varieties, using organic manure, and shifting sowing dates (Duwal et al. 2017). These sorts of initiatives taught by their indigenous knowledge have always helped the Chepang community manage and cope with the changing climate extremes. Documenting these kinds of initiatives can help promote similar kinds of activities in other communities.

7 Insight and Discussions

The Chepang of Benighat Rorang, Dhading, can lead practical mitigation activities as they possess strong links to governing natural resources. The study provides an outline of best practices from indigenous knowledge interlinked with scientific knowledge to contribute to DRR. Both structural and non-structural measures of mitigation were noticed in the Chepang community. The traditional engineering practice for the construction of their houses as well as plantation shifting cultivation were some key examples of resilience practiced by the Chepang as an indigenous measure applied to mitigate the natural hazards. The indigenous knowledge of Chepang has worked as the practiced traditional solution to minimize the impacts of natural hazards. Those applied skills can be documented as traditional innovation and technology.

It is crucial to recognize that indigenous knowledge is not limited to oral or written transmission. The study has discovered that the Chepang community has indigenous knowledge and skill about the construction of houses. So, it is time to include the dissemination of knowledge and practices of such building types and materials to contribute to resilient housing structures in Nepal. Kurnio et al. (2021) also argue that it is essential to educate governments and development partners about indigenous knowledge and its incorporation into earthquake-resistant building designs. Traditional architecture is a crucial reason behind sustainable building design in different cultures and climates because it adopts local environments by using local construction materials and technology (Rijal 2008). A critical factor noticed about the construction of the traditional house of the Chapang is a selection of land. Pande plays an essential role in land selection for the construction; then examines the soil and assures that soil is not frazil supporting the family not to stay at landslide and soil erosion-prone areas. Pande worship and examine the water near selected land, and

they make sure that the water is pure enough to drink and avoid waterborne diseases in the family. However, it might be through shamanism knowledge of the cultural practice of the Chepang but has been helping them mitigate the natural and health hazards.

Similarly, while looking at the nature-based solution to the DRR and mitigation, it was widely noticed throughout that study that the traditional agricultural practices of Chepang have been controlling the soil erosion, conserving forests, managing drought stress, and so on. However, the community is not aware that they have been contributing to the mitigation of natural hazards. The fact that the Chepang community plays a significant role in mitigating natural hazards cannot be ignored. The study also possesses similar findings of (Haque 2019), which has discussed that people in disaster-prone communities have repeatedly demonstrated that, rather than structural methods, local inventive knowledge and practices have solved many problems related to disasters and natural resource management.

Recent development activities and DRR measures have recognized indigenous knowledge as an essential factor in sustainable development; however, there is a gap in putting these measures into action (Silva et al. 2021). The study shows that the community's participation in the discussion can give a relevant and important perspective regarding hazards, which may contribute to addressing in managing and mitigating the risk of those hazards. As memories of past disasters and hazards influence people's perceptions of risks and responses to future disasters and hazards. These disaster memory manifestations provide communities with knowledge, practices, and techniques to survive in a specific environment (Cuaton and Su 2020). Thus, the study urges policymakers and practitioners to incorporate indigenous knowledge of the community for the effective execution of a community-based disaster management approach.

8 Conclusion

The study has identified a significant gap in the integration of indigenous and scientific knowledge and recommends that it be bridged so that development organizations and policymakers can plan effective and practical disaster risk mitigation and management activities in indigenous communities. The study has discovered that the Chepang community has developed mitigation and preparedness knowledge within their context, based on knowledge passed down from previous generations. However, due to a lack of social innovation and handover approaches, indigenous knowledge of Chepang has not properly transformed to the newer generation. Furthermore, the younger generation's lack of commitment and learning attitude is emerging as a major threat in preserving that knowledge and skills.

Acknowledgements The study acknowledges the support provided by the "EFFORT: Enhancing livelihood and Fostering Resilience among the vulnerable communities along Trishuli River basin Project" implemented by Action Nepal and DCA Nepal in Benighat Rorang Rural Municipality, Dhading.

References

Adhikari R (2010) The importance of being a Pande: a performative reading of the shamanistic practices in Chepang community

Beine D (2012) Chepang-then and now life and change among the Chepang of Nepal (First). Blurb

Central Bureau of Statistics G. of N. (2011) National population census 2011. http://dataforall.org/dashboard/nepalcensus/

Cuaton GP, Su Y (2020) Local-indigenous knowledge on disaster risk reduction: Insights from the Mamanwa indigenous peoples in Basey, Samar after Typhoon Haiyan in the Philippines. Int J Disaster Risk Reduct 48:101596. https://doi.org/10.1016/j.ijdrr.2020.101596

de Silva A, Haigh R, Amaratunga D (2021) A systematic literature review of community-based knowledge in disaster risk reduction. In: Multi-hazard early warning and disaster risks. Springer, pp 303–320. https://doi.org/10.1007/978-3-030-73003-1_20

Dhakal S (1970) An anthropological perspective on shifting cultivation: a case study of Khoriya cultivation in the Arun Valley of Eastern Nepal. Occas Pap Sociol Anthropol 6:93–111. https://doi.org/10.3126/opsa.v6i0.1104

Dhungel R (2011) Use of indigenous knowledge in strategies for disaster risk reduction for flood disaster. http://dspace.bracu.ac.bd/xmlui/handle/10361/1819

Duwal S, Neupane PK, Devkota B, Dhoj Y (2017) Climate change imprint and impacts on livelihood of indigenous nationalities: a case of Chepang community from Bhumlichowk Area, Gorkha District, Nepal. Int J Sci Basic Appl Res (IJSBAR) 35(3):173–183. http://gssrr.org/index.php?journal=JournalOfBasicAndApplied

Farooq M, Hussain M, Wahid A, Siddique KHM (2012) Drought stress in plants: an overview. In: Plant responses to drought stress. Springer, Heidelberg, pp 1–33. https://doi.org/10.1007/978-3-642-32653-0_1

Gurung GM (1970) Economic modernization in a Chepang Village in Nepal. Occas Pap Sociol Anthropol 2:32–39. https://doi.org/10.3126/opsa.v2i0.1067

Haque M (2019) Indigenous knowledge and practices in disaster management: experiences of the coastal people of Bangladesh. In: Disaster risk reduction. Springer Singapore, pp 59–72. https://doi.org/10.1007/978-981-10-8845-2_4

Joshi PC, Devi V, Marahatta MPS (2008) Indigenous knowledge for disaster risk reduction in South Asia

Karmacharya R (2015) Changing pattern of socio-cultural life of chepang community: a case study of Dahakhani VDC of Chitwan. Department of Nepali History, Culture and Archaeology Tribhuvan University, Nepal

Khanal B (2014) Social exclusion of the Chepangs in the era of post-political revolution in Nepal-a case study of Dhading District. University of Bergen, Bergen

Khatiwada BP, Ghimire R, Adhikari R, Osti S (2012) Increasing crop water productivity through local crops and technologies: a case from the ethnic Chepang community of Nepal. Hydro Nepal J Water Energy Environ 50–53. https://doi.org/10.3126/hn.v11i1.7204

Kurnio H, Fekete A, Naz F, Norf C, Jüpner R (2021) Resilience learning and indigenous knowledge of earthquake risk in Indonesia. Int J Disaster Risk Reduct 62:102423. https://doi.org/10.1016/j.ijdrr.2021.102423

Linkha TR, Rai DK, Khatiwada SP (2020) Analysis of earthen road construction and land degradation in the Tankhuwakhola watershed of Dhankuta District. Geogr Base 7:113–126. https://doi.org/10.3126/tgb.v7i0.34281

van Hulst M, Koster M, Vermeulen J (2020) Ethnographic research. In: Encyclopedia of public administration and public policy, 3rd edn. Routledge, pp 1–5. https://doi.org/10.1081/E-EPAP3-120051222

Mukul SA, Byg A (2020) What determines indigenous Chepang farmers' swidden land-use decisions in the central hill districts of Nepal? Sustainability 12(13):5326. https://doi.org/10.3390/su12135326

Piya L, Maharjan KL, Joshi NP (2013) Determinants of adaptation practices to climate change by Chepang households in the rural Mid-Hills of Nepal. Reg Environ Change 13(2):437–447. https://doi.org/10.1007/s10113-012-0359-5

Luni P, Lall MK, Prakash JN (2011) Forest and food security of indigenous people: a case of Chepangs in Nepal Luni PIYA. J Int Dev Coop 17(1):113–135

Rahman SA, Rahman MdF, Sunderland T (2012) Causes and consequences of shifting cultivation and its alternative in the hill tracts of eastern Bangladesh. Agrofor Syst 84(2):141–155. https://doi.org/10.1007/s10457-011-9422-3

Rijal A (2008) Living knowledge of the healing plants: ethno-phytotherapy in the Chepang communities from the Mid-Hills of Nepal. J Ethnobiol Ethnomed 4(1):23. https://doi.org/10.1186/1746-4269-4-23

Rijal A (2010) The Chepang and forest conservation in the central mid-hills of Nepal. Biodiversity 11(1–2):71–77. https://doi.org/10.1080/14888386.2010.9712650

Sharma DP (2012) Understanding the Chepangs and shifting cultivation: a case study from rural village of central Nepal. Dhaulagiri J Sociol Anthropol 5:247–262. https://doi.org/10.3126/dsaj.v5i0.6367

Thapa P, Upadhyaya PS (2018) Vulnerability assessment of indigenous communities to climate change in Nepal. J Land Manage Geom Educ 1:41–46

Tuladhar G (2012) Disaster management system in Nepal - policy issues and solutions. J Risk Anal Crisis Response 2(3):166. https://doi.org/10.2991/jrarc.2012.2.3.2

Community Level Risk Assessment Using GIS—An Innovative Method for Participatory Risk Assessment

Rahim Dobariya, Dilshad Bano, Khwaja Momin, Deo Raj Gurung, and Nusrat Nasab

Abstract Identification and prioritization of local level risk through community engagement has long been stressed to inform risk reduction programme. There is a long history of community risk assessment (CRA) as a tool to increase community participation in identifying risk and developing management strategies. The Aga Khan Agency for Habitat (AKAH) as a part of an effort to develop holistic disaster risk reduction programme has developed and internalized innovative community level risk assessment integrating GIS technology with participatory risk assessment (PRA). The GIS framework has made integration of as many indicators as possible while implementing complex risk assessment algorithm. The distinction between living zone and activity zone and assigning different weightages enable attributing higher risk to population and critical assets in contrary to less critical assets. Similarly, assigning different weights for hazard based on onset nature in risk calculation, possible using GIS framework result in scientifically robust as well as more realistic risk products. The consistent backend database of hazard, vulnerability, and risk, with spatial and temporal attributes serves as a valuable resource to understand risk dynamics through monitoring of risk pattern. The multi-temporal database also helps in assessment and evaluation of risk reduction interventions, as risk moderation is partly an impact of the interventions. This innovative approach on community

Disclaimer: The views and opinions expressed in this article are those of the author and do not necessarily reflect of the position of any agency, organization, employer or company. Assumptions made in the analysis are not reflective of the position of any entity other than the author.

R. Dobariya (✉)
Aga Khan Agency for Habitat, 405A/407, Jolly Bhavan 1, 10, New Marine Lines, Mumbai 400 020, India
e-mail: rahim.dobariya@akdn.org

D. Bano
Aga Khan Agency for Habitat, Level 9, Serena Business Complex, Islamabad, Pakistan

K. Momin
Aga Khan Agency for Habitat, Street 10 House # 372, Kabul, Afghanistan

D. R. Gurung · N. Nasab
Aga Khan Agency for Habitat, Tcell Plaza, 10th Floor, 34 Rudaki Avenue, 734025 Dushanbe, Tajikistan

I. Pal et al. (eds.), *Proceedings of the 2nd International Symposium on Disaster Resilience and Sustainable Development*, Lecture Notes in Civil Engineering 294,
https://doi.org/10.1007/978-981-19-6297-4_19

level risk assessment has long informed AKAH's work to build safer habitat across programme areas, for which AKAH Pakistan bagged the World Habitat Gold Award in 2020.

Keywords Community risk assessment · Community-based disaster risk reduction · Aga Khan Agency for Habitat · Geographic Information System · Safer habitat

1 Introduction

World continues to witness increase in catastrophic events as well as increased associated economic cost. The year 2020 saw total of 389 natural disasters, 15,080 disaster related fatalities, 98.4 million affected population, and costed 171.3 billion US$ (CRED 2021). Significant share of the events (41%) and affected population (64%) were in Asia. With 82% of the total fatalities in 2020 globally attributed to extreme temperature and flood, climate change induced events are creating havoc. Past record indicates a rise in climate-related disasters globally over the years, 83% by proportion of the total events that was recorded between 2010–2019 (Freebairn et al. 2020). Many regions across Indian sub-continent continue to witness frequent severe flooding events in recent past. With increase (in intensity and duration) of climate extremes like temperatures and precipitation (Seneviratne et al. 2012), impact on environment and population is foreseen to be more widespread and severe in the future. Evidence suggests that high mountain eco-systems being sensitive to climate change will witness severe impacts in future (Palomo 2017), requiring risk informed development and management programmes, for which understanding of existing and future risks is imperative. As underscored by the Priority 1 in the Sendai Framework for Disaster Risk Reduction 2015–2030 (UNISDR 2015), comprehension of risk is foundational to develop bespoke preparedness and response programmes. Since communities are in the forefront of every disaster and are also the worst affected, emphasis is laid on community specific local level risk management programme to minimize human and economic cost (Dilley 2006).

Community risk assessment (CRA) is a well evolved field within a community-based disaster risk reduction (CBDRR) programme. Every CBDRM begins with a CRA, although approach varies widely by agencies. A quick review of CRA reveals that emphasis is on consensus building through participatory approach, while more recent efforts are towards making the assessment a more inclusive process. In terms of practice, it is evident that CRAs are largely done using analog approach, collecting hazard and socio-economic data using hard copies. Despite the convenience of analog approach, systematic monitoring of evolving risk using a consistent multi-temporal data set is difficult if not impossible, unlike in a digital data environment. Monitoring of evolving risk provides insights into risk dynamics, and also serves as an impact evaluation of risk reduction interventions, both of which are key learnings for improving risk reduction programme. This paper presents the hazard, vulnerability

and risk assessment (HVRA) approach adopted by the Aga Khan Agency for Habitat (AKAH), uniquely integrating GIS and database technology to participatory rapid appraisal (PRA), while generating a rich database of community level hazard and exposure. This paper also presents how situational awareness on the ground supports management decisions, with examples from the countries AKAH operates.

2 Study Area

AKAH's area of operation spreads across five countries (Afghanistan, India, Pakistan, Syria, and Tajikistan) and till date assessments have been completed in more than 2500 settlements spread across 215 districts. Majority (40%) of the settlement are in elevation range of 2000 and 3000 masl, while 29% are in elevation range of 1000 and 2000 masl, 24% are in elevation range of 5 and 1000 masl, and (7%) are above 3000 masl. The AKAH's operational geographies represents multi-hazard environment, prone to debris flow, flash flood, avalanche, landslide, cyclone, and extreme temperature. Out of the total of 2500 assessed settlements, 77% are exposed to multiple hazards and 94% are exposed to at least one type of hazard. More than 13% of settlements fall under high risk from multiple hazards, 58% fall under medium risk, 29% fall under low risk. The region is also prone to prolonged civil unrest and migration as in Afghanistan and Syria. Evidence from the ground reveals that AKAH's geographies is sensitive to climate change and any risk assessment needs to build in climate into the framework.

3 Methodology

The AKAH follows a four-step assessment process (Fig. 1) starting with offsite assessment where living zone, activity zone and open areas are delineated, existing hazard are identified and mapped, using high resolution satellite images. Preliminary assessment is performed using secondary data from official reports, economic surveys, census data, and household surveys. This is followed by onsite assessment where a team comprising of GIS specialist, geologist, engineer, and social mobilizer run a PRA process to collected relevant data and information, in addition to validation of data and information generated during the offsite assessment.

Upon data collection, the third step involves digitization of the data using ArcGIS suite and creating of geodatabase. In accordance with data validation standards, the team checks for comprehensiveness and accuracy of the collected data. Once the integrity of the data is verified, it is run through risk calculation algorithm implemented in Microsoft.Net technology to automatically calculate scores for various dimensions: risk, exposure, vulnerability, susceptibility, coping capacity, adaptive capacity. Different maps are generated using pre-defined layout and symbology

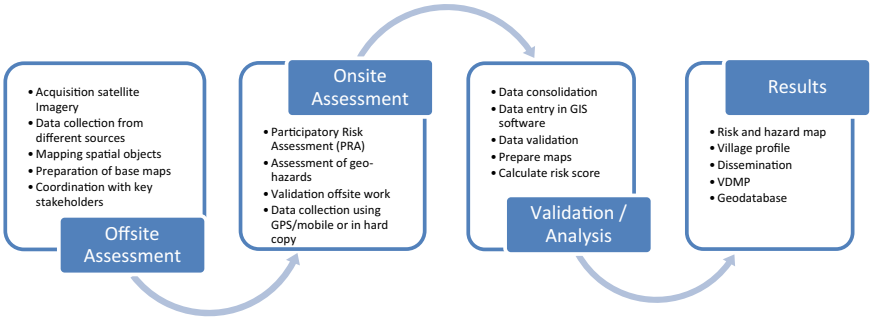

Fig. 1 Four steps HVRA process

guideline, for dissemination purpose. Finally, the maps and information are disseminated to relevant stakeholders including local government departments and communities. The findings are disseminated to community leaders and members through village level dissemination sessions.

4 Indicators and Risk Calculation

The AKAH uses index-based approach for risk calculation. Apart from being flexible the index-based risk methodology is simple to comprehend for risk managers (Rosenblum and Lapp 1989; Satta et al. 2016). Defined as "The combination of the probability of an event and its negative consequences." (UNISDR 2009), risk is an outcome of an interplay between exposure to hazard and vulnerability of the exposed elements. Mathematically it is expressed as Eq. 1.

$$R = \sum_{h=1}^{n} E * V \tag{1}$$

where $\sum_{h=1}^{n} E$ is sum of all the exposures in the community to multi-hazards and V is the vulnerability. Risk is calculated separately for living zone and activity zone to differentiate between risk to population (living zone) and physical area (activity zone), and final risk index (RiskIndex) is arrived at by adding weighted risk of the two zones (Eq. 2). These two zones are delineated using high resolution satellite images on Google Earth platform. Continuous plot of land where houses are located, and density of houses are relatively even demarcated as living zone. In case of a village clearly split into two or more spatially distinct communities, different living zones are digitized. All areas surrounding the living area, where community members visit regularly are identified as activity area. In a rural setting, activity area mainly comprises of houses, the irrigated areas, the exploited forests, and low pastures located close to the village. Since risk to population is of more importance than risk to physical infrastructure, higher weight is given to the living zone than activity zone.

Table 1 Hazard Significance Matrix calculated using return period and hazard intensity

Hazard Return Period	< 10 years	**[0.6]**	**[0.8]**	**[1]**
	10 - 30	**[0.4]**	**[0.6]**	**[0.8]**
	> 30 years	**[0.2]**	**[0.4]**	**[0.6]**
		Low	Medium	High
		Hazard Intensity		

$$\text{RiskIndex (Village)} = 0.8 * \text{RiskIndex (LivingZone)} + 0.2 * \text{RiskIndex (ActivityZone)} \quad (2)$$

The term exposure which is a measure of exposure to hazard is calculated separately for population (living zone) and physical area (activity zone) using Eq. 3 and Eq. 4. As intensity and frequency of hazard is an important consideration in risk calculation, hazard significance value is estimated based on return period and intensity of the hazard (Table 1) and used in exposure to hazard calculation. Return period is classified into three classes: <10 years, 10–30 years, and >30 years, following a practice in Switzerland (Lateltin 1997). Similarly, intensity is classified into three classes (high, medium and low) using an intensity classification scheme (Table S1) based on geometry and features observed in the field.

$$\text{Exposure (Physical Area)} = \text{Exposure (\% Area)} * \text{Hazard (Significance)} * \text{Hazard (Type)} \quad (3)$$

$$\text{Exposure (Population)} = \text{Exposure (\% Population)} * \text{Hazard (Significance)} * \text{Hazard (Type)} \quad (4)$$

The threat from a hazard is also modulated by onset speed of the event (Glade and Alexander, 2013) as it determines ability of the communities to respond timely. Higher significance (100%) is given to sudden onset hazards as it poses a higher risk of injury or death to people, and conversely lower significance (70%) is assigned to slow-onset hazards.

Vulnerability is defined as "The conditions determined by physical, social, economic and environmental factors or processes which increase the susceptibility of an individual, a community, assets or systems to the impacts of hazards." (UNISDR 2009). It is therefore a dynamic and multifaceted dimension, and holistic vulnerability assessment needs to take account of all the dimensions (Schneiderbauer et al. 2017). The AKAH's assessment framework includes 21 indicators, grouped into three dimensions: susceptibility (S), coping capacity (C), and adaptive capacity (A) (Fig. 2). The 21 indicators collected through secondary sources, PRA and field visit, are aggregated into dimensionless value (between 0 and 1) before being averaged to calculate index for different dimensions of vulnerability. The indicators align well with globally adopted framework such as WorldRiskReport (Welle and Birkmann 2015) and INFORM (Doherty et al. 2017). Finally, vulnerability is calculated using Eq. 5, considering positive or negative response of the questions.

$$\mathbf{V} = \frac{(\mathbf{S} + (\mathbf{1} - \mathbf{C}) + (\mathbf{1} - A)}{3} \quad (5)$$

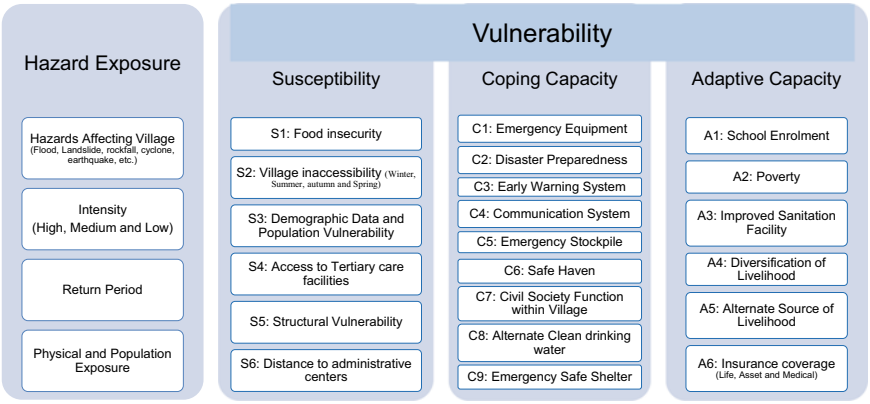

Fig. 2 Conceptual framework of HVRA methodology adopted by AKAH

5 Risk Maps and Database

The final product is a village level risk map where risk level is clearly depicted, along with different hazard types, houses, road network, critical infrastructures like schools and health center, water sources, open area, and emergency infrastructure like stockpile and safe shelter (Fig. 3). Figure 3 shows risk map of Meyanbar 1 village in Shughnan district located in north-east Afghanistan. The settlement has 3.3 km^2 of activity zone area that encompasses entire land area of the hamlet, including one living zone that covers residential area. The settlement perched on a very steep slope along a narrow valley surrounded by high-altitude mountains and difficult terrain, makes it one of the high-risk settlements. The village has 529 residents, out of which 140 of them are residing in medium intensity debris flow hazard zone, 30 of them residing in the high-intensity flood zone, 261 of them residing in high and medium intensity avalanches, and 115 of them residing in a high-intensity landslide zone. It is evident from the map that avalanche, and landslide are the two most prominent threats to the community.

The risk map helps in building community level situational awareness and communicating effectively with stakeholders including community members. The risk map serves as a starting point for development the village disaster management plan (VDMP), a blueprint for community level risk reduction, through a consultative process.

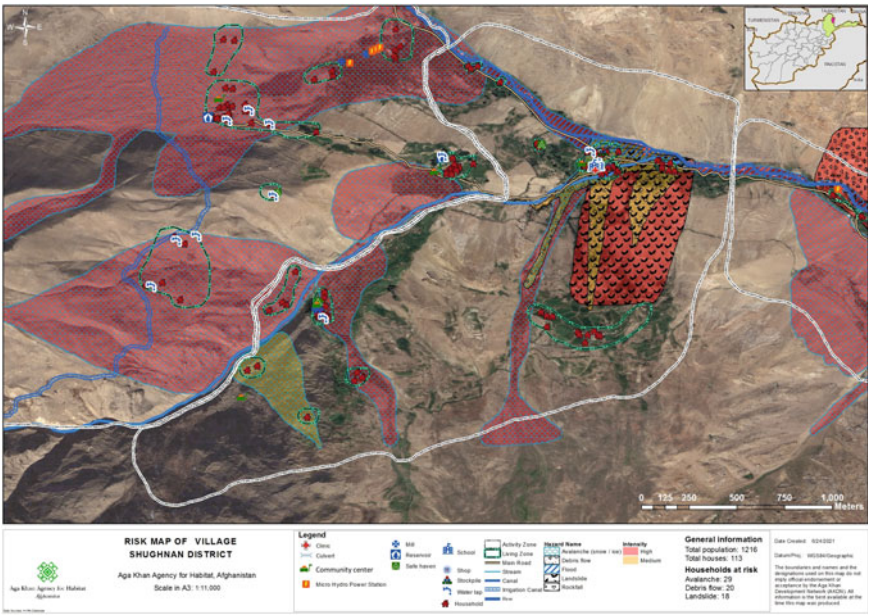

Fig. 3 Risk Map of Meyanbar 1 village in Shughnan district, a high-risk village in Afghanistan

In addition, a comprehensive database of hazard, exposure, and socio-economic parameters is a biproduct of the assessment. Analysis of these backend data informs DRR programming by helping select appropriate interventions based on ground situation, as illustrated in Fig. 4. Figure 4 shows distribution of 116 settlements in Afghanistan, along exposure to hazard on the x-axis and vulnerability on the y-axis, and risk is depicted by color of the circle. The settlement with high vulnerability scores but lower exposure (to hazard) score, those indicated by "A" for example need soft interventions to reduce vulnerability by reducing susceptibility and increasing coping and adaptive capacities. Contrarily, the settlement with high exposure score and lower vulnerability score as represented by "B", needs investment in hazard management such as structural mitigation and early warning interventions to protect lives and infrastructure.

Risk map and database have been the foundation of AKAH's informed DRR programming. Apart from the soft DRR interventions like awareness generation, training and formation of community emergency response teams (CERT), the risk map has been helpful in prioritization of mitigation projects as shown in Immit village in Pakistan (Fig. 5).

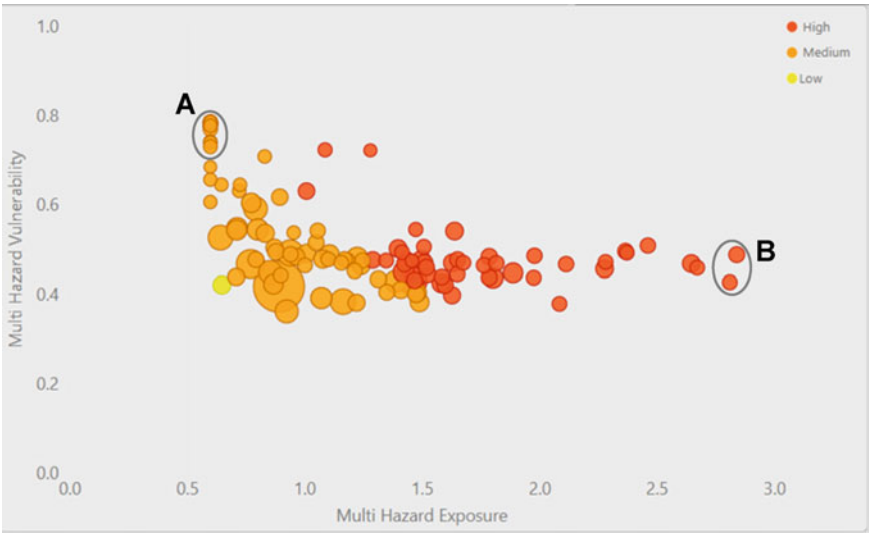

Fig. 4 Risk profiling of assessed settlements and prioritization of DRR interventions

Fig. 5 Photo showing flood protection wall in Immit village in Pakistan

Since the SoP requires that the assessment is done every 3 years or in an event of a catastrophic event, a multi-year consistent database at community level is created over the years, is helpful in monitoring risk evolution. As risk on the ground is modulated by field interventions, the data serves to assess effectiveness of interventions on the ground and thus a tool for programme evaluation.

6 Conclusion

Integrating GIS technology with PRA make the HVRA process more robust by easily ingesting more indicators and implementing more complex algorithms, generating realistic analysis. Differentiating and assigning different weights for living zone and activity zone allows ascribe greater significance to lives of the people and critical assets than physical space. The distinction made between hazard by onset speed in the risk equation develops pragmatic risk scenarios, and thereby helping in developing realistic DRR interventions. The risk maps developed using GIS technology is visually appealing and serves as a good communication tool and easy to reproduce with high degree of consistency.

The rich backend database of hazard, vulnerability, and risk, with spatial and temporal attributes, is an invaluable resource, enabling monitoring of community level risk evolution and providing insights into risk dynamics. Since risk is modulated by impact of the interventions on ground, the multi-temporal database helps perform programme assessment and evaluation.

For this unique approach that has contributed to building safer habitat across AKAH's prgramme areas, AKAH Pakistan bagged the World Habitat Gold Award in 2020.

Acknowledgements The team is grateful to the AKAH management for giving permission to present and publish on AKAH's approach on community level risk assessment and use for informing local level risk reduction. Sincere gratitude to the country technical teams diligently undertaking HVRA across often hard to reach settlements and contributing towards developing resilient communities.

Appendix

Table S1. Scheme for intensity classification for different hazard types

Hazard	Scale	Low	Medium	High
Avalanche	European scale	1—Sluff: (Runout: Small snow slide that cannot bury a person, though there is a danger of falling Potential Damage: Unlikely, but possible risk of injury or death to people. Physical Size: length < 50 m, volume < 100 m^3) 2—Small: (Runout: Stops within the slope Potential Damage: Could bury, injure or kill a person. Physical Size: length < 100 m volume < 1,000 m^3)	3—Medium: (Runout: Runs to the bottom of the slope Potential Damage: Could bury and destroy a car, damage a truck, destroy small buildings or break trees. Physical Size: length < 1,000 m volume < 10,000 m^3)	4—Large: (Runout: Runs over flat areas (significantly less than 30°) of at least 50 m in length, may reach the valley bottom Potential Damage: Could bury and destroy large trucks and trains, large buildings and forested areas. Physical Size: length > 1,000 m, volume > 10,000 m^3)
	Canadian classification	1—Relatively harmless to people 2—Could bury, injure or kill a person	3—Could bury and destroy a car, damage a truck, destroy a small building or break a few trees	4—Could destroy a railway car, large truck, several buildings or a forest area up to 4 hectares 5—Largest snow avalanche known. Could destroy a village or a forest of 40 hectares
	United States classification	1—Sluff or snow that slides less than 50 m (150') of slope distance 2—Small, relative to path	3—Medium, relative to path	4—Large, relative to path 5—Major or maximum, relative to path
Cyclone	Beaufort scale	0–7	8–11	12
	10-min sustained winds	< 28–33 knots (32–38 mph; 52–61 km/h)	34–63 knots (39–72 mph; 63–117 km/h)	64 –>136 knots (74–157 mph; 119–252 km/h)
	India meteorological department	Depression and deep depression	Cyclonic storm and severe cyclonic storm	Very severe cyclonic storm and super cyclonic storm
	National hurricane center	Tropical depression	Tropical storm	Hurricane (1–5)
Flood	Water depth	< 0.3 m	0.3–1 m	1 + metre

(continued)

Table S1. (continued)

Hazard	Scale	Low	Medium	High
Debris Flow	Volume	<50 ($10^3 m^3$)	50–200 ($10^3 m^3$)	>200 ($10^3 m^3$)
	Observational zoning	**Potential** • Located on fan but no clear indicators (levees, lobes, U-shaped etc.) • Abundant debris in the source area > 17° or (30%) • Presence of lake or large • catchment area to collect water	**Inferred** • Still connected with the system (channel can be filled and flow can be diverted) • Reported by people about debris flow events long time ago • Weather indicators (old features) • Abundant debris in the source area with an angle > 17° or (30%)	**Confirmed** • Fresh indicators (levees, lobes, V-shaped channel etc.) along track or fan • Reports by people
Earthquake	Peak ground acceleration	<0.18 g	0.18–0.34 g	0.34 + g
	Velocity	<16 cm/s	16–31 cm/s	31 + cm/s
	MMI	<VI–Strong	VII–Very Strong	>VIII–Destructive
	MSK	<VI–Strong	VII–Very Strong	>VIII–Damaging
	India zone	Zone 2	Zone 3	Zone 4, 5
	Pakistan zone	Zones 1, 2A	Zones 2B, 3	Zone 4
Landslide	Volume	<50 ($10^6 m^3$)	50–500 ($10^6 m^3$)	>500 ($10^6 m^3$)
	Observational zoning	**Potential** – Geology of the area is landslide prone – Steep slope > 20°		**Confirmed** – Open scarps or Open racks – Tilted trees and structure – Water supply to area visible – Recent shallow landslide as secondary processes
Rock fall	Volume	<100 (m^3)	100–1000 (m^3)	>1000 (m^3)
	Observational zoning	**Potential** • Bedded or massive rock >40° • Dip condition horizontal or vertical • >38o from the source area	**Inferred** • Old boulders • Shattered and jointed cliff • >40° slope angle (source area) • >38° (from the source to impact area)	**Confirmed** • Fresh cliff • Fresh boulders in the impact area • Recent events witnessed by the community
All hazards	**Rule of thumb**	**No impact or very limited impact on exposed house**[a]	**Can damage exposed houses**	**Can destroy exposed houses**

[a]The surveyor should only take into account houses that are typical in that particular environment. The surveyor's rule of thumb is simply to estimate the intensity based on the question, should a house be located in the impact zone, to what extent would it be affected by the hazard?

References

Centre for Research on the Epidemiology of Disasters—CRED (2021). Disaster Year in Review 2020: Global Trends and Perspectives

Dilley M (2006) Risk identification a critical component of disaster risk management. World Meteorol Organ Bull 55(1):13–20

Doherty B, Vernaccini L, Marin Ferrer M, Poljansek K, De Groeve T, Luoni S, Garcia JB (2017) Index for risk management - INFORM, European Commission, JRC110749

Freebairn A, Hagon K, Turmine V, Pizzini G, Singh R, Kelly T, Fisher D (2020) World Disasters Report 2020: come heat or high water. International Federation of Red Cross and Red Crescent Societies

Lateltin O (1997) Prise en compte des dangers dus aux mouvements de terrain dans le cadre des activités de l'aménagement du territoire. Recommandations, OFEFP, 42

Palomo I (2017) Climate change impacts on ecosystem services in high mountain areas: a literature review. Mt Res Dev 37(2):179–187

Rosenblum GR, Lapp SA (1989) The use of risk index systems to evaluate risk. In: Risk assessment in setting national priorities. Springer, Boston, pp 183–193

Satta A, Snoussi M, Puddu M, Flayou L, Hout R (2016) An index-based method to assess risks of climate-related hazards in coastal zones: the case of Tetouan. Estuar Coast Shelf Sci 175:93–105

Schneiderbauer S, Calliari E, Eidsvig U, Hagenlocher M (2017) The most recent view of vulnerability. Joint Research Centre (European Commission)

Seneviratne S, Nicholls N, Easterling D, Goodess C, Kanae S, Kossin J, Zwiers FW (2012) Changes in climate extremes and their impacts on the natural physical environment.

UNISDR (2009) UNISDR terminology on disaster risk reduction. United Nations Office for Disaster Risk Reduction, Report. https://unisdr.org/files/7817_UNISDRTerminologyEnglish.pdf. Accessed 19 July 2021

UNISDR (2015) Sendai Framework for Disaster Risk Reduction 2015–2030. In: UN world conference on disaster risk reduction, 2015 March 14–18, Sendai, Japan. Geneva: United Nations Office for Disaster Risk Reduction. https://www.unisdr.org/files/43291_sendaiframeworkfordrren.pdf. Accessed 19 July 2021

Welle T, Birkmann J (2015) The world risk index–an approach to assess risk and vulnerability on a global scale. J Extreme Events 2(01):1550003

Primary and Secondary Data Collection to Conduct Researches, Write Thesis and Dissertation Amidst COVID-19 Pandemic: A Guidepost

Antonio S. Valdez, Tabassam Raza, Martha I. Farolan, Celso I. Mendoza, Leticia Q. Perez, Jose F. Peralta, Richelle I. Valencia, and Harold Anthony Martin P. Lim

Abstract Research has always been regarded by many as tedious because of the difficulties and challenges associated with doing research such as having to forego certain habits like social life. Doing research became even more difficult, especially with regard to limitation on collecting applicable primary and secondary data due to the COVID-19 pandemic lockdowns. It is to be noted that substantive, thorough, sophisticated literature review and intensive pertinent primary data availability are ncessary for doing quality research relevant to the status quo. Various novel approaches have been adopted by scholars through their diverse academic spheres in conducting internationally acceptable research amidst the COVID-19 pandemic. This research aims to come up with a guidepost to facilitate researchers and other stakeholders with fundamental knowledge and skills in conducting substantive, thorough, sophisticated researches that are of international standards. A comparative and

A. S. Valdez · T. Raza (✉) · J. F. Peralta · R. I. Valencia · H. A. M. P. Lim
Graduate School of Business and Director Disaster Risk Management Unit, Philippine School of Business Administration, Manila, Philippines
e-mail: tabassamr@psba.edu

T. Raza
School of Urban and Regional Planning, University of the Philippine, Diliman, Quezon City, Philippines

M. I. Farolan
Malabon City University, Malabon, Philippines

C. I. Mendoza
San Benildo College, Antipolo, Philippines

L. Q. Perez
Marikina Polytechnic College, Marikina, Philippines

C. I. Mendoza
Disaster Preparedness, Mitigation, and Management (DPMM), Asian Institute of Technology, Khlong Nueng, Thailand

L. Q. Perez
City and Regional Planning Department, University of Engineering and Technology, Lahore, Pakistan

I. Pal et al. (eds.), *Proceedings of the 2nd International Symposium on Disaster Resilience and Sustainable Development*, Lecture Notes in Civil Engineering 294,
https://doi.org/10.1007/978-981-19-6297-4_20

diagnostic analysis method is used for analyzing existing literature and policies developed by higher education institutions and schools for doing research in the advent of the COVID-19 pandemic. The output allowed authors to develop a guidepost with rules on using limited primary and extensive secondary data in doing research. The guidepost consists of various sections explaining on how to do research and write theses and dissertations. These sections include among others research title, statement of the problem, research objectives, theoretical and conceptual frameworks, review of related literature, research methodology, analysis and interpretation of data, and conclusion and recommendations. The guidepost is very significant in doing researches and aids researchers in conducting internationally accepted researches with limited primary data and extensive secondary data in the advent of the COVID-19 Pandemic. The guidepost is flexible and can easily be used by local and international institutions' researchers through little modification in context of their research fields.

Keywords Primary and secondary data · COVID-19 · Guidepost · Dissertation · Thesis

1 Introduction and Background

Around the world, people, educators, students, or project proponents find research to be boring, waste of time and make social life miserable to a certain extent. Some are forced by circumstances to conduct researches owing to the requirements imposed by schools as a partial requirement for achieving a degree in college, advance education, or needing points in the employee file for promotion in office position. Very few individuals realize the influence and impact of research on the present set-up of the world. It has become a misplace belief, due to lack of proper information, that research is never a necessity in the world in which we live. Many do not realize that what we have or experience at the moment, like easier and better quality of life comes from products, systems, and methods that originated from research. According to the University of Surrey (2016), searching for information and knowledge through the internet and many other forms of communication would have been impossible without the assistance of research. For example, meteorology is a science that can predict the path of violent storms, hurricanes, and tornadoes, while a lack of Volcanology research would leave a huge proportion of the world vulnerable to the destruction of volcanic eruptions. Thus, nations would have been defenseless to the damaging effect of nature without acquiring knowledge through such research. Further, present medical application for wellness could never be possible without the use of medical and laboratory apparatuses which determine the kind and extent of the ailment of a patient. These apparatuses are indeed developed after rigorous research and experiments. The research therefore is an invaluable tool for building on material knowledge in almost all aspects of life, a most reliable avenue to begin and understand the complexities of various issues; uphold our integrity to detach truth from anything untrue, and serves

as the start for analyzing complicated and confusing sets of data; and research will always be sustenance for the mind (Zarah 2022).

Gathering data for research purposes under normal circumstances is arduous enough. The whole world has been beset by difficulty owing to the existence of COVID-19 a worldwide pandemic. The contagious ailment has forced people to stay home with industries and offices closed to prevent the transmission of the disease (WHO 2020). It has become a constraint then to collect primary data from proposed respondents, or data information coming from offices that were closed for the same reason. The government has imposed tedious and rigid policies preventing people from mingling as a law on health protocols (ODF 2020). Checkpoints were established to ensure that the protocols were observed (IAFT 2020). Various novel approaches have been adopted by scholars through their diverse academic spheres in conducting internationally acceptable research amidst COVID-19 pandemic. This research aims to come up with a guidepost to facilitate researchers and other stakeholders with fundamental knowledge and skills in conducting a substantive, thorough, sophisticated literature review, which is indeed a precondition for doing substantive, thorough, sophisticated research (Boote and Beile 2005). A comparative and diagnostic analysis method is used for analyzing existing literature and policies developed by higher education institutions and schools for doing research in the advent of COVID-19 pandemic. Further, to collect primary data a Google form, consisting of qualitative questions was prepared and sent to regular Master's and Doctoral students gathered from two (2) schools; Pamantasan ng Lungsod ng Marikina and the University of Rizal System, totaling eighteen (18) students. The information gathered after analysis and interpretation of collected data allowed authors to develop a guidepost on using limited primary and extensive secondary data in doing research amidst COVID-19. The guidepost consists of various features with its brief description and instruction on how to write each feature's content towards doing researches and writing academic theses and dissertations. These features include research title; statement of the problem; research objectives: theoretical and conceptual frameworks; review of related literature; research methodology; analysis and interpretation of data; and conclusion and recommendations. The guidepost consists of very significant procedure in crafting internationally acceptable researches with limited primary data and extensive secondary data in the advent of COVID-19 Pandemic. The guidepost is flexible and can easily be used by local and international institutions' researchers through little modification to fit in the context of their research fields not only amidst pandemic but also in normal condition (Raza 2019).

2 Objective of the Study

This research aims to develop a guidepost to facilitate researchers and other stakeholders with fundamental knowledge and skills in conducting substantive, thorough, sophisticated research that are of international standards. To achieve the said objective, this research seeks to answer the following questions:

i. What secondary data collection approaches are recognized to be applied amidst COVID-19 Pandemic?
ii. What are the various novel approaches that have been adopted by scholars during COVID-19 Pandemic?
iii. What are the potential approaches towards internationally acceptable researches during pandemic?
iv. What are the features of the Guidepost to develop internationally accepted researches?

3 Review of Related Literature

As research is a necessity, it cannot stop. Continuance of the activity is now the main problem in the intention to complete research (Bernstein and Walter 2021). Researchers must now learn the use of secondary data and the manner in which it can be obtained. Researchers may find a solution in secondary data which was collected during previous researches, studies and other published or acquired information by other parties in the past.

With the onset of the global COVID-19 pandemic and the efforts to contain it through public health measures, social distancing, lockdown and quarantine measures, the data and assessment landscape is facing long-term impact which could deliver the overdue push for all stakeholders providing international assistance to reinvent not only how to collect data in the coming months but also how to make use of other types of data that is readily available beyond the classic needs assessment/survey data. In a new discussion paper, Wilhelmina Welsch, JIPS' Head of Information Management and Innovation, unpacks immediate and longer-term shifts that will determine how we will work, including as follows (Welsch 2020):

Lean Design: We will have to think a lot more strategically about design and analysis of the questions we need answered.

Definition of Secondary Data: We will have to re-think the definition of and tools for analysis of Secondary Data—GitHub[1] not Reuters.

Act as a documentarian: We will have to act as documentarians with regard to our approaches and, even more importantly, with regards to the challenges and gaps we face, with key elements being reducing and documenting bias as well as being cognizant of who is being left out.

[1] https://github.community/t/what-is-github/1197/2#M3417.

From Face-to-Face to Remote Technologies: We will have to shift from Face-to-Face to remote technologies—where Mixed Methods will remain the key. And we cannot rush the shift.

Focus on Community Engagement: We will have to emphasize community engagement and capitalize on Thick Data.

The following approaches from the above shifts are identified and considered in developing the Guidepost of this research: Adopt remote data collection (Rule of the Thumb); Phone Surveys or self-administered online surveys through Goggle Forms; Web-based Surveys; and data collection by acting as a Documentarian.

As emphasized through an internal survey carried out by United Nations High Commissioner for Refugees (UNHCR), a shift towards remote approaches to primary data collection has brought on several complexities and challenges. Firstly, remote data collection relies heavily on the use of telecommunications and digital tools, such as phone calls, online surveys, virtual communication tools (SMS, WhatsApp, Signal, etc.), and satellite imagery. However, lack of connectivity remains a key issue for many operations looking to leverage remote channels for the collection of information. Secondly, the rapidity with which humanitarian workers have had to adapt to new ways of working also means that we do not always have a good understanding of the preferred communication channels of the community members we are trying to reach. Thirdly, challenges with the remote supervision of data collection activities will directly impact the ability to quality control the information collected. Finally, since there are fewer methods available for data collection, the same may be used over and over, leading to survey fatigue amongst those individuals consulted (UNHCR 2020). These challenges are considered in achieving the main goal of this research, i.e., developing a Guidepost that will be aligned with UNHCR that recommends relying more on secondary data review (SDR), i.e., the process of identifying and assessing data that was collected by someone else for another purpose to determine if it can be used to meet your information needs (Welsch 2020).

A key part of the toolkit by Fiona Samuels in 2020 consists of a list of resources, in terms of the live repository; it brings together experiences of and resources for collecting remote primary data in a COVID-19 era. These materials come from books, journal articles, newspaper articles, blogs and WebPages, and include experiences of doing participatory, qualitative, and quantitative research, through to ethical issues that may be faced and how to deal with them. This resource is periodically updated, and drawn on other organizations compiling similar lists (Samuel 2020).

It is to be noted that the health risks and government measures introduced by COVID-19 have severely limited traditional mechanisms for primary data collection, such as visiting households, doing direct observation and conducting focus group discussions. To continue generating information to support the delivery of life-saving assistance, humanitarian workers are pivoting to remote methodologies for data collection—such as telephone surveys, self-directed surveys, and remote key informant interviews—and are doing more secondary data analysis. Remote data collection is not only a way for UNHCR and partners to continue their work during COVID-19 but also a way to ensure the safety of the people we serve and of

our frontline staff. Further, under secondary data there are two (2) main types; internal which are data gathered from the researcher's organization and external which comes from outside as in government statistics and mass media. See Fig. 1 for more details. On one hand general types of secondary data, there is quantitative which involves numbers like weight of a person, working hours. On the other hand, qualitative entails information that cannot be expressed as numbers like color, feelings, attitudes, and behavior. Secondary data are information that are considered primary in the past and which have been gathered before (Intellspot 2022).

The ability to use secondary data is purely dependent to the original source decision to share the information. People are affected by the different forces of the environment and may consider secondary data as a thing of the past; a careful selection of data therefore is necessary. Using secondary data is analyzing a previously collected and analyzed data and it must match the need for information of a present research. It is therefore a must to consider the integrity and trustworthiness of the secondary data gathered and should have originated from reputable publications in search for consistency of approach.

In actuality (Schutt 2006), the use of secondary data saves time for the researcher without having to collect on his or her own. The effort of collecting data may lead to a larger stored data which would have been impossible for the researcher to collect on his own.

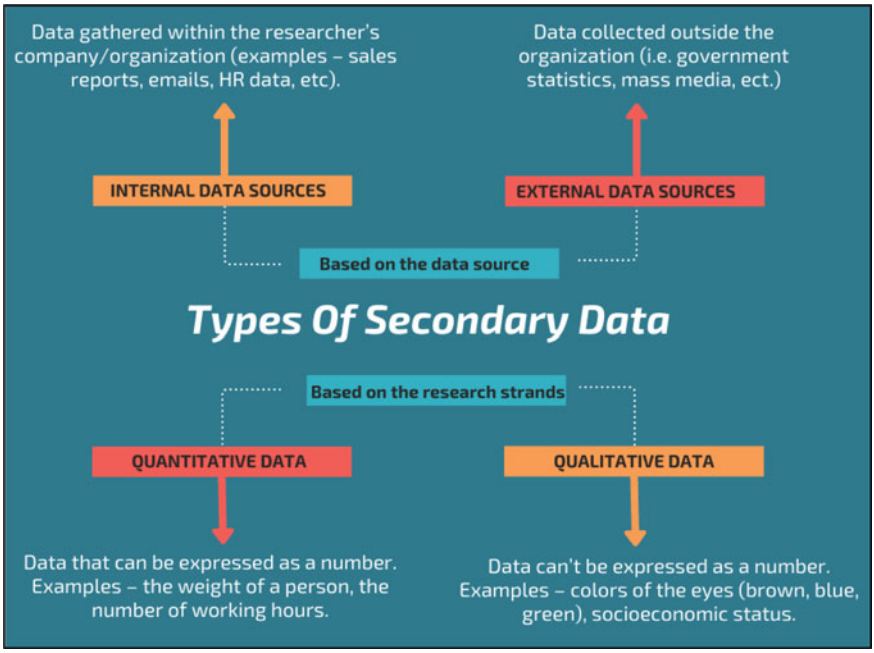

Fig. 1 Types of secondary data based on data source and research strands (*Source* Courtesy of Intellspot 2022)

Every introductory educational, social, and behavioral research textbook contains a chapter or section reviewing prior research as part of the research process (e.g. Babbie 1998; Creswell 2002; Fraenkel and Wallen 2003; Gay and Airasian 2000; McMillan and Schumacher 2001). A researcher cannot perform significant research without first understanding the literature in the field to collect secondary data. Not understanding the prior research clearly puts a researcher at a disadvantage. Different criteria have been suggested to evaluate the quality of research literature reviews and reports (Boote and Beile 2005). Creswell (2002) recommends a five-step process: "identifying terms to typically use in your literature search; locating literature; reading and checking the relevance of the literature; organizing the literature you have selected; and writing a literature review".

All above related literature is considered as significant source for collecting secondary data, thus, incorporated in developing the Guidepost of this research.

4 Methdology

It comprises of primary and secondary data collection to conduct researches, write thesis and dissertation amidst COVID-19 pandemic. Thus, a comparative and diagnostic analysis method is used for analyzing existing literature and policies developed by higher education institutions and schools for doing researches with the advent of COVID-19 pandemic. Further, to collect primary data a Google form, consisting of qualitative questions was prepared and sent to regular Masters' and Doctoral students gathered from two (2) schools; Pamantasan ng Lungsod ng Marikina and the University of Rizal System totaling eighteen (18) students.

A self-made self-directed surveys questionnaire was made to be sent to the respondents online by Google form, consisting of qualitative questions as follow:

i. What is your full understanding of secondary data reference to nature and legality of use?
ii. How do you perceive the practicality of secondary data use in the present circumstance?
iii. What is the viewpoint of your school on the use of secondary data?
iv. What is your notion on the proper secondary data choice?
v. What is your opinion on the general use of secondary data?

4.1 Conceptual Framework of the Study

The Conceptual Framework in Fig. 2 provides a graphical presentation of the sequential methodological activities adapted in this study to develop salient features of the Guidepost to conduct internationally accepted researches for publication.

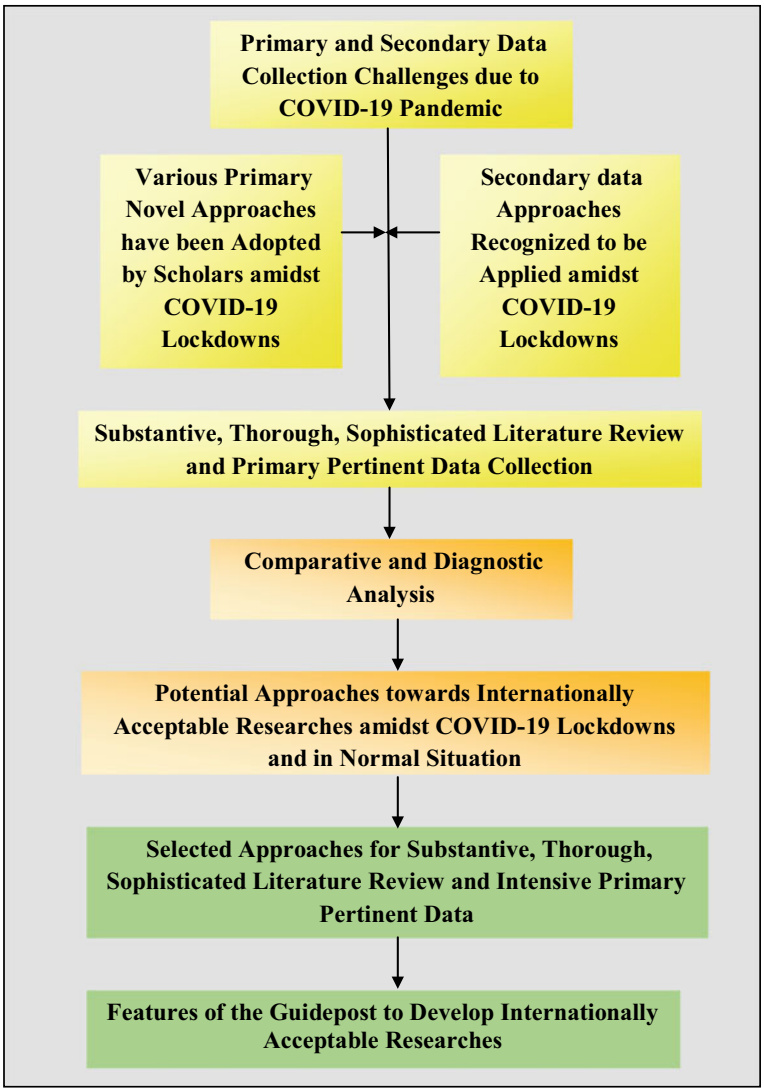

Fig. 2 Conceptual framework of the study

The first activity of the Framework refers to the challenges encountered by researchers in collecting secondary data due to COVID -19 Pandemic lockdown situations. Indeed, the physical movements and visits to the universities, schools, and institutional libraries and public research centers have been restricted due to government protocols regarding lockdown and social distancing to prevent virus spread. The second and third activities deal with the identification of various primary and secondary data collection approaches amidst COVID-10 Pandemic Lockdown. It is

primarily done through writing the sub-heading 22.3 Review of Related Literature of this research. The fourth activity described the available tools in terms of substantive, thorough, sophisticated literature review in identifying pertinent primary data collection approaches. Some of which are mentioned in the sub-heading 22.4 Methodology of this research. The fifth activity portrayed the comparative and diagnostic analysis done in selecting the potential approaches towards internationally acceptable research amidst COVID-19 and during a normal situation. It is stated in the proceeding section. See Fig. 2 for more details about the rest of the activities in the Framework.

5 Findings

For Primary Data Collection

The comparative analysis of the responses received was done and following common answers are obtained:

What is your full understanding of secondary data reference to nature and legality of use?

Answer: I am used to a quantitative approach usually using survey forms in which results are computed through the use of a statistical compendium. Complete knowledge of secondary data use is an approach that I am not very familiar.

ii. How do you perceive the practicality of secondary data use in the present circumstance?

Answer: Provided with knowledge about secondary data, it should be very practical at time that a pandemic is existing and when most organizations and employees are on forced holidays; including most people who are not allowed in the streets and if so allowed, have been prevented to mingle or speak to avoid disease transmission.

iii. What is the viewpoint of your school on the use of secondary data?

Answer: The school has a viewpoint of using valid data that has to be relevant to a present research that is being accomplished.

iv. What is your notion on the proper secondary data choice?

Answer: I believe in the point of the school. If secondary data cannot help resolve the issues raised by the paper, then it is useless.

v. What is your opinion on the general use of secondary data?

Answer: If one intends to pursue a research for whatever use, and primary data becomes impossible to obtain, secondary data should be most important.

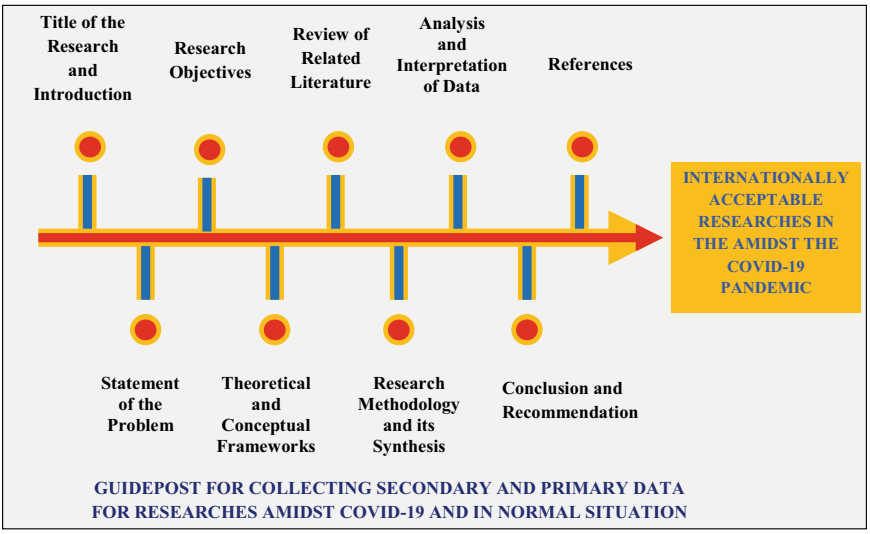

Fig. 3 Guidepost for doing research amidst COVID-19 Pandemic and normal situation

For Secondary Data Collection

To collect the pertinent secondary data for this study a substantive, thorough, sophisticated literature review is done (under subheading 22.3 Review of Related Literature) to answer the research related questions raised to achieve the objective of this research.

5.1 Guidepost for Collecting Secondary and Primary Data for Researches Amidst COVID-19 and in Normal Situation

The comparative and diagnostic analysis in terms of secondary and primary data and corresponding interpretation led to the development of the Guidepost (Fig. 3). It consists of nine (9) major salient features as shown in Fig. 3. The interpretation of the guidepost features plus 6 (+6) is provided in Table 1. To operationalize the Guidepost, one can easily follow the minimum requirements stipulated in terms of 15 steps in Table 1.

In fact and most importantly the Table 1 is provided to comprehend content of each feature with examples in operationalizing the Guidepost.

Table 1 Content of each feature with examples in operationalizing the Guidepost

Step	Feature	Suggested length of the content	Description
1	**Title**	Between 5 to 25 words in length or as instructed by the Publisher	Selecting an appropriate thesis or dissertation topic is one of the most significant aspects of Graduate work. The topic should be the result of thoughtful consideration by the student in cooperation with their advisory committee (TA&MIU, 2020) The research title should describe a) Problem /Issue/Challenge in hand, b) Method/Process, c) Solution, or all: For Example: Development of a Contingency Plan of Development Bank of the Philippines (DBP) towards Pandemic (COVID-19): A 360 Framework
2	**Self validation of the Title/Topic/Research**	This step is for self Validation Purpose. Thus, it should not be included in the content of the research. The researcher/s should comply with all 5 criteria to make the research valid	**Validate the Title/Research by fulfilling following Criteria:** 1. The researcher/s expertise should be aligned with the research/topic under study 2. The coverage of the issue/challenge/problem under study should have wide coverage or impact 3. Availability of substantial related literature/researches; 4. Availability of resources i.e., time, technology, human capital, and funds; and 5. The research should be timely

(continued)

Table 1 (continued)

Step	Feature	Suggested length of the content	Description
3	**Introduction and/or Background**	It should be the first heading of the research manuscript Half (½) to one (1) page content (letter/short size paper) for proposal writing; One (1) to two pages for full manuscript; Consult your University/School guidelines or research committee or committee chair to determine for number of pages required thesis and/or Dissertation writing	It is basically the overall summary of the research. The introduction to a research paper is where you set up your topic and approach for the reader. It has several key goals: The introduction looks slightly different depending on whether your research presents the results of original empirical research or constructs an argument by engaging with a variety of sources (Caulfield 2020),. Essentially, It consists of six parts and can be used as a guide to keep the flow of introduction acceptable under international standards. The heading of the sequence below need not be mentioned in the research content. It is only for indicative purpose: 1. Write Globe to local perspective of the problem/issue/challenge/subject matter under discussion; 2. Provide statement of the problem; (Narrative form) provide also related question/solution/ solution process etc., if any? 3. Provide main objective 4. Methodology; 5. Expected Findings/Conclusion for proposal and Expected recommendations. But for full paper write your findings and recommendations; and 6. Significance of the study/research

(continued)

Table 1 (continued)

Step	Feature	Suggested length of the content	Description
4	**Review of related literature**	Two (2) to four (4) Pages are usually required to write review of related literature. It is suggested to cite at least 20 references to justify your research subject matter	Provide an overview of the most relevant research that has already been conducted. This is a sort of miniature literature review—a sketch of the current state of research into your topic, boiled down to a few sentences (Caulfield 2020). Thus, find published literature consisting of articles, books, chapters, research papers, reports, etc. related to the research topic. At least 20 references need to be cited to justify the research subject matter. It is important to review the related literature and search for recommendations being provided in the literature. Indeed, these recommendations become future research topics. This step should also briefly explain why is certain reference cited and what is its relation or contribution in the ongoing research?

(continued)

Table 1 (continued)

Step	Feature	Suggested length of the content	Description
5	**Statement of the Problem: It also know as argument, challenge, or constraint need to be resolved**	Half (½) to one (1) page content (single space letter/short size paper, the same configuration will be used for the rest of the guidepost) for proposal writing; Half (½) to one (1) page content for full manuscript; and Consult your University/School guidelines or research committee or committee chair to determine for number of pages required thesis and/or Dissertation writing	There are usually two parts of the Statement of the Problem as follows: i. Part I—Narrative/Descriptive Form, the problem written in terms of a statement. For Example: The recent COVID-19 Pandemic event adversely impacted unprecedented losses in the DBP business. It further imposed negative impact on the daily lives of its employees due to the absence of Business Contingency Plan (BCP) ii. Part II—Related Research Questions For Example: What is the level of damages of the bank in terms of its business? What is the negative impact on the lives of employees? What are the main elements of the business? If your research involved testing hypotheses, these should be stated along with your research question (Caulfield 2020). They are usually in null form and can be refers as null hypothesis (Ho) For example, the following hypothesis might respond to the research question above: It was hypothesized that There is no significance difference between negative impact on the lives of employees and COVID-19 impact

(continued)

Table 1 (continued)

Step	Feature	Suggested length of the content	Description
6	**Objective of the study**	One fourth (¼) to one (1) page both for research proposal or full manuscript of a research/ thesis, or dissertation	Rewriting the problem and related research question in terms of proposed solution usually turns them into objectives of the Study: For Example: Solution to statement of the problem can be written as: The main objective of the study is to develop a 360 Business Contingency Plan Regarding Related Question For Example: The research questions can be rewritten in terms of solution particularly as following objectives: 1.To determine the level of damages across different line of products of the Bank 2.To find out the negative impact of the COVID-19 Pandemic impact on the daily lives of the employees 3.To identify the major line of business products of the bank and its total market share
7	**Significance of the study**	At least half (1/2) page or more both for research proposal or full manuscript of a research. Consult your University/School guidelines or research committee or committee chair to determine for number of pages required thesis and/or Dissertation writing	Write about the extent of the beneficiaries i.e. area, communities, or/and institutions, firms, organizations and individuals which will be benefited by this research

(continued)

Table 1 (continued)

Step	Feature	Suggested length of the content	Description
8	**Conceptual and/or theoretical framework of the research**	Depends on the numbers of pages required to develop or craft the conceptual and/or theoretical Framework	Can be verbal or graphical representation of the interrelated activities and processes/Methodology (dependents and independent variables) that will be undertaken during the research work to get desired output i.e. verbal interpretation of the conceptual framework and can be represented by the Abstract in words from
9	**Methodology**	At least 2 page or more as needed both for research proposal or full manuscript. Consult your University/School guidelines or research committee or committee chair to determine for number of pages required thesis and/or Dissertation writing	Detailed Narrative/Descriptive form of the Conceptual Framework and explanation regarding the type of the research, corresponding research methods, and statistical tools; that will be used to collect and interpret data from a specific location. It also briefs on how to do preparation of research and develop Instrument/Questionnaire to collect the pertinent data
10	**Analysis, interpretation of data, and findings**	Number of pages as needed. It is the Expected Output in terms of Proposal; however it refers to actual finding in terms of full manuscript of a research/thesis/dissertation	What output researcher is expecting after processing, analysing, and interpreting pertinent collected data based on his written or unwritten hypothesis?
11	**Conclusion and recommendation**	Consult your University/School guidelines or research committee or committee chair to determine for number of pages required thesis and/or Dissertation writing. However for proposal it is not required	Based on the analysis, interpretation of data and findings, the conclusion can drawn about the overall, thus, the corresponding recommendations should be provided as next step for the future researches

(continued)

Table 1 (continued)

Step	Feature	Suggested length of the content	Description
12	**References**	Number of pages as needed	Consult your committee or committee chair to determine which style is most appropriate for your thesis or dissertation. Your thesis and/or dissertation must follow those standards, methods of citation. (TA&MIU 2020) Use citation style as requested by the publisher e.g., American Psychological Association (APA) Fifth Edition, APA Sixth Edition, or Chicago Fifteen Edition. For this research the authors have used APA Sixth Edition
13	**Timetable and cost (only for proposal writing purposes)**	1 page or as needed	Provide the timetable and resources/funds needed to complete the research work
14	**Miscellaneous/Preliminary material**	Number of pages as needed	Thesis and/or Dissertation must have the following preliminary based on the requirement set by each University, School, or Institution. This includes among others Title Page, Copyright Page, Approval Page, Abstract, Dedication Acknowledgement, Table of Contents, List of Figures, List of Tables, List of Maps, Acronyms/abbreviation, Foreword, and Preface. (TA&MIU 2020)
15	**Supplemental material**	Number of pages as needed	Back matter after the close of the last chapter or section e.g. Endnotes, References/Bibliography, Appendix or Appendices, and Vita. (TA&MIU 2020)
	Total	Maximum of 10 pages are appropriate to write a research proposal. Whereas research manuscript/thesis/dissertation's dependent on the publisher's or research institution's requirement	

6 Conclusion

The data gathered from online/virtual platforms have indicated several important points about secondary data use in research: Among Graduate School students, the

subject of the study, showed unfamiliarity with the use of secondary data in their research accomplishments; Most students are familiar with and used to quantitative research and which actual surveys are being used to obtain information reference to opinions and views on certain issues of the research effort; Respondents acknowledged the difficulty in achieving research work in the face of an existing pandemic where mobilization of people and organizations is limited; Student respondents' schools recognize that secondary data must serve the purpose of relevance to present issues discussed in the research work and should consider that sources of the data should be of reputable publications; and Overall, respondents consider the importance of secondary data for use in research.

The data collection approaches which are recognized to be applied amidst COVID-19 Pandemic: lean design; re-think definition of secondary data; act as a documentarian, from face-to-face to remote technologies, availability of repository, and focus on community engagement are among others.

The ability on use secondary data is purely dependent to the source's decision to share the information. People are affected by the different forces of the environment and may consider secondary data as a thing of the past; a careful selection of data, therefore, is necessary.

Using secondary data in research has proved itself a valuable approach to finding suitable data for one's needs. This should be used more often in research (Martins et al. 2018).

7 Recommendations

- On the issue of non-familiarity with the use of secondary data, it is suggested that students who are exposed to research should be given sufficient knowledge on what secondary data is all about, the rationale for use, and basic rules in adopting information coming from past research by authors in previous studies;
- More emphasis on secondary data should be made part of the lecture in Research Methods as part of the curriculum in schools of the Philippines;
- More examples of research accomplishment using secondary data in all schools should be exhibited to students in order to familiarize and allow the continuance of research when primary data becomes a constraint to achieve;
- Adopt remote data collection (Rule of the Thumb); Phone Surveys or self-administered online surveys through Goggle Forms; Web-based Surveys; and data collection by acting as a Documentarian;
- Using secondary data is analyzing a previously collected and analyzed data. Thus, it should originated from reputable publications and must match the need for information of a present research.
- Live repository can be created by the Universities /Schools consists of a list of resources.
- As usual, researchers should be careful in selecting secondary data, verifying its suitability, documenting any changes or manipulations in the data, checking

whether the data may be safely used to accept of refuse a given set of hypotheses. By doing so, research may be done AT a quicker pace, without loss of quality and confusability (Martins et al. 2018).

References

Babbie E (1998) The practice of social research, Srh. Wadsworth, Belmont

Bernstein G, Walter A (2021) Research practice: perspectives from UX Researchers in a Changing Field. Greggcorp, LLC,: ISBN 0578811170, 9780578811178. https://books.google.com.ph/books/about/Research_Practice.html?id=I8QVzgEACAAJ&redir_esc=y

Boote DN, Beile P (2005) Scholars before researchers: on the centrality of the dissertation literature review in research preparation. Educ Res 34(6): 3–15. http://www.jstor.org/stable/3699805. Accessed 2 Apr 2022

Caulfield J (2020) Writing a research paper introduction | step-by-step guide. Scribbr. https://www.scribbr.com/research-paper/research-paper-introduction/#:~:text=The%20introduction%20to%20a%20research,Position%20your%20own%20approach

Creswell JW (2002) Educational research: planning, conducting, and evaluatingquantitative and qualitative research. Merrill Prentice Hall, Upper Saddle River

Fraenkel JR, Wallen NE (2003) How to design and evaluate research in education, 5th cdn. McGraw-Hill Higher Education, Boston

Gay LR, Airasian PW (2000) Educational research: competencies for analysis and application. Merrill, Upper Saddle Rive

IATF-Inter-agency Task Force for the management of Emergency Infectious Disease (2020) Recommendations for the Management of the Corona Virus Disease 2019 (COVID-19) Situation, Inter-agency Task Force for the management of Emergency Infectious Disease, Resolution No. 3, Series of 2020, March 17, 2020. Manila. https://doh.gov.ph/sites/default/files/health-update/IATF-RESO-13.pdf

Intellspot (2022) Types of secondary data, What is secondary data? Definition and meaning? https://www.intellspot.com/secondary-data/

McMillan JH, Schumacher SA (2001) Research in education: a conceptual introduction, 5th edn. Longman, New York

Open Dialogue Foundation (ODF) (2020) The impact of the COVID-19 crisis on human rights in the Republic of Kazakhstan. https://en.odfoundation.eu/a/27533,the-impact-of-the-covid-19-crisis-on-human-rights-in-the-republic-of-kazakhstan/

Raza T, Rentoy F, Ahmed N, Andres A, Raza TK, Marasigan K, Espinosa R (2019) water challenges and urban sustainable development in changing climate: economic growth agenda for global South. Eur J Sustain Dev 8(4):421–436. https://ecsdev.org/ojs/index.php/ejsd/article/view/907/902

Samue F (2020) Tips for collecting primary data in a COVID-19 era.https://odi.org/en/publications/tips-for-collecting-primary-data-in-a-covid-19-era/

Schutt RK (2006) Investigating the Social world: the process and practice of research, 5th edn. ISBN-13: 978-1412927345, ISBN-10: 141292734X. https://www.amazon.com/Investigating-Social-World-Practice-Research/dp/141292734X

Martins FS, da Cunha JAC, Serra F (2018) Secondary data in research – uses and opportunities. Revista Ibero-Americana de Estratégia 17:01–04. https://doi.org/10.5585/ijsm.v17i4.2723

TA&MIU - Texas A&M International University (2020) Thesis and Dissertation Formatting Manual. Laredo, Texas 78041–1900: Graduate School. https://www.tamiu.edu/cees/arc/documents/thesis.dissertation.formatting.manual.pdf

UNHCR (2020) Data collection in times of physical distancing. https://www.unhcr.org/blogs/data-collection-in-times-of-physical-distancing/

University of Surrey (2016) How does research impact your everyday life? London: Study International, University of Surrey. https://www.studyinternational.com/news/how-does-research-impact-your-everyday-life/#:~:text=For%20example%2C%20without%20meteorology%2C%20we,the%20destruction%20of%20volcanic%20eruptions

Welsch W (2020) The new normal: collecting data amidst a global pandemic. https://www.jips.org/news/the-new-normal-collecting-data-amidst-a-global-pandemic-covid19/

WHO-World Health Organization (2020) COVID 19 transmission estimates by territory, philippines. world health organization

Zarah L (2022) 7 Reasons Why Resaerch is Important. The Arena Media Brands, LLC. https://owlcation.com/academia/Why-Research-is-Important-Within-and-Beyond-the-Academe